Aspects of Higgs Physics and New Physics at the LHC

Zur Erlangung des akademischen Grades eines

DOKTORS DER NATURWISSENSCHAFTEN

von der Fakultät für Physik des

Karlsruher Instituts für Technologie (KIT)

genehmigte

DISSERTATION

von

Dipl.-Phys. Ramona Gröber

aus Leutkirch im Allgäu

Tag der mündlichen Prüfung: 25. April 2014

Referentin: Prof. Dr. Margarete Mühlleitner

Korreferent: Prof. Dr. Dieter Zeppenfeld

Abstract

We study Higgs physics and related issues in the Standard Model (SM) and beyond. In the first part, we present theoretical predictions for Higgs pair production in the SM including higher order corrections in Quantum Chromodynamics (QCD) and the uncertainties on the respective cross sections from various sources. The second part covers supersymmetry. In the framework of the minimal supersymmetric extension of the SM, we investigate decays of light top squarks in the kinematic region where a flavour-changing decay into a charm or up quark and a neutralino or a four-body decay occurs. Furthermore, we discuss the Higgs sector in the next-to-minimal supersymmetric extension of the SM with complex parameters. In particular, we calculate the Higgs boson masses at one-loop order. In addition, we present Higgs boson production cross sections and decay widths. The third part introduces Composite Higgs Models as plausible candidates for physics beyond the SM. We calculate the leading-order cross section for single and double Higgs production via gluon fusion obtained by means of the low-energy theorem (LET) and compare it to the result computed with full mass dependence of the new heavy vector-like fermions. In addition, we calculate the next-to-leading order QCD corrections for double Higgs production in the LET approximation for Composite Higgs Models. Furthermore, we study the effects of fermionic bottom partners on Higgs and electroweak precision observables.

Zusammenfassung

Im Rahmen dieser Doktorarbeit werden Higgsphysik und verwandte Themen im Standardmodell (SM) und darüber hinaus diskutiert. Im ersten Teil werden theoretische Vorhersagen für Higgspaarproduktion im SM inklusive Korrekturen höherer Ordnung und die entsprechenden Unsicherheiten auf die Wirkungsquerschnitte präsentiert. Im zweiten Teil untersuchen wir im Rahmen der minimalen supersymmetrischen Erweiterung des Standardmodells Zerfälle eines leichten Top-Squarks in dem kinematischen Bereich, in dem es mittels eines Flavour-ändernden Prozesses oder in einen Vier-Teilchen-Endzustand zerfallen kann. Zudem wird der Higgssektor in der nächst-minimalen supersymmetrischen Erweiterung des SMs mit komplexen Parametern untersucht, mit Fokus auf der Berechnung der Higgsmassenkorrektur auf Einschleifenniveau. Außerdem diskutieren wir Higgs-Produktionsraten und Zerfälle. Im dritten Teil der Arbeit berechnen wir für Composite Higgs Modelle in führender Ordnung den Wirkungsquerschnitt für die Produktion eines oder zweier Higgsbosonen – sowohl im Niederenergielimes als auch in voller Massenabhängigkeit der schweren neuen Fermionen. Zusätzlich präsentieren wir Ergebnisse für Higgspaarproduktion in nächstführender Ordnung in der starken Kopplungskonstante im Niederenergielimes. Zudem untersuchen wir die Effekte fermionischer Bottom-Partner unter Berücksichtigung der Einschränkungen aus Messungen elektroschwacher Präzisions- und Higgsobservablen.

Contents

CHAPTER 1

Introduction

"I am a firm believer that without speculation there is no good and original observation."
Charles Darwin
Letter to Alfred Russell Wallace, 1857

These are exciting times for particle physics. With the Large Hadron Collider (LHC) at CERN in Geneva, we have a powerful tool at our disposal to study the smallest constituents of nature. The first big success of the LHC could already be announced on 4th July 2012 by the ATLAS and CMS collaborations [1, 2]: The discovery of a new scalar particle with similar properties to the long-sought Higgs boson of the Standard Model (SM) of particle physics.

The SM [3–5] provides a theoretical framework describing the fundamental forces of nature in terms of a gauge field theory, apart from the gravitational force. The Higgs boson is a crucial part of the SM. It emerges as a remnant of the mechanism of electroweak symmetry breaking (EWSB) [6–10], which gives mass to gauge bosons and fermions and is essential for the consistency of the theory. Its discovery hence marks the beginning of a new era of particle physics. The new focus will now consist in the precise determination of its properties, such as its mass, its quantum numbers and its couplings.

Even though the SM describes the so-far gathered data with high accuracy, there are indications that it is not the ultimate theory of nature. Neither is gravitation implemented in the SM nor does the SM provide a candidate for Dark Matter or an explanation for Dark Energy. Furthermore, the Higgs boson mass in the SM seems to be unnatural since contributions from very high-scale physics lead to large quantum corrections to the Higgs boson mass. This poses the question why the Higgs boson

mass scale is so much smaller than the Planck scale, known as the hierarchy problem. A large amount of fine-tuning between the different loop contributions is needed to achieve a Higgs boson mass at the electroweak (EW) scale. This hints to New Physics which becomes relevant at a scale that might be reachable at the LHC. In the past, this theoretical problem acted as a guideline for numerous extensions of the SM.

A solution to many shortcomings of the SM is provided by supersymmetry (SUSY) [11–18]. Supersymmetry is a space-time symmetry which enhances the Poincaré symmetry by additional anti-commuting generators. These generators transform bosonic states into fermionic states and *vice versa*. Each particle is hence paired with a superpartner, which only differs by the spin. None of these superpartners, however, have been discovered yet. Thus, SUSY cannot be an exact symmetry. This problem can be evaded by introducing SUSY breaking sources, leading to different masses for the particles and their superpartners. If SUSY is supposed to solve the naturalness problem of the SM Higgs boson, the discovery reach of the superpartners lies within the range of the LHC. By now, all experiments could only report exclusion limits on the SUSY particle masses, but large parts of the parameter space remain to be explored.

Another interesting alternative to the SM are Composite Higgs Models [19–27]. In these models, the Higgs boson is not a fundamental particle but a composite state emerging from a new strong sector. The Higgs boson will naturally be lighter than the other resonances of the strong sector if it arises as a Goldstone boson of a global symmetry. Due to its Goldstone nature, the Higgs boson is supposed to be massless. If the global symmetry is not exact, however, but explicitly broken, loops of SM fermions and gauge bosons can generate a Higgs boson mass. The phenomenological implications of Composite Higgs Models at the LHC are, apart from deviations in the Higgs boson couplings, the emergence of new resonances of the strong sector. In particular, fermionic resonances which can mix with the top quark are expected to have masses within the reach of the LHC [28–32].

As input from the theory side the experiments need phenomenological studies and precise predictions concerning both SM and New Physics. Precise predictions for the SM are required to detect possible anomalies, in particular because New Physics can also appear indirectly via loop contributions. In order to anticipate where New Physics is supposed to emerge, it is also of great importance to predict the phenomenological implications of New Physics models as accurately as possible. The goal of this thesis is to contribute to this effort. This work is based on the research papers in Refs. [33–37].

The thesis is divided in three parts. The first part deals with the Higgs boson in the SM. Chapter 2 gives an introduction in the SM and motivates physics beyond the SM. In Chapter 3, predictions for Higgs pair production cross sections in the SM are discussed. Higgs pair production is an interesting process giving access to the trilinear Higgs self-coupling [38–40] and hence to the Higgs potential. Thus a measurement of this process is a first step towards the experimental verification of the exact form of the Higgs potential.

The second part of this thesis is dedicated to supersymmetry. After a short introduction in Chapter 4, we discuss in Chapter 5 decays of a light top squark, the superpartner

of the top quark. A relatively light top squark is motivated by the fact that it reduces the amount of fine-tuning of the Higgs boson mass [41]. In Chapter 6, we introduce an extension of the minimal supersymmetric extension of the SM (MSSM) by an additional scalar singlet field, the so-called next-to-minimal supersymmetric extension of the SM (NMSSM) [42–47]. Within this model, the Higgs boson masses at one-loop order are calculated taking into account CP-violation. Additionally, we compute Higgs boson production and decay rates in the NMSSM.

The third part covers Composite Higgs Models. First, an introduction into Composite Higgs Models is given in Chapter 7. Afterwards, the discussion turns to the phenomenology of fermionic resonances of the strong sector. We study in Chapter 8 the impact of top partners on Higgs physics, *i.e.* of fermions that mix with the top quark. In particular, single Higgs boson production and Higgs pair production and their dependence on the spectrum of the new resonances are investigated. Chapter 9 covers the phenomenological implications of bottom partners, taking into account various constraints for instance from electroweak precision tests and the current Higgs results. Chapter 10 summarizes the previous chapters.

Part I.

The Standard Model

CHAPTER 2

The Standard Model

2.1. The Higgs boson in the Standard Model

Five decades after the Higgs mechanism was proposed [6–10] in order to generate masses for the SM particles, the discovery of a Higgs boson with properties compatible with the SM could finally be announced by the ATLAS and CMS collaborations in 2012 [1, 2]. The SM is a gauge theory with a local $SU(3)_C \times SU(2)_L \times U(1)_Y$ gauge group [3–5]. The $SU(3)_C$ symmetry describes QCD where gluons emerge as the gauge bosons. The electroweak (EW) gauge group $SU(2)_L \times U(1)_Y$ unifies weak and electromagnetic forces. A Lagrangian for the SM can be constructed out of symmetry principles. Gauge invariance forbids an explicit mass term for gauge bosons, even though experimentally three EW gauge bosons were found to be massive. Here the Higgs mechanism provides a solution: A complex $SU(2)_L$ doublet ϕ is introduced into the SM with a potential given by

$$-V = \mu^2 \phi^\dagger \phi - \lambda (\phi^\dagger \phi)^2 \,. \tag{2.1}$$

A non-zero minimum of the potential can occur at $\langle \phi^\dagger \phi \rangle = v^2/2 = \mu^2/(2\lambda)$ for $\lambda > 0$ and $\mu^2 > 0$. The vacuum expectation value (VEV) v spontaneously breaks the $SU(2)_L \times U(1)_Y$ symmetry to the $U(1)_{em}$ symmetry of quantum electrodynamics (QED). The VEV v can then be aligned such that the expansion of the Higgs doublet ϕ about the VEV can be written as

$$\phi = \begin{pmatrix} \theta_2 + i\theta_1 \\ \frac{1}{\sqrt{2}}(v + H) - i\theta_3 \end{pmatrix} = e^{i\theta_a \frac{\tau_a}{v}} \frac{1}{\sqrt{2}} \begin{pmatrix} 0 \\ v + H \end{pmatrix} , \tag{2.2}$$

where θ_1, θ_2, θ_3 and H denote four real fields and τ^a are the $SU(2)_L$ generators. The three degrees of freedom θ_a with $a = 1, .., 3$ can be rotated away by a $SU(2)_L$ gauge transformation. They will correspond in the unitary gauge to the longitudinal degrees

of freedom of the massive gauge bosons. One physical degree of freedom is left over – the Higgs boson H.

The gauge symmetry of the SM is a local symmetry. The kinetic term $\mathcal{L}_{kin}$ of the scalar field ϕ hence involves a covariant derivative,

$$\mathcal{L}_{kin} = (D_\mu \phi)^\dagger (D^\mu \phi)\,. \tag{2.3}$$

The covariant derivative reads

$$D_\mu \phi = \left(\partial_\mu - i g_2 W_\mu^a \tau^a - i\frac{1}{2} g_1 B_\mu\right)\phi\,, \tag{2.4}$$

and introduces the $U(1)_Y$ gauge field B_μ and the $SU(2)_L$ gauge fields W_μ^a with $a = 1, ..., 3$. The corresponding gauge couplings are denoted by g_1 and g_2, respectively. Replacing ϕ by Eq. (2.2) in $\mathcal{L}_{kin}$, the bilinear terms in the gauge fields arise with the gauge boson mass squared as coefficient. Additionally, one finds interaction terms of vector bosons with the Higgs bosons in Eq. (2.3), proportional to the mass squared of the gauge boson.

Explicit mass terms for the fermions in the Lagrangian would break $SU(2)_L$ invariance. They can, however, be generated by Yukawa couplings (with $a, b = 1, 2$ and $\epsilon^{12} = 1$)

$$\Delta\mathcal{L}_{yuk} = -y_d \overline{Q}_L \phi\, d_R - y_u \epsilon^{ab} \overline{Q}_{La} \phi_b^\dagger u_R - y_e \overline{L}_L \phi e_R + h.c.\,, \tag{2.5}$$

once ϕ acquires a non-zero VEV. The $SU(2)_L$ quark doublet is denoted by Q_L, the $SU(2)_L$ lepton doublet by L_L, the right-handed up-type fermions by u_R, the down-type fermions by d_R and the right-handed leptons by e_R. Indices in the flavour and gauge space have all been contracted in the above formula. The Higgs boson H itself is massive, with the mass connected by an unique relation to the parameter λ of the Higgs potential, given by $M_H^2 = 2\lambda v^2$. Thus, by the measurement of M_H all unknown parameters of the SM Higgs potential are fixed. The currently measured value of the Higgs boson mass M_H by the ATLAS collaboration is $125.5 \pm 0.2 \pm 0.6$ GeV [48] and $125.7 \pm 0.3 \pm 0.3$ GeV by CMS [49].

Due to the close connection between the Higgs mass and the self-coupling λ, theoretical bounds on λ are directly translated into bounds on M_H. The scale dependence of the coupling λ due to radiative corrections manifests itself by renormalization group running. If the self-coupling λ runs to values smaller than zero before the Planck scale $M_{\text{Planck}} \simeq 10^{19}$ GeV the vacuum becomes unstable. By the requirement of absolute stability a bound on the Higgs mass can be obtained. It turns out that this bound is very near to the measured value and suggests a metastable vacuum [50–52]. Note that the self-coupling λ could also run into a Landau pole at some high scale. In order to avoid this, an upper limit on the Higgs boson mass is given by the so-called *triviality* bound $M_H \lesssim 650$ GeV [53–64], which turns out not to be relevant for the measured Higgs mass.

The SM Higgs boson exhibits another very important feature: It unitarizes longitudinal vector boson scattering. Without Higgs boson exchange the scattering amplitude would increase for high energies with the energy squared leading to a breakdown of

perturbative unitarity at some energy scale Λ. The Higgs boson restores unitarity if the Higgs boson mass is smaller than an upper bound of $M_H \leq 700$ GeV [65], which can easily be fulfilled by the current measurement. However, any deviations in the Higgs boson self-couplings and Higgs boson couplings to vector bosons and fermions would prevent a full restoration of perturbative unitarity.

2.2. Why Beyond the SM Physics?

Even though the SM was quite successful in explaining the experimental data in the last few decades, there still remain some open issues of theoretical or experimental nature that hint to physics beyond the SM. In this section some of them will be shortly described, without any claim of completeness.

Experimental problems:

- In the SM, no mass term for the neutrinos is incorporated. There is, however, experimental evidence [66–69], that neutrinos can oscillate, a phenomenon which can theoretically only be explained, if the mass eigenstates and current eigenstates do not coincide [70]. This implies that neutrinos are massive. The current upper bound on the neutrino masses is a few eV [71].

  A simple extension of the SM, with an additional right-handed, sterile neutrino can solve this problem. For such a sterile neutrino an explicit Majorana mass term can be introduced without violating the SM gauge symmetries (though violating lepton number). The massless neutrino can mix with the massive Majorana neutrino via Yukawa interactions, such that the physical spectrum contains only massive neutrinos, with a very light and a heavy neutrino. This mechanism is called 'seesaw' [72–74].

  If lepton number is conserved, neutrinos are Dirac particles. This, however, requires the strength of the Yukawa interaction to be much smaller than the Yukawa interactions of the other fermions without explaining this hierarchy.

- On experimental side many observations in cosmology *e.g.* orbital velocities of galaxies in clusters or stars in the milky way, gravitational lensing effects [75] or fluctuations in the cosmic microwave background [76, 77] give evidence for a non-baryonic kind of matter, called Dark Matter. A suitable candidate is commonly assumed to be a weakly-interacting massive particle (WIMP) [78], which cannot be provided by the SM. Moreover, observations of distances and associated red shifts of supernovae of type Ia indicate an acceleration of the universe [79, 80], which is explained by a larger energy density of the universe as given by the known and the dark matter together. This means there must be a new energy source, the so-called Dark Energy. The simplest candidate for Dark Energy is a cosmological constant in the Einstein equation, but the origin and size is yet to be explained. Other propositions are *e.g.* modified gravity or spatial inhomogeneity. For a review, see Ref. [81].

- Another cosmological problem is the dominance of matter over antimatter in the

universe. The process leading to an asymmetry between baryons and anti-baryons is called baryogenesis. The necessary conditions are given by the Sakharov criteria [82], which state that a violation of baryon number, a violation of C and CP symmetry and a departure from thermal equilibrium are necessary. The SM can fulfill this conditions, but it turns out that within the SM, the produced amount of net baryons by baryogenesis is too small to explain the baryon asymmetry of the universe. Another connected approach is leptogenesis, which can be incorporated into extensions of the SM concerning the neutrino sector. The asymmetry generated by leptogenesis between leptons and anti-leptons can be transferred to baryons by non-perturbative processes.

Theoretical problems:

- A full description of nature should also include gravitation.
- A unification of all forces is a very appealing scenario. The running gauge couplings in the SM seem to hint to such a possible gauge coupling unification at some high scale $M_{GUT} \approx 10^{16}$ GeV, but they do not fully unify. In Grand Unified Theories (GUT), the SM gauge group is embedded into a larger symmetry group. This is normally accompanied by new particles at a very high scale. Ideally, in GUT models the amount of parameters is reduced with respect to the SM. They also give a possible explanation of charge quantization and predict matter instability.
- Hierarchy problem: The hierarchy problem concerns the question why the Higgs boson mass is so much smaller than the Planck scale. It is closely connected to the issue of fine-tuning. To be more concrete: Quantum corrections to the Higgs boson mass introduce a conceptual problem in the SM [83]. If the SM is seen as an effective theory valid up to some scale Λ, the ratio of the one-loop corrections δM_H^2 to the squared Higgs boson mass M_H^2 reads [84]

$$\frac{\delta M_H^2}{M_H^2} = \frac{3\Lambda^2}{8\pi^2 v^2 M_H^2}(4m_t^2 - M_H^2 - 2M_W^2 - M_Z^2)\,. \tag{2.6}$$

  with m_t, M_W and M_Z denoting the top quark mass, the W boson mass and the Z boson mass, respectively. Numerically, this means that the SM should only be valid up to a scale of roughly 0.5 TeV for a natural theory. A theory is natural if physics at a certain scale is determined by physics at the same scale, hence the ratio $\delta M_H^2/M_H^2$ should be of order 1.

  The problem can be reformulated in terms of a renormalizable theory, if one adds an additional particle at some high scale. For concreteness, it is assumed that the new particle is a new very heavy scalar particle Φ with an interaction term $g_\Phi |H|^2|\Phi|^2$ and a mass m_Φ as it can *e.g.* arise in GUT models. Then the finite terms of the one-loop contribution are given by

$$\delta M_H^2 \approx -\frac{g_\Phi}{16\pi^2} m_\Phi^2 \left(1 - \log\frac{m_\Phi^2}{\mu^2}\right) + ..., \tag{2.7}$$

  with the renormalization scale μ. This means that a large amount of fine-tuning

is necessary for the Higgs boson mass to have a mass value at the scale of EWSB rather than at some high scale m_Φ due to the dependence on m_Φ^2.

In this sense, it is also necessary to distinguish between two different concepts of naturalness: In the strict sense, naturalness means that parameters should be of order one in natural units. There is, however, also the concept of 't Hooft [85], called 'technical naturalness', which states that a small parameter is natural if it is protected by some symmetry. This means *e.g.* that in the SM light fermion masses are technically natural, as the limit $m_f \to 0$ leads to a chirally symmetric Lagrangian and hence enhances the symmetry. For the Higgs boson mass there is no such symmetry protection. Note that most SM extensions address the problem of technical naturalness.

A comment on fine-tuning of the cosmological constant is in order. The energy density of the vacuum, which acts like Einstein's cosmological constant, is by dimensional analysis found to be of the order M^4_{Planck}. Compared to the measured value of the cosmological constant due to cosmic acceleration, this implies a fine-tuning of ~ 120 orders of magnitude, an even more severe fine-tuning than for the Higgs boson mass. One can, however, hope that quantum gravity might solve this problem.

The hierarchy problem plays a special role in all previously discussed points. All the other problems do not give a direct hint to a New Physics scale or, instead point to some very high scale, whereas the hierarchy problem suggests New Physics at the TeV scale. Hence it has acted as a guideline and motivation for model-building and searches for New Physics in the past. In this spirit, many New Physics models were proposed, addressing the hierarchy problem by New Physics at a low scale. In this context, we will discuss supersymmetry (SUSY) and Composite Higgs Models (CHM) in this thesis as possible New Physics scenarios in the second and third part of this thesis.

It should be noted, though, that low-energy modifications to the SM are not the only solutions to the hierarchy problem. Another possibility to circumvent it, is to argue that there is no higher scale introducing any hierarchy to the SM. This can of course only work under the assumption that gravity does not pose any problem and that all hard experimental problems of the SM can be solved at scales below the EWSB scale.[1]

Another, maybe more speculative, idea is based on the multiverse. Under the assumption that there is a multitude of universes, there will be one where the parameters are realized as we observe them. By an anthropic principle, the values of some parameters are selected such that the existence of us as observers is possible. This allows to give bounds on parameters, see *e.g.* Ref. [87] for a discussion of possible values of the cosmological constants by an anthropic principle.

We will now turn back to the SM and discuss the measurement of the Higgs boson self-couplings, which give directly access to the Higgs potential and hence are the last part in the program of establishing experimentally the mechanism of EWSB of the SM.

[1] In Ref. [86] a very simple extension of the SM was proposed by adding three right-handed neutrinos with masses smaller than the EW scale that can solve the issue of neutrino masses, dark matter and baryogenesis at once.

Afterwards, the phenomenological implications of two beyond the SM extensions will be discussed.

CHAPTER 3

Higgs pair production at the LHC

After the Higgs boson discovery one of the major goals of the LHC has become the measurement of the Higgs boson couplings. A special role take in this context the Higgs boson self-couplings. Their measurement allows for a reconstruction of the Higgs potential and hence an experimental verification of the mechanism of EWSB.

Experimentally, the measurement of the Higgs boson self-couplings is a very challenging task, which requires high luminosities for the triple Higgs coupling measurement. The quartic Higgs boson coupling seems to be neither measurable at a high-luminosity upgraded LHC [88–90] nor at a linear collider [38, 91].

The triple Higgs coupling is accessible in Higgs pair production processes. In the SM the most important process at the LHC is double Higgs production via gluon fusion, which is induced by loops of heavy fermions namely top and bottom quarks, followed by Higgs pair production via vector boson fusion (VBF), double Higgs-strahlung off vector bosons and associated production of the Higgs boson pair with top quarks.

In the previous works of Refs. [39, 40] the gluon fusion, the VBF and the Higgs-strahlung production modes were studied and the sensitivity on the extraction of the triple Higgs coupling was investigated. In this work, which is based on Ref. [35], the previous analysis of Refs. [39, 40] is updated by including into the analysis higher order QCD corrections for the three main production processes and by amending the results with modern parton distribution function (PDF) sets. Additionally, the associated production of a Higgs boson pair with a top quark pair is calculated at leading order (LO). The theoretical uncertainties are studied by taking into account uncertainties due to missing higher order calculations by varying the renormalization and factorization scales, the uncertainty on the PDFs and the strong coupling constant α_s and, for the gluon fusion process, the uncertainty stemming from the usage of the heavy quark mass limit for the next-to leading order (NLO) QCD corrections.

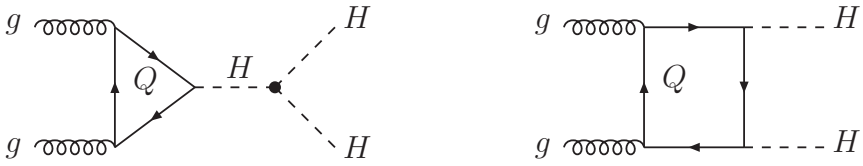

Figure 3.1.: Generic Feynman diagrams for Higgs pair production via gluon fusion at LO. The blob in the diagram indicates the triple Higgs coupling. The symbol Q stands for the top and bottom quark.

In order to explore if the triple Higgs coupling can be measured at the LHC, a parton level analysis is performed for various final states into which the Higgs boson pair can decay. For this analysis we restrict ourselves to the dominant Higgs pair production process. Similar analyses have been performed in Refs. [92–100].

In the first part of this chapter the gluon fusion process and its theoretical uncertainties are discussed. In the second part, VBF with the higher order corrections and the associated theoretical uncertainties will be described and, similarly, the Higgs-strahlung process in the third part. In the fourth part of this chapter a brief summary on the size of the cross sections for all the processes will be given, together with a short investigation on the sensitivity on the triple Higgs coupling. Before concluding in the last section, the fifth part discusses the prospects of measuring the gluon fusion cross section in the three final states $b\bar{b}\tau\bar{\tau}$, $b\bar{b}\gamma\gamma$ and $b\bar{b}W^+W^-$.

3.1. Higgs pair production via gluon fusion

Double Higgs production via gluon fusion is the dominant Higgs pair production process. It is induced by heavy fermion loops – mainly by top quarks, while bottom quark loops contribute with less the 1%. At LO the process is known with the full quark mass dependence and can be found in Refs. [101–104]. Figure 3.1 shows the generic LO Feynman diagrams for the gluon fusion process. There are a triangle and box contributions. The triangle diagram contains the triple Higgs coupling. For the box diagram in Fig. 3.1 we only show one generic diagram. There are three different box contributions corresponding to different momentum configurations.

The QCD corrections to the gluon fusion channel were computed in Ref. [105] at NLO in the low-energy theorem (LET) approximation, which means for the limit of heavy fermion masses in the loop. In the LET approximation, the loop-induced process can be replaced by an effective coupling of gluons to Higgs bosons. In order to improve the NLO result, the LO cross section is taken into account with the full fermion mass dependence in Ref. [105], which improves the results significantly. In Ref. [106], this heavy quark mass approximation was tested by the inclusion of higher order terms in the expansion in $1/m_t$. Recently, in Ref. [107], the LET calculation of Ref. [105] was improved by including the real emission matrix element with the full mass dependence. Furthermore, the next-to-next-to-leading order (NNLO) QCD corrections in

the LET approximation were calculated in Ref. [108]. Threshold resummation in the soft-collinear effective theory of soft gluons in the initial state are given in Ref. [109]. The QCD corrections to this process turn out to be quite large: At NLO the full cross section is almost the double of the LO result. The NNLO corrections are of $\mathcal{O}(20\%)$.

In the following only the NLO QCD corrections in the heavy quark mass limit are taken into account as for the NNLO corrections no public code is available.

For the evaluation of the numerical results I have used the code `HPAIR` [110], with the renormalization and factorization scale set to

$$\mu_0 = \mu_R = \mu_F = M_{HH}\,, \tag{3.1}$$

with M_{HH} denoting the invariant mass of the Higgs boson pair, unless indicated otherwise. We thus obtained a K-factor of

$$K = \frac{\sigma_{NLO}}{\sigma_{LO}} \sim 2\ (1.5) \qquad \text{at } \sqrt{s} = 8\ (100)\ \text{TeV}\,,$$

evaluating the cross section at NLO consistently with the PDFs at NLO, with $\alpha_s(M_Z)$ as given by the PDF set and the evolution of α_s at the corresponding order depending on the evaluated order of the cross section. The cross section at LO, σ_{LO}, was calculated correspondingly with a LO PDF set and the corresponding α_s. At LO the full mass dependence has been taken into account. As reference PDF set we have used the MSTW2008PDF set [111], as it includes error PDFs which allow for an estimation of the theoretical uncertainties. As input parameters we chose

$$\begin{aligned} M_H &= 125\ \text{GeV}\,, & M_Z &= 91.1876\ \text{GeV}, & M_W &= 80.398\ \text{GeV}, \\ m_t &= 173.1\ \text{GeV}\,, & \alpha_s^{LO}(M_Z) &= 0.13939\,, & \alpha_s^{NLO}(M_Z) &= 0.12018\,. \end{aligned} \tag{3.2}$$

3.1.1. Theoretical uncertainties

As described above, the theoretical uncertainties on the inclusive cross section of the gluon fusion process will be estimated by taking into account the following sources of error:

- The uncertainty due to missing higher order corrections is estimated by varying the scale μ_0, *cf.* Eq. (3.1). This gives an estimate of the size of the missing higher order corrections.
- The uncertainties on the PDFs and, related, on α_s. The PDFs are fitted from data. The starting point is a parametrization at some low scale Q_0 in the Bjorken x. With the help of DGLAP equations [112–114], they are then obtained at any scale Q_0 and for any x. Since the PDFs are fitted from the data, they depend on the choice of the data sets and the treatment of the errors on the data, as well as on the parametrization. Furthermore, different groups have a different treatment of heavy quark flavours or use different α_s.
- Specifically for the gluon fusion channel, we additionally estimate the error due to the heavy quark mass approximation for the calculation of the higher order corrections.

In order to obtain the scale uncertainty we varied the scale according to

$$\frac{1}{2}\mu_0 \leq \mu_R = \mu_F \leq 2\mu_0 \,. \tag{3.3}$$

The obtained uncertainty at NLO is quite high: $\Delta^{\mu} \sim 20\%/-17\%$ at $\sqrt{s} = 8$ TeV and $\Delta^{\mu} \sim 12\%/-10\%$ at $\sqrt{s} = 100$ TeV. Note, however, that varying the scale as described in Eq. (3.3) in the LO result would not capture the NLO cross section and could suggest to vary the scale within a larger window. The correction from NLO to NNLO is, however, given in Ref. [108] and turned out to be $\mathcal{O}(20\%)$, reducing the scale uncertainty below 10%. Additionally, for single Higgs production the same scale variation as in Eq. (3.3) is used to estimate the theoretical uncertainty [115, 116], suggesting the scale variation as given in Eq. (3.3).

Another source of a theoretical uncertainty is due to the PDFs. One part of the uncertainties on the PDFs comes from the assumptions made for the parametrization, as *e.g.* different ways of how to parameterize the data, another part comes from theoretical assumptions as *e.g.* on the behaviour for $x \to 0$, 1 or from different input data. These uncertainties are rather hard to estimate. The only possibility is to compare different PDF sets from different groups. A comparison of the prediction of the different PDF sets can be found in Fig. 3.2, where we show in black the MSTW [111] prediction, in red the CT10 [117], in green the ABM11 [118], in blue the GJR08 [119], in violet the HERA 1.5 [120] and in light blue the NNPDF 2.3 [121] prediction as a function of the centre-of-mass (c.m.) energy $\sqrt{s}$. In the small subfigure of Fig. 3.2 the cross sections are normalized to the MSTW prediction. The MSTW PDF set leads to the largest cross section. For $\sqrt{s} = 8$ TeV the ABM11 PDF set gives a cross section which is smaller by 20%. At $\sqrt{s} = 100$ TeV the largest discrepancies of 15% are between the GJR08 PDF set and the MSTW2008 or the GJR08 and the ABM11 PDF set. All the other predictions of the different PDF groups lie in between.

The other source of uncertainty on the PDFs stems from the errors on the fitted data. With the MSTW PDF set these errors can be easily estimated by using the error PDFs [122] provided by the MSTW collaboration. They give additional 2 N_{PDF} sets to determine the variation around the global minimum of the χ^2 distribution obtained from their fit, where N_{PDF} corresponds to the number of fitted parameters. Using the 90% C.L. error PDFs we obtain as an uncertainty

$$\Delta_{PDF} \sim 6\% \; (2.7\%) \quad \text{at } \sqrt{s} = 8 \; (100) \text{ TeV} \,. \tag{3.4}$$

There is additionally an uncertainty on α_s. The MSTW PDF set, however, allows to do a combined analysis on the PDF+α_s uncertainty, by providing PDF sets for the central value of α_s, and in addition for the maximal and minimal values of α_s of a 90% C.L. interval and two values of α_s half between the central value and those maximal and minimal values, with

$$\alpha_s^{NLO}(M_Z) = 0.12018^{+0.00317}_{-0.00386} \; (\text{at } 90\% \text{ C.L.}) \,. \tag{3.5}$$

I hence had to compute the cross section $2N_{PDF} + 1$ times for each of the five values of α_s. For each fixed value of α_s with a central PDF set S_0 and the N_{PDF} error sets

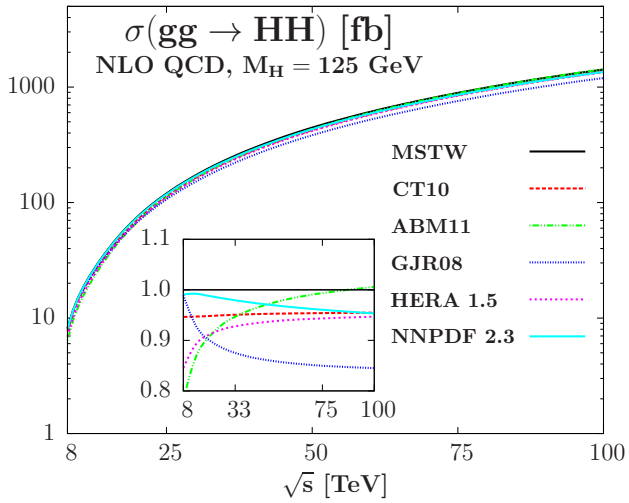

Figure 3.2.: The Higgs pair production via gluon fusion cross section as a function of the c.m. energy $\sqrt{s}$ for different PDF sets. In the insert the cross sections normalized to the MSTW prediction are shown. This figure is already published in Ref. [35].

$S_i^{\pm}$ the PDF error can be calculated with [122]

$$(\Delta\sigma^{\alpha_s}_{PDF})_+ = \sqrt{\sum_{i=1}^{N_{PDF}} \left\{\max\left[\sigma(\alpha_s, S_i^+) - \sigma(\alpha_s, S_0), \sigma(\alpha_s, S_i^-) - \sigma(\alpha_s, S_0), 0\right]\right\}^2} \tag{3.6}$$

$$(\Delta\sigma^{\alpha_s}_{PDF})_- = \sqrt{\sum_{i=1}^{N_{PDF}} \left\{\max\left[\sigma(\alpha_s, S_0) - \sigma(\alpha_s, S_i^+), \sigma(\alpha_s, S_0) - \sigma(\alpha_s, S_i^-), 0\right]\right\}^2} . \tag{3.7}$$

The combined PDF+α_s uncertainty can be obtained from [122]

$$(\Delta\sigma_{\alpha_s+PDF})_+ = \max_{\alpha_s}\left(\{\sigma(\alpha_s, S_0) + (\Delta\sigma^{\alpha_s}_{PDF})_+\}\right) - \sigma(\alpha_s^0, S_0) \tag{3.8}$$

$$(\Delta\sigma_{\alpha_s+PDF})_- = \sigma(\alpha_s^0, S_0) - \min_{\alpha_s}\left(\{\sigma(\alpha_s, S_0) - (\Delta\sigma^{\alpha_s}_{PDF})_-\}\right) . \tag{3.9}$$

Taking into account the combined PDF+α_s uncertainty, and not just the pure PDF uncertainty, leads to larger values

$$\Delta_{PDF+\alpha_s} \sim 8.5\%\ (6.2\%) \quad \text{at } \sqrt{s} = 8\ (100)\ \text{TeV} . \tag{3.10}$$

Note that the given PDF+α_s uncertainties are not large enough to explain the differences in the different prediction using different PDF sets. However, we only calculated the uncertainties from the MSTW PDF set. Possibly, taking into account the error bands from all PDF sets could show an overlap between them. By now, however, the results show that the uncertainty on the combined PDF+α_s error might underestimate the actual uncertainty which can also stem from the different parametrizations.

For the gluon fusion process there is an additional uncertainty, due to the use of the heavy quark mass approximation for the calculation of the higher order corrections. In this limit the loops of heavy quarks can be replaced by an effective ggH and $ggHH$

$\sqrt{s}$ [TeV]	$\sigma^{\text{NLO}}_{gg\to HH}$ [fb]	Scale [%]	PDF [%]	PDF+α_s [%]	EFT [%]	Total [%]
8	8.16	$+20.4\ -16.6$	$+5.8\ -6.0$	$+8.5\ -8.3$	± 10.0	$+41.5\ -33.3$
14	33.89	$+18.2\ -14.7$	$+3.9\ -4.0$	$+7.0\ -6.2$	± 10.0	$+37.2\ -29.8$
33	207.29	$+15.2\ -12.4$	$+2.5\ -2.7$	$+6.2\ -5.4$	± 10.0	$+33.0\ -26.7$
100	1417.83	$+12.2\ -9.9$	$+2.0\ -2.7$	$+6.2\ -5.7$	± 10.0	$+29.7\ -24.7$

Table 3.1.: The Higgs pair production cross section at NLO for the gluon fusion process (in fb) for different c.m. energies (in TeV) taken at the central scale $\mu_F = \mu_R = M_{HH}$, for $M_H = 125$ GeV. The theoretical uncertainties due to the various sources described in the text as well as the total theoretical uncertainty are listed. The results of this table are already published in Ref. [35].

vertex with the help of the LET [123–125]. This approximation, however, is valid for $\sqrt{\hat{s}} \ll m_t$, with $\sqrt{\hat{s}}$ being the partonic c.m. energy, and therefore works much better for single Higgs production, where $\sqrt{\hat{s}} = M_H$. For the double Higgs production, we have $2M_H \leq \sqrt{\hat{s}} \leq \sqrt{s}$. At LO the LET underestimates the total cross section for double Higgs production by $\mathcal{O}(20\%)$ at $\sqrt{s} = 16$ TeV [102]. For distributions it is even worse [92–95]. On the other hand, for NLO corrections the approximation should become better, if the LO cross section is taken into account with the full mass dependence, because the dominant corrections given by the real radiation of a gluon factorize into the LO cross section and a part independent of the masses of the heavy fermions in the loop. Based on the single Higgs production case we estimate the theoretical uncertainty due to the use of the effective vertex for the corrections to

$$\Delta^{EFT} \pm 10\% \,. \tag{3.11}$$

This estimate was recently confirmed by the calculation in Ref. [106], which estimated the finite mass effects by including in the calculation of the NLO cross section higher orders in $1/m_t$.

The various theoretical uncertainties then need to be combined. A quadratic addition of the uncertainties is quite optimistic [115] as it assumes that the uncertainties are uncorrelated. A linear addition is very conservative, so we follow Ref. [126], which calculates the scale uncertainty and then adds the PDF+α_s uncertainty calculated at the minimal and maximal cross sections with respect to the scale variation. The error from the use of the LET for the NLO QCD corrections is then added linearly.

For the gluon fusion process the total cross section and the corresponding theoretical uncertainties can be found in Table 3.1 for collider energies of $\sqrt{s} = 8$, 14, 33 and 100 TeV. It can be inferred from the table that the theoretical uncertainty is quite high (up to ~ 40 % for $\sqrt{s} = 8$ TeV), but decreases a bit with the c.m. energy.

3.2. Higgs pair production via vector boson fusion

Double Higgs production via VBF is the process with the second largest cross section. For the single Higgs production case, its interesting kinematics of two high invariant

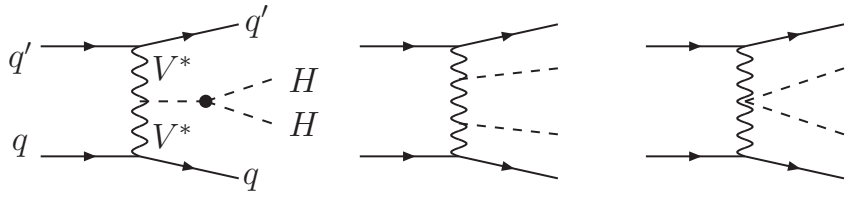

Figure 3.3.: Feynman diagrams for the Higgs pair production process via vector boson fusion, $qq' \to HHqq'$, at LO.

mass tagging jets with larger rapidity gap and a centrally produced Higgs boson make it a very sensitive channel and therefore worthwhile to study it also for the double Higgs production case. We, therefore, determined the NLO QCD corrections for this process and investigated its theoretical uncertainties. The Feynman diagrams for the process at LO can be found in Fig. 3.3.

3.2.1. Higher order corrections

The calculation of higher order QCD corrections for the VBF channel are simplified by the fact that all interference diagrams with a gluon exchange between the two fermion lines disappear due to the colour singlet nature of the exchanged gauge bosons at LO. The NLO QCD corrections then consist only of the known corrections in the structure function approach [127–129]. In the framework of this project, the matrix elements for this process were implemented in the code `VBFNLO` [130, 131], such that the generic QCD corrections for VBF processes can be applied to the double Higgs production case. We found the QCD corrections to be of $\mathcal{O}(7\%)$, by using

$$\mu_0 = \mu_R = \mu_F = Q_{V^*} \,,$$

where Q_{V^*} denotes the momentum of the intermediate vector boson ($V^* = W^*, Z^*$). Note that a cut on $Q_{V^*} \geq 2$ GeV has to be applied, as the PDFs are only available for higher scale values. More details on the higher order corrections can be found in Ref. [35]. The result is in agreement with a previous calculation in Ref. [132] in the context of the two Higgs doublet model. In a recent work [133], the NNLO QCD corrections were calculated but turned out to be quite small. They will not be included in the following discussion on the theoretical uncertainties.

3.2.2. Theoretical uncertainties

In order to determine the theoretical uncertainties we proceeded here very similar to what was done for the gluon fusion production channel. It will therefore be discussed only very briefly. In order to obtain the scale uncertainty we explored the range

$$\frac{\mu_0}{2} \leq \mu_R, \mu_F \leq 2\mu_0 \,, \tag{3.12}$$

using $\frac{1}{2} \leq \mu_R/\mu_F \leq 2$ after checking that this restriction does not modify the result. The scale uncertainty for this process is quite small $\sim \pm 2\%$ at 8 TeV and even smaller

$\sqrt{s}$ [TeV]	$\sigma^{NLO}_{qq'HH}$ [fb]	Scale [%]		PDF [%]		PDF+α_s [%]		Total [%]	
8	0.49	+2.3	−2.0	+5.2	−4.4	+6.7	−4.4	+9.0	−6.4
14	2.01	+1.7	−1.1	+4.6	−4.1	+5.9	−4.1	+7.6	−5.1
33	12.05	+0.9	−0.5	+4.0	−3.7	+5.2	−3.7	+6.1	−4.2
100	79.55	+1.0	−0.9	+3.5	−3.2	+5.2	−3.2	+6.2	−4.1

Table 3.2.: The total Higgs pair production cross section at NLO for the vector boson fusion process at the LHC for different c.m. energies at a central scale $\mu_F = \mu_R = Q_{V^*}$ for $M_H = 125$ GeV. Additionally, the theoretical uncertainties of various sources and the total theoretical uncertainty are given. The results of this table are already published in Ref. [35].

at higher energies. Note that the NLO QCD corrections decrease the theoretical uncertainties due to higher order corrections considerably. At LO the scale uncertainty is still $\sim 8\%$ at 8 TeV.

The PDF+α_s uncertainty dominates the theoretical error with +7%/-4% for $\sqrt{s} = 8$ TeV and +5%/-3% at $\sqrt{s} = 100$ TeV. For this process we add up the PDF+α_s and the scale uncertainty linearly, justified by the fact that the scale uncertainty is very small. This thus leads to the same result as the procedure described for the gluon fusion process.

In Table 3.2 the cross section at NLO QCD for different c.m. energies with the corresponding theoretical uncertainties can be found. The total theoretical uncertainty is much lower than for the gluon fusion production mode, maximally amounting to 9%.

3.3. Double Higgs-strahlung

At LO the Higgs-strahlung process has been calculated a long time ago in Ref. [134]. The two Higgs bosons can be radiated from either a Z boson or a W boson. At LO the radiation off a W boson dominates [39, 40] over the corresponding process with a Z boson. As a central scale for this process we chose ($V = W, Z$)

$$\mu_0 = \mu_R = \mu_F = M_{VHH}\,, \tag{3.13}$$

where M_{VHH} denotes the invariant mass of the vector boson and two Higgs final state. The Feynman diagrams for the process at LO can be found in Fig. 3.4.

3.3.1. Higher order corrections

For double Higgs-strahlung off vector bosons $q\bar{q} \to V^* \to VHH$ the NLO QCD corrections can be inferred from the long known correction to the Drell-Yan process

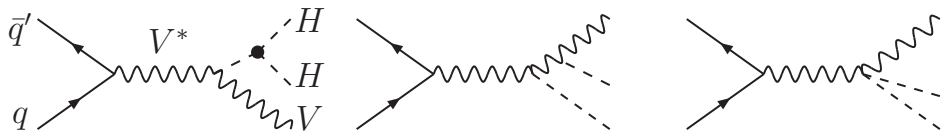

Figure 3.4.: Feynman diagrams for the Higgs pair production via Higgs-strahlung off a vector boson, $q\bar{q} \to VHH$ ($V = W, Z$), at LO.

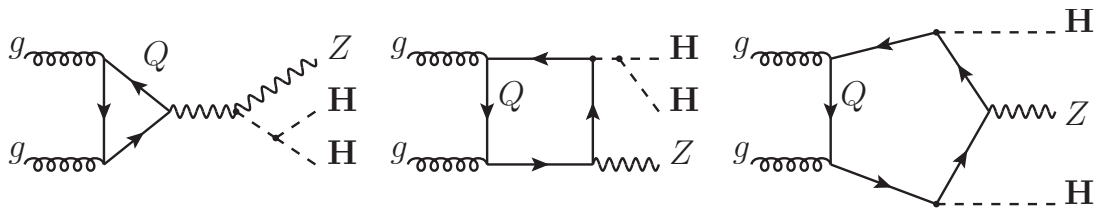

Figure 3.5.: Generic Feynman diagrams for the process $gg \to ZHH$, which are part of the NNLO QCD corrections for the process $pp \to ZHH$.

$q\bar{q} \to V$ [135–137], as the process can be viewed as the Drell-Yan production $q\bar{q} \to V^*$ followed by the splitting $V^* \to VHH$ with an off-shell vector boson with squared momentum k^2 and $(2M_H + M_V)^2 \leq k^2 \leq \hat{s}$. The NNLO QCD corrections consist of the known Drell-Yan NNLO QCD corrections [138–140]. For double Higgs-strahlung off a Z boson, there is an additional contribution from gluon-initiated one-loop diagrams (see Refs. [140–142] for single-Higgs radiation), which are of the same order as the NNLO QCD corrections.[1] For the double Higgs-strahlung process, this means that the contributions from $gg \to ZHH$ stemming from triangle, box and pentagon diagrams need to be included. The Feynman diagrams can be found in Fig. 3.5. The process is mediated by heavy quark loops. For the box and pentagon diagrams this is due to the Higgs coupling to the fermion loop: Since the Higgs coupling to fermions is proportional to their mass, light quark loops are negligible. For the triangle diagram, the reason is that the contribution of the quarks of one $SU(2)_L$ doublet cancels if the masses of the quarks in the doublet are degenerate, meaning that for the light quarks this contribution is negligible as their masses are nearly degenerate. For the calculation of this process I used `FeynArts/FormCalc/LoopTools` [147–150]. The results were cross-checked in a second independent calculation.

The $gg \to ZHH$ contribution is of $\mathcal{O}(20 - 30\%)$ depending on the c.m. energy. Note that this contribution is much more important than in the single Higgs production case where $gg \to ZH$ only contributes with less than 5%. The reason is, that, in addition, we have the contribution from the pentagon diagram which involves two top Yukawa couplings. Also the destructive interference of the triangle and box diagram in the case of single Higgs production is softened.

[1] Note that in Ref. [143–146] it was shown that additional contributions to the NNLO QCD corrections via an effective ggZ vertex with the initial states qg or $q\bar{q}$ are negligably small.

$\sqrt{s}$ [TeV]	$\sigma_{WHH}^{\text{NNLO}}$ [fb]	Scale [%]		PDF [%]		PDF+α_s [%]		Total [%]	
8	0.21	+0.4	−0.5	+4.3	−3.4	+4.3	−3.4	+4.7	−4.0
14	0.57	+0.1	−0.3	+3.6	−2.9	+3.6	−3.0	+3.7	−3.3
33	1.99	+0.1	−0.1	+2.9	−2.5	+3.4	−3.0	+3.5	−3.1
100	8.00	+0.3	−0.3	+2.7	−2.7	+3.8	−3.4	+4.2	−3.7

Table 3.3.: The total Higgs pair production cross sections at NNLO QCD for the $q\bar{q}' \to WHH$ process at the LHC for different c.m. energies at the central scale $\mu_F = \mu_R = M_{WHH}$ for $M_H = 125$ GeV. Additionally, the theoretical uncertainties of various sources and the total theoretical uncertainty are given. The results of this table are already published in Ref. [35].

In total, we obtain as K-factors for $\sqrt{s} = 14$ TeV

$$K = \frac{\sigma_{NNLO}}{\sigma_{LO}} = 1.32(1.52) \qquad \text{for } WHH \ (ZHH)\,, \tag{3.14}$$

for which we have set $\alpha_s^{NNLO}(M_Z) = 0.11707$. In our calculation we have included the full CKM matrix elements in the quark luminosities and initial state bottom quark contributions.

3.3.2. Theoretical uncertainties

For the theoretical uncertainties on the Higgs-strahlung process I proceeded in the same way as was done for the VBF production mode. The scale was varied within the range $\mu_0/2 \leq \mu_R = \mu_F \leq 2\mu_0$. The uncertainty due to missing higher order corrections, which is deduced from the scale variation, for the WHH process turns out to be very small, less than 1%. For the ZHH process the scale uncertainty is, however, higher because of the additional contribution of the gluon induced diagrams at NNLO. For this subchannel these are the LO contributions, which means that they still show a large scale uncertainty. Since they are, however, part of the NNLO corrections the scale uncertainty for the ZHH production process is still below $\sim 5\%$.

The combined PDF+α_s uncertainty is for both processes roughly between 3-4%. This, in the end, adds up to a theoretical uncertainty of less then 5% for the WHH production channel and of less then 9% for ZHH. More details can be found in Table 3.3 for WHH production and in Table 3.4 for ZHH production.

3.4. Cross sections and sensitivity on the triple Higgs coupling at the LHC

With the higher order corrections of the last section at hand, we can now compare the cross sections of the different production modes. Additionally to the already discussed

$\sqrt{s}$ [TeV]	$\sigma_{ZHH}^{\text{NNLO}}$ [fb]	Scale [%]		PDF [%]		PDF+α_s [%]		Total [%]	
8	0.14	$+3.0$	-2.2	$+3.8$	-3.0	$+3.8$	-3.0	$+6.8$	-5.3
14	0.42	$+4.0$	-2.9	$+2.8$	-2.3	$+3.0$	-2.6	$+7.0$	-5.5
33	1.68	$+5.1$	-4.1	$+1.9$	-1.5	$+2.7$	-2.6	$+7.9$	-6.7
100	8.27	$+5.2$	-4.7	$+1.9$	-2.1	$+3.2$	-3.2	$+8.4$	-8.0

Table 3.4.: Same as Table 3.3 for ZHH production using the central scale $\mu_F = \mu_R = M_{ZHH}$. The results of this table are already published in Ref. [35].

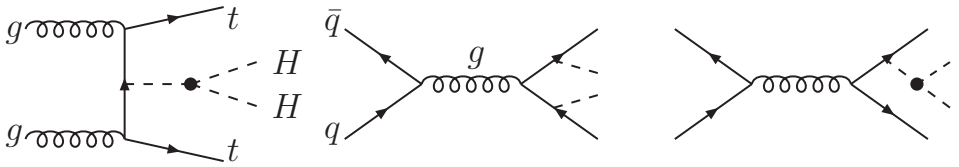

Figure 3.6.: Example Feynman diagrams for the process $pp \to t\bar{t}HH$.

processes of gluon fusion, vector boson fusion and Higgs-strahlung off W or Z bosons, we calculated the associated production of a Higgs boson pair with a top quark pair at LO with the help of `Madgraph/MadEvent`[151, 152]. I provided a cross-check for this calculation. Only the diagrams involving strong interactions need to be included for the process. The inclusion of the electroweak contributions barely changes the result. Generic Feynman diagrams for the $pp \to t\bar{t}HH$ process can be found in Fig. 3.6. For the scale of the process we used $\mu_0 = m_t + \frac{1}{2}M_{HH}$. The final results for the cross sections can be found in Fig. 3.7, which shows in red the gluon fusion cross section at NLO QCD, in green the VBF cross section at NLO QCD, in blue the WHH and ZHH cross sections at NNLO and in violet the $t\bar{t}HH$ cross section at LO. The cross sections are roughly three order of magnitudes smaller than the corresponding single Higgs production processes. The gluon fusion production mode dominates over the others by at least one order of magnitude. Note that the $t\bar{t}HH$ process has a larger cross section in Fig. 3.7 than the WHH and ZHH production modes in contrast to the single Higgs production case. In Ref. [153], where this process was investigated, the hierarchy was found to be inverse. We checked, however, that the process is very sensitive to the scale choice and has therewith large uncertainties on the cross section. Another scale choice can invert the order of the two processes and can therefore reconcile our result with the one in Ref. [153]. The issue about the best scale choice for this process can only be solved by including higher order corrections. In Ref. [107] the NLO QCD corrections were recently calculated. Even though the scale choice differs from ours, the results are in good agreement.

In order to investigate the sensitivity on the triple Higgs coupling λ_{HHH}, we rescale it in terms of the SM triple Higgs coupling, $\lambda_{HHH}^{SM} = 3M_H^2/v$, for the gluon fusion, VBF and Higgs-strahlungs production channels to obtain the maximal possible sensitivity, similar to what has been done in Refs. [38, 39]. This does not give any information on New Physics models, as in most New Physics models, not only the triple Higgs

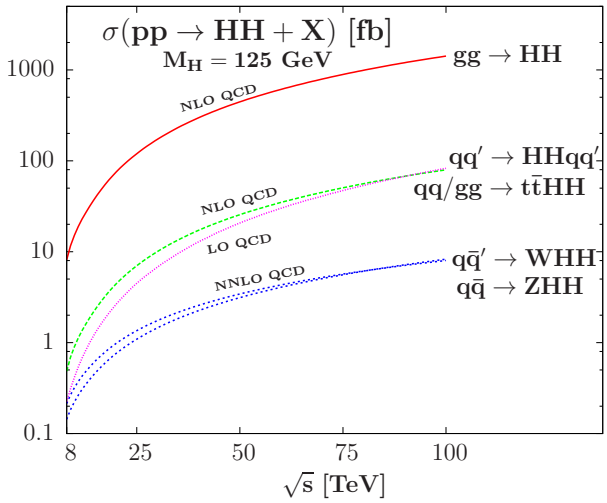

Figure 3.7.: The cross sections as functions of the c.m. energy for the gluon fusion process (red/full) at NLO QCD, VBF (green/dashed) at NLO QCD, WHH and ZHH (blue/dotted) at NNLO QCD and $t\bar{t}HH$ (violet/small dotted) at LO QCD. This plot is already published in Ref. [35].

coupling is modified but there might also be some other important contributions to the process from *e.g.* dimension six operators or new particles running in the loop. It merely tests how well a certain production process needs to be known to extract the SM triple Higgs coupling with a certain accuracy. Figure 3.8 shows the sensitivity on the SM triple Higgs coupling for the c.m. energies $\sqrt{s} = 8$, 14, 33 TeV. The left plots in Fig. 3.8 show the total cross section as a function of the variation of the triple Higgs coupling $\kappa = \lambda_{HHH}/\lambda^{SM}_{HHH}$, the right plots are normalized to the value of the cross section at $\kappa = 1$ corresponding to the SM result. As can be inferred from the plots, the VBF production channel is the most sensitive one, followed by gluon fusion. The minimal cross section for production in the VBF channel is obtained for $\kappa \approx 2$, for gluon fusion at $\kappa \approx 3$ and for WHH and ZHH production at $\kappa \approx -1$. The sensitivity on the triple Higgs coupling decreases with the energy for all the shown processes as the diagram involving the triple Higgs coupling is generally suppressed by the Higgs boson propagator with the partonic c.m. energy $\sqrt{\hat{s}}$.

3.5. Prospects of measuring Higgs pair production at the LHC

The prospects of measuring the Higgs pair production process at the LHC are investigated in the following in a parton level analysis. As the cross sections are very small, we will concentrate on the main production channel gluon fusion. In order to keep the signal from becoming too small, one of the Higgs bosons should at least decay via the dominant decay mode: $H \to b\bar{b}$. For the decays of the second Higgs boson, a first possibility would be to also consider the second Higgs boson decaying into $b\bar{b}$, but this final state is overwhelmed by the large $4b$ QCD background [94]. We, therefore, consider the

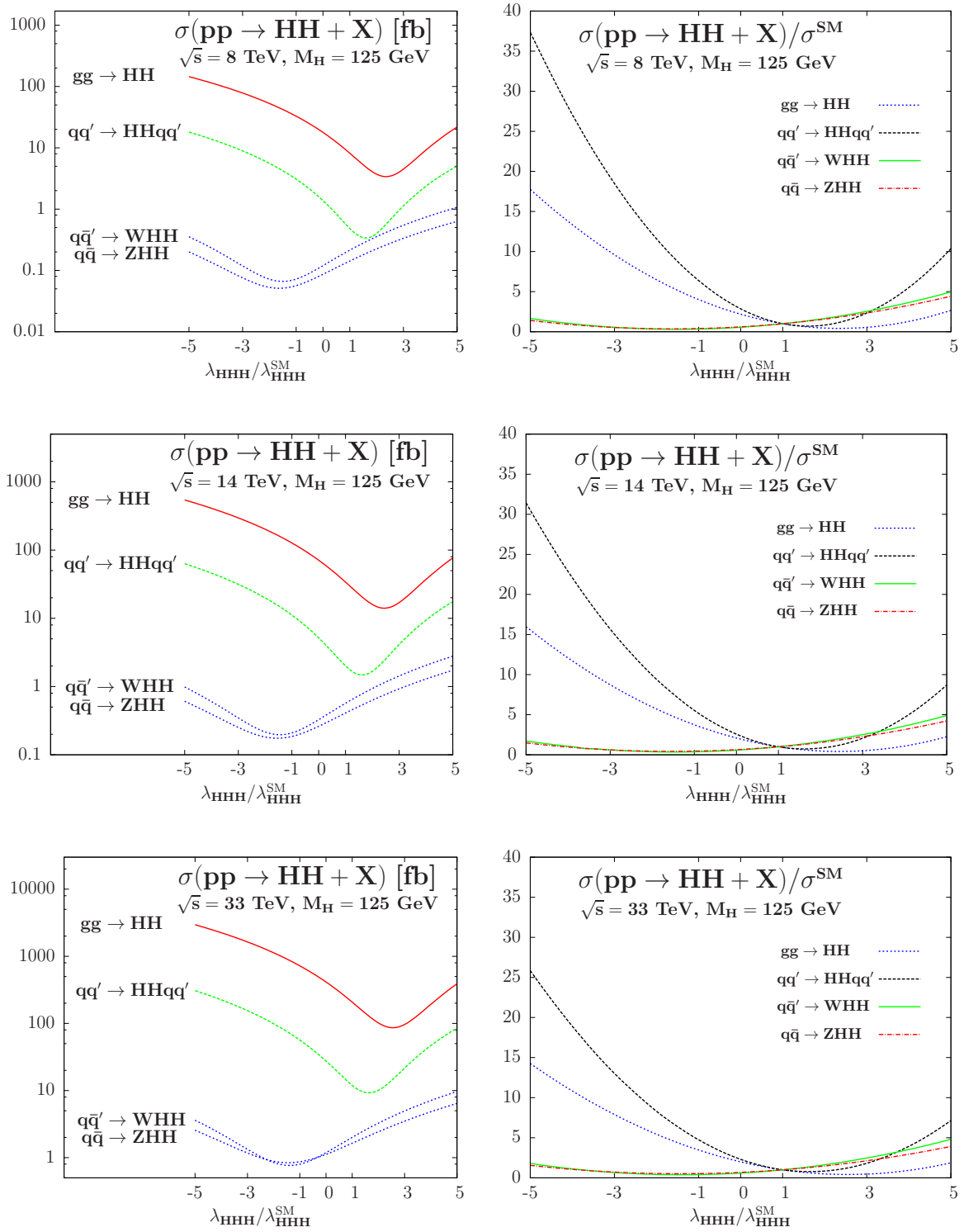

Figure 3.8.: The sensitivity on the triple Higgs coupling for the gluon fusion process, the VBF process and WHH and ZHH production for the c.m. energies $\sqrt{s} = 8$ TeV (upper plots), 14 TeV(plots in the middle), 33 TeV (lowest plots). The plots on the left show the total cross section as a function of the variation of the triple Higgs coupling, the plot on the right are normalized to the prediction for no variation of the SM triple Higgs coupling ($\lambda_{HHH}/\lambda^{SM}_{HHH}$). These plots are already published in Ref. [35].

final states $b\bar{b}\tau\bar{\tau}$, $b\bar{b}\gamma\gamma$ and $b\bar{b}W^*W^*$ with the off-shell W bosons decaying leptonically. Following the recommendations of the LHC Higgs cross section working group [115], we use for the branching ratios of the 125 GeV SM Higgs boson, $BR(H \to b\bar{b}) = 0.577$, $BR(H \to \tau\bar{\tau}) = 0.0612$, $BR(H \to W^*W^*) = 0.215$ and $BR(H \to \gamma\gamma) = 0.00228$. The general approach will be exemplified for the $b\bar{b}\gamma\gamma$ final state, whereas the results of the other final states will be only summarized shortly. More details can be found in Ref. [35].

For the calculation of the signal, the LO matrix element of `HPAIR` [110] was implemented into `Pythia 6` [154]. The NLO QCD corrections were taken into account via a K-factor of $K = 1.88$ [115]. The background processes were calculated with `Madgraph 5` [152]. Again, higher order corrections were taken into account with multiplicative K-factors. For the evaluation of the cross sections the MSTW2008 PDF set was used as before. As c.m. energy we use throughout this section $\sqrt{s} = 14$ TeV.

3.5.1. The $b\bar{b}\gamma\gamma$ final state

In this subsection the results of the $b\bar{b}\gamma\gamma$ final state study of Ref. [35, 155] are summarized. More studies for this final state can be found in Refs. [95, 99, 100]. Background processes for this final state are the QCD continuum processes $b\bar{b}\gamma\gamma$ and the production of a Higgs boson in association with a $t\bar{t}$ pair with the Higgs boson decaying into photons and the top quarks into W bosons and bottom quarks. Another background stems from the associate production of a single Higgs boson with a Z boson with the Higgs boson decaying to $\gamma\gamma$ and the Z boson to $b\bar{b}$. For the QCD continuum process no higher order corrections are taken into account, whereas for $t\bar{t}H$ production a K-factor of 1.1 was used and for ZH production a NNLO K-factor of 1.33. The K-factors were taken from Ref. [115]. First, some basic selection cuts were applied, namely:

- Cuts on the p_T of the leptons $p_{T,\ell} > 20$ GeV and on the pseudorapidity $|\eta_\ell| < 2.4$, on the p_T of the jets $p_{T,jets} > 20$ GeV and their pseudorapidity $|\eta_{jet}| < 2.4$ to reduce the $t\bar{t}H$ background;
- $p_{T,b} > 30$ GeV, $|\eta_b| < 2.4$, and $\Delta R(b,b) > 0.4$ (with ΔR being the distance of the two b quarks in the pseudorapidity and azimuthal plane, $\Delta R = \sqrt{(\Delta\eta)^2 + (\Delta\phi)^2}$) for the b-quark;
- $p_{T,\gamma} > 30$ GeV, $|\eta_\gamma| < 2.4$ and $\Delta R(\gamma,\gamma) > 0.4$ for the photons;
- the reconstruction of the Higgs mass in the windows 112.5 GeV $< M_{b\bar{b}} <$ 137.5 GeV and 120 GeV $< M_{\gamma\gamma} <$ 130 GeV;
- $\Delta R(\gamma, b) > 0.4$;

and we require exactly one bottom quark pair and one photon pair. We assume a b-tagging efficiency of 70%. Based on the boosted Higgs boson topology one can apply further cuts to reduce the background. As can be inferred from Fig. 3.9 (right) a cut on the invariant mass M_{HH} of the Higgs boson pair can reduce the background as the signal itself peaks at higher values of M_{HH}, so we applied $M_{HH} > 350$ GeV. In the left plot of Fig. 3.9 it can be seen that a cut on the $p_{T,H} > 100$ GeV can further remove background

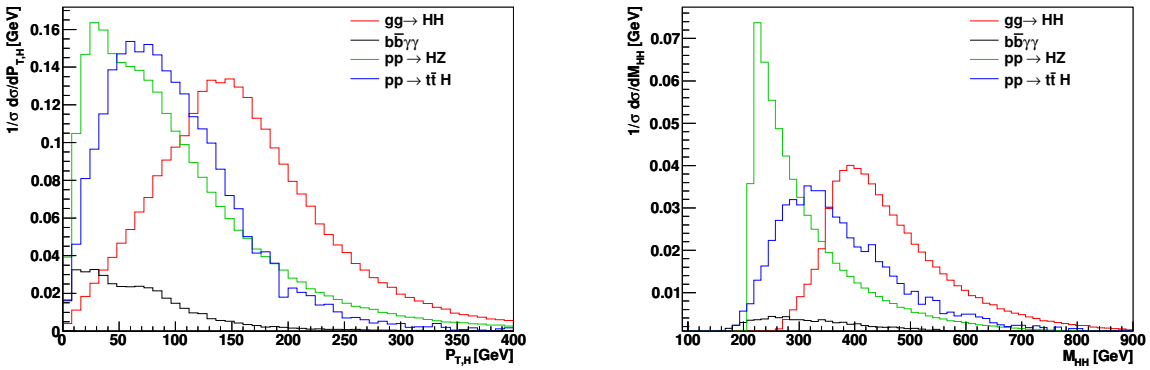

Figure 3.9.: Normalized differential cross sections of signal (in red) and background processes with respect to the transverse momentum of one Higgs boson, $p_{T,H}$, (left plot) or the invariant mass M_{HH} (right plot). These plots are already published in Ref. [35].

	HH	$b\bar{b}\gamma\gamma$	$t\bar{t}\gamma\gamma$	ZH	S/B	$S/\sqrt{B}$
σ_{NLO} [fb]	$8.92 \cdot 10^{-2}$	$5.05 \cdot 10^{3}$	1.39	$3.33 \cdot 10^{-1}$	$1.77 \cdot 10^{-5}$	$6.87 \cdot 10^{-2}$
M_H from b's	$4.37 \cdot 10^{-2}$	$4.01 \cdot 10^{2}$	$8.70 \cdot 10^{-2}$	$1.24 \cdot 10^{-3}$	$1.09 \cdot 10^{-4}$	$1.20 \cdot 10^{-1}$
M_H from γ's	$3.05 \cdot 10^{-2}$	1.78	$2.48 \cdot 10^{-2}$	$3.73 \cdot 10^{-4}$	$1.69 \cdot 10^{-2}$	1.24
Cut on M_{HH}	$2.73 \cdot 10^{-2}$	$3.74 \cdot 10^{-2}$	$7.45 \cdot 10^{-3}$	$1.28 \cdot 10^{-4}$	$6.07 \cdot 10^{-1}$	7.05
Cut on $p_{T,H}$	$2.33 \cdot 10^{-2}$	$3.74 \cdot 10^{-2}$	$5.33 \cdot 10^{-3}$	$1.18 \cdot 10^{-4}$	$5.44 \cdot 10^{-1}$	6.17
Cut on $\lvert\eta_H\rvert$	$2.04 \cdot 10^{-2}$	$1.87 \cdot 10^{-2}$	$3.72 \cdot 10^{-3}$	$9.02 \cdot 10^{-5}$	$9.06 \cdot 10^{-1}$	7.45
Cut on $\Delta R(b,b)$	$1.71 \cdot 10^{-2}$	0.00	$3.21 \cdot 10^{-3}$	$7.44 \cdot 10^{-5}$	5.21	16.34

Table 3.5.: Cross sections of the signal and the various backgrounds for $\sqrt{s} = 14$ TeV for the different cuts as described in the text, the signal to background ratio S/B and the significance $S/\sqrt{B}$ for $\int \mathcal{L} = 3000$ fb^{-1} in the $b\bar{b}\gamma\gamma$ channel. This table is already published in Ref. [35].

events without cutting away too many signal events. In addition, we applied a cut on the pseudorapidity of the Higgs bosons of $|\eta_H| < 2$ and the isolation of the two b quark jets to be $\Delta R(b,b) < 2.5$. The latter in particular significantly reduces the $b\bar{b}\gamma\gamma$ continuum background, since this background does not show a boosted topology. The cross sections for the various cuts for signal and background processes as well as the signal over background ratio S/B and the significance $S/\sqrt{B}$ are summarized in Table 3.5. As final significance 16.34 is obtained for an integrated luminosity of $\int \mathcal{L} = 3000$ fb^{-1}, corresponding to 51 signal events. The channel therefore seems promising. A more detailed analysis including fake rates and a detector simulation, however, needs to be performed by the experimental collaborations in order to give a more realistic picture.[2]

[2] A rough detector simulation has been included in Ref. [35]. The significance was reduced to $S/\sqrt{B} = 6.46$.

3.5.2. The $b\bar{b}\tau\bar{\tau}$ and $b\bar{b}W^+W^-$ final states

The $b\bar{b}\tau\bar{\tau}$ final state as been studied in Refs. [35, 94, 96]. We consider for the analysis background processes from the QCD-QED continuum processes $b\bar{b}\tau\bar{\tau}$ and $b\bar{b}\tau\bar{\nu}_\tau\bar{\tau}\nu_\tau$ with the latter stemming mostly from the pair-production of top quarks with subsequent decay of the top quarks to $t \to bW^+ \to b\bar{\tau}\nu_\tau$. Additionally, there is a background of the associate production of a single Higgs boson with a Z boson, similar to the $b\bar{b}\gamma\gamma$ final state. We applied the following basic acceptance cuts, assuming a b-tagging efficiency of 70% and a τ-tagging efficiency of 50% [156, 157]

- $p_{T,b} > 30$ GeV and $|\eta_b| < 2.4$ for the b-quark;
- $p_{T,\tau} > 30$ GeV and $|\eta_\tau| < 2.4$ for the τ-lepton pair;
- the reconstruction of the Higgs mass in the windows 112.5 GeV $< M_{b\bar{b}} <$ 137.5 GeV and 100 GeV $< M_{\tau\tau} <$ 150 GeV.

In addition, similar to the $b\bar{b}\gamma\gamma$ final state we applied cuts on the invariant mass of the Higgs boson pair of $M_{HH} > 350$ GeV and we restricted $p_{T,H} > 100$ GeV. This leads to a significance $S/\sqrt{B} = 6.71$ for $\int \mathcal{L} = 3000$ fb^{-1}, corresponding to 330 signal events. It therefore seems promising, but depends strongly on how well the Higgs boson mass can be reconstructed from the bottom quark pair and the τ-leptons. More details on the analysis can be found in Ref. [35].

The $b\bar{b}W^+W^-$ final state has been studied in Refs. [35, 96, 97]. We consider only the leptonic W boson decays $W \to \ell\nu_\ell$ ($\ell = e, \mu$) with a branching ratio of 10.8% for $\ell = e$ or μ. This channel, however, is quite difficult because, due to the missing energy of the W decays, the mass of the Higgs boson decaying into W bosons cannot be reconstructed. It, therefore, does not allow for such a significant background reduction as for the previously discussed final states $b\bar{b}\gamma\gamma$ and $b\bar{b}\tau\bar{\tau}$. In the end, after taking into account all the $b\bar{b}\ell_1\nu_{\ell_1}\ell_2\nu_{\ell_2}$ continuum background processes and applying cuts on transverse momenta and pseudorapidities of the leptons and b-quarks, assuming a Higgs boson mass reconstruction of the bottom quark pair as in the previous channels and applying some more advanced cuts on the missing transverse energy and the transverse mass of the leptons, the significance and the background to signal ratio is still quite small. Therefore, this channel is not very promising. Note, that in Ref. [97] it was pointed out, that semi-leptonic decays of the W boson pair might show more encouraging prospects. A more detailed discussion on the leptonic decays of the W boson pair for the $b\bar{b}W^+W^-$ final state can be found in Ref. [35].

3.6. Summary

In this chapter, the prospects of measuring the triple Higgs coupling have been discussed, based on Ref. [35]. The triple Higgs coupling can be measured in Higgs pair production processes. The most important one is Higgs pair production via gluon fusion followed by VBF, associated production with a top quark pair and Higgs-strahlung off a vector boson. In the framework of this thesis and Ref. [35], higher order corrections

to gluon fusion, VBF and Higgs-strahlung were included. For VBF, the matrix element had to be implemented into `VBFNLO` to obtain the NLO QCD corrections. For Higgs-strahlung off vector bosons the NLO and NNLO QCD corrections were taken over from the Drell-Yan process. In addition, in this thesis we calculated gluon-induced double Higgs-strahlung off a Z boson, which is of the same order in the perturbative expansion as the NNLO QCD corrections. This calculation involves one-loop two-to-three diagrams. The theoretical uncertainties for gluon fusion, VBF and Higgs-strahlung have been determined. For gluon fusion they are quite high, whereas for VBF and Higgs-strahlung they are below 10%. Within the SM, we studied how sensitive the different processes are to the triple Higgs coupling.

The last part of this chapter shortly summarized the prospects of measuring the gluon fusion process at the LHC at $\sqrt{s} = 14$ TeV, discussed in Ref. [35], to get access to the triple Higgs coupling. The final states $b\bar{b}\gamma\gamma$ and $b\bar{b}\tau\bar{\tau}$ seem promising, whereas $b\bar{b}W^+W^-$ with leptonic W decays does not.

Part II.

Supersymmetry

CHAPTER 4

Supersymmetric extensions of the Standard Model

In 1967, Coleman and Mandula published a no-go-theorem [158] which states that all possible symmetries of an interacting quantum field theory are restricted to the Poincaré algebra and internal symmetry generators commuting with the Poincaré group. The restrictions of the Coleman-Mandula theorem are evaded in supersymmetry (SUSY) by allowing for Fermi-type generators, which act as anticommutating spinors. Haag, Lopuszanski and Sohnius showed in 1974 [159] that the SUSY algebra as a generalization of the Lie algebra, is indeed the only graded Lie-algebra [160] (*i.e.* an algebra with anticommutators and spinor generators) of symmetries of the S matrix consistent with an interacting quantum field theory. This in itself provides a motivation for SUSY as the maximal possible symmetry.

In SUSY, single-particle states are included in irreducible representations of the superalgebra. These representations contain both fermionic and bosonic degrees of freedom. Supersymmetric transformations convert fermions into bosons and *vice versa*. The SUSY generators commute with gauge transformations, which make the bosons and the fermions in one supersymmetric multiplet identical in quantum numbers and mass.

In addition to symmetry considerations, SUSY is motivated by the fact that many shortcomings of the SM can be solved. For instance, one of the main motivations for low-energy SUSY is, that the quadratic dependence of the Higgs boson mass on the cut-off is cured. In a supersymmetric theory, bosonic loops exactly cancel all fermionic loop contributions in the Higgs boson mass. In contrast to the prediction of degenerate masses for the members of one supermultiplet, none of the superpartners have been observed yet. Hence, SUSY must be broken. If SUSY is broken softly, meaning that no SUSY breaking operators of dimension four or higher are added in the SUSY breaking part, the Higgs mass corrections are only logarithmically divergent, and not quadratically as in the SM. The Higgs boson mass becomes then technically natural, see Section 2.2. A moderate amount of fine-tuning will, however, be introduced due to

the current bounds from direct searches for SUSY particles. In order to break SUSY, the Lagrangian has to be extended by terms parameterizing this breaking. The coefficients of the soft-SUSY breaking operators in the Lagrangian are in general treated as unknown parameters. This means, that many new parameters are introduced into the theory. The number of parameters can be reduced by assumptions on the SUSY breaking mechanism. In viable SUSY breaking models an additional 'hidden' sector is needed, from which the SUSY breaking is communicated by messenger particles to the visible sector. Candidates for messenger particles are *e.g.* heavy chiral supermultiplets charged under the SM gauge groups in gauge mediated SUSY breaking models, or in gravity mediated SUSY breaking models, SUSY breaking is communicated by gravitational interactions.

In supersymmetric extensions of the SM new renormalizable operators can arise leading to proton decay, which has not been observed so far. Such operators can be forbidden if a discrete symmetry, called R-parity, is introduced. Superpartners get different charges under R-parity. If R-parity is indeed perserved, the lightest SUSY particle (LSP) is stable. In case the LSP is uncharged and colourless, it provides a natural candidate for Dark Matter. Additional benefits of SUSY are the successful unification of the gauge couplings and a dynamical mechanism for electroweak symmetry breaking. In most SUSY models, the sign of the Higgs boson mass squared parameter is driven to negative values by renormalization group running, whereas the signs of the other mass parameters stay positive.

4.1. The SUSY algebra

Supersymmetric transformations are generated by an operator Q through

$$Q_a^i|\text{boson}>=|\text{fermion}>, \quad Q_a^i|\text{fermion}>=|\text{boson}> . \tag{4.1}$$

The exact type of fermions and bosons related to each other as well as the number of generators Q with the supercharge index $i = 1, ..., N$ depend on the specific framework. The generators Q are complex, anticommuting spinors, transforming under the Lorentz group as $(\frac{1}{2}, 0)$, their conjugate $Q^\dagger$ transforms as $(0, \frac{1}{2})$. The spinor indices a can take the values $a = 1, 2$. In the following, we will consider only $N = 1$ SUSY, corresponding to one generator Q and its complex hermitian conjugate $Q^\dagger$. The SUSY algebra is an extension of the Poincaré algebra with the additional anticommutator and commutator relations

$$\{Q_a, Q_b^\dagger\} = 2\sigma_{ab}^\mu P_\mu \tag{4.2}$$

$$\{Q_a, Q_b\} = \{Q_a^\dagger, Q_b^\dagger\} = 0 \tag{4.3}$$

$$[Q_a, P^\mu] = [Q_a^\dagger, P^\mu] = 0 \tag{4.4}$$

$$[M^{\mu\nu}, Q_a] = -(\sigma^{\mu\nu})_{ab} Q^b , \tag{4.5}$$

with $\sigma^\mu = (1, \sigma^i)$, $\bar{\sigma}^\mu = (1, -\sigma^i)$ and $\sigma^{\mu\nu} = i(\sigma^\mu\bar{\sigma}^\nu - \bar{\sigma}^\nu\sigma^\mu)/4$ and σ^i the Pauli spin matrices ($i = 1, 2, 3$). The operator P^μ is the four momentum acting as generator for

space-time translations of the Poincaré algebra and $M^{\mu\nu}$ represents the six Lorentz generators [161].

Single-particle states transform under irreducible representations of the super-algebra, so-called supermultiplets. They contain both bosonic and fermionic degrees of freedom. According to Eq. (4.4), P^2 commutes with Q and $Q^\dagger$ so that all particles of the same multiplet must have the same mass. Different masses can only be obtained by SUSY breaking. The same quantum numbers under the SM gauge group arise for all degrees of freedom of one supermultiplet, due to the commutation of the SM gauge group with Q and $Q^\dagger$.

Supermultiplets can be assembled in superfields, which live in superspace. The superspace has, in addition to the usual spacetime coordinates, anticommuting coordinates, which can be expressed in terms of Grassmann spinors θ and $\bar{\theta}$. The superspace coordinate y^μ is then defined as

$$y^\mu = x^\mu - i\theta\sigma^\mu\bar{\theta}\,, \tag{4.6}$$

with the usual bosonic space-time coordinate x^μ. This formalism was introduced for $N = 1$ SUSY in Ref. [162].

For $N = 1$ SUSY, there are two possible SUSY representations under the additional assumption of renormalizability of the resulting Lagrangian, namely chiral supermultiplets and vector supermultiplets. A chiral supermultiplet contains a Weyl spinor and a complex scalar field. A vector supermultiplet can be reduced in the Wess-Zumino gauge [163] to a massless spin-1 field and a massless Weyl spinor.[1] A mass for the gauge boson can be obtained by EWSB. The fermionic superpartner of the gauge field is a Majorana fermion, as gauge bosons transform in the adjoint representation, which is a real representation, of the corresponding gauge groups.

A supersymmetric Lagrangian for interacting chiral superfields is given by

$$\mathcal{L} = \int d^4\theta\, K(\Phi, \Phi^\dagger) + \left[\int d^2\theta\, W(\Phi) + h.c.\right], \tag{4.7}$$

with Φ denoting a generic chiral superfield, K the Kähler potential, leading to kinetic terms, and W the superpotential. The Kähler potential is real. In general, the superpotential can have the form $W = f\,\Phi + m/2\,\Phi^2 + \lambda/3\,\Phi^3$, with generic coupling constants f, m, λ. Invariance under supersymmetry dictates that W only depends on Φ, not on $\Phi^\dagger$. The superpotential is hence holomorphic.

For a gauge invariant Lagrangian the kinetic terms are minimally coupled to a vector superfield V. The Kähler potential becomes then

$$K(\Phi, \Phi^\dagger) = \Phi^\dagger e^{igT^aV^a}\Phi\,, \tag{4.8}$$

with V^a denoting the vector superfields, g the coupling constant and T^a the generators of the gauge group. Additionally, kinetic terms for the vector superfields need to be introduced via superfield strength tensors.

[1] Expansion of both the chiral and vector superfield in the Grassmann variables θ and $\bar{\theta}$ yields an additional auxiliary field, which can, however, be eliminated by applying the equations of motion.

Superfield	spin 0	spin 1/2	$SU(3) \times SU(2) \times U(1)$
$\hat{Q}$	$\tilde{Q} = (\tilde{u}_L \;\; \tilde{d}_L)$	$(u_L \;\; d_L)$	$(3, 2, 1/6)$
$\hat{U}^c$	$\tilde{u}_R^*$	$u_R^\dagger$	$(\bar{3}, 1, -2/3)$
$\hat{D}^c$	$\tilde{d}_R^*$	$d_R^\dagger$	$(\bar{3}, 1, 1/3)$
$\hat{L}$	$\tilde{L} = (\tilde{\nu}_L \;\; \tilde{e}_L)$	$(\nu_L \;\; e_L)$	$(1, 2, -1/2)$
$\hat{E}^c$	$\tilde{e}_R^*$	$e_R^\dagger$	$(1, 1, 1)$
$\hat{H}_u$	$\phi_u = (H_u^+ \;\; H_u^0)$	$(\tilde{H}_u^+ \;\; \tilde{H}_u^0)$	$(1, 2, 1/2)$
$\hat{H}_d$	$\phi_d = (H_d^0 \;\; H_d^-)$	$(\tilde{H}_d^0 \;\; \tilde{H}_d^-)$	$(1, 2, -1/2)$

Table 4.1.: Chiral superfields of the MSSM and their particle content with their respective representations/quantum numbers under SM gauge group. The index c denotes charge conjugation.

Superfield	spin 1/2	spin 1	$SU(3) \times SU(2) \times U(1)$
$\hat{W}$	$\tilde{W}_1 \, \tilde{W}_2 \, \tilde{W}_3$	$W_1 \, W_2 \, W_3$	$(1, 3, 0)$
$\hat{B}$	$\tilde{B}$	B	$(1, 1, 0)$
$\hat{G}$	$\tilde{g}$	g	$(8, 1, 0)$

Table 4.2.: Vector superfields of the MSSM and their particle contents with their respective representations/quantum numbers under the SM gauge group.

We will now turn to a discussion of the Minimal Supersymmetric Extension of the SM (MSSM). More detailed discussions on SUSY in general can be found in many textbooks and reviews, see *e.g.* Refs. [15, 18, 161, 164].

4.2. The Minimal Supersymmetric Extension of the Standard Model

The MSSM is minimal in the sense that the spectrum contains the minimal amount of necessary particles. Each chirality component of a SM Dirac fermion is part of a chiral supermultiplet, each SM vector boson is part of a vector supermultiplet. The Higgs boson is introduced as part of a chiral supermultiplet. One Higgs boson superfield is, however, not sufficient. A second $SU(2)$ Higgs doublet is needed for gauge anomaly cancelation. In addition, the second superfield with a different hypercharge is required to assign a mass to both up-type and down-type fermions due to the holomorphy of the superpotential. The particle content of the MSSM is detailed in Table 4.1 and Table 4.2, where only the the quark and lepton superfields of the first generation are shown.

The superpotential of the MSSM expressed in terms of the superfields is given by

$$W_{MSSM} = \epsilon_{ab}\Big(y_u \hat{Q}^a \hat{H}_u^b \hat{U}^c + y_d \hat{H}_d^a \hat{Q}^b \hat{D}^c + y_e \hat{H}_d^a \hat{L}^b \hat{E}^c - \mu \hat{H}_d^a \hat{H}_u^b\Big)\,, \tag{4.9}$$

with $\epsilon_{12} = \epsilon^{12} = 1$. The dimensionless Yukawa couplings y_u, y_d and y_e are in general 3×3 matrices in flavour space. The new parameter, μ, has mass dimension one. Due to our ignorance on the exact mechanism of SUSY breaking, the SUSY breaking part of the Lagrangian will be parameterized in the most general way by explicit SUSY breaking terms. We require that SUSY is broken softly. This means that all SUSY breaking terms must have positive mass dimension. For the MSSM, the soft-SUSY breaking Lagrangian reads

$$\begin{aligned}
\mathcal{L}^{\text{soft}}_{\text{MSSM}} = & -m_{H_d}^2 |\phi_d|^2 - m_{H_u}^2 |\phi_u|^2 - \tilde{Q}^* m_{\tilde{Q}}^2 \tilde{Q} - \tilde{u}_R^* m_{\tilde{U}}^2 \tilde{u}_R \\
& - \tilde{d}_R^* m_{\tilde{D}}^2 \tilde{d}_R - \tilde{L}^* m_{\tilde{L}}^2 \tilde{L} - \tilde{e}_R^* m_{\tilde{E}}^2 \tilde{e}_R \\
& - \epsilon_{ab}(\tilde{u}_R^* y_u A_u \tilde{Q}^a \phi_u^b + \tilde{d}_R^* y_d A_d \phi_d^a \tilde{Q}^b + \tilde{e}_R^* y_e A_e \phi_d^a \tilde{L}^b - B\mu\, \phi_d^a \phi_u^b + h.c.) \\
& - \frac{1}{2}(M_1 \tilde{B}\tilde{B} + M_2 \tilde{W}_i \tilde{W}_i + M_3 \tilde{g}\tilde{g} + h.c.)\,,
\end{aligned} \tag{4.10}$$

where we have introduced the soft-SUSY breaking mass parameters m_{H_d}, m_{H_u}, $m_{\tilde{Q}}$, $m_{\tilde{U}}$, $m_{\tilde{D}}$, $m_{\tilde{E}}$, $m_{\tilde{L}}$, M_1, M_2 and M_3, the parameter B and the soft-SUSY breaking trilinear couplings A_u, A_d and A_e. Note that in general the soft-SUSY breaking mass parameters $m_{\tilde{U}}$, $m_{\tilde{D}}$, $m_{\tilde{E}}$ and $m_{\tilde{L}}$ and the trilinear couplings A_u, A_d and A_e are 3×3 matrices in flavour space. We will now shortly highlight the different sectors needed for the discussion in the following two sections.

4.2.1. The Higgs boson sector

The two complex Higgs doublets of the MSSM lead to five physical Higgs bosons on top of the three usual SM Goldstone bosons: Two charged Higgs bosons $H^\pm$ and three neutral ones. If CP is conserved, one is CP-odd, A, and two are CP-even, h and H. Spontanous symmetry breaking can take place, so that the masses of the massive vector bosons are generated when the two Higgs doublets ϕ_u and ϕ_d acquire VEVs

$$\langle \phi_d \rangle = \frac{1}{\sqrt{2}} \begin{pmatrix} v_d \\ 0 \end{pmatrix}\,, \qquad \langle \phi_u \rangle = \frac{1}{\sqrt{2}} \begin{pmatrix} 0 \\ v_u \end{pmatrix}\,. \tag{4.11}$$

A relative phase between the Higgs doublets can be absorbed by a redefinition of either ϕ_u or ϕ_d. With $v^2 = v_u^2 + v_d^2 \approx 246$ GeV, the gauge boson masses are given by the usual relations in terms of the VEV v. It is useful to define

$$\tan\beta = \frac{v_u}{v_d}\,. \tag{4.12}$$

The range of $\tan\beta$ is restricted by perturbativity of the bottom and top Yukawa couplings. In addition, the requirement of dynamical EWSB, meaning that the correct sign for the determinant of the squared Higgs mass matrix is obtained by RGE running,

restricts $\tan\beta$ to $1 \lesssim \tan\beta \lesssim 60$. In the SM, the negative sign of the mass squared term was introduced by hand, see Eq. (2.1). The mass of the charged Higgs boson is obtained by diagonalizing all terms bilinear in H_d^- and H_u^+. This leads to a massless charged Goldstone boson and a charged Higgs boson with mass

$$M_{H^\pm}^2 = \left(\frac{B\mu}{v_u v_d} + \frac{1}{4}g_2^2\right) v^2 \,. \tag{4.13}$$

The mass matrix of the CP-odd components can be obtained similarly. Its diagonalization leads to a massless Goldstone boson and the CP-odd Higgs boson with mass

$$m_A^2 = \frac{2B\mu}{s_{2\beta}} \,. \tag{4.14}$$

We introduced the short-hand notations $s_x = \sin x$, $c_x = \cos x$ and $t_x = \tan x$. It is convenient to replace the parameter B by the CP-odd Higgs boson mass. Then the CP-even Higgs boson mass matrix is given by

$$M_{\Phi\Phi}^2 = \begin{pmatrix} m_A^2 s_\beta^2 + M_Z^2 c_\beta^2 & -(m_A^2 + M_Z^2) s_\beta c_\beta \\ -(m_A^2 + M_Z^2) s_\beta c_\beta & m_A^2 c_\beta^2 + M_Z^2 s_\beta^2 \end{pmatrix} . \tag{4.15}$$

The neutral Higgs boson masses follow from this as

$$m_{h,H}^2 = \frac{1}{2}\left(m_A^2 + M_Z^2 \mp \sqrt{(m_A^2 + M_Z^2)^2 - 4M_Z^2 m_A^2 c_{2\beta}^2}\right) . \tag{4.16}$$

From this formula it can be inferred that at tree level the lighter Higgs boson mass is bounded to be smaller than $m_h \leq M_Z c_{2\beta}$. In order to lift the Higgs boson mass to the measured value of 125 GeV, loop corrections are essential. In particular, the leading corrections to the Higgs boson masses come from top quark and top squark loops. Including these corrections, the lightest CP-even Higgs boson mass is found to be smaller than $m_h < 132$ GeV [161], for a typical scale of the SUSY spectrum of $M_{SUSY} = 1$ TeV.

4.2.2. Gauginos and higgsinos

The spin-1/2 partners of the gauge bosons and Higgs bosons, called gauginos and higgsinos can mix. The mass eigenstates of the neutral components are called neutralinos, $\tilde{\chi}^0$, the mass eigenstates of the charged components are called charginos, $\tilde{\chi}^\pm$. The only exception is the gluino $\tilde{g}$, which does not mix with the other gauginos and higgsinos, due to its non-trivial quantum number under $SU(3)_C$. Hence, the gluino mass is directly given by the parameter M_3 in the soft-SUSY breaking Lagrangian in Eq. (4.10).

The masses of the four neutralinos are obtained by diagonalizing the mass matrix. In the $\psi^0 = (\tilde{B}, \tilde{W}_3, \tilde{H}_d^0, \tilde{H}_u^0)$ basis the mass matrix for the neutralinos reads

$$M_N = \begin{pmatrix} M_1 & 0 & -c_\beta M_Z s_W & M_Z s_\beta s_W \\ 0 & M_2 & c_\beta M_W & -M_W s_\beta \\ -c_\beta M_Z s_W & c_\beta M_W & 0 & -\mu \\ M_Z s_\beta s_W & -M_W s_\beta & -\mu & 0 \end{pmatrix} , \tag{4.17}$$

The sine of the Weinberg angle is denoted by s_W and is given by $s_W = g_1/\sqrt{g_1^2 + g_2^2}$. The mass matrix is diagonalized by means of a unitary transformation $\mathcal{N}$, yielding

$$\text{diag}(m_{\tilde{\chi}_1^0}, m_{\tilde{\chi}_2^0}, m_{\tilde{\chi}_3^0}, m_{\tilde{\chi}_4^0}) = \mathcal{N}^* M_N \mathcal{N}^\dagger \,. \tag{4.18}$$

The mass eigenstates $\tilde{\chi}_i^0$ are mass-ordered, with $\tilde{\chi}_1^0$ being the lightest neutralino. The chargino masses will be given in Section 6.1.2 in the context of the NMSSM.

4.2.3. Squark sector

The superpartners of the left- and right-handed SM fermions can mix. We will restrict ourselves in this discussion to the superpartner of the quarks, the squarks. In the general case of flavour violation, all flavour eigenstates can mix, such that we can define a six-component vector

$$\tilde{q} = \begin{pmatrix} \tilde{q}_L \\ \tilde{q}_R \end{pmatrix} . \tag{4.19}$$

The 6×6 mass matrix for the up-type squarks reads

$$M_{\tilde{u}}^2 = \begin{pmatrix} m_{\tilde{Q}}^2 + M_Z^2(T_L^3 - Q_{\tilde{u}} s_W^2) c_{2\beta} \mathbb{1} + m_u m_u^\dagger & -m_u(A_u^* + \mu/t_\beta) \\ -(A_u^T + \mu^*/t_\beta) m_u^\dagger & m_{\tilde{U}}^2 + Q_{\tilde{u}} M_Z^2 c_{2\beta} s_W^2 \mathbb{1} + m_u^\dagger m_u \end{pmatrix} , \tag{4.20}$$

and for the down-type quarks

$$M_{\tilde{d}}^2 = \begin{pmatrix} m_{\tilde{Q}}^2 + M_Z^2(T_L^3 - Q_{\tilde{d}} s_W^2) c_{2\beta} \mathbb{1} + m_d m_d^\dagger & -m_d(A_d^* + \mu t_\beta) \\ -(A_d^T + \mu^* t_\beta) m_d^\dagger & m_{\tilde{D}}^2 + Q_{\tilde{d}} M_Z^2 c_{2\beta} s_W^2 \mathbb{1} + m_d^\dagger m_d \end{pmatrix} , \tag{4.21}$$

where we introduced the fermion mass matrices $m_u = y_u v_u/\sqrt{2}$ and $m_d = y_d v_d/\sqrt{2}$. The soft-SUSY breaking masses $m_{\tilde{Q}}$, $m_{\tilde{U}}$, $m_{\tilde{D}}$ and trilinear couplings A_u and A_d are 3×3 matrices. In general, they are non-diagonal and hence provide new sources of flavour violation. The third component of the $SU(2)_L$ generator is denoted by $T_{\tilde{L}}^3$, the charge operator is called $Q_{\tilde{f}}$. The sfermions are rotated into mass eigenstates $\tilde{f}^m$ by means of an unitary transformation

$$\tilde{q}^m = \tilde{W}^{\tilde{q}} \tilde{q} \,, \tag{4.22}$$

with

$$\text{diag}(m_{\tilde{q}_1}^2, ..., m_{\tilde{q}_6}^2) = \tilde{W}^{\tilde{q}} M_{\tilde{q}}^2 \tilde{W}^{\tilde{q}\dagger} \tag{4.23}$$

and $\tilde{q} = \tilde{u}, \tilde{d}$. The masses are ordered, starting from the lightest eigenvalue. It is often useful to work in the super-CKM basis [165]. In this basis the quark masses matrices are diagonal and the squarks are rotated in parallel to the quarks. All terms are flavour-diagonal in this basis, apart from soft-SUSY breaking masses and trilinear couplings. The squarks are hence rotated to

$$\tilde{q}_L' = U_L \tilde{q}_L \,, \qquad \tilde{q}_R' = U_R \tilde{q}_R \tag{4.24}$$

where the generation indices are suppressed and $U_{L/R}$ are the matrices which rotate the left-handed/right-handed quark current eigenstates to their respective mass eigenstates. A further transformation with a 6×6 matrix W rotates the squarks into the mass eigenstates $\tilde{q}^m$

$$\tilde{q}_s^m = W_{st}^{\tilde{q}} \begin{pmatrix} \tilde{q}'_L \\ \tilde{q}'_R \end{pmatrix}_t = W_{si}^{\tilde{q}} \tilde{q}'_{Li} + W_{s\,i+3}^{\tilde{q}} \tilde{q}'_{Ri} \,, \tag{4.25}$$

with $s, t = 1, ..., 6$ and $i = 1, 2, 3$. The bases of Eq. (4.22) and (4.25) are connected via

$$\tilde{W}_{si}^{\tilde{q}} = W_{sj}^{\tilde{q}} U_{ji}^L \,, \qquad \tilde{W}_{s\,i+3}^{\tilde{q}} = W_{s\,j+3}^{\tilde{q}} U_{ji}^R \,, \tag{4.26}$$

where summation over $j = 1, 2, 3$ implied. Without flavour violation in the soft-SUSY breaking sector the 3×3 matrices entering the squark mass matrices in Eqs. (4.20) and (4.21) are diagonal in the super-CKM basis, such that the 6×6 squark mass matrices become block-diagonal and can hence be reduced to three 2×2 matrices for the three flavour eigenstates $\tilde{u}, \tilde{c}$, and $\tilde{t}$ or $\tilde{d}, \tilde{s}$, and $\tilde{b}$, respectively.

CHAPTER 5

Light stop decays

In this chapter we consider the phenomenology of light top squarks. Their lightness is motivated by naturalness arguments, since the amount of fine-tuning of the EW scale is significantly driven by the top squark [41]. A 125 GeV Higgs boson in the MSSM can only be obtained if the loop corrections to its mass are large. In particular, top squarks and quarks give the leading contribution to these loop corrections. For such a large Higgs boson mass, two scenarios are possible: either the top squarks are rather heavy or they are maximally mixed. The latter case allows for one lighter top squark and refers to scenarios with a large stop mixing parameter $X_t = (A_t - \mu \cot\beta)/m_S$, with the average stop mass $m_S^2 = m_{\tilde{t}_1} m_{\tilde{t}_2}$. This can be seen by means of the following formula for the leading corrections to the lightest Higgs boson mass in the decoupling limit $m_A \gg M_Z$ [166]

$$m_h^2 = M_Z^2 \cos^2 2\beta + \frac{3m_t^4}{2\pi^2 v^2}\left(\log\left(\frac{m_S^2}{m_t^2}\right) + X_t^2\left(1 - \frac{X_t^2}{12}\right)\right) . \tag{5.1}$$

The lightest stop masses, that can lead to the observed Higgs mass value, can be obtained for $m_S \approx 500$ GeV and $X_t^2 \approx 6$. The maximal mixing scenario turns out to optimally reduce the amount of fine-tuning for given M_H [167]. A light top squark can also be helpful to create the correct relic abundance due to co-annihilation, in particular for stop-neutralino mass differences between $15 - 30$ GeV or $m_A \approx 2m_{\tilde{\chi}_1^0}$, see Ref. [168–171].[1]

In this chapter we consider very light top squarks, with masses below the kinematic threshold for the decays $\tilde{t}_1 \to t\tilde{\chi}_1^0$ of a top squark $\tilde{t}_1$ into a top quark t and a neutralino $\tilde{\chi}_1^0$ and for decays $\tilde{t}_1 \to bW\tilde{\chi}_1^0$ into neutralino, bottom quark and W boson. We assume

[1] A light stop can also be helpful for successful baryogenesis within the MSSM. It turns out, however, that it would require stop masses below the top quark mass [172–177], which is in tension to the direct searches for light top squarks by ATLAS [178].

that the lightest stop is the next-to-lightest supersymmetric particle (NLSP) and the lightest neutralino is the lightest supersymmetric particle (LSP). The light top squark can then decay into $\tilde{t}_1 \to (u/c)\tilde{\chi}_1^0$ [179–181] and $\tilde{t}_1 \to b\tilde{\chi}_1^0 f\bar{f}'$ [182], where f and $\bar{f}'$ denote generic light fermions.

The strongest limits on light stop masses in this kinematic region are given by ATLAS [178], which exclude light top squark masses up to ~ 230 GeV for $m_{\tilde{\chi}_1^0} \approx 200$ GeV. Another analysis has recently been performed by the CMS collaboration [183] with a similar outcome as the ATLAS analysis, but depending on the mass splitting between the neutralino and the stop mass. Tevatron [184, 185] and LEP results [186, 187] give weaker bounds on the stop masses than the recent ATLAS and CMS searches. All these analyses assume a branching ratio of 100% for the decay $\tilde{t}_1 \to c\tilde{\chi}_1^0$. Reference [188] pointed out, that similar results on the bounds on the lightest stop mass could also be obtained from already existing searches for monojets [189, 190] or searches with final states including more than two jets [191, 192] by the CMS razor analysis [193], for $BR(\tilde{t}_1 \to b\tilde{\chi}_1^0 f\bar{f}) = 100\%$.

The decays $\tilde{t}_1 \to (u/c)\tilde{\chi}_1^0$ are flavour violating. In general, the MSSM exhibits many new sources of flavour violation, such that the decays $\tilde{t}_1 \to (u/c)\tilde{\chi}_1^0$ can directly occur at tree level. In the case of flavour violation we will hence denote the light stop $\tilde{u}_1$, as it is a mixture of all up-type flavours but with the largest component being stop-like.[2] Precise measurements of flavour observables from K, D and B processes, however, strongly restrict the new sources of flavour violation. The flavour structure of New Physics models must hence be highly non-generic. A framework for suppression of flavour-violating interactions is given by means of the *Minimal Flavour Violation* (MFV) concept [194–196].

In this chapter we compute the decay widths for the two-body decays $\tilde{u}_1 \to (u/c)\tilde{\chi}_1^0$ and the four-body decay $\tilde{u}_1 \to b\tilde{\chi}_1^0 f\bar{f}'$. If the flavour-violating coupling is very small the four-body decay can become important. Compared to the existing works of Ref. [179–181], we take into account a flavour-violating coupling of a charm/up quark to a $\tilde{u}_1$ and a neutralino already at tree-level and compute the NLO QCD corrections to the decay width. For the four-body decay, in contrast to the work in Ref. [182], we allow for flavour violation and we take into account the full mass dependence on the third generation quarks and leptons.

The chapter is structured as follows. In Section 5.1 we will shortly discuss the concept of MFV. Then we will discuss the decays $\tilde{u}_1 \to (u/c)\tilde{\chi}_1^0$ in Section 5.2 and the decay $\tilde{u}_1 \to b\tilde{\chi}_1^0 f\bar{f}'$ in Section 5.3. Afterwards, we show the numerical impact of our calculation in Section 5.4. In the last section, a short summary will be given.

[2] In the text, we will still refer to it as the 'light stop' but keeping in mind, that it also has components from other flavours.

5.1. Minimal Flavour Violation

In the SM, all flavour and CP-violation originates from the Yukawa sector[3] and is parameterized in terms of the Cabbibo-Kobayashi-Maskawa (CKM) matrix [197, 198]. Generic New Physics models exhibit new sources of flavour and CP-violation. Limits on electron and neutron electric dipole moments, however, set tight bounds on the amount of CP-violation. Equivalently, flavour observables, in particular *e.g.* $K^0 - \bar{K}^0$ mixing, lead as well to large bounds on the scale of New Physics under the assumption of a generic $\mathcal{O}(1)$ flavour structure. Flavour transitions can be parameterized by effective four-fermion interactions. These effective operators are suppressed by the scale of New Physics, which would generate such an effective operator. If the New Physics scale of such an operator is the TeV-scale, the flavour structure of the model cannot be generic. The coupling constant of the operator must be small. A solution is provided by the MFV ansatz [194–196]. Essentially, MFV means that all flavour and CP-violating interactions are linked to the structure of the SM Yukawa couplings. It can be formally described in the following way: In the SM, there are three families with two $SU(2)_L$ doublets denoted by Q_L and L_L and with three $SU(2)_L$ singlets denoted by U_R, D_R and E_R. The largest global symmetry of their kinetic terms that commutes with the gauge group is a $U(3)^5$ symmetry. The latter can be decomposed into an $SU(3)^5$, that we call flavour symmetry, and a $U(1)^5$ factor. In the following, we will concentrate on the quark sector and thus define

$$SU(3)_q^3 = SU(3)_{Q_L} \times SU(3)_{U_R} \times SU(3)_{D_R} \,. \tag{5.2}$$

The flavour symmetry is not exact, since it is broken by the Yukawa couplings. Formally, the invariance under the flavour group can be restored by promoting the Yukawas $y_{u/d}$ to non-dynamical fields, called spurions, with the following transformation under $SU(3)_q^3$

$$y_u \sim (3, \bar{3}, 1)_{SU(3)_q^3} \,, \qquad\qquad y_d \sim (3, 1, \bar{3})_{SU(3)_q^3} \,. \tag{5.3}$$

In analogy, this can be extended to the lepton sector with an $SU(3)_l^2$ symmetry.[4] An effective theory then satisfies MFV if all the operators constructed by the SM fields and the spurions are formally invariant under the flavour symmetry and CP. This means that in MFV all sources of flavour and CP-violation are completely determined by the CKM matrix.

Such an approach can be implemented for SUSY as well. In general, the MSSM has many new flavour-violating sources given by the soft-SUSY breaking masses and trilinear couplings, see *e.g.* Section 4.2.3. Employing MFV, the soft-SUSY breaking squark

[3] In general, strong interactions in the SM could break CP as well. Experimental evidence, in particular from the measurement of the electric dipole moment of the neutron, suggests, however, that QCD does not violate CP. The puzzling question why QCD does not exhibit any CP-violation is commonly known as the 'strong CP-problem'.

[4] Note that in SUSY the $SU(3)_{L_L}$ can be enlarged to $SU(4)_{L_L}$ by including the $\hat{H}_d$ field into a generalized lepton multiplet [199].

masses and trilinear couplings can be written as [196, 200]

$$m^2_{\tilde{Q}} = \tilde{m}^2(a_1 \mathbb{1} + b_1\, y_u\, y_u^\dagger + b_2\, y_d\, y_d^\dagger + b_3\, y_d\, y_d^\dagger\, y_u\, y_u^\dagger + b_4\, y_u\, y_u^\dagger\, y_d\, y_d^\dagger)\,, \tag{5.4}$$

$$m^2_{\tilde{U}} = \tilde{m}^2(a_2 \mathbb{1} + b_5\, y_u^\dagger\, y_u)\,, \tag{5.5}$$

$$m^2_{\tilde{D}} = \tilde{m}^2(a_3 \mathbb{1} + b_6\, y_d^\dagger\, y_d)\,, \tag{5.6}$$

$$A_u = A(a_4 \mathbb{1} + b_7\, y_d\, y_d^\dagger + b_9\, y_u\, y_u^\dagger)\,, \tag{5.7}$$

$$A_d = A(a_5 \mathbb{1} + b_8\, y_u\, y_u^\dagger + b_{10}\, y_d\, y_d^\dagger)\,, \tag{5.8}$$

where we have introduced the coefficients a_i $(i = 1, ..., 5)$ and b_j $(j = 1, ..., 10)$, the mass parameter $\tilde{m}$ and the trilinear coupling A. The Yukawa couplings y_u and y_d, the soft-SUSY breaking masses $m_{\tilde{Q}}$, $m_{\tilde{U}}$ and $m_{\tilde{D}}$ and the trilinear soft-SUSY breaking couplings A_u and A_d are 3×3 matrices in flavour space. Often universality of the soft-SUSY breaking masses and trilinear terms is assumed, meaning the coefficients b_i are set to zero. For example, in supergravity models all soft-SUSY breaking masses are universal at a scale close to the Planck scale. In models with gauge-mediated SUSY breaking, the soft-SUSY breaking terms are universal at the mass scale of the messenger particles. The assumption of universality is, however, not invariant under renormalization group evolution. Coefficients b_i are induced by renormalization group equation (RGE) running. If the scale of universality is large, as *e.g.* it is in supergravity scenarios, then their typical size can be rather large.

As can be seen in Eqs. (5.4–5.8), MFV implies that the soft-SUSY breaking masses and trilinear couplings are nearly degenerate, leading to squark masses with tightly constrained mass splittings. However, we want to discuss scenarios with light stop quark masses, meaning that the 3rd generation squark mass is supposed to be much smaller than the squark masses of the other generations. In such a case the MFV assumptions can be relaxed a bit by an intermediate breaking of the $SU(3)$ flavour symmetry factors into $SU(2)$ [201]. In the past, some flavour observables have exhibited a slight tension, which can even be eased a bit, if the flavour symmetry of the quark sector is reduced to an $SU(2)^3$ [202].

5.2. Flavour-violating two-body decays of a light squark

In this section, we will discuss the decays $\tilde{u}_1 \to c\tilde{\chi}_1^0$ and $\tilde{u}_1 \to u\tilde{\chi}_1^0$. The latter is typically suppressed by two orders of magnitude with respect to the former, due to the smaller CKM matrix element for transitions of the third generation to the first, if $\tilde{u}_1$ is mainly stop-like. We will hence mainly refer in the discussion to the $\tilde{u}_1 \to c\tilde{\chi}_1^0$ decay, but results for the $\tilde{u}_1 \to u\tilde{\chi}_1^0$ decay were obtained in the same way. In Ref. [179], the authors have considered the decay $\tilde{u}_1 \to c\tilde{\chi}_1^0$ with a vanishing $c - \tilde{\chi}_1^0 - \tilde{u}_1$ coupling at tree level. The process then takes place at one-loop order by loops of charged particles, *i.e.* W bosons, charginos or charged Higgs bosons. The divergences (in scalar self-energy diagrams) are canceled by the introduction of a soft counterterm at the Planck

scale, which leads to a large logarithm, namely $\log \Lambda_{Planck}/M_W$, at the weak scale, which has been chosen to be M_W in their calculation. This large logarithm stems from flavour off-diagonal terms induced in the soft-SUSY breaking masses by RGE running. Reference [179] argues that in view of the large logarithm, the non-logarithmic terms in the decay width can be neglected. In Refs. [180, 181], these non-logarithmic terms for the decay at one loop at the MFV scale μ_{MFV} with universal soft-SUSY breaking masses and trilinear couplings were then given, meaning the process has been calculated at full one-loop order under the assumption of a vanishing $c - \tilde{\chi}_1^0 - \tilde{t}$ coupling at tree level. The results have been compared to Ref. [179] and it has been shown that the non-logarithmic terms contribute with $\mathcal{O}(10\%)$ to the partial decay width. For a reliable result the large logarithms need to be resummed. This is provided by solving the RGEs for the scalar soft-SUSY breaking masses. Furthermore, Refs. [180, 181] compare their results with the flavour-violating tree-level process, with the $c-\tilde{\chi}_1^0-\tilde{u}_1$ coupling induced by RGE running. They come to the conclusion that a resummation of the logarithms is important, if the scale μ_{MFV}, at which the soft-SUSY breaking masses and trilinear couplings are universal, is large.

In this section, we will describe the calculation of the one-loop SUSY-QCD (sQCD) corrections to the $\tilde{u}_1 \to c\tilde{\chi}_1^0$ decay width assuming that this decay can already occur at tree level.

5.2.1. Tree-level decay width

At tree level the decay width of the lightest up-type squark into a charm quark and the lightest neutralino is given by

$$\Gamma = \frac{1}{16\pi} m_{\tilde{u}_1} \sqrt{\left(1 - \frac{(m_c + m_{\tilde{\chi}_1^0})^2}{m_{\tilde{u}_1}^2}\right)\left(1 - \frac{(m_c - m_{\tilde{\chi}_1^0})^2}{m_{\tilde{u}_1}^2}\right)} \left[-4\, g_{211}^L g_{211}^R \frac{m_c m_{\tilde{\chi}_1^0}}{m_{\tilde{u}_1}^2} + \left(1 - \frac{m_c^2 + m_{\tilde{\chi}_0}^2}{m_{\tilde{u}_1}^2}\right)\left((g_{211}^L)^2 + (g_{211}^R)^2\right)\right], \tag{5.9}$$

with $m_{\tilde{u}_1}$ denoting the up-type squark mass, $m_{\tilde{\chi}_1^0}$ the neutralino mass and m_c the charm quark mass. The couplings g^L and g^R are given by

$$g_{ijk}^L = \frac{2\sqrt{2}}{3} g_1 \mathcal{N}_{k1}^* W_{j\,i+3}^{\tilde{u}*} - \frac{\sqrt{2} m_{u_i}}{v \sin\beta} \mathcal{N}_{k4}^* W_{ji}^{\tilde{u}*}, \tag{5.10}$$

$$g_{ijk}^R = -\frac{\sqrt{2}}{6} \left(g_1 \mathcal{N}_{k1} + 3 g_2 \mathcal{N}_{k2}\right) W_{ji}^{\tilde{u}*} - \frac{\sqrt{2} m_{u_i}}{v \sin\beta} \mathcal{N}_{k4} W_{j\,i+3}^{\tilde{u}*}, \tag{5.11}$$

for the quark indices $i = 1, .., 3$, the squark indices $j = 1, ..., 6$ and the neutralino indices $k = 1, ..., 4$. The mass of the up-type quark i is denoted by m_{u_i}. Flavour non-diagonal matrix elements in Eqs. (5.10, 5.11) from the squark mixing matrix $W^{\tilde{u}}$ as introduced in Eq. (4.22) are necessary for non-vanishing couplings. They will automatically be generated by RGE running, if we evolve the parameters of the model to $\mu \neq \mu_{MFV}$.

The charm mass in Eq. (5.9) can usually be neglected. Only if the mass difference between the decaying squark and the neutralino becomes comparable with the charm

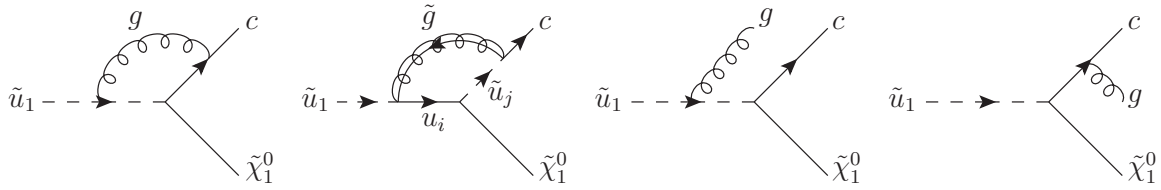

Figure 5.1.: Feynman diagrams showing the NLO sQCD corrections to $\tilde{u}_1 \to c\tilde{\chi}_1^0$.

quark mass or if the lightest neutralino is mostly higgsino-like, the charm mass can play a role. In mSUGRA models the lightest neutralino for a 173.2 GeV top quark is never higgsino-like [203]. In general, the lightest neutralino is mainly bino-like if $|M_1| < |\mu|$ (for $|M_2| < |M_1|$ it could also be wino-like). The parameters $|M_2|$ and $|\mu|$ determine also the chargino masses directly. The exclusion limits on charginos go up to ≈ 800 GeV [204] if the decay of a chargino into a slepton is kinematically allowed or for decoupled sleptons up to 315 GeV [204, 205]. Both exclusion limits are given under some assumptions on branching fractions and masses of the sparticles. The lightest neutralino can only be mainly wino or higgsino-like, if its mass value is close to the mass of one of the charginos. In scenarios, where the lightest neutralino is much lighter that the charginos, the neutralino will thus be mainly bino-like. For the tree-level decay width, we have taken into account the charm quark mass, while at one-loop order we have neglected it.

5.2.2. The decay at one loop

The Feynman diagrams for the one-loop process of $\mathcal{O}(\alpha_s\alpha)$ can be found in Fig. 5.1. The first two diagrams show the virtual contributions given by vertex corrections involving gluons and gluinos in the loop. Gluinos can in general couple to two different flavours of quarks and squarks, hence we have introduced the indices i and j into the Feynman diagram. The two last Feynman diagrams show the real corrections due to radiation of a gluon off the squark and off the charm quark.

Virtual corrections:

The virtual corrections have been calculated with `FeynArts/FormCalc` [147–150]. The results for the gluon contributions are the same as for the decay $\tilde{t}_1 \to t\tilde{\chi}_1^0$ given in Refs. [206–208]. The gluino contributions could not be checked against the literature, as they involve flavour-changing loop couplings.

The virtual corrections involve ultraviolet (UV), infrared (IR) and collinear divergences. We distinguish between UV-poles, which show up as $1/\epsilon_{UV}$ using dimensional regularization, which regularizes the divergent integrals by going to $D = 4 - 2\epsilon$ dimensions, and IR and collinear poles which show up as $1/\epsilon_{IR}$. Combined collinear and IR divergences lead even to poles in $1/\epsilon_{IR}^2$. The IR divergences of virtual and real corrections cancel according to the Kinoshita-Lee-Nauenberg theorem [209, 210]. In our case, also the collinear divergences of virtual and real corrections cancel completely, as we do not have massless particles in the initial state. The UV divergences cancel in the renor-

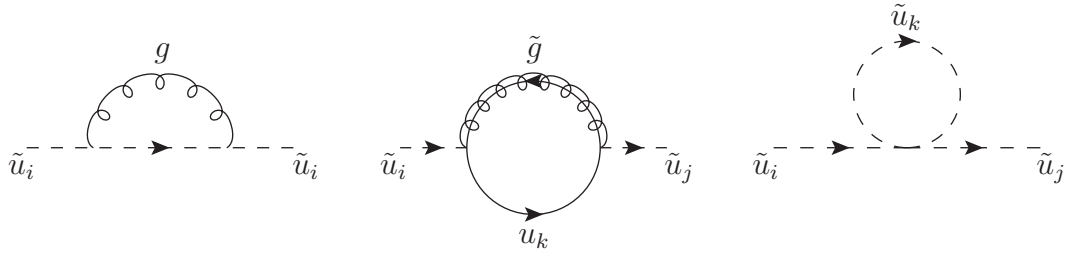

Figure 5.2.: Feynman diagrams for the one-loop sQCD corrections to the self-energies $\tilde{\Sigma}_{ij}(p^2)$ of the squarks.

malization procedure. The specific steps will be discussed in the following in more detail.

Renormalization of UV divergences:

The virtual corrections to the decay at one loop are divergent and hence need to be renormalized. We adopt a complete on-shell scheme, meaning we demand for all counterterms on-shell renormalization conditions. The bare fermion and sfermion fields with superscript (0) need to be replaced by the renormalized ones

$$\tilde{u}^{(0)} \to \left(1 + \frac{1}{2}\delta Z^{\tilde{u}}\right)\tilde{u}\,, \quad u^{(0)}_{L/R} \to \left(1 + \frac{1}{2}\delta Z^{L/R}\right)u_{L/R}\,, \tag{5.12}$$

with the help of wave-function renormalization constants $\delta Z^{\tilde{u}}$ and $\delta Z^{L/R}$. The wave-function renormalization constants of the squark fields are given by $(i, j = 1, ..., 6)$

$$\delta Z^{\tilde{u}}_{ij} = \begin{cases} -\frac{1}{2}\widetilde{\mathrm{Re}}\frac{\partial\tilde{\Sigma}_{ii}(p^2=m^2_{\tilde{u}_i})}{\partial p^2} & \text{if } i = j\,, \\ \frac{2}{m^2_{\tilde{u}_i} - m^2_{\tilde{u}_j}}\widetilde{\mathrm{Re}}\,\tilde{\Sigma}_{ij}(p^2 = m^2_{\tilde{u}_j}) & \text{if } i \neq j\,, \end{cases} \tag{5.13}$$

where $\widetilde{\mathrm{Re}}$ only takes the real part of the one-loop integrals but keeps the complex structure of the parameters. The self-energies $\tilde{\Sigma}_{ij}$ are calculated from the Feynman diagrams shown in Fig. 5.2. The indices i and j denote the flavour indices of the external particles. Note that we only calculate corrections $\propto \alpha_s$. This means that in the third diagram of Fig. 5.2, featuring a quartic squark coupling, only the terms proportional to α_s need to be taken into account. In principle, there is also a diagram involving a quartic coupling between up-type and down-type squarks. This diagram, however, turns out to be zero due to the flavour structure.

Defining the following structure for the quark self-energies

$$\Sigma_{ij}(p^2) = \not{p}\Sigma^L_{ij}(p^2)P_L + \not{p}\Sigma^R_{ij}(p^2)P_R + \Sigma^l_{ij}(p^2)P_L + \Sigma^r_{ij}(p^2)P_R \tag{5.14}$$

with $P_{L/R} = (1 \mp \gamma_5)/2$, the wave-function renormalization constants for the quarks

read

$$\delta Z_{ij}^{L/R} = \frac{2}{m_i^2 - m_j^2} \widetilde{\mathrm{Re}} \left(m_j^2 \Sigma_{ij}^{L/R}(m_j^2) + m_i m_j \Sigma_{ij}^{R/L}(m_j^2) \right.$$
$$\left. + m_i \Sigma_{ij}^{l/r}(m_j^2) + m_j \Sigma_{ij}^{r/l}(m_j^2) \right) \qquad \text{for } i \neq j\,, \tag{5.15}$$

$$\delta Z_{ii}^{L/R} = -\widetilde{\mathrm{Re}}\, \Sigma_{ii}^{L/R}(m_i^2) - m_i \frac{\partial}{\partial p^2} \widetilde{\mathrm{Re}} \left(m_i (\Sigma_{ii}^{L/R}(p^2) + \Sigma_{ii}^{R/L}(p^2)) \right.$$
$$\left. + \Sigma_{ii}^{l/r}(p^2) + \Sigma_{ii}^{r/l}(p^2) \right) \Big|_{p^2 = m_i^2} \qquad \text{for } i = j\,, \tag{5.16}$$

with $i, j = 1, .., 3$. The masses m_i/m_j will later on be identified with the quark masses m_{u_i}/m_{u_j}. The self-energies are calculated from the Feynman diagrams shown in Fig. 5.3. Note that in the calculation of the self-energies of the fermions special care needs to be taken: for the calculation of fermion self-energies it is important to take into account that dimensional regularization breaks SUSY, as it leads to a mismatch between fermionic and bosonic degrees of freedom. Thus, a SUSY restoring counterterm needs to be introduced. An alternative approach perserving SUSY is provided by dimensional reduction [211, 212], where the space-time dimension for the nominator in the loop integral, in particular for the γ-algebra, is kept in four dimensions. We follow the latter approach.

A second subtle point is that the gluon diagram in Fig. 5.3 does not have any scale and should hence be zero. But it exhibits UV and IR divergences. If they are to be canceled separately, one needs to take into account that this diagram is given by $1/\epsilon_{UV} - 1/\epsilon_{IR}$.

In addition to the quark and squark fields, their mixing matrices need to be renormalized. The mixing matrix counterterms δu and $\delta \tilde{w}$ relate the bare mixing matrices $U^{(0)}$ and $\tilde{W}^{(0)}$ with the renormalized ones

$$U_{ij}^{(0)L/R} \to (\delta_{ik} + \delta u_{ik}^{L/R}) U_{kj}^{L/R}\,, \qquad i, j, k = 1, 2, 3\,, \tag{5.17}$$

$$\tilde{W}_{st}^{(0)} \to (\delta_{sr} + \delta w_{sr}) \tilde{W}_{rt}\,, \qquad s, r, t = 1, ..., 6\,. \tag{5.18}$$

Summation over common indices is implied. The bare and renormalized mixing matrices need to be unitary. The counterterms hence have to be defined anti-hermitian [213]. They are thus chosen such that they cancel the anti-hermitian part of the wave-function

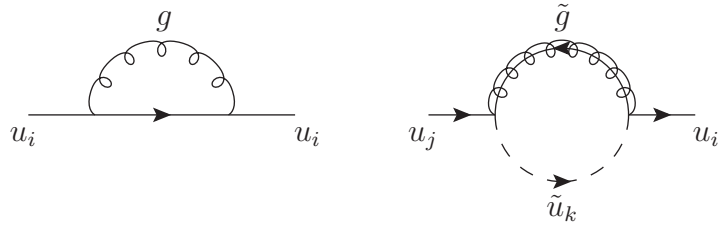

Figure 5.3.: Feynman diagrams for the one-loop sQCD corrections to the self-energy of the quark.

renormalization constants

$$\delta u^{L/R} = \frac{1}{4}\left(\delta Z^{L/R} - \delta Z^{L/R\dagger}\right), \tag{5.19}$$

$$\delta \tilde{w} = \frac{1}{4}\left(\delta Z^{\tilde{u}} - \delta Z^{\tilde{u}\dagger}\right). \tag{5.20}$$

We define the counterterms on-shell. Note that the on-shell definition of the mixing matrix counterterms is known to be gauge dependent [214–217]. We adopt the prescription of Ref. [217], where it was stated that the result obtained in the Feynman-'t Hooft gauge corresponds to the gauge-independent one.

In the Yukawa part of the coupling, the bare fermion mass $m^{(0)}$ needs to be replaced by the renormalized one

$$m^{(0)}_{u_i} \to m_{u_i} + \delta m_{u_i} \tag{5.21}$$

with the counterterm δm_{u_i} given by

$$\delta m_{u_i} = \frac{1}{2}\widetilde{\mathrm{Re}}\left[m_{u_i}\left(\Sigma^L_{ii}(m^2_{u_i}) + \Sigma^R_{ii}(m^2_{u_i})\right) + \Sigma^l_{ii}(m^2_{u_i}) + \Sigma^r_{ii}(m^2_{u_i})\right]. \tag{5.22}$$

Note, that even if the fermion mass is set to zero, a counterterm arises nevertheless, due to the Σ^l and Σ^r contributions of the gluino diagram of Fig. 5.3, see *e.g.* also Ref. [218].

With these ingredients at hand, we can define the counterterm Lagrangian in the basis of the mass eigenstates of the squark, neutralino and quark as

$$\mathcal{L}_{\bar{u}\tilde{u}\tilde{\chi}^0_1} = \bar{u}_i(g^L_{ijk} + \delta g^L_{ijk})P_L\tilde{u}_j\tilde{\chi}^0_k + \bar{u}_i(g^R_{ijk} + \delta g^R_{ijk})P_R\tilde{u}_j\tilde{\chi}^0_k\,. \tag{5.23}$$

The counterterms δg^L and δg^R are given by

$$\begin{aligned}
\delta g^L_{ijk} =& \frac{2\sqrt{2}}{3} g_1 \mathcal{N}^*_{k1}\left(\sum_{n=1}^{3}\left[\frac{1}{2}\delta Z^{R\dagger}_{in} W^{\tilde{u}*}_{j\,n+3} + W^{\tilde{u}*}_{j\,n+3}\delta u^R_{in}\right] + \sum_{m=1}^{6}\left[\delta\tilde{w}^*_{jm} W^{\tilde{u}*}_{m\,i+3} + \frac{1}{2}W^{\tilde{u}*}_{m\,i+3}\delta Z^{\tilde{u}}_{mj}\right]\right) \\
& - \frac{\sqrt{2}}{v\sin\beta}\mathcal{N}^*_{k4}\left(\sum_{n=1}^{3}\left[\delta_{ni}\delta m_{u_n} W^{\tilde{u}*}_{ji} + \frac{1}{2}\delta Z^{R\dagger}_{in} W^{\tilde{u}*}_{jn} m_{u_n} + m_{u_i} W^{\tilde{u}*}_{jn}\delta u^L_{in}\right]\right. \\
& \left. + \sum_{m=1}^{6}\left[m_{u_i}\delta\tilde{w}^*_{jm} W^{\tilde{u}*}_{mi} + m_{u_i}\frac{1}{2}W^{\tilde{u}*}_{mi}\delta Z^{\tilde{u}}_{mj}\right]\right), \qquad (5.24) \\
\delta g^R_{ijk} =& -\frac{\sqrt{2}}{6}\left(\mathcal{N}_{k1} + 3g_2\mathcal{N}_{k2}\right)\left(\sum_{n=1}^{3}\left[\frac{1}{2}\delta Z^{L\dagger}_{in} W^{\tilde{u}*}_{jn} + W^{\tilde{u}*}_{jn}\delta u^L_{in}\right] + \right. \\
& \left. \sum_{m=1}^{6}\left[\delta\tilde{w}^*_{jm} W^{\tilde{u}*}_{mi} + \frac{1}{2}W^{\tilde{u}*}_{mi}\delta Z^{\tilde{u}}_{mj}\right]\right) \\
& - \frac{\sqrt{2}}{v\sin\beta}\mathcal{N}_{k4}\left(\sum_{n=1}^{3}\left[\delta_{ni}\delta m_{u_n} W^{\tilde{u}*}_{j\,i+3} + \frac{1}{2}\delta Z^{L\dagger}_{in} m_{u_n} W^{\tilde{u}*}_{j\,n+3} + m_{u_i} W^{\tilde{u}*}_{j\,n+3}\delta u^R_{in}\right] + \right. \\
& \left. \sum_{m=1}^{6}\left[m_{u_i}\delta\tilde{w}^*_{jm} W^{\tilde{u}*}_{m\,i+3} + m_{u_i}\frac{1}{2}W^{\tilde{u}*}_{m\,i+3}\delta Z^{\tilde{u}}_{mj}\right]\right), \qquad (5.25)
\end{aligned}$$

with the fermion flavour index $i = 1, 2, 3$, the squark index $j = 1, ..., 6$ and the neutralino index $k = 1, ..., 4$. We only sum over the indices if indicated. In the expressions in Eqs. (5.24) and (5.25) only the previously discussed counterterms are needed. All other parameters do not get any QCD contributions at one-loop level.

There is another subtle point that we have not discussed yet. The wave-function renormalization constants δZ_{ij} in Eq. (5.15) and $\delta Z^{\tilde{u}}_{ij}$ in Eq. (5.13) have a vanishing denominator for degenerate masses of particle i and j. In particular, if the first and second generation fermion masses are set to zero, this becomes problematic. The problem is solved though by renormalizing both the fields and the mixing matrices on-shell, as the combination of the renormalization constants is non-singular, see *e.g.* Ref. [219] for the case of degenerate squark masses. We thus replace for degenerate fermions

$$\begin{aligned}\frac{1}{2}\delta Z^{L/R\dagger}_{ij} + \delta u^{L/R}_{ij} =& \frac{1}{4}\left(\delta Z^{L/R}_{ij} + \delta Z^{L/R\dagger}_{ij}\right) \xrightarrow{m_{u_i}=m_{u_j}} -\frac{1}{2}\,\widetilde{\mathrm{Re}}\;\Sigma^{L/R}_{ij}(m^2_{u_i}) \\ & - m_{u_i}\frac{\partial}{\partial p^2}\widetilde{\mathrm{Re}}\left(m_{u_i}(\Sigma^{L/R}_{ij}(p^2) + \Sigma^{R/L}_{ij}(p^2)) \right. \\ & \left. + \Sigma^{l/r}_{ij}(p^2) + \Sigma^{r/l}_{ij}(p^2)\right)\Big|_{p^2=m^2_{u_i}}\,, \end{aligned} \tag{5.26}$$

and

$$\begin{aligned}&\frac{1}{2}\delta Z^{L/R\dagger}_{ij} m_{u_j} + \delta u^{R/L}_{ij} m_{u_i} = \frac{1}{2}\delta Z^{L/R\dagger}_{ij} m_{u_j} + \frac{1}{4}\left(\delta Z^{R/L}_{ij} - \delta Z^{R/L\dagger}_{ij}\right) m_{u_i} \\ &\xrightarrow{m_{u_i}=m_{u_j}} \frac{1}{2}\widetilde{\mathrm{Re}}\left[m_{u_i}\Sigma^{R/L}_{ij}(m^2_{u_i}) + 2\Sigma^{r/l}_{ij}(m^2_{u_i})\right] - \frac{1}{2}\frac{\partial}{\partial p^2}\widetilde{\mathrm{Re}}\left[m^3_{u_i}\Sigma^{L/R}_{ij}(p^2) + m^3_{u_i}\Sigma^{R/L}_{ij}(p^2)\right. \\ &\left. + m^2_{u_i}\Sigma^{l/r}_{ij}(p^2) + m^2_{u_i}\Sigma^{r/l}_{ij}(p^2)\right]\Big|_{p^2=m^2_{u_i}}\,. \end{aligned} \tag{5.27}$$

We do not sum in Eqs. (5.26) and (5.27) over common indices. Equations (5.26) and (5.27) have been derived by using $\delta Z^{\dagger}_{ij} = \delta Z_{ij}(m_i \leftrightarrow m_j)$ in Eq. (5.15). The latter relation follows from the hermiticity of the Lagrangian, implying that the self-energies obey $\Sigma_{ij} = \gamma_0\Sigma^{\dagger}_{ij}\gamma_0$, with Σ_{ij} defined in Eq. (5.14). For degenerate squark masses, we use

$$\frac{1}{2}\delta Z^{\tilde{u}}_{st} + \delta\tilde{w}^{\dagger}_{ts} = \frac{1}{4}\left(\delta Z^{\tilde{u}}_{st} + \delta Z^{\tilde{u}\dagger}_{st}\right) \xrightarrow{m_{\tilde{u}_s}=m_{\tilde{u}_t}} -\frac{1}{2}\widetilde{\mathrm{Re}}\frac{\partial}{\partial p^2}\tilde{\Sigma}_{st}(p^2)\Big|_{p^2=m^2_{\tilde{u}_s}}\,. \tag{5.28}$$

Real corrections:

For the computation of the real corrections we follow Ref. [220]. The Feynman diagrams are the last two diagrams in Fig. 5.1. We use the following parametrization

$$r^2 := \frac{(p_{\tilde{u}} - p_c - p_g)^2}{m^2_{\tilde{u}_1}} = \frac{m^2_{\tilde{\chi}^0_1}}{m^2_{\tilde{u}_1}}\,, \tag{5.29}$$

$$p_c\, p_g = \frac{m^2_{\tilde{u}_1}}{2}(1-r)^2 y\,, \tag{5.30}$$

$$p_{\tilde{u}_1}\, p_g = \frac{m^2_{\tilde{u}_1}}{2}(1-r^2)(1-z)\,, \tag{5.31}$$

with $p_{\tilde{u}_1}$, p_c and p_g denoting the four-momenta of the squark, the charm quark and the gluon, respectively. As a first step the squared matrix elements of the diagrams three and four of Fig. 5.1 and their interference term need to be calculated. Then they need to be integrated over the three-particle phase space. We regularize the phase space integral by going from four dimensions to $D = 4 - 2\epsilon$ dimensions, with $\epsilon = \epsilon_{IR}$. The three-particle phase space integral is given by

$$\begin{aligned} d\Phi^{(3)}(p_c, p_{\tilde{\chi}_1^0}, p_g, p_{\tilde{u}_1}) =& d\Phi^{(2)}(p_c, p_{\tilde{\chi}_1^0}, p_{\tilde{u}_1}) \frac{(1-r)^2}{16\pi^2} \frac{(m_{\tilde{u}_1}^2)^{1-\epsilon}(4\pi)^\epsilon}{\Gamma(1-\epsilon)} \left(\frac{1+r}{1-r}\right)^{2\epsilon} \\ & \int_0^1 dz (r^2 + (1-r^2)z)^{-\epsilon} \int_0^{y_{max}} dy y^{-\epsilon} (y_{max} - y)^{-\epsilon} , \end{aligned} \tag{5.32}$$

where $p_{\tilde{\chi}_1^0}$ denotes the four-momentum of the neutralino. The upper integration limit y_{max} reads

$$y_{max} = \frac{(1+r)^2 z(1-z)}{(z - r^2 z + r^2)} . \tag{5.33}$$

The two-particle phase space $d\Phi^{(2)}$ can either be evaluated in four dimensions or in D dimensions after the cancellation of the divergences with the virtual corrections. We are only interested in the total decay width, for which the phase space integration can be performed analytically, thus we can directly cancel the IR and collinear divergences against the ones occurring in the virtual corrections without introducing a subtraction counterterm.

The full result of the decay width at NLO QCD can be found in Appendix A. My results for this process have been numerically cross-checked by a second independent calculation [221]. I have implemented them into the `SDECAY` [222] routine of `SUSY-HIT` [223]. For `SUSY-HIT` to cope with the SUSY Les Houches Accord 2 (SLHA2) [224] input files, the read-in routine had to be modified. A new routine `SD_lightstop2bod` and some follow-up routines have been implemented into `SUSY-HIT` to evaluate the discussed decay.

5.3. Four-body decay of a light squark

The light squark can also decay via a four-body decay. Especially, if the flavour-violating coupling $c - \tilde{\chi}_1^0 - \tilde{u}_1$ is very small, the four-body decay can dominate as it has flavour-conserving subprocesses. The process was computed for the first time in Ref. [182]. Compared to Ref. [182], we allow for flavour-violating couplings at tree level and take into account the full mass dependence on the third generation quarks and fermions. Due to the flavour violation, not only a $b\tilde{\chi}_1^0 f \bar{f}'$ final state is considered, as would be in the $\tilde{t}_1$ decay in a non-flavour violating theory, but more generally, $\tilde{u}_1 \to d_i \tilde{\chi}_1^0 f \bar{f}'$ with d_i denoting a down-type fermion with flavour index $i = 1, 2, 3$. The final state fermions can be $f, \bar{f}' = u, d, c, s, b, \tau, \mu, e, \nu_e, \nu_\mu, \nu_\tau$. The Feynman diagrams for the process are shown in Fig. 5.4. In addition to the shown Feynman diagrams, there are diagrams with an exchange of a neutral particle *e.g.* a neutralino or a gluino which can only proceed via flavour-violating couplings. They will not be considered

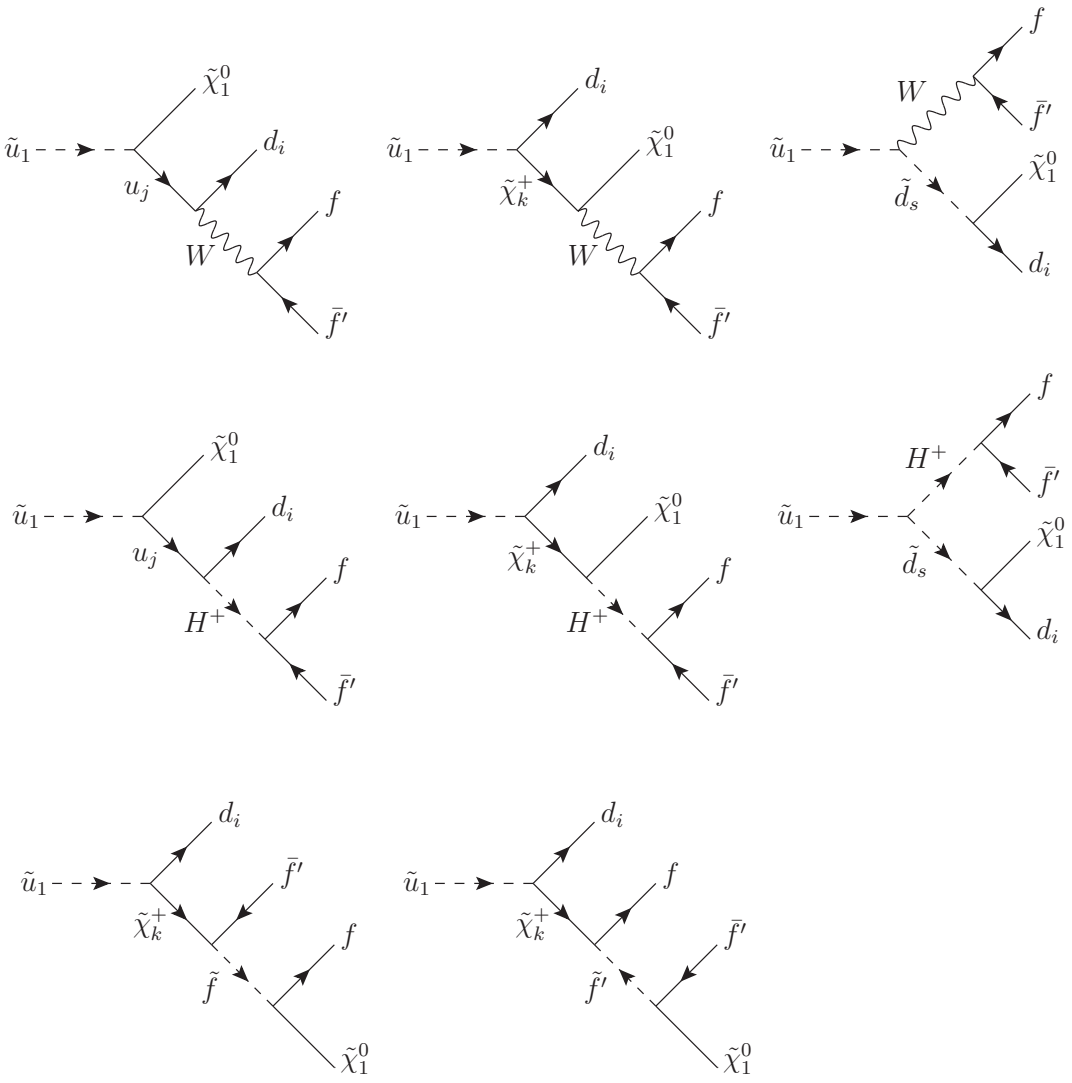

Figure 5.4.: Feynman diagrams for the decay $\tilde{u}_1 \to d_i \tilde{\chi}_1^0 f \bar{f}'$. The indix i can take values $i = 1, ..., 3$. The indices j, k, and s imply a summation over the three generations of fermions, the two chargino indices and the six down-type squark indices, respectively. The arrows in the plots are chosen according to the Feynman rules in Ref. [161]. The arrows on the chargino lines show the charge flow. Neutralino lines do not have an arrow to indicate their Majorana nature.

for phenomenological studies, but we checked explicitly that they are negligibly small. The Feynman diagrams of Fig. 5.4 include fermion number flow violating interactions. We have followed the techniques in Ref. [225] for the evaluation of such diagrams.[5]

The calculation was done with two independent approaches: I have performed the calculation by hand, but evaluating the traces with `FeynCalc` [230]. The cross-check was performed with `FeynArts/FormCalc` [147–150]. I have implemented my results

[5]Earlier works giving the Feynman rules for Majorana fermions can be found in Refs. [226–229].

into SUSY-HIT [223] in a new routine SD_lightstop4bod and follow-up routines. For the numerical evaluation of the process, the phase space generator RAMBO [231] was used.

There is one caveat in the numerical evaluation of this process: The masses of the propagating particles can potentially get quite important loop corrections, which we take into account by using the output of a spectrum generator. These loop corrections of the particle masses, however, lead to an artificial gauge dependence of the process due to a mismatch of the perturbative order of the particle masses with the couplings. In order to deal with this issue, we have cancelled the gauge dependence obtained in a general R_ξ gauge, before setting the masses to their loop-corrected values. The thus obtained result corresponds to the one obtained in the unitary gauge.

We find that the most important contribution comes from the first diagram of Fig. 5.4 with a top quark and a W boson as propagating particles. Note that Ref. [182] finds the most important contribution to be the second diagram of Fig. 5.4, with W and chargino propagators. The reason that we find something different is that in the parameter space we have considered the top quark is lighter than the charginos such that the virtuality of the top exchange diagrams is smaller and the respective diagram can hence dominate the process.

5.4. Numerical analysis

In this section we study the numerical impact of our calculation on the decay widths and branching ratios of the light up-type squark. In order to do so, we have generated the spectrum with the code SPheno [232, 233]. The code allows for flavour violation.[6] For the CKM matrix we used[7]

$$V_{CKM} = \begin{pmatrix} 0.9742 & 0.2257 & 0.0036 \\ -0.2256 & 0.9733 & 0.0425 \\ 0.0061 & -0.0422 & 0.9991 \end{pmatrix} . \tag{5.34}$$

The top quark mass was set to $m_t = 173.3$ GeV; for the bottom quark mass $m_b = 4.89$ GeV and for the τ lepton mass $m_\tau = 1.77$ GeV was used. The strong coupling constant at NLO was taken to be $\alpha_s^{\overline{\rm DR}}(M_Z) = 0.10665$ in the evaluation of the NLO QCD corrections of the two-body decay widths. As SUSY parameter set, we have

[6] Another spectrum calculator allowing for flavour violation is SOFTSUSY [234]. The results of these codes seem to be in good agreement, taken into account the uncertainties due to *e.g.* different treatment of higher order corrections to the sparticle masses [235, 236]. The only significant deviation can be found in the case of flavour violation and large difference between the soft-SUSY breaking squark masses.

[7] These CKM matrix elements have been obtained from the Wolfenstein parameterization [237] of the CKM matrix. The input for the Wolfenstein parameters is given by $\lambda = 0.2257$, $A = 0.814$, $\bar{\rho} = 0.135$ and $\bar{\eta} = 0.349$, see Ref. [238].

chosen

$$\begin{aligned} \tan\beta = 10\,, \quad \mu = 900\text{ GeV}\,, \quad m_A = 600\text{ GeV}\,, \quad M_2 = 650\text{ GeV}\,, \\ M_3 = 1530\text{ TeV}\,, \quad m_{\tilde{Q}} = 1.5\text{ TeV}\,, \quad (m_{\tilde{U}})_{11} = (m_{\tilde{U}})_{22} = 1.5\text{ TeV}\,, \\ (m_{\tilde{U}})_{33} = 480\text{ GeV}\,, \quad m_{\tilde{D}} = 1.5\text{ TeV}\,, \quad m_{\tilde{L}} = m_{\tilde{E}} = 1\text{ TeV}\,, \\ A_d = A_e = 0\,, \quad (A_u)_{11} = (A_u)_{22} = 0\,, \quad (y_u A_u)_{33} = 1.4\text{ GeV}\,. \end{aligned} \tag{5.35}$$

The soft-SUSY breaking masses as well as the trilinear couplings have to be understood as 3×3 diagonal matrices with the given values generation universal if not explicitly indicated otherwise. The bino soft-SUSY breaking mass M_1 is allowed to vary between 272 GeV and 344 GeV.

The output scale in the spectrum generator was set to 300 GeV. As can be seen from the above values, the input was taken to be flavour diagonal with the exception of the CKM matrix. Flavour off-diagonal matrix elements in the squark sector were generated by RGE running. Our input corresponds to the MFV assumption with the exception that the $SU(3)^3$ flavour symmetry of the quark sector is broken to an $SU(2) \times SU(3)^2$ by setting the third generation soft-SUSY breaking squark mass $(m_{\tilde{U}})_{33}$ to a lower value than the other soft-SUSY breaking squark masses.

The resulting sparticle masses are all above the current exclusion limits. For example, the gluino mass for this parameter set is $m_{\tilde{g}} = 1.5$ TeV and hence above the exclusion limits of Refs. [239–242]. The squark masses, apart from the lightest mostly stop-like squark, are all found to be roughly at $m_{\tilde{Q}} = 1.45$ TeV and hence evade the exclusion limits of Refs. [239, 242]. The sleptons in the investigated scenarios have masses of around 1 TeV. They are not excluded yet [204, 243]. The charginos in this scenario have masses larger than $m_{\tilde{\chi}^\pm_{1,2}} \geq 660$ GeV. If the decay of the lightest chargino into sleptons is kinematically forbidden, the strongest exclusion limits are only ≈ 315 GeV [204, 205], such that our scenario is save. The lightest up-type squark mass is $m_{\tilde{u}_1} = 350$ GeV and hence not excluded by the ATLAS search on light top squarks in Ref. [178] in the kinematic region we are interested in.

We also verified that the point is compatible with the results of the Higgs searches: The exclusion limit on heavy Higgs bosons was tested with the help of `HiggsBounds` [244, 245]. The compatibility with the excess of a Higgs boson at 125 GeV was checked with `HiggsSignals` [246]: the light Higgs boson with a mass of 123.9 GeV in this scenario is compatible with the excess at 68% C.L.. Additionally, we checked flavour observables in particular from rare B decays ($B_s \to \mu^+\mu^-$ [247], $B \to \mu^+\mu^-$ [248], $B^- \to \tau^-\nu_\tau$ [249], $B^+ \to \tau^+\nu_\tau$ [250] and $B \to X_s\gamma$ [251]) with the help of `SuperIsoRelic` [252–254]. The code `SuperIsoRelic` can also compute the relic density. We demand the relic density $\Omega_c h^2$ to be smaller than 0.123 for our parameter points, in accordance with the measurement of the WMAP [255] and the Planck satellite [77] of

$$\Omega_c h^2 = 0.1196 \pm 0.0031 \qquad \text{(Planck at 68\%C.L.)}\,. \tag{5.36}$$

If the relic density we obtain in our model is smaller than the lower bound given by the Planck experiment, we assume that the neutralino is not the only Dark Matter particle,

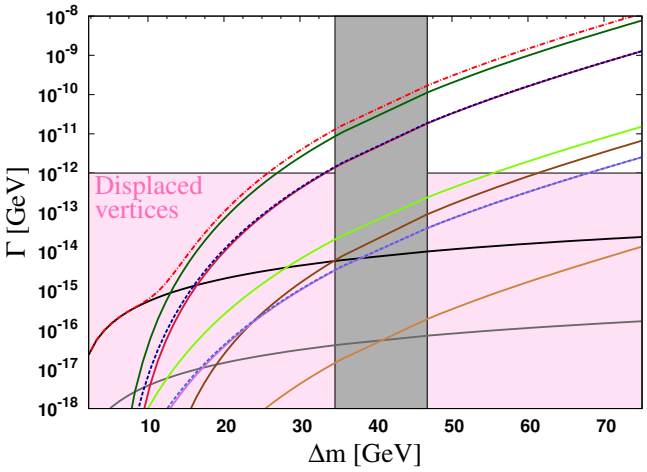

Figure 5.5.: Decay widths Γ for the decays of $\tilde{u}_1$ to the final states $c\tilde{\chi}_1^0$ (black), $u\tilde{\chi}_1^0$ (gray), $b\tilde{\chi}_1^0 jj$ (dark green), $b\tilde{\chi}_1^0(\bar{\mu}\nu_\mu/\bar{e}\nu_e)$ (dark blue/dashed), $b\tilde{\chi}_1^0\bar{\tau}\nu_\tau$ (dark red), $j\tilde{\chi}_1^0 jj$ (light green), $b\tilde{\chi}_1^0\bar{b}j$ (brown), $j\tilde{\chi}_1^0(\bar{\mu}\nu_\mu/\bar{e}\nu_e)$ (light blue/dashed), $j\tilde{\chi}_1^0\bar{\tau}\nu_\tau$ (pink), $j\tilde{\chi}_1^0\bar{b}j$ (light brown). The red dashed-dotted line shows the total decay width. Total decay widths below 10^{-12} GeV lead to displaced vertices as indicated by the pink region. The gray area is excluded by a too large relic density.

but that we have instead a multi-component Dark Matter scenario. More details on the constraints imposed on the parameter points can be found in Ref. [221].

In order to show the numerical results, we have varied M_1 and fixed all parameters as described above. We introduce the parameter $\Delta m = m_{\tilde{u}_1} - m_{\tilde{\chi}_1^0}$ describing the mass difference between the lightest squark mass and the lightest neutralino mass, as the decay widths will in particular depend on this.

In Fig. 5.5 the decay widths as a function of Δm are shown. The decay widths were evaluated at the scale of the decaying particle, *i.e.* $\mu = m_{\tilde{u}_1}$. The mass difference Δm in the plot is varied within the kinematic region of interest *i.e.*, the mass splitting was only varied up to the kinematic threshold of the decay $\tilde{u}_1 \to b\tilde{\chi}_1^0 W^+$. We do not consider in our plot $\Delta m < 2$ GeV. For very small Δm the light squark will be quasi-stable, such that exclusions due to the observations from big bang nucleosynthesis from *e.g.* the observation of H, D, He and Li abundances need to be taken into account, as the decay products of the decays of the quasi-stable squarks during nucleosynthesis can lead to various effects such as the dissociation of the light elements [256]. Not going below $\Delta m = 2$ GeV, we are not yet in the region were the lifetime of the squark is sufficiently long such that these bounds become relevant.

The red dashed-dotted line in Fig. 5.5 shows the total decay width. The decay width into the final state $c\tilde{\chi}_1^0$ is shown by a black line, the one into the final state $u\tilde{\chi}_1^0$ by a gray line. The dark green line shows the decay with into the final state $b\tilde{\chi}_1^0 jj$, the light green line into the final state $j\tilde{\chi}_1^0 jj$. The symbol j stands here for quarks of the first or second generation or the respective antiquarks. The dark blue dashed line corresponds to the decay widths into the final states $b\tilde{\chi}_1^0\bar{\mu}\nu_\mu$ or $b\tilde{\chi}_1^0\bar{e}\nu_e$, the light blue dashed line to

the decay widths into the final states $j\tilde{\chi}_1^0\bar{\mu}\nu_\mu$ or $j\tilde{\chi}_1^0\bar{e}\nu_e$. The respective final states with muons or electrons have both almost the same decay width. The only difference in the calculation arises for the diagrams with sleptons or sneutrinos as propagating particles (last two Feynman diagrams of Fig. 5.4), but these contributions are so small that the difference between μ or e final state is completely negligible. The decay widths of the squark into $b\tilde{\chi}_1^0\bar{\tau}\nu_\tau$ and $j\tilde{\chi}_1^0\bar{\tau}\nu_\tau$ are shown in dark red and pink, respectively. The pink line is nearly completely below the light blue dashed line, since the τ final states differs from the respective μ and e final state only by the mass of the τ, which in contrast to the μ and e mass was not set to zero. The decay width into the final state $b\tilde{\chi}_1^0\bar{b}j$ is shown as a dark brown line; the decay width into the final state $j\tilde{\chi}_1^0\bar{b}j$ as light brown line. The gray region in the figure is excluded due to a too large relic density. If the total decay width is below 10^{-12} GeV (pink region), displaced vertices are possible. The minimal decay length that allows a measurement of the lifetime of the decaying particle is strongly detector dependent. We assume 0.1 mm, corresponding to a lifetime of $\tau \approx 0.3$ ps and a total decay width of $\Gamma \approx 10^{-12}$ GeV for a velocity of the decaying particle of $v \approx c$ [257].[8]

From Fig. 5.5, it can be inferred that the total decay width of the light up-type squark is rather small. Such a small decay width allows the squark to hadronize before it decays. In our computation of the decay width we did not take into account any long distance effects from hadronization. Since we consider the inclusive decay, the long distance effects can be estimated to be of $\mathcal{O}(\Lambda_{QCD}/m_{\tilde{u}_1})$ or even $\mathcal{O}(\Lambda_{QCD}^2/m_{\tilde{u}_1}^2)$ (with $\Lambda_{QCD} \approx 200$ MeV denoting the scale at which QCD becomes perturbative), if the energy release in the decay is much larger than Λ_{QCD}, see *e.g.* Refs. [260–262] with a similar argument for rare B decays. Hence hadronization effects can be neglected here.

In Fig. 5.6, the branching ratios are shown. The colour code is the same as in Fig. 5.5: The black line shows the branching ratio for the decay $\tilde{u}_1 \to c\tilde{\chi}_1^0$, the gray line shows the one for the final state $u\tilde{\chi}_1^0$, the dark green line the one for the four-body decay into final state $b\tilde{\chi}_1^0 jj$, the dark blue dashed line the branching ratios for both the final states $b\tilde{\chi}_1^0\bar{\mu}\nu_\mu$ and $b\tilde{\chi}_1^0\bar{e}\nu_e$ final states, the dark red line the branching ratio into the final state $b\tilde{\chi}_1^0\bar{\tau}\nu_\tau$. All other final states have too small branching ratios to be seen in the plot. The gray region is again excluded by a too large relic density. As can be seen from this figure, the assumption of the experimental analyses of a branching ratio of 100% for the final state $c\tilde{\chi}_1^0$ is not valid here for $\Delta m \gtrsim 7$ GeV. From both Fig. 5.5 and Fig. 5.6, it can be inferred that for this parameter point, the four-body decays dominate for large mass splittings Δm between the squark and the neutralino mass. In the region with small mass splitting the decay $c\tilde{\chi}_1^0$ dominates. The reason is that for the four-body decay more phase space is needed, hence the decay width decreases strongly with Δm. The size of the two-body decay widths strongly depends on the size of the flavour violation. Typically, the decay width into $u\tilde{\chi}_1^0$ is $\mathcal{O}(1\%)$ of the decay width into $c\tilde{\chi}_1^0$ for a mainly stop-like $\tilde{u}_1$, due to the suppression of flavour transitions $t \to u$ compared to $t \to c$ by two orders of magnitude, as long as the

[8] Studies on displaced vertices have been performed by the experimental collaborations mainly in the context of R-parity violating SUSY, see *e.g.* Refs. [258, 259]. They can, however, not directly be applied to our case.

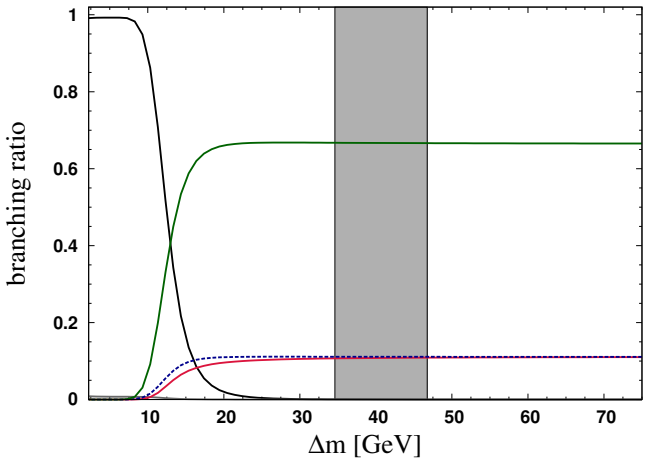

Figure 5.6.: Branching ratios of the light stop decays into the final states $c\tilde{\chi}_1^0$ (black), $u\tilde{\chi}_1^0$ (gray), $b\tilde{\chi}_1^0 jj$ (dark green), $b\tilde{\chi}_1^0\bar{\mu}\nu_\mu$, $b\tilde{\chi}_1^0\bar{e}\nu_e$ (both in dark blue dashed) and $b\tilde{\chi}_1^0\bar{\tau}\nu_\tau$ (dark red) as a function of Δm.

flavour-violating sources are restricted to the CKM matrix. For the four-body decays, the decay $\tilde{u}_1 \to b\tilde{\chi}_1^0 jj$ dominates by roughly a factor 6 over the decays to $b\tilde{\chi}_1^0\bar{\mu}\nu_\mu$ and $b\tilde{\chi}_1^0\bar{e}\nu_e$. The reason is that for the four-body decay the first two Feynman diagrams of Fig. 5.4 give the most important contributions. The only difference between the final states of the decays into $b\tilde{\chi}_1^0 jj$ and $b\tilde{\chi}_1^0\bar{\mu}\nu_\mu/b\tilde{\chi}_1^0\bar{e}\nu_e$ in these two diagrams are given by a colour factor of three for the decays into $b\tilde{\chi}_1^0 jj$ and, additionally, a sum over the CKM matrix elements for $j = u, c, d, s$. Hence, the final state $b\tilde{\chi}_1^0 jj$ has a factor 6 larger decay width with respect to $b\tilde{\chi}_1^0\bar{\mu}\nu_\mu$ and $b\tilde{\chi}_1^0\bar{e}\nu_e$. The decay width into the final state $b\tilde{\chi}_1^0\bar{\tau}\nu_\tau$ is a bit smaller than that into $b\tilde{\chi}_1^0\bar{\mu}\nu_\mu$ and $b\tilde{\chi}_1^0\bar{e}\nu_e$, as we did not set m_τ to zero.

In order to estimate the impact of the one-loop corrections on the two-body decays, we show in Fig. 5.7 the K-factor, defined as

$$K = \frac{\Gamma_{NLO}}{\Gamma_{LO}}\,, \tag{5.37}$$

as a function of Δm for the decay $\tilde{u}_1 \to c\tilde{\chi}_1^0$. The line for the final state $u\tilde{\chi}_1^0$ is similar and hence it is not shown in Fig. 5.7. From the figure it can be inferred that the NLO corrections are $\mathcal{O}(10\%)$ for large Δm and can be up to $\mathcal{O}(30\%)$ for small Δm.

In Fig. 5.8 we estimate the impact of our calculation for the four-body decay. The left plot of Fig. 5.8 shows, for the sum over all final states of the four-body decays, the effects of the inclusion of the third generation masses. More precisely, we have plotted $\Gamma(m_b = 4.89\ \text{GeV}, m_\tau = 1.77\ \text{GeV})/\Gamma(m_b = 0, m_\tau = 0)$ as a function of the mass difference Δm. From the figure it can be inferred, that the finite mass effects are quite important. They lead to a at least 10% smaller decay width. For small mass splittings the mass effects are of course much more important, due to the phase space, which becomes significantly smaller if finite masses of the final state particles are taken into account.

In the right plot of Fig. 5.8, we show the impact of the inclusion of flavour-violating

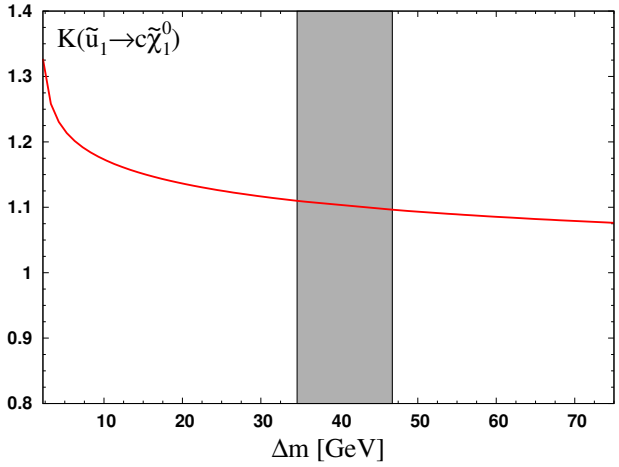

Figure 5.7.: The K-factor, $K = \Gamma_{NLO}/\Gamma_{LO}$, for the decay $\tilde{u}_1 \to c\tilde{\chi}_1^0$ as a function of Δm. The gray area is excluded by a too large dark matter abundance.

couplings for the computation of the four-body decay. For this purpose, we show the total decay width of the four-body decay without flavour violation $\Gamma_{no\,FV}$, for which we have excluded all diagrams with flavour transitions in the computation of the four-body decay, divided by the decay width with flavour violation as a function of Δm. The decay width of the four-body decay here again is the sum over all possible final states. As it can be inferred from the plot, the impact for large Δm is tiny. For small Δm the effect becomes larger, mainly due to the fact that the flavour non-violating final states of the four-body decay are kinematically closed. The flavour-violating final states can still be kinematically open as they do not necessarily involve a bottom quark in the final state.

5.5. Summary and Outlook

In this chapter we have studied the decays of a very light top squark in the kinematic region where only four-body decays or flavour changing two-body decays are possible. We have analyzed the two-body decays at one-loop order allowing for a flavour-changing coupling already at tree level. We found that the K-factor increases with decreasing mass splitting between the squark mass and the neutralino mass. The one-loop corrections roughly increase the decay width by $\mathcal{O}(10\% - 30\%)$. For the four-body decay we have improved the previous work of Ref. [182] by including the mass dependence of the third generation fermions. In addition, we allowed for flavour violation. We found that the effects of the flavour-violating couplings in the four-body decay for the investigated parameters are rather small. The inclusion of the masses of the third generation fermions for the four-body decay, however, was shown to be quite important. The branching ratio of the four-body decay can be quite significant, even 100%, in contrast to the assumptions made for exclusion limits of the light stops [178, 183].

A phenomenological analysis of the different parameter regions is planned for the future.

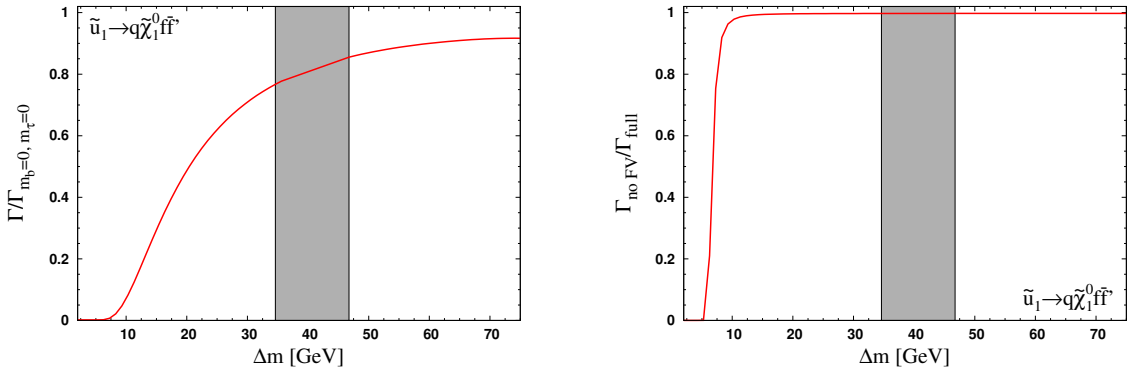

Figure 5.8.: *Left plot:* The decay width of the sum of the different final states of the four-body decays divided by the corresponding decay width with bottom quark mass and τ mass set to zero, as a function of Δm. *Right plot:* The sum of all four-body decay widths without flavour violation divided by the decay width of all four-body decays with flavour violation, as a function of Δm. The gray area is excluded by a too large dark matter abundance.

In the end our results can directly be compared to the exclusion limits on the light top squark. Our analysis shows, that the exclusion limits will possibly be weakened, as taking into account the four-body decay leads to a branching ratio into the two-body decay which is not 100%. However, the experiments assumed in their analysis, that the branching ratio into the final state $c\tilde{\chi}_1^0$ is 100%.

CHAPTER 6

Higgs bosons in the NMSSM with complex parameters

The NMSSM has in addition to the two Higgs doublets of the MSSM an extra complex scalar singlet field. Apart from the usual benefits of a supersymmetric theory, the introduction of the complex singlet field in the NMSSM is motivated by the fact that the μ-problem [263] of the MSSM can be solved. The μ-problem originates from the μ-term of the MSSM,

$$-W_{\mathrm{MSSM},\mu} = \mu\epsilon_{ab}\hat{H}_d^a\hat{H}_u^b \tag{6.1}$$

which generates the so-called little hierarchy problem. Being a supersymmetric mass parameter, the only natural values of the μ-term are the Planck-scale M_{Planck} or zero. Both values, however, are not allowed *e.g.* by the requirement of a successful EWSB. For EWSB, the μ-parameter needs to be of the order of the weak or SUSY scale. Another reason, which forbids these values for μ, is *e.g.* also an cosmologically unacceptable massless axion in the spectrum for $\mu = 0$ [263]. In the NMSSM the problem is solved by introducing the singlet superfield $\hat{S}$ coupling to the doublet fields $\hat{H}_u$ and $\hat{H}_d$, which generates dynamically a μ-term of the order of the weak or SUSY scale by acquiring a VEV v_s

$$-W_{\mathrm{NMSSM},\mu} = \lambda\epsilon_{ab}\hat{S}\hat{H}_d^a\hat{H}_u^b \quad \rightarrow \quad \mu_{eff} = \frac{\lambda\langle S\rangle}{\sqrt{2}} \equiv \frac{\lambda v_s}{\sqrt{2}}\,. \tag{6.2}$$

An additional advantage of the NMSSM is that it needs less fine-tuning in order to lift the lightest Higgs boson mass up to 125 GeV. The tree-level bound on the lightest Higgs boson mass squared in the MSSM is given by $M_h^2 \leq M_Z^2\cos^2 2\beta$, in the NMSSM it is increased to $M_{H_1}^2 \leq M_Z^2(\cos^2 2\beta + 2\lambda^2/(g_1^2+g_2^2)\sin^2 2\beta)$.[1] Therefore, loop corrections

[1] This corresponds to the mass value obtained by diagonalizing the submatrix of the $SU(2)_L$ doublets of the Higgs boson mass matrix [264].

to the Higgs boson mass, which go logarithmically with the soft-SUSY breaking scale, can be smaller than in the MSSM to achieve the 125 GeV Higgs boson mass, and hence less fine-tuning is necessary. Nevertheless, loop corrections to the Higgs boson mass are still essential in order to obtain the experimentally measured Higgs boson mass value.

In general, many parameters of the NMSSM can be complex. This can lead already at tree level to CP-violation in the Higgs sector, in contrast to the MSSM. The 3 CP-even neutral Higgs bosons and the 2 CP-odd neutral Higgs bosons of the NMSSM then become mixtures of both CP-even and CP-odd components. CP-violation is strongly restricted by the measurement of electric dipole moments (EDMs), in particular from the non-observation of EDMs for thorium monoxide, thallium, neutron and mercury [265–268]. However, the phase combinations occuring in the EDMs can be different from the ones inducing a mixing between CP-even and CP-odd components in the Higgs sector, such that the effect of the CP-violating phases on the Higgs boson masses can still be sizable [269–273]. New sources of CP-violation compared to the SM are necessary for a successful baryogenesis [274].

This chapter is structured as follows: In Section 6.1 the NMSSM with complex parameters at tree level is introduced. In Section 6.2 we discuss the Higgs boson masses at one-loop level with special focus on the renormalization. Compared to previous works on Higgs boson mass corrections in the NMSSM [275–283] and the complex NMSSM [284–289], this work employs a Feynman-diagrammatic based calculation in a mixed on-shell-$\overline{\text{DR}}$ scheme, similar to what was done in Ref. [290] for the real NMSSM. Section 6.3 deals with Higgs boson production and decays in the complex NMSSM. In Section 6.4, numerical results of the one-loop calculation of the Higgs boson masses are given. Section 6.5 summarizes the main results. The results of this chapter have been published in Refs. [33, 37, 291].

6.1. The NMSSM with complex parameters

The superpotential of the NMSSM can be separated into a part equal to the one of the MSSM and an NMSSM specific part, which contains the new singlet superfield. The superpotential then reads

$$W_{\text{NMSSM}} = \underbrace{\epsilon_{ab}\Big(y_u \hat{Q}^a \hat{H}_u^b \hat{U}^c + y_d \hat{H}_d^a \hat{Q}^b \hat{D}^c + y_e \hat{H}_d^a \hat{L}^b \hat{E}^c\Big)}_{W_{\text{MSSM}}} - \epsilon_{ab}\lambda \hat{S} \hat{H}_d^a \hat{H}_u^b + \frac{1}{3}\kappa \hat{S}^3 \ . \quad (6.3)$$

The notation corresponds to the one of Section 4.2. The parameters κ and λ can have complex values. The cubic term in the singlet field is necessary in order to break the accidental Peccei-Quinn symmetry explicitly to avoid an axion in the spectrum, which would be very strongly constraint by cosmology [71]. A linear term in the singlet field and a quadratic term in the singlet field in the superpotential are not forbidden by $SU(3) \times SU(2) \times U(1)$ invariance. They are, however, unwanted as they need to be of the order of the SUSY scale and, would thereby introduce a similar problem as the

original μ-problem [264]. We, therefore, consider the simpler version of the NMSSM without these terms. The NMSSM Lagrangian in this form exhibits a discrete $\mathbb{Z}_3$ symmetry corresponding to invariance under a multiplication of all components of a chiral superfield by $e^{i\,2/3\pi}$. Note that the $\mathbb{Z}_3$ invariance leads to the so-called domain wall problem, for more details see *e.g.* Ref. [292].

In the following we assume y_u, y_d and y_e to be diagonal, neglecting any generation mixing. In such a case, they can always be chosen to be real as their phases can be absorbed into the quark fields. The soft-SUSY breaking part of the Lagrangian reads

$$\mathcal{L}^{\text{soft}}_{\text{NMSSM}} = \mathcal{L}^{\text{soft}}_{\text{MSSM}} - m_S^2|S|^2 + (\epsilon_{ab} A_\lambda \lambda S \phi_d^a \phi_u^b - \frac{1}{3} A_\kappa \kappa S^3 + h.c.)\,, \tag{6.4}$$

where the soft-SUSY breaking trilinear couplings A_λ and A_κ and the soft-SUSY breaking mass m_S in the NMSSM specific part have been introduced. The soft-SUSY breaking Lagrangian part $\mathcal{L}^{soft}_{MSSM}$ is given in Eq. (4.10). The $B\mu$ term of the MSSM is replaced by the λA_λ term of Eq. (6.4) and hence must be set to zero in $\mathcal{L}^{soft}_{MSSM}$ in Eq. (4.10). In the soft-SUSY breaking part of the Lagrangian the component fields, denoted without a hat, are used. All trilinear couplings in the soft-SUSY breaking Lagrangian can be complex valued, whereas among the soft-SUSY breaking masses, only the ones for the gaugino fields $\tilde{B}$, $\tilde{W}$ and $\tilde{G}$ can have a non-zero CP-violating phase. The kinetic and gauge parts of the Lagrangian cannot contain any phases. The only other source for CP-violating phases are relative phases between the Higgs boson fields. Expanding them around the VEVs yields

$$\begin{gathered}\phi_d = \begin{pmatrix} \frac{1}{\sqrt{2}}(v_d + h_d + i a_d) \\ h_d^- \end{pmatrix}\,, \qquad \phi_u = e^{i\varphi_u} \begin{pmatrix} h_u^+ \\ \frac{1}{\sqrt{2}}(v_u + h_u + i a_u) \end{pmatrix}\,, \\ S = \frac{e^{i\varphi_s}}{\sqrt{2}}(v_s + h_s + i a_s)\,,\end{gathered} \tag{6.5}$$

and one thus obtains two further phases φ_u and φ_s. In case of vanishing phases the neutral components h_i and a_i with $i = d,\ u,\ s$ correspond to the CP-even and CP-odd parts of the neutral components of ϕ_u, ϕ_d and S. The charged components are denoted by h_d^- and h_u^+, see also Section 4.2. Exploiting that the phases of the Yukawa couplings can be chosen arbritrarily, the phase of the up-type Yukawa coupling is set to $\phi_{y_u} = -\phi_u$ while the down-type and the charged lepton-type ones are assumed to be real. This corresponds to a field redefinition of the up-type fermion fields by a phase $\phi_u/2$ and leads to real values for the fermion masses. This phase is then reintroduced in some of the couplings of the fermions to other particles, such as the coupling of the up- and down-type quarks to the W bosons.

6.1.1. The Higgs sector at tree level

For non-vanishing VEVs v_u, v_d and v_s of the two Higgs doublet and the Higgs singlet fields the tadpole conditions must be fulfilled, which means that all terms linear in the Higgs field must vanish

$$t_\phi \equiv \left\langle \frac{\partial V_{\text{Higgs}}}{\partial \phi} \right\rangle = 0 \quad \text{for} \quad \phi = h_d, h_u, h_s, a_d, a_u, a_s. \tag{6.6}$$

By using that the complex parameters can be expressed by their absolute value and a phase, respectively, the only phase combinations appearing in the Higgs sector are

$$\varphi_x = \varphi_{A_\lambda} + \varphi_\lambda + \varphi_s + \varphi_u \,, \tag{6.7}$$
$$\varphi_y = \varphi_\kappa - \varphi_\lambda + 2\varphi_s - \varphi_u \,, \tag{6.8}$$
$$\varphi_z = \varphi_{A_\kappa} + \varphi_\kappa + 3\varphi_s \,. \tag{6.9}$$

The tadpole conditions for the CP-even components then read,

$$\begin{aligned} t_{h_d} =& \left[m_{H_d}^2 + \frac{M_Z^2 c_{2\beta}}{2} - v_s t_\beta \, |\lambda| \left(\frac{|A_\lambda|}{\sqrt{2}} c_{\varphi_x} + |\kappa| \, \frac{v_s}{2} c_{\varphi_y} \right) \right. \\ & \left. + |\lambda|^2 \left(\frac{2 s_\beta^2 M_W^2 s_W^2}{e^2} + \frac{v_s^2}{2} \right) \right] \frac{2 c_\beta M_W s_W}{e} \,, \end{aligned} \tag{6.10}$$

$$\begin{aligned} t_{h_u} =& \left[m_{H_u}^2 - \frac{M_Z^2 c_{2\beta}}{2} - \frac{|\lambda| \, v_s}{t_\beta} \left(\frac{|A_\lambda|}{\sqrt{2}} c_{\varphi_x} + |\kappa| \frac{v_s}{2} c_{\varphi_y} \right) \right. \\ & \left. + |\lambda|^2 \left(\frac{2 c_\beta^2 M_W^2 s_W^2}{e^2} + \frac{v_s^2}{2} \right) \right] \frac{2 s_\beta M_W s_W}{e} \,, \end{aligned} \tag{6.11}$$

$$\begin{aligned} t_{h_s} =& m_S^2 v_s - \left[s_{2\beta} |\lambda| \left(\frac{|A_\lambda|}{\sqrt{2}} c_{\varphi_x} + |\kappa| v_s c_{\varphi_y} \right) \right. \\ & \left. - |\lambda|^2 v_s \right] \frac{2 M_W^2 s_W^2}{e^2} + |\kappa|^2 v_s^3 + \frac{1}{\sqrt{2}} |A_\kappa| |\kappa| v_s^2 c_{\varphi_z} \,, \end{aligned} \tag{6.12}$$

and for the CP-odd components, they yield

$$t_{a_d} = \frac{M_W s_W s_\beta}{e} |\lambda| v_s \left(\sqrt{2} |A_\lambda| s_{\varphi_x} - |\kappa| v_s s_{\varphi_y} \right) \,, \tag{6.13}$$
$$t_{a_u} = \frac{1}{t_\beta} t_{a_d} \,, \tag{6.14}$$
$$t_{a_s} = \frac{2 M_W^2 s_W^2 s_{2\beta}}{e^2} |\lambda| \left(\frac{1}{\sqrt{2}} |A_\lambda| s_{\varphi_x} + |\kappa| v_s s_{\varphi_y} \right) - \frac{1}{\sqrt{2}} |A_\kappa| |\kappa| v_s^2 s_{\varphi_z} \,. \tag{6.15}$$

We have expressed the tadpole conditions directly in terms of the SM input parameters that we will use later on for the renormalization procedure. With the help of Eqs. (6.10–6.12) the soft-SUSY breaking masses m_{H_u}, m_{H_d} and m_S can be eliminated. The tadpole conditions t_{a_d} and t_{a_s} each eliminate one of the phase combinations in Eqs. (6.7–6.9)

and they lead to

$$c_{\varphi_x} = \pm\sqrt{1 - \frac{|\kappa|^2 v_s^2}{2|A_\lambda|^2} s_{\varphi_y}^2}\,, \tag{6.16}$$

$$c_{\varphi_z} = \pm\sqrt{1 - 18\frac{M_W^4 s_W^4 s_{2\beta}^2 |\lambda|^2}{e^4 |A_\kappa|^2 v_s^2} s_{\varphi_y}^2}\,, \tag{6.17}$$

with e denoting the electric charge. The tadpole condition for t_{a_u} does not lead to a new linear independent condition and can therefore not be used to eliminate any further parameters.[2] In the end, at tree level in the Higgs sector there is one phase left, namely the phase combination φ_y. Note that the signs in Eqs. (6.16, 6.17) are undetermined. They are additional input parameters. In general, however, not all of the possible sign combinations work for a specific parameter point.

The mass matrix for the neutral Higgs bosons can be obtained by collecting all bilinear terms of the Lagrangian. In a first step, a rotation $\mathcal{R}^G$ is performed in order to extract the Goldstone field G

$$\begin{aligned} &\Phi = (h_d, h_u, h_s, A, a_s, G)^T = \mathcal{R}^G (h_d, h_u, h_s, a_u, a_d, a_s)^T \\ &\text{with} \quad \mathcal{R}^G = \begin{pmatrix} \mathbb{1} & 0 \\ 0 & \mathcal{G} \end{pmatrix} \quad \text{and} \quad \mathcal{G} = \begin{pmatrix} s_{\beta_n} & c_{\beta_n} & 0 \\ 0 & 0 & 1 \\ c_{\beta_n} & -s_{\beta_n} & 0 \end{pmatrix}. \end{aligned} \tag{6.18}$$

At tree level the mixing angle is given by $\beta_n = \beta = \arctan v_u/v_d$. The thus obtained basis Φ needs to be rotated by another unitary transformation in order to obtain the mass eigenstates

$$\mathcal{R} M_{\Phi\Phi} \mathcal{R}^T = \text{diag}\Big((M_{H_1}^{(0)})^2, ..., (M_{H_5}^{(0)})^2, 0\Big) =: \mathcal{D}_H\,. \tag{6.19}$$

The diagonal matrix $\mathcal{D}_H$ is ordered in the masses, with M_{H_1} being the lightest Higgs boson mass. The subscript (0) always denotes the tree-level Higgs boson masses. The 6×6 Higgs boson mass matrix $M_{\Phi\Phi}$ in the basis Φ is given in Appendix C, directly written in terms of the input parameters used for the renormalization.

The charged Higgs boson mass matrix can be read from the Lagrangian $\mathcal{L} = (h_d^+, h_u^+) M_{h^+h^-} (h_d^-, h_u^-)^T$ and yields

$$M_{h^+h^-} = \frac{1}{2}\begin{pmatrix} t_\beta & 1 \\ 1 & \frac{1}{t_\beta} \end{pmatrix}\left[M_W^2 s_{2\beta} + |\lambda| v_s \left(\sqrt{2}|A_\lambda| c_{\varphi_x} + |\kappa| v_s c_{\varphi_y}\right) - 2|\lambda|^2 \frac{M_W^2 s_W^2}{e^2} s_{2\beta}\right]. \tag{6.20}$$

This mass matrix can be diagonalized by a rotation with the angle β_c, with $\beta_c = \beta$ at tree level. Thus, one obtains a vanishing mass for the charged Goldstone boson $G^\pm$ and a mass of

$$M_{H^\pm}^2 = M_W^2 + \frac{|\lambda| v_s}{s_{2\beta}}\left(\sqrt{2}|A_\lambda| c_{\varphi_x} + |\kappa| v_s c_{\varphi_y}\right) - 2|\lambda|^2 \frac{M_W^2 s_W^2}{e^2}\,, \tag{6.21}$$

[2] The reason is that the a_u and a_d states are rotated into the neutral Goldstone boson G and the CP-even Higgs boson interaction state A. In the basis of (A, G) there is only a tadpole condition for A.

for the charged Higgs boson $H^\pm$.

6.1.2. The neutralino and chargino sectors

In the NMSSM there exists an additional neutralino state compared to the four neutralinos of the MSSM, which is, in the interaction eigenstates, the superpartner of the scalar singlet, and will be named $\tilde{S}$ in the following. The other neutral components are the fermionic superpartners of the ϕ_u and ϕ_d fields, $\tilde{H}_u^0$ and $\tilde{H}_d^0$, the bino $\tilde{B}$ and the neutral component of the winos $\tilde{W}_3$. These particles can mix through a non-diagonal mass matrix, in the basis $\psi^0 = (\tilde{B}, \tilde{W}_3, \tilde{H}_d^0, \tilde{H}_u^0, \tilde{S})^T$,

$$M_N = \begin{pmatrix} M_1 & 0 & -c_\beta M_Z s_W & M_Z s_\beta s_W e^{-i\varphi_u} & 0 \\ 0 & M_2 & c_\beta M_W & -M_W s_\beta e^{-i\varphi_u} & 0 \\ -c_\beta M_Z s_W & c_\beta M_W & 0 & -\lambda \frac{v_s}{\sqrt{2}} e^{i\varphi_s} & -\frac{\sqrt{2} M_W s_\beta s_W \lambda e^{i\varphi_u}}{e} \\ M_Z s_\beta s_W e^{-i\varphi_u} & -M_W s_\beta e^{-i\varphi_u} & -\lambda \frac{v_s}{\sqrt{2}} e^{i\varphi_s} & 0 & -\frac{\sqrt{2} M_W c_\beta s_W \lambda}{e} \\ 0 & 0 & -\frac{\sqrt{2} M_W s_\beta s_W \lambda e^{i\varphi_u}}{e} & -\frac{\sqrt{2} M_W c_\beta s_W \lambda}{e} & \sqrt{2}\kappa v_s e^{i\varphi_s} \end{pmatrix}, \tag{6.22}$$

which needs to be diagonalized, in order to obtain mass eigenstates. The diagonalization of the mass matrix can be performed with the help of the unitary 5×5 matrix $\mathcal{N}$

$$\mathrm{diag}(m_{\tilde{\chi}_1^0}, m_{\tilde{\chi}_2^0}, m_{\tilde{\chi}_3^0}, m_{\tilde{\chi}_4^0}) = \mathcal{N}^* M_N \mathcal{N}^\dagger . \tag{6.23}$$

The fermionic superpartners of the charged Higgs bosons, $\tilde{H}_d^\pm$ and $\tilde{H}_u^\pm$, and of the charged components of the Winos $\tilde{W}^\pm = (\tilde{W}_1 \mp i\tilde{W}_2)/\sqrt{2}$, can be arranged into

$$\psi_R^- = \begin{pmatrix} \tilde{W}^- \\ \tilde{H}_d^- \end{pmatrix}, \quad \psi_L^+ = \begin{pmatrix} \tilde{W}^+ \\ \tilde{H}_u^+ \end{pmatrix} . \tag{6.24}$$

The mass term has the form $(\psi_R^-)^T M_C \psi_L^+ + h.c.$, with the chargino mass matrix

$$M_C = \begin{pmatrix} M_2 & \sqrt{2} s_\beta M_W e^{-i\varphi_u} \\ \sqrt{2} c_\beta M_W & \lambda \frac{v_s}{\sqrt{2}} e^{i\varphi_s} \end{pmatrix} . \tag{6.25}$$

The chargino mass matrix can be diagonalized with the help of two unitary matrices, U and V, as the left- and right-handed spinors are different. This leads to

$$\mathrm{diag}(m_{\tilde{\chi}_1^\pm}, m_{\tilde{\chi}_2^\pm}) = U^* M_C V^\dagger . \tag{6.26}$$

Again the mass eigenstates $\tilde{\chi}_i^\pm$ are mass-ordered. Note that the soft-SUSY breaking masses M_1 and M_2 in the neutralino/chargino sector can be complex. An R-symmetry, however, can be applied to rotate away either the phase of M_1 or M_2.[3]

[3]The R-symmetry assigns to fields and Grassmann coordinates a $U(1)$ charge [18]. As the R-symmetry transforms the different components of the super-field in a different way, the R-symmetry is broken, but it allows to rotate away a non-physical phase. It can be applied very similarly to the MSSM to rotate away *e.g.* the phase of M_2 [293, 294]. Additionally, to the assignments of Refs. [293, 294] the singlet field obtains a charge of 1/3 under R-symmetry.

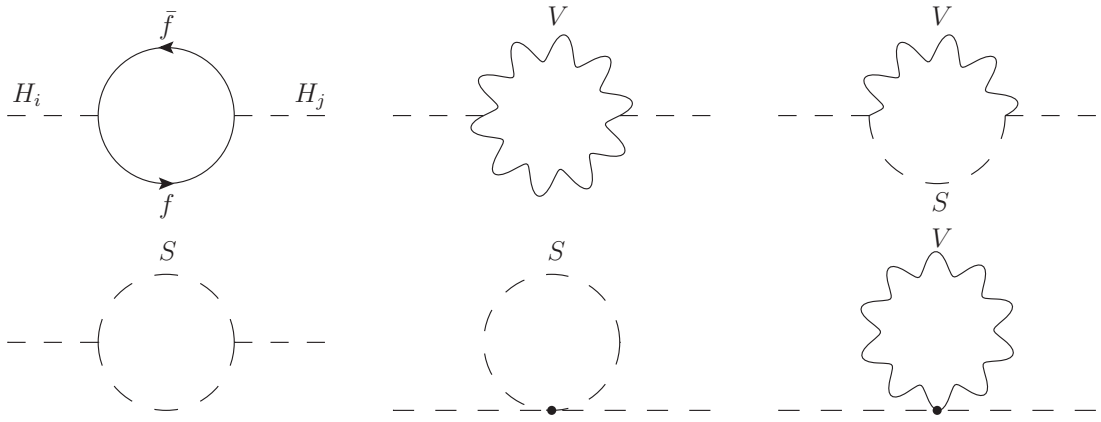

Figure 6.1.: Generic Feynman diagrams for the calculation of $\Sigma_{ij}(p^2)$. The label f generically stands for all contributing fermions, like the quarks, leptons and gauginos, and the ghost fields; the label V for vector bosons and the label S for the scalar particles, such as sfermions, Higgs bosons and Goldstone bosons.

6.2. Higgs boson masses at one loop

At one loop the Higgs boson mass gets corrections via loop contributions which contribute to the renormalized self-energy $\hat{\Sigma}_{ij}$ at momentum p. The self-energy diagrams are given by two-point functions for the two Higgs bosons i and j. Figure 6.1 shows the generic Feynman diagrams, for scalar loop particles S, vector bosons V and fermions f, where f generically also stands for the ghost contributions. All of these contributions are needed for the calculation of the unrenormalized self-energy $\Sigma_{ij}(p^2)$ with incoming momentum p. The renormalized self-energies $\hat{\Sigma}_{ij}$ are then given in terms of the unrenormalized ones and the counterterms by

$$\hat{\Sigma}_{ij}(p^2) = \Sigma_{ij}(p^2) + \frac{1}{2}p^2\left[\delta\mathcal{Z}^\dagger + \delta\mathcal{Z}\right]_{ij} - \frac{1}{2}\left[\delta\mathcal{Z}^\dagger\mathcal{D}_H + \mathcal{D}_H^\dagger\delta\mathcal{Z}\right]_{ij} - [\mathcal{R}\delta\mathcal{M}_{\Phi\Phi}\mathcal{R}^\dagger]_{ij}\,, \quad (6.27)$$

with $i,j = 1,...,6$ and $H_6 = G$ the Goldstone boson. The diagonalized mass matrix $\mathcal{D}_H$ was introduced in Eq. (6.19). The matrix $\delta\mathcal{M}_{\Phi\Phi}$ is the counterterm matrix, which needs to be introduced to renormalize the parameters appearing in the mass matrix given in Appendix C. The 6×6 wave-function renormalization constant matrix $\delta\mathcal{Z}$ is defined by

$$\delta\mathcal{Z} = \mathcal{R}\delta\mathcal{Z}_\Phi\mathcal{R}^\dagger \quad \text{with} \quad \Phi \to \left(\mathbb{1} + \frac{1}{2}\delta\mathcal{Z}_\Phi\right)\Phi\,, \qquad \delta\mathcal{Z}_\Phi = \mathcal{R}^G\delta\mathcal{Z}_\phi\mathcal{R}^{G\dagger}\,, \quad (6.28)$$

and

$$\delta\mathcal{Z}_\phi = \mathrm{diag}(\delta Z_{H_u},\, \delta Z_{H_d},\, \delta Z_S, \delta Z_{H_d},\, \delta Z_{H_u},\, \delta Z_S)\,. \quad (6.29)$$

Note that due to $SU(2)_L$ invariance, both CP-even and CP-odd current eigenstates of one multiplet have the same wave-function renormalization constant. The wave-

function renormalization constants can be calculated from the derivatives of the unrenormalized self-energies in the following way:

$$\delta Z_{H_d}(|\mathcal{R}_{i1}|^2 + |\mathcal{R}_{i4}\sin\beta + \mathcal{R}_{i6}\cos\beta|^2) + \delta Z_{H_u}(|\mathcal{R}_{i2}|^2 + |\mathcal{R}_{i4}\cos\beta - \mathcal{R}_{i6}\sin\beta|^2) + \delta Z_S(|\mathcal{R}_{i3}|^2 + |\mathcal{R}_{i5}|^2) = -\frac{\partial\Sigma_{ii}(p^2 = (M^{(0)}_{H_i})^2)}{\partial p^2}\Big|_{\text{div}} \quad \text{with} \quad i = 1,..,6\ . \tag{6.30}$$

The subscript 'div' means that we only take into account terms proportional to $\Delta = 2/(4-D) - \gamma_E + \ln 4\pi$ with γ_E denoting the Euler constant and D the number of dimensions. The value $D = 4$ characterizes the divergence. Note that these are six equations with three variables. We used the three equations of (6.30) with $i = 1, 2, 3$, but checked explicitly, that the others are also fulfilled. The mixing matrix element R_{i6} is zero if $i \neq 6$, leading to a simplification of the given Eqs. (6.30) for the considered cases. A $\overline{\text{DR}}$ scheme for the wave-function renormalization constants, as is used in Eqs. (6.30), is convenient, because it avoids the occurrence of unphysical threshold effects [295–297].

6.2.1. Renormalization of the parameters

As a first step in the renormalization of the Higgs boson mass matrix, one needs to define a parameter set that will be used throughout the calculation consistently. Instead of the original parameter set entering the Higgs potential, obtained from Eqs. (6.3, 6.4),

$$m^2_{H_d}, m^2_{H_u}, m^2_S, \varphi_{A_\kappa}, \varphi_{A_\lambda}, |A_\lambda|, g_1, g_2, v_u, v_d, v_s, \varphi_s, \varphi_u, |\lambda|, \varphi_\lambda, |\kappa|, \varphi_\kappa, |A_\kappa|\,, \tag{6.31}$$

the following parameters were used

$$\underbrace{t_{h_d}, t_{h_u}, t_{h_s}, t_{a_d}, t_{a_s}, M^2_{H^\pm}, M^2_W, M^2_Z, e}_{\text{on-shell}}, \underbrace{\tan\beta, v_s, \varphi_s, \varphi_u, |\lambda|, \varphi_\lambda, |\kappa|, \varphi_\kappa, |A_\kappa|}_{\overline{\text{DR}}}\,, \tag{6.32}$$

as the first parameters are "physical" quantities[4] for which physical on-shell renormalization conditions can be found. The transformation rules for going from the parameters given in Eq. (6.31) to the ones in Eq. (6.32) can be found in Appendix B. In the following the renormalization conditions for the parameters will shortly be discussed.

Tadpole parameters:

The renormalized tadpoles are obtained by replacing the unrenormalized ones by $t_\phi \to t_\phi + \delta t_\phi$ with $\phi = h_d, h_u, h_s, a_d, a_s$. The counterterm δt_ϕ is calculated from the one-loop irreducible tadpole diagrams T_{H_i} of the ith Higgs boson by requiring that the tadpole condition remains equal to zero at one loop,

$$\delta t_\phi = \mathcal{R}^\dagger T_{H_i}\,, \tag{6.33}$$

[4]Whether the tadpole parameters can be called physical quantities is debateable. Since their introduction is motivated by physical interpretation, we call in a slight abuse of language the renormalization conditions for the tadpoles on-shell.

with H_i denoting the Higgs boson mass eigenstates. Note that setting this condition at one loop, leads to a simplification of the calculation of the unrenormalized Higgs self-energies: no diagrams in Fig. 6.1 with tadpoles need to be taken into account as they are automatically set to zero.

Gauge boson masses M_W, M_Z and charged Higgs boson mass $M_{H^\pm}$:

By replacing the unrenormalized masses by $M^2 \to M^2 + \delta M^2$ the counterterms in the on-shell scheme are given by

$$\begin{aligned} \delta M_W^2 &= \widetilde{\mathrm{Re}}\, \Sigma^T_{WW}(p^2 = M_W^2)\,, \quad \delta M_Z^2 = \widetilde{\mathrm{Re}}\, \Sigma^T_{ZZ}(p^2 = M_Z^2)\,, \\ \delta M_{H^\pm}^2 &= \widetilde{\mathrm{Re}}\, \Sigma_{H^+H^-}(p^2 = M_{H^\pm}^2)\,. \end{aligned} \tag{6.34}$$

The index T denotes the transverse part of the unrenormalized gauge boson self-energy.

The electric charge e:

In order to obtain the renormalized electric charge, the bare charge is replaced by $e \to (1 + \delta Z_e)e$. The counterterm is defined in the Thomson limit, by requiring that the full $e^+e^-\gamma$ coupling for on-shell external particles and vanishing photon momentum is equal to the physical electric charge, leading to

$$\delta Z_e = \frac{1}{2}\frac{\partial \Sigma^T_{\gamma\gamma}(p^2 = 0)}{\partial p^2} + \frac{s_W}{c_W}\frac{\Sigma^T_{\gamma Z}(p^2 = 0)}{M_Z^2}\,. \tag{6.35}$$

Again, the index T denotes the transverse part of the gauge boson self-energy. Note that the sign between the unrenormalized self-energies $\Sigma_{\gamma\gamma}$ and $\Sigma_{\gamma Z}$ depends on the convention for the covariant derivative. For the convention used here, see Eq. (2.4).

The ratio of the vacuum expectation values $\tan\beta$

The bare $\tan\beta$ needs to be replaced by $\tan\beta \to \tan\beta + \delta\tan\beta$. The counterterm $\delta\tan\beta$ is obtained from

$$\delta\tan\beta = \frac{\tan\beta}{2}\left(\delta Z_{H_u} - \delta Z_{H_d}\right)\Big|_{\mathrm{div}}\,, \tag{6.36}$$

using a $\overline{\mathrm{DR}}$ condition to renormalize $\tan\beta$. There are several other options on how to renormalize $\tan\beta$ which all suffer either from gauge dependence, numerical instability or process dependence. As was pointed out in Ref. [298], the condition in Eq. (6.36) is a fair compromise, as it leads to numerically stable results, is process- and gauge-independent for the important class of R_ξ gauges. Note that the angle β also appears as the mixing angle of *e.g.* the charged Higgs boson mass matrix. As we do not renormalize the Higgs boson mixing matrices, since they will only get a finite contribution [297], the angles β need to be separated into the ones which stem from the ratio of the VEVs and the ones stemming from angles in the mixing matrices.

The vacuum expectation value v_s, the couplings λ and κ and the phases φ_u and φ_s:

In the bare Lagrangian these parameters need to be replaced in the following way:

$$\begin{aligned} v_s &\to v_s + \delta v_s\,, \quad \varphi_u \to \varphi_u + \delta\varphi_u\,, \quad \varphi_s \to \varphi_s + \delta\varphi_s\,, \\ \lambda &\to \lambda + \delta|\lambda| e^{i\varphi_\lambda} + i\lambda\delta\varphi_\lambda\,, \quad \kappa \to \kappa + \delta|\kappa| e^{i\varphi_\kappa} + i\kappa\delta\varphi_\kappa\,. \end{aligned} \tag{6.37}$$

In order to determine the above counterterms from the neutralino/chargino sector the counterterms of M_1 and M_2 have to be derived, even though not needed for the Higgs sector. They enter through the replacements of the bare mass parameters by

$$M_1 \to M_1 + \delta|M_1|e^{i\varphi_{M_1}} + iM_1\delta\varphi_{M_1}\,, \quad M_2 \to M_2 + \delta|M_2|e^{i\varphi_{M_2}} + iM_2\delta\varphi_{M_2}\,. \tag{6.38}$$

With the decomposition of the fermionic self-energy as in Eq. (5.14) for the renormalized self-energies $\hat{\Sigma}$ and the relations

$$\Big[m_{f,i}\Big(\widetilde{\mathrm{Re}}\,\hat{\Sigma}^L(p^2) + \widetilde{\mathrm{Re}}\,\hat{\Sigma}^R(p^2)\Big) + \widetilde{\mathrm{Re}}\,\hat{\Sigma}^l(p^2) + \widetilde{\mathrm{Re}}\,\hat{\Sigma}^r(p^2)\Big]_{ii} = 0\,, \tag{6.39}$$

$$\Big[m_{f,i}\Big(\widetilde{\mathrm{Re}}\,\hat{\Sigma}^L(p^2) - \widetilde{\mathrm{Re}}\,\hat{\Sigma}^R(p^2)\Big) - \widetilde{\mathrm{Re}}\,\hat{\Sigma}^l(p^2) + \widetilde{\mathrm{Re}}\,\hat{\Sigma}^r(p^2)\Big]_{ii} = 0\,, \tag{6.40}$$

derived from the renormalization conditions, with $m_{f,i}$ being the mass of either the ith chargino or neutralino, the following conditions for the charginos can be found

$$\begin{aligned}\mathrm{Re}(U^*\delta M_C V^\dagger)|_{\mathrm{div}} &= \frac{1}{2}\Big[m_{\tilde{\chi}_i^\pm}\Big(\Sigma^L_{\chi^+}(p^2) + \Sigma^R_{\chi^+}(p^2)\Big) + \Sigma^l_{\chi^+}(p^2) + \Sigma^r_{\chi^+}(p^2)\Big]_{ii}|_{\mathrm{div}} \\ &=: \mathrm{Re}\,\delta m_{\chi^+_{ii}}\,, \end{aligned} \tag{6.41}$$

$$\begin{aligned}\mathrm{Im}(U^*\delta M_C V^\dagger)|_{\mathrm{div}} &= \frac{i}{2}\Big[\Sigma^r_{\chi^+}(p^2) - \Sigma^l_{\chi^+}(p^2) + im_{\tilde{\chi}_i^\pm}(U^*\,\mathrm{Im}\delta Z_R^C U^T + V\,\mathrm{Im}\delta Z_L^C V^\dagger)\Big]_{ii}|_{\mathrm{div}} \\ &=: \mathrm{Im}\,\delta m_{\chi^+_{ii}}\,. \end{aligned} \tag{6.42}$$

For the neutralinos, one finds instead

$$\mathrm{Re}(\mathcal{N}^*\delta M_N\mathcal{N}^\dagger)_{ii}|_{\mathrm{div}} = \Big[m_{\tilde{\chi}_i^0}\Sigma^L_{\chi^0}(p^2) + \frac{1}{2}\Big(\Sigma^l_{\chi^0}(p^2) + \Sigma^r_{\chi^0}(p^2)\Big)\Big]_{ii}|_{\mathrm{div}} =: \mathrm{Re}\,\delta m_{\chi^0_{ii}}\,, \tag{6.43}$$

$$\begin{aligned}\mathrm{Im}(\mathcal{N}^*\delta M_N\mathcal{N}^\dagger)_{ii}|_{\mathrm{div}} &= \frac{i}{2}\Big[\Sigma^r_{\chi^0}(p^2) - \Sigma^l_{\chi^0}(p^2) + 2im_{\tilde{\chi}_j^0}(\mathcal{N}^*\mathrm{Im}\delta Z^N\mathcal{N}^\dagger)\Big]_{ii}|_{\mathrm{div}} \\ &=: \mathrm{Im}\,\delta m_{\chi^0_{ii}}\,, \end{aligned} \tag{6.44}$$

where we used that $\hat{\Sigma}^{L,R} = (\hat{\Sigma}^{L,R})^\dagger$ and $\hat{\Sigma}^l = (\hat{\Sigma}^r)^\dagger$. The imaginary parts of the field renormalization constants δZ^N, δZ_L^C and δZ_R^C can be chosen freely. For convenience we chose $\mathrm{Im}\,\delta Z^N = 0$, $\mathrm{Im}\,\delta Z_R^C = 0$ and $\mathrm{Im}\,\delta Z_L^C = 0$. The counterterm matrices δM_N and δM_C are derived from the mass matrices of the neutralinos in Eq. (6.22) and of the charginos in Eq. (6.26) by expanding them in the counterterms at one loop. For explicit formulae, see Ref. [33]. The chargino/neutralino sector provides fourteen equations for the eleven parameters. We use for the renormalization of v_s, λ, κ φ_u and φ_s a $\overline{\mathrm{DR}}$ scheme. Hence, it does not matter which of these equations are used. In principle, the counterterms could be taken directly from the Higgs sector. However, determining them from the chargino/neutralino sector provides an additional consistency check. The phases of the complex parameters determined from the chargino/neutralino sector turn out to get a vanishing counterterm. This behaviour was also noticed in Ref. [299] for the complex MSSM.

The absolute value A_κ

The bare A_κ needs to be replaced by $A_\kappa \to A_\kappa + \delta|A_\kappa|e^{i\varphi_{A_\kappa}} + i\delta\varphi_{A_\kappa}A_\kappa$, with φ_{A_κ} and $\delta\varphi_{A_\kappa}$ being substituted by the tadpole t_{a_s} and and its counterterm δt_{a_s}. The counterterm can then be derived from the Higgs boson self-energies with

$$\mathcal{R}_{i5}\mathcal{R}_{j5}\hat{\Sigma}_{ij}(M_{a_s a_s}) = 0 \quad \Leftrightarrow \quad \delta M_{a_s a_s} = \mathcal{R}_{i5}\mathcal{R}_{j5}\Sigma_{ij}(M_{a_s a_s}) \; . \tag{6.45}$$

The counterterm $\delta M_{a_s a_s}$ contains δA_κ. We renormalize A_κ in the $\overline{\text{DR}}$ scheme, meaning that only the divergent part is taken.

I have performed the calculation of all the self-energies and tadpoles with `FeynArts/FormCalc` [147–150] and derived the renormalization conditions. The results were checked by a second independent calculation [300].

6.2.2. Loop-corrected Higgs boson masses and mixing matrices

The squared one-loop corrected masses are extracted as the zeros of the determinant of the two-point function $\hat{\Gamma}$,

$$\hat{\Gamma}(p^2) = i\Big(\mathbb{1}\cdot p^2 - \mathcal{M}_{1\text{l}}\Big) \;\; \text{with} \;\; \Big(\mathcal{M}_{1\text{l}}\Big)_{ij} = \Big(M^{(0)}_{H_i}\Big)^2\delta_{ij} - \hat{\Sigma}_{ij}(p^2) \quad i,\, j = 1,\ldots,5 \; , \tag{6.46}$$

with the one-loop corrected Higgs boson mass matrix $\mathcal{M}_{1\text{l}}$ and the renormalized self-energy as given in Eq. (6.27). The Higgs boson masses at one loop are then calculated in an iterative procedure. We will exemplify the procedure here for the nth Higgs boson mass. In a first step, the momentum squared p^2 in Eq. (6.46) is set to the tree-level mass of the nth Higgs boson. The Higgs boson mass matrix $\mathcal{M}_{1l}$ is then diagonalized, with the nth eigenvalue being the input for p^2 in the next iteration step. As soon as the thus obtained Higgs boson mass does not change within a certain precision, for which we assumed 10^{-9}, the procedure ends and the one-loop corrected Higgs boson mass is given by the nth eigenvalue of the matrix $\mathcal{M}_{1\text{l}}$. This procedure is applied for all the $n = 1, ..., 5$ Higgs bosons. We did not include the Goldstone boson into this procedure but explicitly checked that the numerical result is basically unchanged, and that if the Goldstone boson is included, it gets a mass of zero. Furthermore, it was shown in Ref. [301] that it is sufficient to include the mixing with the neutral Goldstone boson. The inclusion of the mixing with the longitudinal Z boson and the Goldstone boson leads to the same result as only including the mixing with the Goldstone boson.

Note that with this procedure, we include terms beyond one-loop order, as through the calculation of the determinant of the Higgs boson mass matrix higher order terms occur. As discussed in Ref. [295] for the MSSM, this is justified by the fact, that these corrections improve the numerical accuracy of the one-loop corrections significantly, therefore this is called *improved one-loop corrections* in literature, see *e.g.* Ref. [295]. These corrections are the dominant ones, apart from the QCD corrections occurring at two-loop order. With the above described procedure, we can hence significantly improve the accuracy of the results.

We have compared our thus obtained results against other methods for the calculation of the Higgs boson mass of the renormalized two point function, as *e.g.* the $p^2 = 0$

approximation, where the one-loop corrected mass is obtained by diagonalizing $\mathcal{M}_{1l}$ after setting $p^2 = 0$. The numerical differences in the obtained loop-corrected masses were always acceptably small for the parameter points we checked.

The mixing matrix at one loop is determined as the matrix which diagonalizes the one-loop corrected Higgs boson mass matrix $\mathcal{M}_{1l}$ calculated at $p^2 = 0$. This procedure yields a unitary mixing matrix. Another possibility would be to follow Ref. [296], where the mixing matrices at one loop are calculated by finite wave-function renormalization factors for the MSSM. This procedure has the advantage that it guarantees the correct on-shell properties of the Higgs bosons. But the mixing matrix is not unitary anymore. We have extended this procedure to the case of a 5×5 Higgs boson mass matrix and checked the results that we obtained with the $p^2 = 0$ approximation against the thus obtained result. The results were numerically in good agreement, so that we stuck to the simpler and faster method, applying the $p^2 = 0$ approximation for the determination of the Higgs boson mixing matrix.

6.3. Higgs boson production and decays

In this section the Higgs boson production processes and Higgs boson decays, needed for the numerical analysis in the next section, are summarized. The second part of this section is based on Ref. [37]. The Higgs boson couplings will be generically denoted by g with an appropriate subscript throughout this section. Note that the couplings denoted by g are reduced couplings, the factors, which were factored out of the couplings, can be found in Appendix D.

6.3.1. Neutral Higgs boson production

Neutral Higgs bosons are dominantly produced at the LHC through the gluon fusion production process, followed by vector boson fusion (VBF), Higgs-strahlung off a vector boson (VH) and associated production with top quarks. The cross section for VBF, Higgs-strahlung and associated production with top quarks can be obtained from the known results of the MSSM, after adjusting the Higgs boson couplings. For the gluon fusion process, it is slightly more complicated, since the pseudoscalar and scalar contributions need to be combined. They do not interfere, as it can easily be seen from the Lorentz structure of the matrix elements. The LO gluon fusion cross section is given by

$$\sigma_{LO}(ggH_i) = \frac{M_{H_i}^2}{s} \int_{\tau=M_H^2/s}^1 \frac{dx}{x} f_g(x,\mu_F^2) f_g(\tau/x,\mu_F^2) \sigma_{H_i}^0 \,, \tag{6.47}$$

with the gluon PDFs, f_g, evaluated at the factorization scale μ_F and with

$$\sigma_{H_i}^0 = \frac{G_F \alpha_s^2(\mu)}{512\sqrt{2}\pi} \left(\left| \sum_{q=t,b} g_{H_i q\bar{q}}^S A_{1/2}^S(\tau_q) + g_{H_i \tilde{q}\tilde{q}} \frac{M_Z^2}{m_{\tilde{q}}^2} A_0(\tau_{\tilde{q}}) \right|^2 + 4 \left| \sum_{q=t,b} g_{H_i q\bar{q}}^P A_{1/2}^P(\tau_q) \right|^2 \right) , \tag{6.48}$$

where we defined $\tau_x = 4m_x^2/M_{H_i}^2$. The Fermi constant is denoted by G_F. We have set the scales to $\mu = \mu_F = M_{H_i}/2$. The loop-functions are given by

$$A_{1/2}^S(\tau) = 2\tau\Big[1 + (1-\tau)\, f(\tau)\Big]\,, \tag{6.49}$$

$$A_{1/2}^P(\tau) = \tau f(\tau)\,, \tag{6.50}$$

$$A_0(\tau) = -\tau\Big[1 - \tau f(\tau)\Big]\,, \tag{6.51}$$

with

$$f(\tau) = \begin{cases} \arcsin^2\left(\frac{1}{\sqrt{\tau}}\right) & \tau \geq 1\,, \\ -\frac{1}{4}\left[\ln\left(\frac{1+\sqrt{1-\tau}}{1-\sqrt{1-\tau}}\right) - i\pi\right]^2 & \tau < 1\,. \end{cases} \tag{6.52}$$

For the NMSSM the QCD corrections can be taken over from the MSSM. The NLO QCD corrections can be found in Refs. [302–306] in the LET approximation and with the full mass dependence in Refs. [307–309]. The full mass dependence on the squark masses was calculated in Ref. [310]. In the large top mass approximation the NNLO QCD corrections are given in Refs. [138, 311–314]. For the numerical computation, I have modified the publicly available code `HIGLU` [315] to adapt it to the complex NMSSM. The above described higher-order corrections are included in the numerical evaluation.

The NMSSM VBF and VH cross sections can easily be obtained from the respective SM cross sections by multiplying them with the appropriate modification factor:

$$\sigma(qqH_i/VH_i) = \left(\frac{g_{H_iVV}}{g_{HVV}^{SM}}\right)^2 \sigma^{SM}(qqH^{SM}/VH^{SM})\,, \tag{6.53}$$

where the coupling g_{H_iVV} can be found in Appendix D. The SM VBF cross section is taken into account at NLO QCD [127–129, 316] and was computed with the code `VV2H` [110]. The SM VH cross section is taken at NLO QCD [137, 316] and was calculated with the publicly available code `V2HV` [110]. Note that in supersymmetric theories the VBF and VH cross sections are always reduced compared to the SM, but summing over all Higgs bosons leads to the SM result due to the following sum rule of the Higgs boson to vector boson couplings

$$\sum_{i=1}^{5}\left(\frac{g_{H_iVV}}{g_{HVV}^{SM}}\right)^2 = 1\,. \tag{6.54}$$

Analogously to Higgs-strahlung and VBF, the cross section for Higgs production via associated production with a top quark pair can be obtained by modifying the Higgs boson to top quark coupling by

$$\sigma(H_i t\bar{t}) = \left(\frac{g_{H_it\bar{t}}}{g_{Ht\bar{t}}^{SM}}\right)^2 \sigma^{SM}(H^{SM}t\bar{t})\,. \tag{6.55}$$

The SM cross section is taken at NLO QCD, as provided in Ref. [317–320], from the LHC Higgs cross section working group homepage [321].

6.3.2. Higgs boson decays

The Higgs boson decays for both the real and the complex NMSSM are implemented in the publicly available code `NMSSMCALC` [37], which is based on `HDECAY` [223, 322, 323]. The implementation includes for the dominant decays higher order QCD corrections by adapting them from the MSSM case as given in `HDECAY`. For the decays of the neutral Higgs bosons into bottom quarks the SUSY-QCD corrections and the approximate SUSY-electroweak corrections are included. The decays into strange quarks include the dominant resummed SUSY-QCD corrections and the decays into a τ pair the resummed electroweak corrections.

Many Higgs boson decays can simply be obtained by adapting them from the MSSM by adjusting the couplings of the Higgs bosons. Some cases, especially in the complex NMSSM are more involved as the Higgs bosons are admixtures of CP-even and CP-odd components. The relevant two-body decays for the numerical analysis in this thesis, will therefore shortly be described here. For the Higgs boson off-shell decays we refer to the program code of `NMSSMCALC`. For Higgs boson decays into scalar particles or W and Z bosons the couplings simply need to be adjusted at tree level. QCD corrections can be taken over from the MSSM, electroweak corrections can, however, not be used. Higgs boson decays into fermions can be obtained at tree level from the real MSSM case by adding the scalar and the pseudoscalar decay widths of the real NMSSM, leading to

$$\Gamma_{H_i f\bar{f}} = \frac{G_F c_f}{4\pi\sqrt{2}} M_{H_i} m_f^2 \sqrt{1-4\left(\frac{m_f}{M_H}\right)^2}\left[\left(g^S_{H_i f\bar{f}}\right)^2\left(1-4\left(\frac{m_f}{M_H}\right)^2\right)+\left(g^P_{H_i f\bar{f}}\right)^2\right], \tag{6.56}$$

for $M_H > 2m_f$. For the decays into quarks we define $c_f = 3$, for the decays into the leptons $c_f = 1$. The reduced coupling $g^{S/P}_{H_i f\bar{f}}$ is given in Appendix D.

The decays of neutral Higgs bosons into gluons are mediated by loops of heavy quarks, with the dominant contribution coming from the heaviest quark, namely the top quark, and by squark loops. The decay widths are given by

$$\Gamma(H_i \to gg) = \frac{G_F \alpha_s^2 M_{H_i}^3}{64\sqrt{2}\pi^3}\left(\left|\sum_{q=t,b,c} g^S_{H_i q\bar{q}} A^S_{1/2}(\tau_q) + \sum_{\tilde{q}} \frac{M_Z^2}{m_{\tilde{q}}^2} g_{H_i\tilde{q}\tilde{q}} A_0(\tau_{\tilde{q}})\right|^2 + 4\left|\sum_{q=t,b,c} g^P_{H_i q\bar{q}} A^P_{1/2}(\tau_q)\right|^2\right), \tag{6.57}$$

with the loop functions in Eqs. (6.51) and the coupling conventions in Appendix D. The sum over $\tilde{q}$ includes all squark mass eigenstates. The QCD corrections are included in `NMSSMCALC` up to N^{3}LO in the limit of heavy quark masses [302, 306, 308, 324–330]. The squark loops were taken at NLO QCD in the limit of heavy squark masses [331].

The Higgs decays into photons are mediated by loops of top, bottom and charm quarks, τ leptons and squarks, sleptons, charginos, charged Higgs bosons and W bosons. The largest contribution stems from the W boson loops. The decay widths within the

complex NMSSM are then given by

$$\Gamma(H_i \to \gamma\gamma) = \frac{G_F \alpha^2 M_{H_i}^3}{128\pi^3\sqrt{2}} \left(\left| \sum_f c_f e_f^2 \, g^S_{H_i f\bar{f}} A^S_{1/2}(\tau_f) + \sum_{\tilde{\chi}_j^\pm} \frac{M_W}{M_{\tilde{\chi}_j^\pm}} g^S_{H_i \tilde{\chi}_j^+ \tilde{\chi}_j^-} A^S_{1/2}(\tau_{\tilde{\chi}_j^\pm}) \right. \right.$$
$$\left. + g_{H_i WW} A_1(\tau_W) + \frac{M_Z^2}{2M_{H^\pm}^2} g_{H_i H^+ H^-} A_0(\tau_{H^\pm}) + \sum_{\tilde{f}} c_f e_f^2 \frac{M_Z^2}{m_{\tilde{f}}^2} \, g_{H_i \tilde{f}\tilde{f}} A_0(\tau_{\tilde{f}}) \right|^2$$
$$\left. + 4 \left| \sum_f c_f e_f^2 \, g^P_{H_i f\bar{f}} A^P_{1/2}(\tau_f) + \sum_{\tilde{\chi}_j^\pm} \frac{M_W}{M_{\tilde{\chi}_j^\pm}} g^P_{H_i \tilde{\chi}_j^+ \tilde{\chi}_j^-} A^P_{1/2}(\tau_{\tilde{\chi}_j^\pm}) \right|^2 \right) , \tag{6.58}$$

with $f = t, b, c, \tau$ and $\tilde{f} = \tilde{q}, \tilde{\tau}_1, \tilde{\tau}_2$. With $\tilde{q}$ we denote all squark mass eigenstates and $c_f = 3$, 1 denotes the colour factor of the (s)quarks and the (s)tau. The loop functions for $A^{S,P}_{1/2}$ and A_0 can be found in Eq. (6.51). The loop function A_1 is given by

$$A_1(\tau) = -\left[2 + 3\tau + 3\tau(2-\tau) f(\tau)\right] , \tag{6.59}$$

with $f(\tau)$ as defined in Eq. (6.52). The QCD corrections for the quark [326, 332–337] and squark loops [310] can be taken over from the MSSM.

For the loop-induced process $H \to Z\gamma$, the determination of the tree-level decay width proceeds analogously to the Higgs decays into photons and it is not needed for the analysis of the Higgs boson masses in the next section, as due to its smallness it will only affect the total decay width in a negligible manner. Hence it will not be given here explicitly, but it can be found in the program code of `NMSSMCALC`. As part of this thesis, I have provided cross checks for all the Higgs boson couplings, the above described Higgs boson decays and various other decays in the implementation of the complex NMSSM in the code `NMSSMCALC`.

6.4. Numerical analysis

The numerical analysis of the Higgs boson masses in the complex NMSSM was done with a self-written `Mathematica` [338] code using the `LOOPTOOLS` [148, 149] library. A slightly different implementation but based on the described work is publicly available as part of a `FORTRAN` code in `NMSSMCALC` [37, 291]. The latter is adapted to the SUSY Les Houches 2 (SLHA2) convention [224]. In the SLHA2 convention the complex parameters are split into real and imaginary parts, and not into absolute value and phase. This leads to a numerically slightly different result. For the numerical results in this section, the renormalization procedure as described in this chapter was used.

For the numerical values of the input parameters we follow the SLHA [339] and compute the parameters M_W^2 and e from the SLHA pre-defined input values for the Fermi constant $G_F = 1.16637 \cdot 10^{-5}$ GeV^{-2}, the Z boson mass $M_Z = 91.187$ GeV and the electroweak coupling $\alpha = 1/137$. If not stated otherwise, we use the running $\overline{\text{DR}}$ top quark mass m_t at the scale $Q = \sqrt{m_{\tilde{Q}_3} m_{\tilde{t}_R}}$, with $m_{\tilde{Q}_3}$ and $m_{\tilde{t}_R}$ denoting the soft-SUSY

breaking masses of the third generation squarks, obtained from the top quark pole mass $m_t = 173.2$ GeV by taking the routines for the renormalization group running of the parameters of `NMSSMTools` [340–342]. All other parameters were evolved to this scale with `NMSSMTools` as well. In the same way we obtain the running $\overline{\text{DR}}$ bottom quark mass starting from the SLHA input value $m_b(m_b)^{\overline{\text{MS}}} = 4.19$ GeV. For the light quarks we chose $m_u = 2.5$ MeV, $m_c = 1.27$ GeV, $m_d = 4.95$ MeV, $m_s = 101$ MeV and for the τ lepton mass $m_\tau = 1.777$ GeV.

For the analysis of the Higgs boson masses a scenario needs to be found which fulfills the phenomenological constraints. To begin with, we require the most SM-like Higgs boson to have a mass value close to the measured value. Due to the experimental and theoretical uncertainties on the Higgs boson mass, the Higgs boson mass window is chosen to be

$$120 \text{ GeV} < M_{H_i}^{SM-like} < 130 \text{ GeV}\,. \tag{6.60}$$

Additionally, the Higgs rates should be SM-like, meaning we demanded for the significance of the SM-like Higgs boson to lie within 20% of the value for the significance of the SM Higgs boson with the same mass. The significance was been estimated to be given by $S = N_s/\sqrt{N_b}$, where N_s denotes the number of signal events and N_b the number of background events, to be within a window of $\pm 20\%$ compared to the SM, for the most SM-like Higgs boson with a mass in the interval given in Eq. (6.60). This in the end leads to the criterion

$$0.8\sigma_{tot}^{SM} < \sigma_{tot}^{NMSSM} < 1.2\sigma_{tot}^{SM}\,, \tag{6.61}$$

with

$$\begin{aligned}\sigma_{tot} = &\Big(\sigma(ggH_i) + \sigma(qqH_i) + \sigma(WH_i) + \sigma(ZH_i) + \sigma(t\bar{t}H_i)\Big) \\ &\Big[BR(H \to \gamma\gamma)^2 + 16BR(H \to W^+W^-)^2 BR(W^+ \to \bar{\ell}\nu_l)^2 BR(W^+ \to \ell\bar{\nu}_l)^2 \\ &+16BR(H \to ZZ)^2 BR(Z \to \ell\ell)^2 BR(Z \to \ell\ell)^2\Big]\,.\end{aligned} \tag{6.62}$$

In σ_{tot}, the NMSSM value is calculated with the cross sections and branching ratios of the most SM-like Higgs boson, hence $H_i = H^{SM-like}$. For σ_{tot}^{SM} the cross sections and branching ratios are given by the values obtained in the SM with a mass of the SM Higgs boson equal to the mass of the NMSSM Higgs boson in σ_{tot}^{NMSSM}, *i.e.* $M_H = M_{H_i}^{SM-like}$. I performed this check of the compatibility with the Higgs results by computing the cross sections and branching ratios as outlined in Section 6.3.[5] The branching ratios of the vector boson decays into lepton final states were taken to be

$$BR(W^+ \to \ell\bar{\nu}_l) = 0.108\,, \quad BR(Z \to \ell\ell) = 0.0366\,. \tag{6.63}$$

Note that in the analysis only the Higgs boson discovery channels, *i.e.* $\gamma\gamma$, $\ell\bar{\ell}\ell\bar{\ell}$ with $\ell = e$, μ and $\ell\bar{\nu}_l\bar{\ell}\nu_l$, are included, as at the time of the analysis in June 2012 an evidence of a Higgs boson was only seen in these channels. Our results here are based on the 7 TeV

[5] The Higgs boson branching ratios were calculated with the help of an early version of `NMSSMCALC`.

run of the LHC, denoted in the following by LHC7. Furthermore, we have checked whether one of the non-SM like Higgs bosons is excluded by the searches at LHC, LEP [343, 344] or TEVATRON [345][6], with the program `HiggsBounds` [346, 347]. Again these bounds were taken from the data available in June 2012. The main intention of this section is to show the importance of the one-loop corrections for the Higgs boson mass calculation and to study the influence of the CP-violating phases on the Higgs mass predictions at one loop. The findings presented here will not change qualitatively by taking into account the newer, now available data.

For a numerical study, we started out from some of the benchmark points given in Ref. [348], but modified them a bit. All the points lead to the correct relic density in the limit of the real NMSSM, as we checked with `MicrOMEGAs` [342]. All the scenarios are taken with the parameters evolved to the scale $Q = \sqrt{m_{\tilde{t}_R} m_{\tilde{Q}_3}}$ and with the soft-SUSY breaking parameters of the sleptons and the up, down, charm, strange and bottom squarks given by

$$\begin{aligned} & m_{\tilde{U}} = m_{\tilde{D}} \;=\; m_{\tilde{Q}_{1,2}} \;=\; m_{\tilde{E}} \;=\; m_{\tilde{L}} \;=\; 1 \text{ TeV}\,, \\ & A_x = 1 \text{ TeV} \qquad (x = u, c, d, s, e, \mu, \tau)\,, \\ & A_b \approx 1 \text{ TeV}\,. \end{aligned} \tag{6.64}$$

This leads to masses of the the sleptons and the squarks of the first and second generation of ~ 1 TeV. At the time of the analysis, these values were still allowed by the direct searches for squarks and sleptons.

6.4.1. Scenario 1: SM-like H_3

The parameter set for this scenario is given by

$$\begin{aligned} & |\lambda| = 0.72\,, \quad |\kappa| = 0.20\,, \quad \tan\beta = 3\,, \quad M_{H^\pm} = 629 \text{ GeV}\,, \quad |A_\kappa| = 27 \text{ GeV} \\ & |\mu| = 198 \text{ GeV}\,, \quad |A_b| = 963 \text{ GeV}\,, \quad |A_t| = 875 \text{ GeV}\,, \quad M_1 = 145 \text{ GeV}\,, \\ & M_2 = 200 \text{ GeV}\,, \quad M_3 = 600 \text{ GeV}\,. \end{aligned} \tag{6.65}$$

The parameters λ and κ cannot be chosen too high in order to keep them perturbative up to the GUT scale. In Ref. [349] an upper bound of

$$\lambda^2 + \kappa^2 \lesssim 0.5 \tag{6.66}$$

for λ and κ at the electroweak scale was given. Note that the bound in Eq. (6.66) is only a rough guideline. The actual bound also depends on $\tan\beta$. In Ref. [348], it was also shown that our parameter choice of λ and κ in Eq. (6.65) is still perturbative up to the GUT scale with extra matter above the TeV-scale, which would influence the analysis here in no other way. For the analysis we set all CP-violating phases to zero

[6] We only gave the references for the most stringent bounds at the time of our analysis. More references can be found in the manual of `HiggsBounds` [346, 347] for version 3.8.0.

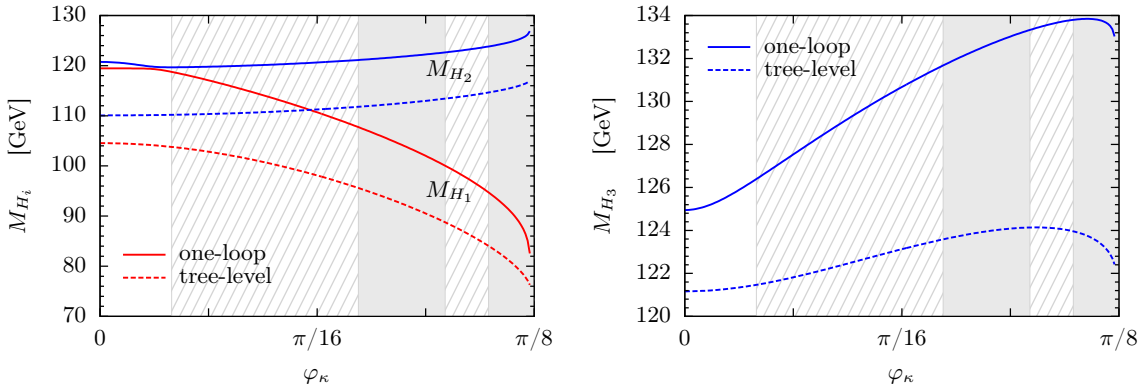

Figure 6.2.: *Left:* Tree-level (dashed) and one-loop corrected (full) Higgs boson masses for H_1 (red) and H_2 (blue) as a function of φ_κ. *Right:* Tree-level (dashed) and one-loop (full) mass, M_{H_3}, of the most SM-like Higgs boson in the CP-conserving limit as a function of φ_κ. The exclusion region due to LEP, Tevatron and LHC7 data is shown as a gray area, the region with the SM-like Higgs boson not being compatible with an excess of data around 125 GeV as dashed area. These plots are already published in Ref. [33].

and subsequently turn on specific phases to study their respective influence. The signs of the tree-level CP-violating phases in Eqs. (6.16, 6.17) are chosen as

$$\text{sign } \cos\varphi_x = +1\,, \qquad \text{sign } \cos\varphi_z = -1\,. \tag{6.67}$$

The left- and right-handed soft-SUSY breaking mass parameters in the stop sector are given by $m_{\tilde{Q}_3} = 490$ GeV and $m_{\tilde{t}_R} = 477$ GeV, leading to relatively light stop masses $m_{\tilde{t}_1} = 363$ GeV and $m_{\tilde{t}_2} = 616$ GeV. Newest ATLAS and CMS searches for stops restrict masses in that region significantly, see *e.g.* Refs. [350, 351]. In this scenario, in the limit of CP-conservation, the one-loop corrected H_3 plays the role of the SM-like Higgs boson with a mass $M_{H_3} = 125$ GeV compatible with present LHC searches. In the following we discuss for various complex phase choices the phenomenology of the three lightest Higgs bosons. The two heavier ones receive mass corrections of maximally 2 GeV leading to masses of ~ 642 GeV so that they were not excluded by collider searches in June 2012, with H_4 being mostly CP-odd and H_5 mostly CP-even. Their masses are not displayed in the plots.

In a first example, we discuss CP-violation occuring already at tree level by varying the phase φ_κ and, through this the phase φ_y which is the only relevant phase combination at tree level. The value of φ_κ is not restricted by EDMs, as it leaves the phase entering the prediction of the EDMs unchanged [287]. Note that by varying φ_κ also the phases φ_{A_κ} and φ_{A_λ} are varied in order to fulfill the tadpole conditions. They are, however, not taken as input parameters here.

In Fig. 6.2 (left plot) the tree-level and one-loop masses of the two lightest Higgs boson mass eigenstates $H_{1,2}$ are shown as a function of φ_κ. The limit $\varphi_\kappa = 0$ corresponds to the real NMSSM. The phase can only be varied up to a value of $\pi/8$, since for higher values the tadpole conditions, Eqs. (6.10–6.15), do not give valid solutions for

the phases φ_x and φ_z anymore, since they become complex. The tree-level and one-loop corrected masses of the SM-like H_3 are shown in Fig. 6.2 (right plot). The gray areas in the plots are the ones which are excluded by the searches for the other Higgs boson by either LEP, LHC7 or Tevatron. As described above we obtained them with `HiggsBounds`. This excludes the regions $0.074\,\pi < \varphi_\kappa < 0.099\,\pi$ and $\varphi_\kappa > 0.112\,\pi$. Again, these exclusions were obtained in June 2012 and do not correspond to the newest LHC results. The dashed region marks the parameter region where the criterion of compatibility with the Higgs excess around 125 GeV stated in Eq. (6.61) cannot be fulfilled anymore. The dashed region starts at $\varphi_\kappa > 0.021\pi$. As can be seen from Fig. 6.2 the one-loop corrections to the Higgs boson mass are very important. For this example they are up to 15 GeV for the two lightest Higgs boson. For the third lightest Higgs boson, for $\varphi_\kappa = 0$, they are about 4 GeV, but for larger values of φ_κ they can become more important. It can also be seen that indeed both at tree level and at one loop the Higgs boson masses are sensitive to a variation of φ_κ. At one loop even the slope of the curves can change compared to the tree-level curve, as *e.g.* for M_{H_3} in the right plot of Fig. 6.2.

In order to have a measure for the CP-violation we define ($i = 1, 2, 3$)

$$r^i_{\rm CP} \equiv (\mathcal{R}_{i1})^2 + (\mathcal{R}_{i2})^2 + (\mathcal{R}_{i3})^2 \,, \tag{6.68}$$

with $r^i_{CP} = 1$ for a completely CP-even Higgs boson and $r^i_{CP} = 0$ for a completely CP-odd Higgs boson. The CP-even singlet component of the Higgs bosons is given by $\mathcal{R}_{i3}$. In Fig. 6.3, the amount of CP-violation as a function of φ_κ is shown in the left plot, while the right plot displays the CP-even singlet component squared. It can be inferred from the plots that for $\varphi_\kappa = 0$ the lightest Higgs boson is CP-even but mostly singlet like, whereas the second lightest Higgs boson is CP-odd. Both the lightest and the second lightest Higgs bosons interchange their roles at $\varphi_\kappa \sim 0.02$. The most SM-like Higgs boson is, for $\varphi_\kappa = 0$, a CP-even state with no singlet component. For increasing values of φ_κ it becomes a CP-mixed state, which is then excluded at the LHC by not showing a SM-like signature anymore.

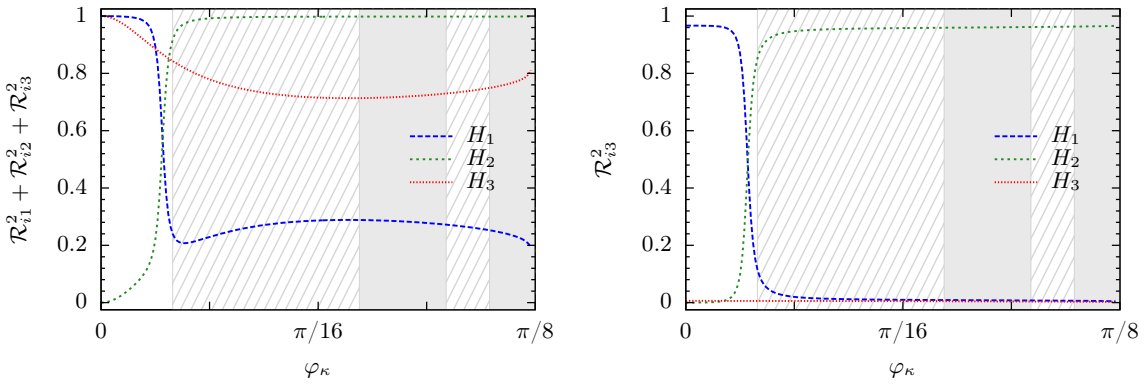

Figure 6.3.: The amount of CP violation $r^i_{\rm CP}$ for H_i ($i = 1, 2, 3$) as a function of φ_κ (left plot). The amount of CP-even singlet component $(\mathcal{R}_{i3})^2$ as a function of φ_κ (right plot). This figure is already published in Ref. [33].

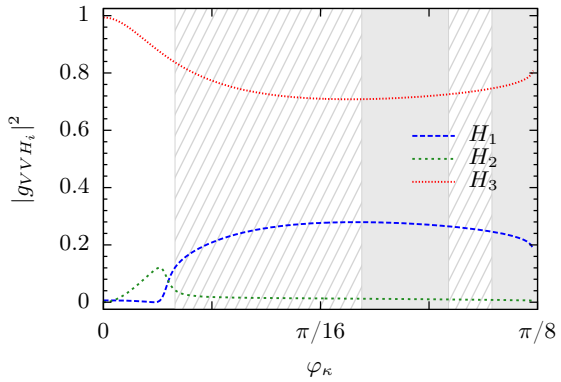

Figure 6.4.: The H_i coupling to V ($V = Z, W$) bosons squared ($i = 1, 2, 3$) normalized to the SM coupling, $|g_{VVH_i}|^2$, as a function of φ_κ. This plot is published in Ref. [33].

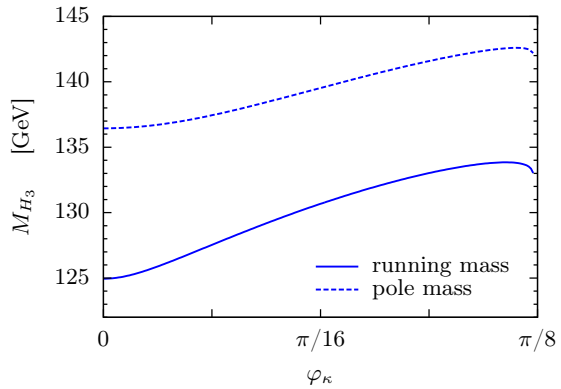

Figure 6.5.: The one-loop corrected mass of the SM-like Higgs H_3 evaluated with the top and bottom running $\overline{\text{DR}}$ masses (full) and with the corresponding pole masses (dashed). This figure is already published in Ref. [33].

Finally, Fig. 6.4 shows the coupling squared of the Higgs bosons to the V bosons ($V = Z, W$), normalized to the SM as a function of φ_κ. The vector bosons couple only to the CP-even, non-singlet components of the Higgs bosons.

In order to get an estimate of the theoretical uncertainty due to the unknown higher-order corrections, the one-loop corrections to the Higgs boson masses calculated with the top and bottom pole masses, $m_t = 173.2$ GeV and $m_b = 4.88$ GeV, are compared to the results for the one-loop corrected masses evaluated with the running $\overline{\text{DR}}$ top and bottom quark masses $m_{t,b}$ at the scale $Q = \sqrt{m_{\tilde{Q}_3} m_{\tilde{t}_R}}$. In this scenario they are $m_t = 153.4$ GeV and $m_b = 2.55$ GeV. The result can be found in Fig. 6.5. The absolute values of the corrections change quite a bit and are larger for higher top quark masses. The slope of the curve is, however, in both cases nearly the same. The theoretical uncertainty due to the different quark mass renormalization schemes can then conservatively be estimated to be about 10%.

In the previous example, the dependence of the Higgs boson masses on a CP-violating phase which enters the Higgs sector at tree level was discussed. It is, however, possible

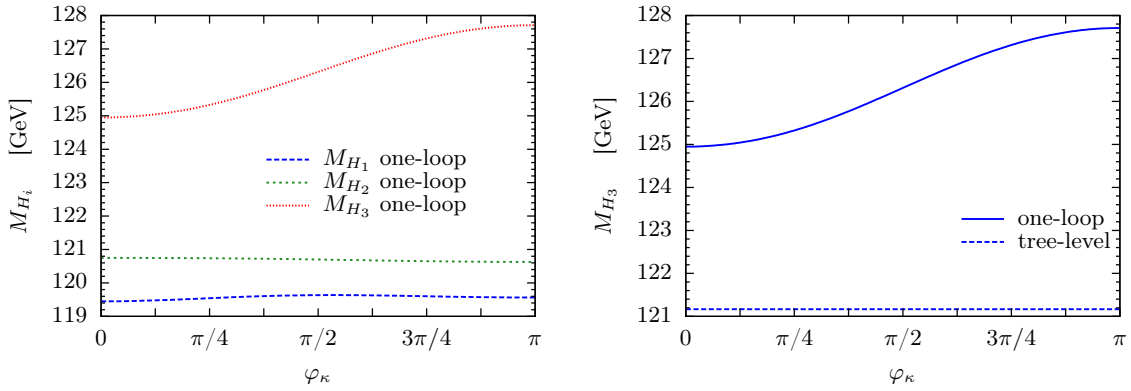

Figure 6.6.: One-loop corrected Higgs boson masses M_{H_i} $(i = 1, 2, 3)$ as a function of $\varphi_\kappa = \varphi_\lambda$ (left plot). Tree-level (dashed) and one-loop corrected (full) mass for H_3 as a function of $\varphi_\kappa = \varphi_\lambda$ (right plot). These plots are already published in Ref. [33].

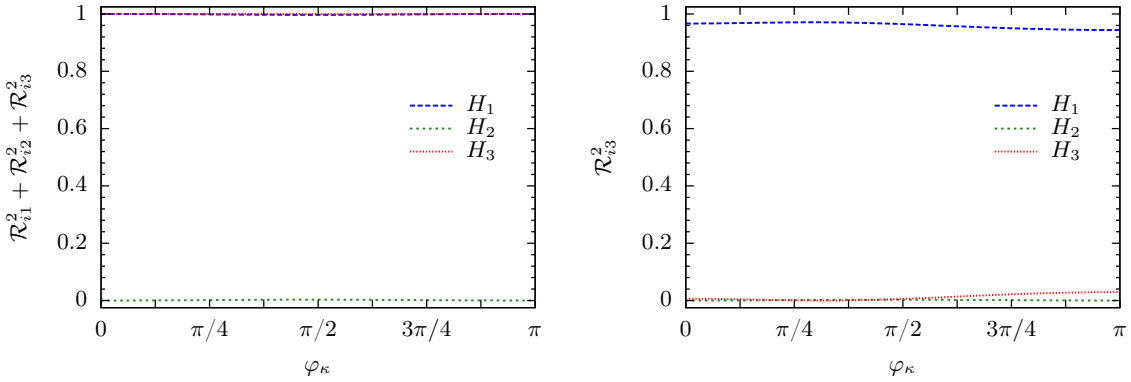

Figure 6.7.: The amount of CP violation $r^i_{\rm CP}$ for H_i $(i = 1, 2, 3)$ as a function of $\varphi_\kappa = \varphi_\lambda$ (left). The amount of CP-even singlet component $(\mathcal{R}_{i3})^2$ as a function of $\varphi_\kappa = \varphi_\lambda$ (right). This figure is already published in Ref. [33].

that the phases only enter at one-loop level. In order to explore this possibility we vary the phase φ_κ by an equal amount as the phase φ_λ in order to keep the phase φ_y constant such that CP-violation is only introduced radiatively. Figure 6.6 (left plot) shows the one-loop corrected masses of the three lightest Higgs states $H_{1,2,3}$ as a function of $\varphi_\kappa = \varphi_\lambda$. In Fig. 6.6 (right plot) a comparison between the tree-level and one-loop corrected mass of the SM-like Higgs boson H_3 is provided. The tree-level mass shows, of course, no dependence on φ_κ. The one loop mass M_{H_3} changes by only ~ 3 GeV for φ_κ varying from 0 to π, and the loop-corrected masses for $H_{1,2}$ show almost no dependence on the CP-violating phase. The reason is the following: the main correction to the Higgs boson masses stem from the top squarks. The phase φ_λ enters the stop quark mass matrix. The third lightest Higgs boson H_3 has the largest h_u component and therefore has a large coupling to up-type quarks and squarks. Therefore, it is most sensitive to a change in the top squark masses. For M_{H_1} (M_{H_2}) the mass corrections are of about 15 (11) GeV. With mass values around 120 GeV they could lead to additional signals at the LHC if they were SM-like. In the left plot of

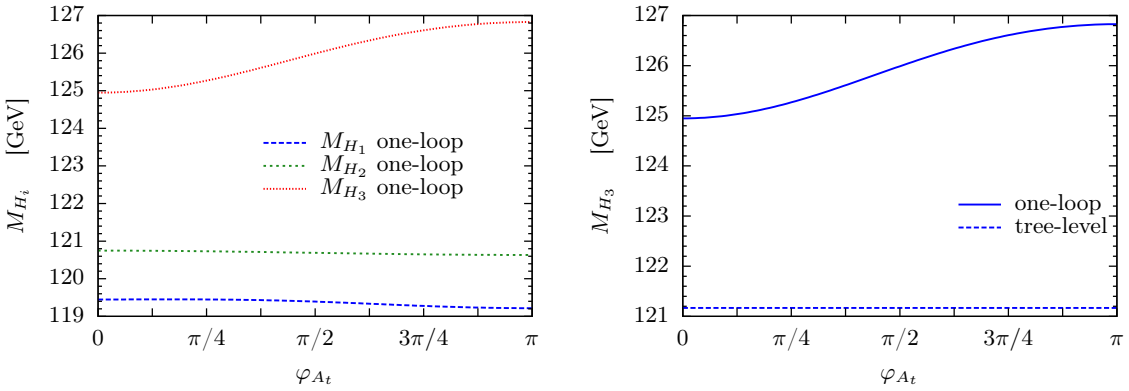

Figure 6.8.: One-loop corrected Higgs boson masses M_{H_i} $(i = 1, 2, 3)$ as a function of φ_{A_t} (left). Tree-level (dashed) and one-loop (full) mass M_{H_3} as a function of φ_{A_t} (right). These plots are already published in Ref. [33].

Fig. 6.7 the amount of CP-violation of H_1, H_2, H_3 is shown, whereas the right plot shows the CP-even singlet component squared. With their masses around 120 GeV the two lightest Higgs boson are within the discovery region of the LHC. However, due to the CP-odd nature of H_2 and the singlet character of H_1, the signals are considerably reduced. The whole shown region for the variation of $\varphi_\kappa = \varphi_\lambda$ was hence still allowed in June 2012.

Another possibility to study radiatively induced CP-violation is to vary a phase of a parameter which only enters at loop level, such as the phases of the trilinear couplings A_t, A_b or A_τ or the soft-SUSY breaking gaugino masses M_1 or M_2. The gaugino mass M_3 enters only at two-loop level and is therefore not relevant here. The effects of the phase φ_{M_3} were though studied for the MSSM in *e.g.* Ref. [297], showing that they can be quite significant. The largest effect here is to be expected from a variation of A_t, as the stop sector gives the most important contributions to the Higgs boson mass corrections at one loop. We thus restrict ourselves to study this case.

Figure 6.8 shows in the left plot the one-loop corrected masses for H_1, H_2, H_3 as a function of φ_{A_t}. The right plot in Fig. 6.8 compares the tree-level (dashed line) and the one-loop mass (solid line) of H_3. Again, M_{H_1} and M_{H_2} show barely any dependence on φ_{A_t} because of the same argument as given before. The mass M_{H_3} varies over the given range of φ_{A_t} by 2 GeV. In Fig. 6.9 the Higgs boson mass of H_3 is shown for different values of the renormalization scale. The blue long-dashed line is for the renormalization scale $\mu_{ren} = 250$ GeV. The green short dashed line corresponds to our standard choice of $\mu_{ren} = Q = 500$ GeV and the red dotted line corresponds to $\mu_{ren} = 1000$ GeV. The uncertainty due to unknown higher order corrections can then be estimated to be of $\mathcal{O}(4\%)$. This might, however, underestimate the uncertainty slightly, as we only renormalized part of the parameters in a $\overline{\text{DR}}$ scheme. The on-shell renormalized counterterms do not show any dependence on the renormalization scale. Checking the dependence of the Higgs boson mass corrections on the renormalization scheme of the quark masses by using either pole or running masses might in this case give a more realistic picture of the theoretical uncertainty. As mentioned before in

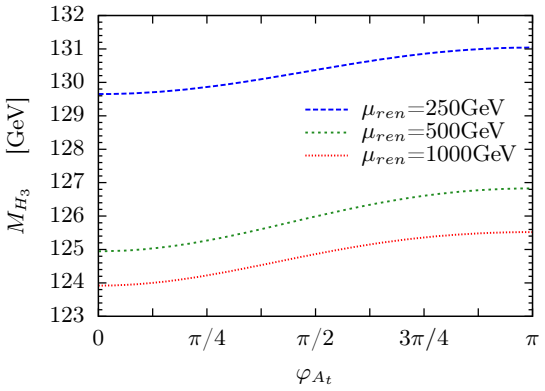

Figure 6.9.: One-loop corrected Higgs boson masses M_{H_3} as a function of φ_{A_t} for three different renormalization scales, $\mu_{ren} = 250$ (blue/long-dashed), 500 (green/short-dashed) and 1000 GeV (red/dotted). This plot is already published in Ref. [33].

Fig. 6.5 this leads to an estimate of the uncertainty of 10%.

6.4.2. Scenario 2: SM-like H_1 or H_2

In this scenario the following parameter set was chosen

$$\begin{aligned} &|\lambda| = 0.65\,, \quad |\kappa| = 0.25\,, \quad \tan\beta = 3\,, \quad M_{H^\pm} = 619 \text{ GeV}\,, \quad |A_\kappa| = 18 \text{ GeV}\,, \\ &|\mu| = 199 \text{ GeV}\,, \quad |A_b| = 971 \text{ GeV}\,, \quad |A_t| = 1143 \text{ GeV}\,, \quad M_1 = 105 \text{ GeV}\,, \\ &M_2 = 200 \text{ GeV}\,, \quad M_3 = 600 \text{ GeV}\,, \quad \text{sign } \cos\varphi_x = +1\,, \qquad \text{sign } \cos\varphi_z = -1\,. \end{aligned} \tag{6.69}$$

The left- and right-handed soft-SUSY breaking mass parameters in the stop sector were set to $m_{\tilde{Q}_3} = 642$ GeV and $m_{\tilde{t}_R} = 632$ GeV, leading to $m_{\tilde{t}_1} = 514$ GeV and $m_{\tilde{t}_2} = 768$ GeV. The renormalization scale is set to $\mu_{ren} = 650$ GeV. The values of λ and κ in Eq. (6.69) respect the bound of Eq. (6.66). We again vary the phase φ_κ. The results can be found in Fig. 6.10 which shows in the left plot the Higgs boson masses of H_1 and H_2 at tree level as a dashed line, and at one loop as a solid line. The right plot in Fig. 6.10 shows the couplings of the respective Higgs boson to vector bosons normalized to the SM coupling as a function of φ_κ at tree level as a dashed line and at one loop as a solid line. The gray area is the area where one of the Higgs bosons is excluded by direct searches of the LHC7, Tevatron or LEP. In the dashed area the most SM-like Higgs boson is not compatible anymore with the imposed constraint of Eq. (6.61). The plots show the variation of φ_κ for which the tadpole conditions can be fulfilled. From the plots it can be inferred that the one-loop corrections are very important leading to an increase of up to ~ 20 GeV for the lightest Higgs boson mass. The lightest Higgs boson has for $\varphi_\kappa = 0$ a very SM-like vector boson coupling. At $\varphi_\kappa \sim 3\pi/64$ the Higgs boson H_1 and H_2 interchange their roles and H_2 becomes more SM-like. Unfortunately, this phenomenological very interesting cross-over is in the area which is incompatible with the Higgs boson excess at 125 GeV.

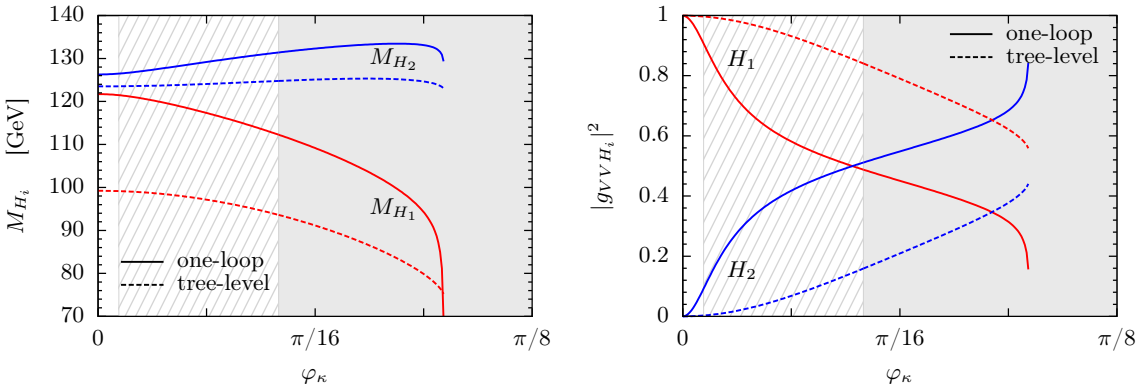

Figure 6.10.: Left: Tree-level (dashed) and one-loop corrected (full) Higgs boson masses as a function of φ_κ for H_1 (red) and H_2 (blue). Right: The H_1 (red) and H_2 (blue) Higgs couplings squared to two V bosons ($V = W, Z$) normalized to the SM coupling as a function of φ_κ at tree level (dashed) and at one loop (full). The exclusion region due to LEP, Tevatron and LHC7 data is shown as gray area, the region with the SM-like Higgs boson not being compatible with an excess of data around 125 GeV as dashed area. These plots are already published in Ref. [33].

Figure 6.11 in the left plot shows the amount of CP-violation $r^i_{\rm CP}$ of the three lightest Higgs bosons; the right plot in Fig. 6.11 shows the CP-even singlet component squared of the Higgs bosons, as a function of φ_κ. The lightest Higgs boson is first mainly CP-even, the second lightest is CP-odd. There is a cross-over between the two of them at $\varphi_\kappa \sim 3\pi/64$. The third lightest Higgs boson is mainly CP-even singlet like and therefore not excluded by the searches.

6.5. Summary

In this chapter the neutral Higgs boson sector of the complex NMSSM was analyzed with the main focus on the one-loop corrections to the Higgs boson masses. In the complex NMSSM the Higgs bosons are a superposition of CP-even and CP-odd components. The mass corrections were calculated at one-loop order in a Feynman diagrammatic approach in a mixed on-shell–$\overline{\rm DR}$ renormalization scheme. It was shown that these corrections are very important. We studied the influence of the phases of the complex parameters which either enter the Higgs sector at tree level already or only at one loop. The dependence can be quite significant.

In addition, we have briefly discussed the neutral Higgs boson production and Higgs boson decays. This was needed to give exclusions due the most SM-like Higgs boson not being compatible the excess at 125 GeV. In addition, we checked whether one of the non-SM like Higgs bosons is excluded by the searches at LHC, LEP or Tevatron. Our scenarios show that not only the lightest Higgs boson can play the role of the SM-like Higgs boson but also the second or third lightest, as the lighter ones can be

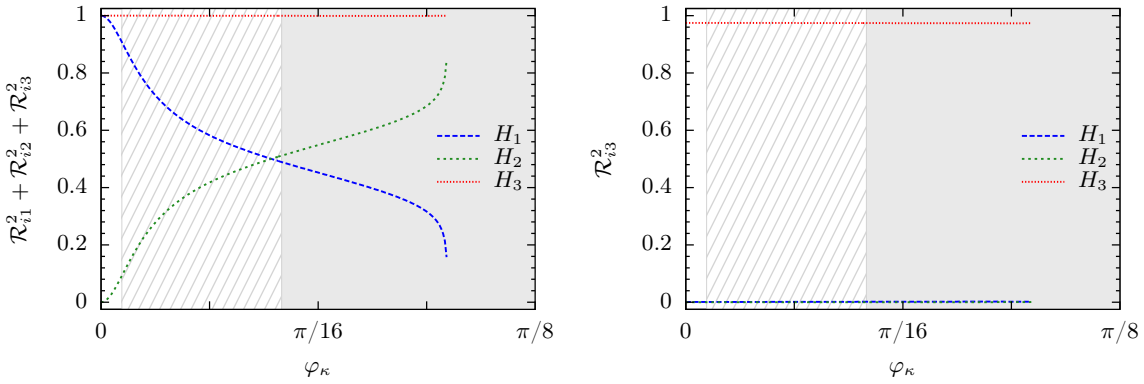

Figure 6.11.: The amount of CP violation r^i_{CP} for H_i $(i = 1, 2, 3)$ as a function of φ_κ (left). The amount of CP-even singlet component $(\mathcal{R}_{i3})^2$ as a function of φ_κ (right). This figure is already published in Ref. [33].

mainly singlet or CP-odd like and therefore escape the searches so far.

Part III.

Composite Higgs Models

CHAPTER 7

Composite Higgs Models

An alternative to stabilize the electroweak scale against UV physics is provided by theories with an additional strong sector. Similar to QCD, a number of new resonances emerge. Their masses arise through the strong dynamics of the new gauge sector. The theory is asymptotically free, but becomes strong and confining at the electroweak scale. Then the hierarchy between the scales of the strong sector and the Planck scale arises naturally like in QCD. Such a class of models are known as technicolour models and were originally proposed in the late 1970's by Weinberg and Susskind [352, 353].

A related concept is the one of Composite Higgs Models, which was developed in the 1980's. Composite Higgs Models are based on the idea that a Higgs boson arises as a pseudo-Nambu Goldstone boson from an additional strong sector, and is thus naturally lighter than the other resonances of the strong sector [19–25].

These ideas were revived in the 2000's with the 'holographic' Higgs models [26, 27, 354] in terms of five dimensional models. The composite Higgs boson was identified with the fifth component of a gauge field living in a five-dimensional space-time with Anti-de-Sitter (AdS) metric. The physics of such models is the same as the low-energy effective description of a strongly-interacting conformal field theory (CFT) with a breaking of the conformal symmetry by the elementary sector. In this thesis, we will stick to the four-dimensional approach in order to study the phenomenology of these models.

One of the key ingredients in Composite Higgs Models is the pseudo Goldstone nature of the Higgs boson. A global symmetry G is broken to a subgroup H_1 at a scale f with $n = \dim(G) - \dim(H_1)$ Goldstone bosons arising from this symmetry breaking pattern. A subgroup H_0 of G is gauged by external vector bosons and can be identified with the SM gauge group. An embedding for the SM gauge group into H_1 has to exist, in order not to break the gauge symmetry by the strong sector. The coset G/H_1 needs to contain at least one $SU(2)_L$ doublet to be identified with the Higgs doublet. Hence, of the n Goldstone bosons, three can be identified with the longitudinal modes

of the massive vector bosons. Interactions of the SM fields with the strong sector must respect the SM gauge symmetry but, in general, will break the global symmetry G. These interactions give rise to a Higgs potential, which is generated by loops of SM fermions and gauge bosons and can break the electroweak symmetry. By naive dimensional analysis the Higgs mass scale is hence $M_H \sim \mathcal{O}(v)$ and the mass scale of the strong resonances is $m_\rho \approx g_\rho f$ with the coupling $1 \lesssim g_\rho \lesssim 4\pi$. The Higgs boson is thus naturally lighter than the other resonances of the strong sector.

In the models we will consider in the following, the Higgs potential arises directly at one-loop order. In such model a mild tuning, given by $\Delta = 1/\xi$ with $\xi = v^2/f^2$, is unavoidable [27]. The explicit symmetry breaking terms are given by linear couplings of the SM fermions ψ to an operator $\mathcal{O}$ of the strong sector $\mathcal{L} = \lambda\bar{\psi}\mathcal{O}$. This implies that the SM fermions are mixtures of composite and elementary fermions, which is commonly known as 'partial compositeness'. Note that the Higgs potential cannot be generated by the gauge bosons alone as they align the vacuum along the $SU(2)_L \times U(1)_Y$ preserving direction. Therefore, couplings of the fermions to the strong sector are necessarily needed to break the global symmetry. In the following section, strongly-interacting models will be discussed in a model independent way. After that we will turn to a discussion on explicit models with the main focus on minimal models.

7.1. The Strongly-Interacting Light Higgs Lagrangian

A low-energy, model-independent description of the idea of a composite Higgs boson is given in terms of the strongly-interacting light Higgs (SILH) Lagrangian [355], which can in general be applied for models in which the Higgs boson arises as a pseudo-Nambu Goldstone boson. In particular, it can be applied if $\xi = v^2/f^2 \ll 1$. The deviations with respect to the SM are then parameterized in terms of dimension-six operators. The only possible dimension-five operator gives mass to neutrinos [356]. We will not include this operator in our description, as for an $\mathcal{O}(1)$ coupling constant the bound on neutrino masses requires a suppression scale of about $\mathcal{O}(10^{13}$ GeV). The operator is hence not relevant for our analysis.

Due to its Goldstone nature the Higgs doublet has a shift symmetry. Coefficients for the different operators can be obtained by symmetry considerations. Operators violating the symmetry must be suppressed by at least the same coupling as represented in the renormalizable SM counterpart. For instance, a higher dimensional operator in the Higgs doublet ϕ given by $(\phi^\dagger\phi)^3$ is suppressed by the coupling of its SM counterpart, given in this case by $\mathcal{L} = -\lambda(\phi^\dagger\phi)^2$. The SILH Lagrangian for the Higgs doublet ϕ then reads [355]

$$\begin{aligned}\mathcal{L}_{SILH} = &\frac{c_H}{2f^2}\partial^\mu\left(\phi^\dagger\phi\right)\partial_\mu\left(\phi^\dagger\phi\right) + \frac{c_T}{2f^2}\left(\phi^\dagger\overleftrightarrow{D^\mu}\phi\right)^2 + \frac{c_r}{2f^2}\phi^\dagger\phi(D^\mu\phi)^\dagger(D_\mu\phi) \\ &- \frac{c_6\lambda}{f^2}\left(\phi^\dagger\phi\right)^3 + \left(\frac{c_y y_f}{f^2}\phi^\dagger\phi\bar{f}_L\phi f_R + h.c.\right) \\ &+ \frac{ic_W g_2}{2m_\rho^2}\left(\phi^\dagger\sigma^i\overleftrightarrow{D^\mu}\phi\right)(D^\nu W_{\mu\nu})^i + \frac{ic_B g_1}{2m_\rho^2}\left(\phi^\dagger\overleftrightarrow{D^\mu}\phi\right)(\partial^\nu B_{\mu\nu})\end{aligned} \tag{7.1}$$

$$+\frac{ic_{HW}g_2}{16\pi^2 f^2}\left(D^\mu\phi\right)^\dagger\sigma^i\left(D^\nu\phi\right)W^i_{\mu\nu}+\frac{ic_{HB}g_1}{16\pi^2 f^2}\left(D^\mu\phi\right)^\dagger\left(D^\nu\phi\right)B_{\mu\nu}$$
$$+\frac{c_\gamma g_1^2}{16\pi^2 f^2}\frac{g_2^2}{g_\rho^2}\phi^\dagger\phi B_{\mu\nu}B^{\mu\nu}+\frac{c_g g_s^2}{16\pi^2\, f^2}\frac{y_t^2}{g_\rho^2}\phi^\dagger\phi G^a_{\mu\nu}G^{a\mu\nu}\,,$$

with the SM Yukawa couplings y_f and the SM gauge couplings g_1, g_2 and g_s. The abbreviation

$$\phi^\dagger\overleftrightarrow{D_\mu}\phi=\phi^\dagger D_\mu\phi-(D_\mu\phi)^\dagger\phi\,, \tag{7.2}$$

has been introduced. The gauge field strengths $W_{\mu\nu}$ and $G_{\mu\nu}$ are defined by

$$[D_\mu,D_\nu]=-igF^a_{\mu\nu}T^a \qquad \text{with} \quad F_{\mu\nu}=W_{\mu\nu},\,G_{\mu\nu}\,, \tag{7.3}$$

with g denoting the respective gauge coupling and T^a the generators of the gauge group. For the $U(1)$ field strenght $B_{\mu\nu}$, Eq. (7.3) can be simplified to $B_{\mu\nu}=\partial_\mu B_\nu-\partial_\nu B_\mu$. The coefficients c_i in Eq. (7.1) are expected to be of order one. The coefficient c_T, however, must be strongly suppressed. The reason is that the SM Higgs sector is actually invariant under a global $SU(2)_L\times SU(2)_R$, called custodial symmetry. The $SU(2)_L\times SU(2)_R$ symmetry is broken by Yukawa and gauge interactions, but it protects the relation between the W boson and Z boson mass from large corrections. The term associated with the coefficient c_T breaks the custodial symmetry. We will hence set c_T to zero in the following. Note that the term associated with c_r is not part of the original formulation of the SILH Lagrangian in Ref. [355]. Together with the term with coefficient c_H, it makes a field redefinition necessary in order to have a canonically normalized kinetic term.

Another useful description of a strongly-coupled Higgs boson is given in terms of the effective chiral Lagrangian. We will not discuss this Lagrangian any further but refer to the literature [357, 358]. For large values of ξ, the SILH Lagrangian is not an accurate description anymore. A resummation in ξ needs to be performed, as it is provided by explicit model constructions. In the next sections, we will discuss such explicit models.

7.2. Explicit Composite Higgs Models

A simple model fulfilling our requirement of a global symmetry with the SM gauge group as a subgroup is given by the $SU(3)$. This is, however, not a good choice, as the custodial $SU(2)_L\times SU(2)_R$ symmetry group is not contained in $SU(3)$. The unbroken subgroup hence needs to be enlarged to an $SO(4)$ global symmetry, with the algebra $SO(4)\cong SU(2)_L\times SU(2)_R$. Another rank 2 group is $SO(5)$ [359] ($SU(3)$ is also rank 2). Minimal Composite Higgs Models (MCHM) are thus based on an $SO(5)/SO(4)$ coset, leading to four Goldstone bosons with three becoming the longitudinal modes of the massive vector bosons and one physical Higgs boson. Before focusing on minimal realizations some comments on extensions are in order. Enlarged global symmetries normally lead to an enlarged Higgs boson spectrum. A simple extension is *e.g.* based on an $SO(6)/SO(5)$ coset and contains an extra singlet field [360] compared to the minimal model. Apart from the interesting phenomenology arising through the additional

Higgs boson, this extension has additional benefits such as the possibility of successful baryogenesis [361].[1] Other possible extensions are *e.g.* $SO(6)/SO(4) \times SO(2)$ or $Sp(6)/Sp(4) \times SU(2)$ leading to effective two-Higgs doublet models [362].

We will now turn to the discussion of MCHM with $SO(5)$ as global symmetry group. In order to assign the correct hypercharges, the symmetry needs to be enlarged by a $U(1)$ factor, with charge X, so that in the end the MCHM is based on an $SO(5) \times U(1)_X/SO(4) \times U(1)_X$ coset. The SM gauge group $SU(2)_L \times U(1)_Y$ is embedded into $SO(4) \times U(1)_X$ with $Y = T_R^3 + X$. The four Goldstone bosons $h^{\hat{a}}$ ($\hat{a} = 1, ..., 4$) are introduced by means of a field Σ with

$$\Sigma = \Sigma_0 \exp(\Pi(x)/f), \qquad \Sigma_0 = (0,0,0,0,1)\,, \qquad \Pi(x) = -i\sqrt{2}T^{\hat{a}}h^{\hat{a}}(x)\,, \tag{7.4}$$

and $T^{\hat{a}}$ denoting the generators of the coset $SO(5)/SO(4)$, which are defined in Appendix E. The low-energy physics of the strong sector can be described in terms of a non-linear σ-model

$$\mathcal{L}_{kin} = \frac{f^2}{2}\left(D_\mu\Sigma\right)\left(D^\mu\Sigma\right)^T\,, \quad \text{with} \quad D_\mu\Sigma = \partial_\mu\Sigma - ig_1B_\mu\Sigma(T_R^3+X) - ig_2W_\mu^a\Sigma T_L^a\,. \tag{7.5}$$

For further discussion the explicit form of the Goldstone field is useful. It can be obtained from Eq. (7.4) and (E.10) and reads

$$\Sigma = \frac{\sin h/f}{h}(h_1, h_2, h_3, h_4, h\cot(h/f))\,, \qquad h = \sqrt{\sum_{\hat{a}=1}^{4} h_{\hat{a}}^2}\,. \tag{7.6}$$

In the unitary gauge three of the degrees of freedom become the longitudinal modes of the gauge bosons. By means of a unitary gauge transformation, Σ can thus be simplified to

$$\Sigma = (0,0,0,\sin(H/f),\cos(H/f))\,, \tag{7.7}$$

with the VEV aligned in the h_4 direction ($H = h_4$). The Lagrangian in Eq. (7.5) then reads

$$\mathcal{L}_{kin} = \frac{1}{2}\partial_\mu H\partial^\mu H + \frac{f^2}{4}\sin^2\left(\frac{H}{f}\right)\left[g_2^2W_\mu^+W^{\mu-} + \frac{g_2^2}{2\cos^2\theta_W}Z^\mu Z_\mu\right]\,. \tag{7.8}$$

By expanding the Higgs field around the VEV[2] $H = \langle H\rangle + h$ in zeroth order and by identifying

$$\xi = \frac{v^2}{f^2} = \sin^2\left(\frac{\langle H\rangle}{f}\right)\,, \tag{7.9}$$

the usual relation between v and the gauge boson masses can be obtained. Note that ξ can have values between zero and one, with $\xi = 0$ corresponding to the SM limit and $\xi = 1$ to the technicolour limit, in which the scale of the strong sector corresponds to the

[1] Note also that $SO(6) \cong SU(4)$, hinting to a possible four-dimensional UV completion with fermions, since the global symmetry of the kinetic term of N fundamental Weyl fermions is $SU(N)$.

[2] Note that we slightly changed our notation here: The fluctuation of the Higgs field H around the VEV is now called h throughout of this part of the thesis. The Higgs boson mass will hence be denoted by m_h.

EWSB scale. The Higgs boson to gauge boson couplings can be obtained by expanding in higher orders in $H = \langle H \rangle + h$. In terms of the corresponding SM couplings, they are given by ($V = W, Z$)

$$g_{hVV} = g_{hVV}^{\mathrm{SM}} \sqrt{1-\xi}\,, \qquad g_{hhVV} = g_{hhVV}^{\mathrm{SM}} \,(1-2\xi)\,. \tag{7.10}$$

The g_{hVV} and g_{hhVV} couplings are hence reduced compared to the SM for all possible values of ξ. Due to the modified Higgs boson vector boson couplings, the Higgs boson cannot fully unitarize the longitudinal vector boson scattering anymore. This leads to a characteristic increase of this process with the energy and can be viewed as a kind of 'smoking gun' signature of such a class of models [355, 358]. However, it is experimentally very challenging to be measured. Unitarity of longitudinal vector boson scattering can be restored by the inclusion of further resonances of the strong sector [363].

The Higgs boson to fermion couplings and Higgs self-couplings can only be calculated once a representation for the fermions is chosen. The simplest choice for an $SO(5)$ representation is the spinorial representation corresponding to a **4**. It was, however, shown in Ref. [364] that such a model has problems to evade the constraints from $Zb_L\bar{b}_L$ and we will thus not discuss it any further here. Instead we will discuss models with the fermions transforming in the fundamental and the antisymmetric representation of $SO(5)$. For fermions transforming in the symmetric representation (a **14**), we refer to the works in Refs. [32, 365].

7.2.1. Fermions transforming in the fundamental representation

The fundamental representation of the $SO(5)$ is a **5**. This model is often abbreviated by MCHM5 in literature. As already mentioned, linear couplings of the SM fermions to the strong sector can break the global symmetry explicitly and hence generate a Higgs potential. Such terms will also generate a mass for the corresponding SM fermion by mixing with the strong sector. Explicit mass terms for the SM fermions are thus not needed. The mixing will be connected to the mass of the fermion and is thus most interesting for the heaviest SM fermion, the top quark. We will therefore concentrate the discussion on the third generation quarks. We introduce a single five-plet of new fermions with a $U(1)$ charge $X = 2/3$ since this will lead to the desired new fermions which mix with the top quark. The new multiplet decomposes into

$$\psi = \frac{1}{\sqrt{2}} \begin{pmatrix} d - \chi_1 \\ -i(d + \chi_1) \\ u + u_1 \\ i(u - u_1) \\ \sqrt{2}T \end{pmatrix}. \tag{7.11}$$

The fermionic states have been directly expressed in terms of $SO(4)$ eigenstates. In Table 7.1 the isospin quantum numbers $T_{L/R}$ and their third component $T^3_{L/R}$, the hypercharge Y and the electric charge Q_{el} for the fermions in Eq. (7.11) are given.

	u	u_1	T	d	χ_1
T_L^3	1/2	-1/2	0	-1/2	1/2
T_L	1/2	1/2	0	1/2	1/2
T_R^3	-1/2	1/2	0	-1/2	1/2
T_R	1/2	1/2	0	1/2	1/2
Y	1/6	7/6	2/3	1/6	7/6
$Q_{el} = T_L^3 + Y$	2/3	2/3	2/3	-1/3	5/3

Table 7.1.: Quantum numbers under $SU(2)_L \times SU(2)_R$, the hypercharge Y and the electric charge Q_{el} of the composite fermions in ψ. The isospin quantum numbers are denoted by $T_{L/R}$, their third component by $T_{L/R}^3$.

As can be inferred from the Table, the new $SU(2)_L$ doublet $\tilde{Q} = (u, d)$ has the same quantum numbers as the the doublet Q_L of the left-handed top and bottom quark. A term invariant under the SM gauge group can thus be formed such that the SM doublet of the left-handed top and bottom quark can mix with the $SU(2)_L$ doublet $\tilde{Q}$ on Lagrangian level. The singlet field T has the same quantum numbers as the right-handed top quark t_R. Furthermore, another charged 2/3 fermion u_1 and an exotic fermion χ_1 with charge 5/3 were introduced. With these ingredients at hand, the Lagrangian reads

$$\begin{aligned}\mathcal{L}_f &= i\bar{q}_L \not{D} q_L + i\bar{t}_R \not{D} t_R + i\bar{b}_R \not{D} b_R + i\overline{\psi}_L \not{D} \psi_L + i\overline{\psi}_R \not{D} \psi_R \\ &\quad - yf(\overline{\psi}_L \Sigma^T)(\Sigma \psi_R) - M_5 \bar{\psi}_L \psi_R + \text{h.c.} \\ &\quad - \lambda_q \overline{Q}_L \tilde{Q}_R - \lambda_t \overline{T}_L t_R + \text{h.c.}\,,\end{aligned} \tag{7.12}$$

with the mass M_5 of the five-plet, the coupling y of the Goldstone field to the new fermions and the linear couplings λ_q and λ_t of the strong sector to the SM fermions. The covariant derivative is given by ($a = 1, 2, 3$)

$$D_\mu \psi = \left[\partial_\mu - i g_2 W_\mu^a T_L^a - i g_1 B_\mu (T_R^3 + X)\right] \psi\,, \qquad \text{with} \qquad X = (2/3)\mathbb{1}_5\,. \tag{7.13}$$

The new fermions introduced in Eq. (7.11) are vector-like, namely both left- and right-handed components transform in the same way under the SM gauge group. A mass term can thus be written down without violating the $SU(2)_L \times U(1)_Y$ symmetry. Note that we did not introduce any explicit mass term for the top and bottom quark in Eq. (7.12). The top quark gets its mass through mixing with the 2/3 charged fermions, the so-called top partners. The mass matrix for the top-like quarks reads (with $s = \sin\langle H\rangle/f = v/f$ and $c = \cos\langle H\rangle/f$)

$$-\mathcal{L}_m = \overline{\begin{pmatrix} t_L \\ u_L \\ u_{1,L} \\ T_L \end{pmatrix}} \underbrace{\begin{pmatrix} 0 & \lambda_q & 0 & 0 \\ 0 & M_5 + \frac{fys^2}{2} & \frac{fys^2}{2} & \frac{yfsc}{\sqrt{2}} \\ 0 & \frac{fys^2}{2} & M_5 + \frac{fys^2}{2} & \frac{yfsc}{\sqrt{2}} \\ \lambda_t & \frac{yfsc}{\sqrt{2}} & \frac{yfsc}{\sqrt{2}} & M_5 + yfc^2 \end{pmatrix}}_{M_t} \begin{pmatrix} t_R \\ u_R \\ u_{1,R} \\ T_R \end{pmatrix} + \text{h.c.}\,. \tag{7.14}$$

The mass matrix can be diagonalized by a bi-unitary transformation with

$$\left(U_L^t\right)^\dagger M_t U_R^t = M_t^{diag}\,. \tag{7.15}$$

Before EWSB ($v = 0$) the mass matrix is diagonalized by the rotations

$$\begin{aligned}
\begin{pmatrix} Q_L \\ \tilde{Q}_L \end{pmatrix} &\to \begin{pmatrix} \cos\phi_L & \sin\phi_L \\ -\sin\phi_L & \cos\phi_L \end{pmatrix} \begin{pmatrix} Q_L \\ \tilde{Q}_L \end{pmatrix}\,, \qquad \tan\phi_L = \frac{\lambda_q}{M_5} \\
\begin{pmatrix} t_R \\ T_R \end{pmatrix} &\to \begin{pmatrix} \cos\phi_R & \sin\phi_R \\ -\sin\phi_R & \cos\phi_R \end{pmatrix} \begin{pmatrix} t_R \\ T_R \end{pmatrix}\,, \qquad \tan\phi_R = \frac{\lambda_t}{M_5 + yf}\,.
\end{aligned} \tag{7.16}$$

The masses of the new fermions are then given by

$$\frac{M_5}{c_L}\,, \qquad M_5\,, \qquad \frac{yf + M_5}{c_R}\,, \tag{7.17}$$

with $s_{L,R} = \sin\phi_{L,R}$ and $c_{L,R} = \cos\phi_{L,R}$. The lightest mass eigenstate, identified with the top quark, obtains a mass only at $\mathcal{O}(v/f)$ given by

$$m_t = y \sin\phi_L \sin\phi_R \frac{v}{\sqrt{2}}\,. \tag{7.18}$$

The parameter $\sin\phi_R$ is fitted to the experimental top quark mass. Note that y and $\sin\phi_L$ cannot be chosen too small in order to obtain the correct mass value for m_t. The Goldstone coupling y is however perturbative only below 4π.

The Lagrangian of Eq. (7.12) does not give rise to a bottom quark mass, as there is no new fermionic resonance with the same quantum numbers than the right-handed bottom quark. It can, however, be introduced by adding a $\mathbf{5_{-1/3}}$. In order to avoid additional parameters which would then arise, we introduce a bottom quark mass via an *ad hoc* Yukawa coupling

$$\mathcal{L}_b = -\lambda_b \overline{Q}_L \phi b_R + \text{h.c.}\,. \tag{7.19}$$

As will be shown in the next subsection, a bottom quark mass can also easily be introduced by resorting to larger representations of the fermions. For later use, we will also give the Higgs boson couplings to fermions. They can be obtained by expanding the bilinear terms in the fermion fields in higher orders in $H = \langle H\rangle + h$. The interaction Lagrangian of one Higgs boson with two fermions is given by

$$-\mathcal{L}_{ht\bar{t}} = y\,h\,\overline{\begin{pmatrix} t_L \\ u_L \\ u_{1,L} \\ T_L \end{pmatrix}} \underbrace{\begin{pmatrix} 0 & 0 & 0 & 0 \\ 0 & sc & sc & \frac{1-2s^2}{\sqrt{2}} \\ 0 & sc & sc & \frac{1-2s^2}{\sqrt{2}} \\ 0 & \frac{1-2s^2}{\sqrt{2}} & \frac{1-2s^2}{\sqrt{2}} & -2sc \end{pmatrix}}_{\tilde{G}_{hf\bar{f}}} \begin{pmatrix} t_R \\ u_R \\ u_{1,R} \\ T_R \end{pmatrix} + \text{h.c.} \tag{7.20}$$

and the interaction of two Higgs bosons with two fermions reads

$$-\mathcal{L}_{hht\bar{t}} = \frac{y}{2f}\, h^2 \overline{\begin{pmatrix} t_L \\ u_L \\ u_{1,L} \\ T_L \end{pmatrix}} \underbrace{\begin{pmatrix} 0 & 0 & 0 & 0 \\ 0 & 1-2\,s^2 & 1-2\,s^2 & -2\sqrt{2}sc \\ 0 & 1-2\,s^2 & 1-2\,s^2 & -2\sqrt{2}sc \\ 0 & -2\sqrt{2}sc & -2\sqrt{2}sc & -2\,(1-2\,s^2) \end{pmatrix}}_{\tilde{G}_{hhf\bar{f}}} \begin{pmatrix} t_R \\ u_R \\ u_{1,R} \\ T_R \end{pmatrix} + \text{h.c.}\,. \quad (7.21)$$

The coupling matrices are rotated to the mass eigenstates by

$$y(U_L^t)^\dagger \tilde{G}_{hf\bar{f}} U_R^t = G_{hf\bar{f}}\,, \quad \text{and} \quad y(U_L^t)^\dagger \tilde{G}_{hhf\bar{f}} U_R^t = G_{hhf\bar{f}}\,. \quad (7.22)$$

If all new fermionic resonances are above the cut-off of the effective theory, we are left with only the pure Higgs non-linearities, expressed by means of ξ. The Higgs boson to fermion couplings are then given by (see *e.g.* Ref. [27, 366])

$$g_{hff} = g_{hff}^{SM} \frac{1-2\xi}{\sqrt{1-\xi}} \quad \text{and} \quad g_{hhff} = -g_{hff}^{SM} \frac{4\xi}{v} \quad (7.23)$$

The g_{hff} and g_{hhff} couplings as defined in Eq. (7.23) can of course be obtained from Eq. (7.22) by taking the limit of very heavy top partners masses. Note that the g_{hhff} coupling does not exist in the SM. The trilinear Higgs self-coupling reads

$$g_{hhh} = g_{hff}^{SM} \frac{1-2\xi}{\sqrt{1-\xi}}\,. \quad (7.24)$$

Coupling matrices of the fermions with vector bosons can be obtained from the covariant derivative as defined in Eq. (7.13).

7.2.2. Fermions transforming in the antisymmetric representation

The antisymmetric representation is a ten-plet of $SO(5)$. We assign a $U(1)$ charge of $X = 2/3$. Our approach in this discussion will be very similar to the previous subsection. But as the results will be needed in the phenomenological study, we will nevertheless repeat here some steps, pointing to the differences compared to the fundamental representation case. The decomposition of the **10** under $SU(2)_L \times SU(2)_R$ is given by

$$\mathbf{10} = (\mathbf{2},\mathbf{2}) \oplus (\mathbf{3},\mathbf{1}) \oplus (\mathbf{1},\mathbf{3})\,. \quad (7.25)$$

The fermion ten-plet reads

$$\mathcal{Q} = \frac{1}{2} \begin{pmatrix} 0 & -(u+u_1) & \frac{i(d-\chi)}{\sqrt{2}} + \frac{i(d_1-\chi_1)}{\sqrt{2}} & \frac{d+\chi}{\sqrt{2}} - \frac{d_1+\chi_1}{\sqrt{2}} & d_4+\chi_4 \\ u_1+u & 0 & \frac{d_1+\chi_1}{\sqrt{2}} + \frac{d+\chi}{\sqrt{2}} & \frac{i(d_1-\chi_1)}{\sqrt{2}} - \frac{i(d-\chi)}{\sqrt{2}} & -i(d_4-\chi_4) \\ -\frac{i(d_1-\chi_1)}{\sqrt{2}} - \frac{i(d-\chi)}{\sqrt{2}} & -\frac{d_1+\chi_1}{\sqrt{2}} - \frac{d+\chi}{\sqrt{2}} & 0 & u_1-u & t_4+T_4 \\ \frac{d_1+\chi_1}{\sqrt{2}} - \frac{d+\chi}{\sqrt{2}} & \frac{i(\chi_1-d_1)}{\sqrt{2}} + \frac{i(d-\chi)}{\sqrt{2}} & u-u_1 & 0 & -i(t_4-T_4) \\ -d_4-\chi_4 & i(d_4-\chi_4) & -t_4-T_4 & i(t_4-T_4) & 0 \end{pmatrix}. \quad (7.26)$$

	u	u_1	t_4	T_4	d	d_1	d_4	χ	χ_1	χ_4
T_L^3	0	0	-1/2	1/2	-1	0	-1/2	1	0	1/2
T_L	1	0	1/2	1/2	1	0	1/2	1	0	1/2
T_R^3	0	0	1/2	-1/2	0	-1	-1/2	0	1	1/2
T_R	0	1	1/2	1/2	0	1	1/2	0	1	1/2
Y	2/3	2/3	7/6	1/6	2/3	-1/3	1/6	2/3	5/3	7/6
$Q_{el} = T_L^3 + Y$	2/3	2/3	2/3	2/3	-1/3	-1/3	-1/3	5/3	5/3	5/3

Table 7.2.: Quantum numbers of the new vector-like fermions under $SU(2)_L \times SU(2)_R$, the hypercharge Y and the electric charge Q_{el}.

For convenience we have chosen a two-indexed way of writing the ten-plet. The action of the generators in Eqs. (E.10–E.12) on the representation is given by the commutator, as shown in Appendix E. The quantum numbers of the specific fermions appearing in Eq. (7.26) can be found in Table 7.2. The fermions u_1 and d_1 can mix with a right-handed top and bottom quark, respectively, as they have the same quantum numbers. The $SU(2)_L$ doublet $\tilde{Q} = (T_4, d_4)$ can mix with the SM doublet Q_L of left-handed top and bottom quarks. In contrast to the fundamental representation, we have now all ingredients at hand to introduce the bottom quark mass via partial compositeness without introducing another representation. The Lagrangian is then, analogously to Eq. (7.12), given by

$$\begin{aligned}\mathcal{L} =& i\,\mathrm{Tr}(\bar{\mathcal{Q}}_R \not{D} \mathcal{Q}_R) + i\,\mathrm{Tr}(\bar{\mathcal{Q}}_L \not{D} \mathcal{Q}_L) + i\bar{q}_L \not{D} q_L + i\bar{b}_R \not{D} b_R + i\bar{t}_R \not{D} t_R \\ & - M_{10}\mathrm{Tr}(\bar{\mathcal{Q}}_R \mathcal{Q}_L) - yf\left(\Sigma^\dagger \bar{\mathcal{Q}}_R \mathcal{Q}_L \Sigma\right) + h.c. \\ & - \lambda_t \bar{t}_R u_{1L} - \lambda_b \bar{b}_R d_{1L} - \lambda_q (\bar{T}_{4R}, \bar{d}_{4R}) Q_L + h.c.\,.\end{aligned} \tag{7.27}$$

In order to form an $SO(5)$ invariant, the trace must be taken in the kinetic terms. The mass matrices for the 2/3 charged fermions, the $-1/3$ charged fermions and the 5/3 charged fermions can be derived now from the bilinear terms in the Lagrangian in zeroth order in the $H = \langle H \rangle + h$ expansion, and are given by

$$-\mathcal{L}_{m_t} = \overline{\begin{pmatrix} t_L \\ u_L \\ u_{1L} \\ t_{4L} \\ T_{4L} \end{pmatrix}} \begin{pmatrix} 0 & 0 & 0 & 0 & \lambda_q \\ 0 & \tilde{m}_a & -\frac{1}{4}fys^2 & -\frac{1}{4}fycs & -\frac{1}{4}fycs \\ \lambda_t & -\frac{1}{4}fys^2 & \tilde{m}_a & \frac{1}{4}fycs & \frac{1}{4}fycs \\ 0 & -\frac{1}{4}fycs & \frac{1}{4}fycs & \tilde{m}_b & -\frac{1}{4}fys^2 \\ 0 & -\frac{1}{4}fycs & \frac{1}{4}fycs & -\frac{1}{4}fys^2 & \tilde{m}_b \end{pmatrix} \begin{pmatrix} t_R \\ u_R \\ u_{1R} \\ t_{4R} \\ T_{4R} \end{pmatrix} + h.c.\,, \tag{7.28}$$

$$-\mathcal{L}_{m_b} = \overline{\begin{pmatrix} b_L \\ d_L \\ d_{1L} \\ d_{4L} \end{pmatrix}} \begin{pmatrix} 0 & 0 & 0 & \lambda_q \\ 0 & \tilde{m}_a & -\frac{1}{4}fys^2 & fy\frac{cs}{2\sqrt{2}} \\ \lambda_b & -\frac{1}{4}fys^2 & \tilde{m}_a & -fy\frac{cs}{2\sqrt{2}} \\ 0 & fy\frac{cs}{2\sqrt{2}} & -fy\frac{cs}{2\sqrt{2}} & \tilde{m}_c \end{pmatrix} \begin{pmatrix} b_R \\ d_R \\ d_{1R} \\ d_{4R} \end{pmatrix} + h.c.\,, \tag{7.29}$$

and

$$-\mathcal{L}_{m_\chi} = \overline{\begin{pmatrix} \chi_L \\ \chi_{1L} \\ \chi_{4L} \end{pmatrix}} \begin{pmatrix} \tilde{m}_a & -\frac{1}{4}fys^2 & fy\frac{cs}{2\sqrt{2}} \\ -\frac{1}{4}fys^2 & \tilde{m}_a & -fy\frac{cs}{2\sqrt{2}} \\ fy\frac{cs}{2\sqrt{2}} & -fy\frac{cs}{2\sqrt{2}} & \tilde{m}_c \end{pmatrix} \begin{pmatrix} \chi_R \\ \chi_{1R} \\ \chi_{4R} \end{pmatrix} + h.c.\,, \tag{7.30}$$

with

$$\tilde{m}_a \equiv \frac{1}{4}fys^2 + M_{10}\,, \qquad \tilde{m}_b \equiv \frac{1}{2}fy(1-\frac{1}{2}s^2) + M_{10}\,, \qquad \tilde{m}_c \equiv \frac{1}{2}fyc^2 + M_{10}\,. \tag{7.31}$$

The transformation into the mass eigenstates is defined, in analogy to Eq. (7.15), by

$$\left(U_L^{t/b/\chi}\right)^\dagger M_{t/b/\chi} U_R^{t/b/\chi} = M_{t/b/\chi}^{diag}\,. \tag{7.32}$$

In order to gain an analytic understanding, the mass matrix can be diagonalized before EWSB, *i.e.* for $v = 0$. This can be done by the following rotations

$$\begin{aligned}
\begin{pmatrix} Q_L \\ \tilde{Q}_L \end{pmatrix} &\to \begin{pmatrix} \cos\phi_L & \sin\phi_L \\ -\sin\phi_L & \cos\phi_L \end{pmatrix} \begin{pmatrix} Q_L \\ \tilde{Q}_L \end{pmatrix}\,, && \tan\phi_L = \lambda_q/(M_{10} + fy/2)\,, \\
\begin{pmatrix} t_R \\ u_{1R} \end{pmatrix} &\to \begin{pmatrix} \cos\phi_{Rt} & \sin\phi_{Rt} \\ -\sin\phi_{Rt} & \cos\phi_{Rt} \end{pmatrix} \begin{pmatrix} t_R \\ u_{1R} \end{pmatrix}\,, && \tan\phi_{Rt} = \lambda_t/M_{10}\,, \\
\begin{pmatrix} b_R \\ d_{1R} \end{pmatrix} &\to \begin{pmatrix} \cos\phi_{Rb} & \sin\phi_{Rb} \\ -\sin\phi_{Rb} & \cos\phi_{Rb} \end{pmatrix} \begin{pmatrix} b_R \\ d_{1R} \end{pmatrix}\,, && \tan\phi_{Rb} = \lambda_b/M_{10}\,.
\end{aligned} \tag{7.33}$$

This results in the following masses of the top partners

$$M_{10}\,, \quad \frac{M_{10}}{\cos\phi_{Rt}}\,, \quad M_{10} + \frac{fy}{2}\,, \quad \frac{M_{10} + \frac{fy}{2}}{\cos\phi_L}\,, \tag{7.34}$$

and masses of the bottom partners

$$M_{10}\,, \quad \frac{M_{10}}{\cos\phi_{Rb}}\,, \quad \frac{M_{10} + \frac{fy}{2}}{\cos\phi_L}\,. \tag{7.35}$$

The mass matrix of the 5/3 charged fermions can be diagonalized exactly leading to

$$M_{10}\,, \quad M_{10}\,, \quad M_{10} + \frac{fy}{2}\,. \tag{7.36}$$

At LO in v/f, we obtain for the top and bottom quark masses

$$m_t = \frac{y\,v}{4}\sin\phi_L \sin\phi_{Rt}\,, \qquad m_b = \frac{y\,v}{2\sqrt{2}}\sin\phi_L \sin\phi_{Rb}\,. \tag{7.37}$$

Note that the mass formula for the top quark mass is suppressed compared to the fundamental representation, meaning that the parameters need to be chosen larger to

fulfill the requirement of the correct top quark mass. As can be inferred from Eq. (7.37), either $\sin\phi_L$ or $\sin\phi_{Rb}$ needs to be small to fit the small bottom quark mass. Since $\sin\phi_L$ cannot be too small, to achieve the correct top quark mass, $\sin\phi_{Rb}$ will be small, implying that the right-handed bottom quark is mainly fundamental.

The Higgs coupling matrices can be obtained from the bilinear terms of the Lagrangian by expanding the mass matrices in the interaction eigenstates up to first order in the Higgs field h. They read

$$
\begin{aligned}
&-\mathcal{L}_{ht\bar{t}} = \\
&y\,h\,\overline{\begin{pmatrix} t_L \\ u_L \\ u_{1L} \\ t_{4L} \\ T_{4L} \end{pmatrix}}
\underbrace{\begin{pmatrix}
0 & 0 & 0 & 0 & 0 \\
0 & \frac{1}{2}sc & -\frac{1}{2}sc & \frac{1}{4}(2s^2-1) & \frac{1}{4}(2s^2-1) \\
0 & -\frac{1}{2}sc & \frac{1}{2}sc & \frac{1}{4}(1-2s^2) & \frac{1}{4}(1-2s^2) \\
0 & \frac{1}{4}(2s^2-1) & \frac{1}{4}(1-2s^2) & -\frac{1}{2}sc & -\frac{1}{2}sc \\
0 & \frac{1}{4}(2s^2-1) & \frac{1}{4}(1-2s^2) & -\frac{1}{2}sc & -\frac{1}{2}sc
\end{pmatrix}}_{\tilde{G}_{ht\bar{t}}}
\begin{pmatrix} t_R \\ u_R \\ u_{1R} \\ t_{4R} \\ T_{4R} \end{pmatrix} + h.c.\,, \\
&-\mathcal{L}_{hb\bar{b}} = y\,h\,\overline{\begin{pmatrix} b_L \\ d_L \\ d_{1L} \\ d_{4L} \end{pmatrix}}
\underbrace{\begin{pmatrix}
0 & 0 & 0 & 0 \\
0 & \frac{1}{2}sc & -\frac{1}{2}sc & \frac{1}{2\sqrt{2}}(1-2s^2) \\
0 & -\frac{1}{2}sc & \frac{1}{2}sc & \frac{1}{2\sqrt{2}}(2s^2-1) \\
0 & \frac{1}{2\sqrt{2}}(1-2s^2) & \frac{1}{2\sqrt{2}}(2s^2-1) & -sc
\end{pmatrix}}_{\tilde{G}_{hb\bar{b}}}
\begin{pmatrix} b_R \\ d_R \\ d_{1R} \\ d_{4R} \end{pmatrix} + h.c.\,.
\end{aligned}
\tag{7.38}
$$

In analogy to Eq. (7.22) the Higgs boson couplings to the top quarks and bottom quarks in the mass eigenstates are given by

$$
y(U_L^t)^\dagger \tilde{G}_{ht\bar{t}} U_R^t = G_{ht\bar{t}}\,, \quad \text{and} \quad y(U_L^b)^\dagger \tilde{G}_{hb\bar{b}} U_R^b = G_{hb\bar{b}}\,. \tag{7.39}
$$

We do not give the Higgs couplings to the 5/3 charged fermions here, as they only interact with the Higgs boson with very small off-diagonal couplings. Couplings to the Goldstone bosons can be derived by the replacements

$$
h_1 \to \frac{G^- - G^+}{i\sqrt{2}}, \qquad h_2 \to -\frac{G^- + G^+}{\sqrt{2}}, \qquad h_3 \to G_0\,, \tag{7.40}
$$

in the Lagrangian in Eq. (7.27). The couplings of the Goldstone bosons with the fermions can be found in explicit form in Ref. [36].

With the heavy new vector-like fermions integrated out, the model with fermions transforming in the antisymmetric representation has exactly the same Higgs boson couplings as the one with the fundamental representation [27]. Note that in the holographic Composite Higgs Model of Ref. [27] with fermions in the **10** representation, one representation per generation is required. Simplified models with only one new multiplet are often dubbed by 'two site' models.

7.3. Concluding remarks

Our approach for defining the explicit models was guide-lined by the principle of minimality. In addition to the operators present in the Lagrangians in Eq. (7.12) or

Eq. (7.27), extra operators such as *e.g.*

$$\Delta\mathcal{L} = i\, y'_L(\overline{\psi}_L\Sigma^T)\not{D}(\Sigma\psi_L) + i\, y'_R(\overline{\psi}_R\Sigma^T)\not{D}(\Sigma\psi_R)\,, \tag{7.41}$$

can be introduced into the Lagrangian (7.12). We restrict ourselves, however, to the necessary set of operators, meaning that their couplings are set to zero. We also do not introduce any further sources of $SO(5)$ breaking other than the linear couplings of the SM fermions with the strong sector. In general, it is *e.g.* possible to introduce different masses for the different $SU(2)_L$ multiplets of vector-like fermions, which would not break the SM gauge group but only the global symmetry $SO(5)$. With our approach, we end up with a minimal amount of new parameters. Compared with the SM, only four new parameters both in the model with the fundamental and in the model with the antisymmetric representation are introduced.

Until now, we did not give any motivation why the fermionic resonances need to be included in the effective theory approach. In Refs. [28–31] the explicit form of the Higgs potential for minimal Composite Higgs Models with fermions transforming in different representations was calculated. This results in a relation between the Higgs boson mass and the masses of the fermionic resonances. The Higgs mass turns out to be in general too large in the considered models, but light top partners, typically at around a TeV for moderate values of ξ, can cure the tension with the experimentally measured Higgs mass value. Based on Weinberg sum rules, Ref. [31] derived for the $SO(5)/SO(4)$ model with fermions in the fundamental representation a mass bound for the lightest top partner of

$$m_{T,lightest} \lesssim \frac{m_h \pi v}{m_t\sqrt{N_c}\sqrt{\xi}}\,, \tag{7.42}$$

is found, with N_c denoting the number of colours. For the antisymmetric representation the same formula can be applied. Of course, the upper mass bound on the lightest top partner mass is complementary with bounds of direct searches. Combining both, large values of ξ are excluded. Recently in Ref. [367], it was shown that the bound on the lightest resonance mass can be relaxed by $\mathcal{O}(10\%)$ if loop corrections of heavy new gluons are taken into account.

Finally, a remark on UV-completions of Composite Higgs Models is in order. All the models presented here are effective theories, with a cut-off scale $\Lambda = 4\pi f$, of an underlying yet unknown theory. An interesting question is of course the underlying dynamics of such a theory. As already mentioned, there exist some extra-dimensional approaches, in which the low-energy theory is described by the first few Kaluza-Klein states. A true UV-completion of extra dimensional models, however, relies on the knowledge of a (string) theory of gravity [368]. Four-dimensional approaches can be classified in two groups: The supersymmetric UV-completions and the non-supersymmetric ones. A supersymmetric UV-completion was proposed *e.g.* in Refs. [369, 370], with the usual SUSY spectrum showing up at energies above ~ 10 TeV and gauge and fermion resonances of the strong sector at lower energies. A non-supersymmetric UV-completion is *e.g.* given in Ref. [371] and relies on four-fermion operators. Embeddings into theories with fundamental fermionic matter were discussed in Ref. [372] for an $SO(6)/SO(5)$ coset.

CHAPTER 8

Phenomenology of Top Partners in Composite Higgs Models

The next two chapters are dedicated to the phenomenological implications of Composite Higgs Models on LHC physics. As discussed in the previous chapter, fermionic resonances, in particular top partners, need to be light to accommodate the correct Higgs boson mass and are hence within the reach of the LHC. In this spirit, this chapter will be devoted to study the influences of top partners on Higgs physics, in particular on single and double Higgs production via gluon fusion. The structure of the loop-induced Higgs boson to two gluon coupling which mediates the dominant Higgs production channel at the LHC can be approximated by the low-energy theorem (LET) [123–125]. The application of the LET on Composite Higgs Models is discussed in both a model-independent way and for an explicit model with top partners, taking into account constraints on the masses of the top partner from electroweak precision tests (EWPTs) and from direct searches of new vector-like fermions. The discussion is based on Ref. [34].

The LET is especially useful for the calculation of higher order QCD corrections for the single and double Higgs production processes via gluon fusion, as it reduces the loop order by one. We will discuss the NLO QCD corrections to Higgs pair production in Composite Higgs Models within the LET approach in Section 8.3 of this chapter.

8.1. The low-energy theorem in Composite Higgs Models

With the help of the LET, the loop-induced interactions of the Higgs boson with gluons can be replaced by effective couplings for a zero momentum Higgs boson. The LET

prediction for the Higgs boson coupling to gluons can be obtained by treating the Higgs field H as a background field, as zero momentum of the Higgs boson implies that it is a constant field. We can then treat the masses of each heavy particle p_i as field dependent. They enter the QCD gauge coupling as threshold corrections

$$\frac{1}{g_s^2(\mu)} = \frac{1}{g_s^2(\Lambda)} - \frac{11 - 2/3 n_f}{8\pi^2} \log\left(\frac{\Lambda}{\mu}\right) - \frac{1}{8\pi^2} \sum_{p_i} \delta b_{p_i} \log \frac{m_{p_i}^2(H)}{\mu} \,, \tag{8.1}$$

with n_f the number of fermions and $\delta b = 2/3$ if p_i is a Dirac fermion. We assumed that the particles p_i transform as triplets under $SU(3)_C$. The effective Lagrangian is then simply derived from the kinetic terms of the gluons [373]

$$-\frac{1}{4g_s^2(\mu)} G^a_{\mu\nu} G^{a\,\mu\nu} \,, \tag{8.2}$$

with the field strength $G_{\mu\nu}$ as defined in Eq. (7.3) and reads

$$\mathcal{L}_{eff} = \frac{g_s^2}{64\pi^2} G^a_{\mu\nu} G^{a\,\mu\nu} \sum_{p_i} \delta b_{p_i} \log m_{p_i}^2(H) \,. \tag{8.3}$$

By expanding the field-dependent masses of the heavy fermions around the VEV $\langle H \rangle$, the effective Higgs-gluon couplings are given by

$$\mathcal{L}_{h^n gg} = \frac{g_s^2}{96\pi^2} G^a_{\mu\nu} G^{a\,\mu\nu} \left(A_1 h + \frac{1}{2} A_2 h^2 + \ldots \right) \,, \tag{8.4}$$

where we have defined

$$A_n \equiv \left(\frac{\partial^n}{\partial H^n} \log\det \mathcal{M}^2(H) \right)_{\langle H \rangle} \,, \tag{8.5}$$

with $\mathcal{M}^2 \equiv \mathcal{M}^\dagger \mathcal{M}$, and $\mathcal{M}$ is the heavy fermion mass matrix. Later on, the explicit form of the coefficients A_1 and A_2 will be useful. They read

$$A_1 = \frac{1}{\langle H \rangle} \left[\frac{\partial}{\partial(\log H)} \log\det \mathcal{M}^2(H) \right]_{\langle H \rangle} \,, \tag{8.6}$$

$$A_2 = \frac{1}{\langle H \rangle^2} \left[\left(\frac{\partial^2}{\partial(\log H)^2} - \frac{\partial}{\partial(\log H)} \right) \log\det \mathcal{M}^2(H) \right]_{\langle H \rangle} \,. \tag{8.7}$$

In the SM, only the effects of the top quark can be integrated out by the LET. The bottom quark mass is too light, such that an expansion in small external momentum, from which the LET arises as the zeroth coefficient, is not suitable. The field dependent mass of the top quark in the SM can be written as $m_t(H) = y_t H/\sqrt{2}$. Using $A_n = (-1)^{n+1}(n-1)!/v^n$ Eq. (8.5) can be resummed to

$$\mathcal{L}_{h^n gg} = \frac{g_s^2}{48\pi^2} G^a_{\mu\nu} G^{a\,\mu\nu} \log\left(1 + \frac{h}{v}\right) \,. \tag{8.8}$$

The corresponding operator for a chiral fermion is given generically by $G^a_{\mu\nu}G^{a\,\mu\nu}\log(H^\dagger H)$, for a vector-like fermion it is instead $G^a_{\mu\nu}G^{a\,\mu\nu}H^\dagger H$. The effects of these two operators on double Higgs production were discussed in Ref. [373].

In a first step, the LET predictions for single and double Higgs boson production will be given in a model independent way. Using the SILH Lagrangian given in Eq. (7.1), expressions for the hgg and $hhgg$ couplings can easily be derived. The contributions split in three parts. The first part stems from the top quark mass, given in the effective approach by

$$m_t(H) = \frac{y_t H}{\sqrt{2}}\left(1 - c_y\frac{H^2}{2f^2}\right) . \tag{8.9}$$

The second part is generated by the contributions of the heavy fermions. In the effective Lagrangian of Eq. (7.1), this is encoded in the operator with coefficient c_g, such that we end up with

$$\frac{1}{2}\left(\frac{\partial}{\partial\log H}\log\det\mathcal{M}^2(H)\right)_{H=v} = 1 - c_y\frac{v^2}{f^2} + 3c_g\frac{y_t^2}{m_\rho^2}v^2 , \tag{8.10}$$

$$\frac{1}{2}\left(\left(\frac{\partial^2}{\partial(\log H)^2} - \frac{\partial}{\partial\log H}\right)\log\det\mathcal{M}^2(H)\right)_{H=v} = -1 - c_y\frac{v^2}{f^2} + 3c_g\frac{y_t^2}{m_\rho^2}v^2 . \tag{8.11}$$

Finally, one needs to take into account the proper canonical normalization of the Higgs boson kinetic term. The SILH Lagrangian contains an additional kinetic term,

$$\Delta\mathcal{L}_{h\,kin} = \frac{1}{2f^2}\left(c_H + \frac{c_r}{4}\right)(\langle H\rangle + h)^2\partial_\mu h\partial^\mu h , \tag{8.12}$$

such that a field redefinition needs to be performed. The field redefinition to first order in ξ is given by

$$h \to h - \frac{\xi}{2}\left(c_H + \frac{c_r}{4}\right)\left(h + \frac{h^2}{v} + \frac{h^3}{3v^2}\right) . \tag{8.13}$$

Finally, taking into account the relation between v and $\langle H\rangle$ with a first order correction term in ξ

$$v^2 = \langle H\rangle^2\left(1 + \frac{c_r}{4}\frac{\langle H\rangle^2}{f^2}\right) , \tag{8.14}$$

leads to the effective Higgs to gluon couplings given by

$$\mathcal{L}_{hgg} = \frac{g_s^2}{48\pi^2}G^a_{\mu\nu}G^{a\,\mu\nu}\frac{h}{v}\left[1 - c_y\frac{v^2}{f^2} + 3c_g\frac{y_t^2}{m_\rho^2}v^2 - \frac{c_H}{2}\xi\right] , \tag{8.15}$$

$$\mathcal{L}_{hhgg} = \frac{g_s^2}{96\pi^2}G^a_{\mu\nu}G^{a\,\mu\nu}\frac{h^2}{v^2}\left[-1 - c_y\frac{v^2}{f^2} + 3c_g\frac{y_t^2}{m_\rho^2}v^2 - \frac{c_r}{4}\xi\right] . \tag{8.16}$$

Note that often the expressions given in terms of the determinant of the mass matrix as in Eqs. (8.4) and (8.5) are more useful, especially if there are several top partners.[1] After having derived the effective vertices in terms of a model independent Lagrangian, we

[1]Both the terms of Eq. (8.4) and the shifts due to the canonical normalization of the kinetic term need to be taken into account.

will turn now to a discussion in terms of an explicit model with fermions transforming in the fundamental representation, as introduced in Section 7.2. More results derived in a model independent way can be found in Ref. [34], including also a discussion on the LET for the Higgs to photon couplings.

8.2. Low-energy theorem for a model with top partners

For the discussion of the LET in an explicit model, we will stick to the minimal $SO(5)/SO(4)$ model with the fermions transforming in the fundamental representation as introduced in Section 7.2.1. A discussion of the LET in Littlest Higgs Models or in the Minimal Composite Higgs Model with fermions transforming in the spinorial representation can be found in Ref. [34]. We will first shortly review some constraints on new fermions from electroweak precision tests and direct searches, based on the results obtained in Ref. [34] in 2012. Since then, the exclusion limits on direct searches have been updated. These updated limits will be discussed in more detail in in Section 9.2, in terms of a different model with the fermions transforming in a **10** of $SO(5)$.

8.2.1. Constraints from electroweak precision data and direct searches for fermions transforming in the fundamental representation

New Physics models are strongly constrained by the measurement of the resonant production of a Z boson at LEP with high precision. For Composite Higgs Models, constraints from the electroweak precision tests (EWPTs) were discussed widely in literature [374, 375], also regarding models with top partners [376–380]. For this work, the results of Ref. [380] have been updated by including a newer measurement of the W boson mass based on Tevatron results [381, 382], leading to the new world average value [383]

$$M_W = 80.385 \pm 0.015 \text{ GeV}\,. \tag{8.17}$$

A further discussion on EWPTs will be delayed to Section 9.1. For the constraints on the new vector-like fermions from direct searches, we took into account several searches for pair-produced heavy fermions with subsequent decays into $WbWb$, $ZtZt$ and $WtWt$ final states. They are based on the data available in June 2012 [384–393]. A list of the experimental searches included into our analysis can be found in Table 8.1, with the respective excluded mass range of the new vector-like fermion ψ. Even though we will discuss in more detail the constraints in Section 9.2, the general way of obtaining them will be given here. The reason is that the presentation of the results from the experimental collaborations has changed since June 2012. At that time, the constraints were given for the different channels assuming for each branching ratios of 100%. The newer constraints are given in terms of branching ratios of the new fermions.

The search results given in Table 8.1 are all based on pair-production of the heavy fermions. As this is a pure QCD process, the cross section $\sigma(pp, p\bar{p} \to \psi\bar{\psi})$ only

exp.	search	L [fb^{-1}]	M_ψ [GeV] range	arXiv Ref.
CMS [384–387]	$WbWb$ (1 lepton)	4.7	$[400, 625]$	1209.0471
	$WbWb$ (2 leptons)	5.0	$[350, 600]$	1203.5410
	$WtWt$	4.9	$[450, 650]$	1204.1088
	$ZtZt$	1.14	$[250, 550]$	1109.4985
ATLAS [388–391]	$WbWb$	1.04	$[250, 500]$	1202.3076
	$WqWq$	1.04	$[300, 500]$	1202.3389
	$WtWt$ (1 lepton)	1.04	$[300, 600]$	1202.6540
	$WtWt$ (2 leptons)	1.04	$[300, 600]$	1202.5520
CDF [392, 393]	$WbWb$	5.6	$[180, 500]$	1107.3875
	$WtWt$	4.8	$[260, 425]$	1101.5728

Table 8.1.: List of experimental searches for pair-produced heavy fermions included in our analysis of collider constraints. For this table, see also Ref. [34].

depends on the mass of the new vector-like fermion ψ, denoted generically by M_ψ. The constraint from *e.g.* a search for $\psi\bar{\psi} \to WbWb$ at the LHC will then read

$$\sigma_{QCD}(pp \to \psi\bar{\psi}) \times BR(\psi \to Wb)^2 \leq \sigma_{exp}\,, \tag{8.18}$$

where σ_{exp} is the experimental upper bound on the cross section. The QCD pair production cross section was obtained with the code `HATHOR` [394] at approximate NNLO. The branching ratios of the decays of the vector-like fermions were computed with the formulae given in Appendix F. Both the heavy -1/3 charged fermion d as well as χ_1 have branching ratios of 100% into Wt. The results of the searches in the $WtWt$ final state can be straightforwardly applied to both cases.

All the searches reported here were for $\sqrt{s} = 7$ TeV. These results can be projected to $\sqrt{s} = 8$ TeV. This is done in the following way: Backgrounds in searches for top partners are mainly given by top quark pair production, which is increased by 42% by going from $\sqrt{s} = 7$ TeV to $\sqrt{s} = 8$ TeV. The search strategy relies on a cut on the $t\bar{t}$ invariant mass, whose distribution is not significantly changed by the energy increase, as was explicitly checked with `MadGraph 5` [152]. The upper limit on the cross section is hence softened in the Gaussian approximation by a factor of $\sqrt{1.42} \cong 1.19$. The large luminosity of the 8 TeV run is nevertheless tightening the limit on the cross section, lowering it by a square root factor of the luminosity in every channel. We have assumed $\int \mathcal{L} = 15$ fb^{-1} for the 2012 run. The resulting constraints were $m_\chi \geq 700$ GeV for 5/3 charged fermions χ and $m_T \gtrsim 500$ GeV, with T denoting generically a top partner.

Note that at the time of the completion of this thesis, the actual data constrained the masses a bit tighter: For m_χ the strongest bound comes from a CMS dedicated search for 5/3 charged fermions [395] leading to a limit of

$$m_\chi \geq 770 \text{ GeV} \tag{8.19}$$

and for top partners from an ATLAS search [396], excluding top partners up to

$$m_T \geq 850 \text{ GeV} \quad \text{for} \quad BR(T \to ht) = 100\%\,. \tag{8.20}$$

8.2.2. The low-energy theorem for single Higgs production

The cross section for single Higgs production in this model can easily be derived in the LET approximation by applying Eq. (8.4) since the kinetic term of the Higgs boson is already canonically normalized. Thus, only the determinant of the mass matrix of the top-like fermions given in Eq. (7.14) needs to be derived, which yields

$$\det \mathcal{M}^{\dagger}(H)\mathcal{M}(H) = \frac{M_5^4 y^2 f^2 \sin^2\phi_L \sin^2\phi_R}{8\cos^2\phi_L \cos^2\phi_R}(M_5 + yf)^2 \sin^2\left(\frac{2H}{f}\right) . \tag{8.21}$$

Hence, this leads to $A_1 = (2/v)(1-2\xi)/\sqrt{1-\xi}$ with $\sin^2(\langle H\rangle/f) = \xi$. The cross section is then modified, compared to the SM cross section, according to

$$\frac{\sigma(pp \to h)}{\sigma(pp \to h)_{SM}} = \left(\frac{1-2\xi}{\sqrt{1-\xi}}\right)^2 . \tag{8.22}$$

Compared to the results given in Eq. (8.15) for the model independent parametrization of the strong dynamics, this result here is valid to all orders in ξ as it provides the resummed result within this model. Equation (8.22) is independent of the details of the heavy spectrum, meaning that it does not depend on the couplings λ_i or the masses M_i of the heavy new fermions, but solely on the Higgs boson non-linearities given by ξ. This behaviour always takes place if the heavy mass matrix takes the form

$$\det \mathcal{M}^2 = F(H/f) \times P(\lambda_i, M_i, f) \quad \text{with} \quad F(0) = 0\,. \tag{8.23}$$

It can then easily be seen that the LET prediction becomes independent of the masses and of the couplings of the new heavy top partners. In Ref. [397] the origin of this factorization was discussed by means of a spurion analysis. It was also shown that this factorization can break down if the top quark mixes with more than one composite operator. This and the introduction of bottom partner mixing with the SM bottom quark can lead to a dependence of the cross section on the composite masses and couplings. This statement will be further discussed in Section 9.3. The question, which needs to be addressed now, is how well the LET result approximates the full cross section including all top-like fermions in full mass dependence. The full cross section was computed with a self-written `FORTRAN` code. For the purpose of showing numerical results, a scan was performed over the parameter space retaining only points allowed by EWPTs. The mass matrix for the top quarks of Eq. (7.14) was diagonalized numerically without any approximations. The result can be found in Fig. 8.1 which shows the $\sigma(pp \to h)/\sigma^{SM}(pp \to h)$ ratio as a function of the lightest resonance mass for $\xi = 0.25$. Showing the ratio of the cross sections has the advantage that QCD K-factors cancel out under the assumption that the higher order corrections are the same in both cases. This is approximately true as was shown in Ref. [398]. The green points in Fig. 8.1 are still allowed by EWPTs and direct searches for vector-like fermions. The gray points are excluded by direct searches and the orange points are the projected exclusions for the 8 TeV run 2012. They are by now excluded. The black line in the plot shows for comparison the result obtained with the LET in Eq. (8.22). As can be inferred from the plot, the LET very well describes the full cross section. The cross

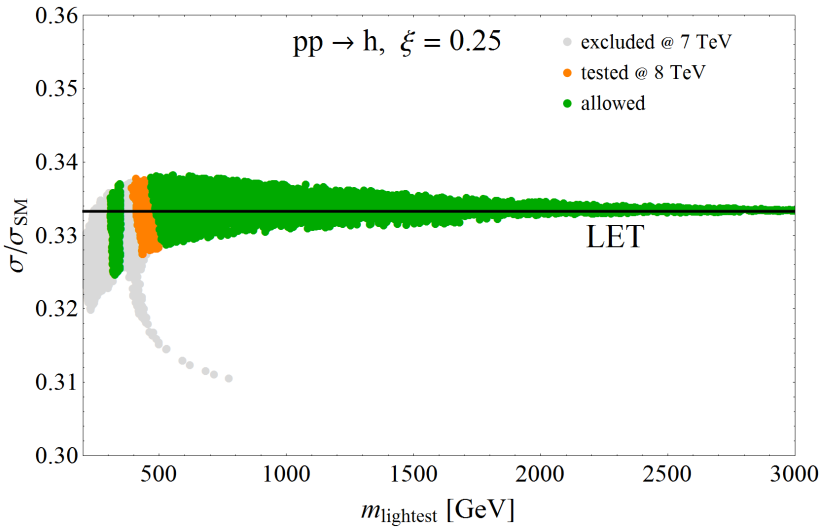

Figure 8.1.: The MCHM5 cross section for single Higgs production through gluon fusion (including the exact dependence on top and heavy fermion masses), normalized to the SM cross section (computed retaining the m_t dependence), as a function of the mass of the lightest fermion resonance m_{lightest} for $m_h = 125\,\text{GeV}$. The compositeness parameter is set to $\xi = 0.25$. Green points are allowed, gray points are excluded by current collider constraints, whereas orange points show the projected exclusions at LHC8 in 2012 and are by now excluded. For comparison, the cross section ratio computed with the LET approximation in Eq. (8.22) is shown as a black line. This figure is already published in Ref. [34].

section barely depends on the details of the heavy spectrum, as it shows not much dependence on the mass of the lightest new fermion. The reason is that the shift in the top Yukawa coupling originating from the heavy top partner spectrum cancels with the loop contributions of the heavy fermions.[2] Remark, finally, that Eq. (8.22) coincides with the result obtained if only the Higgs non-linearities are taken into account, *i.e.* by rescaling the SM cross section by the correction factor of the top Yukawa coupling in the limit where all the fermionic resonances are very heavy.

8.2.3. The low-energy theorem for double Higgs production

The double Higgs production in the LET approximation has two contributions. They are depicted in Fig. 8.2 and consist of an effective vertex of two gluons with two Higgs bosons and an effective coupling of two gluons to a single Higgs boson which then splits into a Higgs boson pair. The latter can be obtained from the single Higgs production case by multiplying with the triple Higgs boson coupling and the Higgs boson propagator. For the former, the contribution A_2 in Eq. (8.4) has to be computed.

[2]Note, that in Refs. [399, 400] the idea of lifting the degeneracy between the Higgs gluon and the Higgs top quark coupling by using $pp \to hj$ production was discussed.

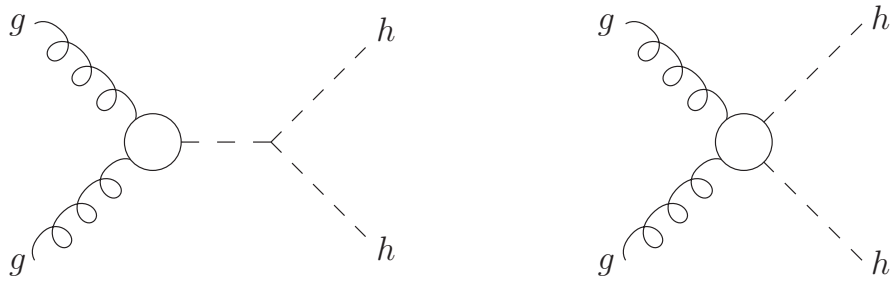

Figure 8.2.: Feynman diagrams for double Higgs production in the LET approximation.

We find

$$A_2 = -\frac{2}{v^2}\frac{1}{1-\xi}\,. \tag{8.24}$$

The partonic cross section is then given by

$$\hat{\sigma}_{gg\to hh} = \frac{G_F^2\alpha_s^2(\mu)\hat{s}}{128(2\pi)^3}\,\frac{1}{9}\sqrt{1-\frac{4m_h^2}{\hat{s}}}\,C_{\rm LET}^2(\hat{s})\,, \tag{8.25}$$

with

$$C_{\rm LET}(\hat{s}) = \frac{3m_h^2}{\hat{s}-m_h^2}\left(\frac{1-2\xi}{\sqrt{1-\xi}}\right)^2 - \frac{1}{1-\xi}\,, \tag{8.26}$$

and $\sqrt{\hat{s}}$ denoting the partonic c.m. energy, connected to the hadronic c.m. energy $\sqrt{s}$ by $\hat{s} = \tau s$, with τ denoting the product of the two proton momentum fractions of the gluons. The hadronic cross section is obtained by convolution with the parton distribution functions f_g of the gluon in the proton,

$$\sigma = \int_{4m_h^2/s}^1 d\tau \int_\tau^1 \frac{dx}{x} f_g(x,\mu)\, f_g(\tau/x,\mu)\, \hat{\sigma}_{gg\to hh}(\tau s)\,. \tag{8.27}$$

As renormalization and factorization scale we chose $\mu = \mu_F = \mu_r = \sqrt{\hat{s}}$. The parton distribution functions of the MSTW2008 collaboration [111] were used. For $\xi \to 0$ the SM result can be reproduced in Eq. (8.27). The LET is, as for single Higgs production, independent of the spectrum of heavy new fermions and only depends on the Higgs non-linearities expressed in terms of the parameter ξ. For comparison, the full cross section for Higgs boson pair production is calculated. The Feynman diagrams can be found in Fig. 8.3. There are two triangle contributions, one involving the triple Higgs boson coupling and one involving a two Higgs boson two fermion coupling. Note that the two Higgs boson two fermion coupling is an effective coupling of dimension-five and hence vanishes in the SM limit as $\xi \to 0$. This diagram leads to a quite strong enhancement of the cross section compared to the SM for large values of ξ, as it is not suppressed by an extra propagator. In the context of Composite Higgs Models, this was first noticed in Ref. [366]. The sensitivity on this novel Higgs coupling to fermions was investigated in Ref. [401].

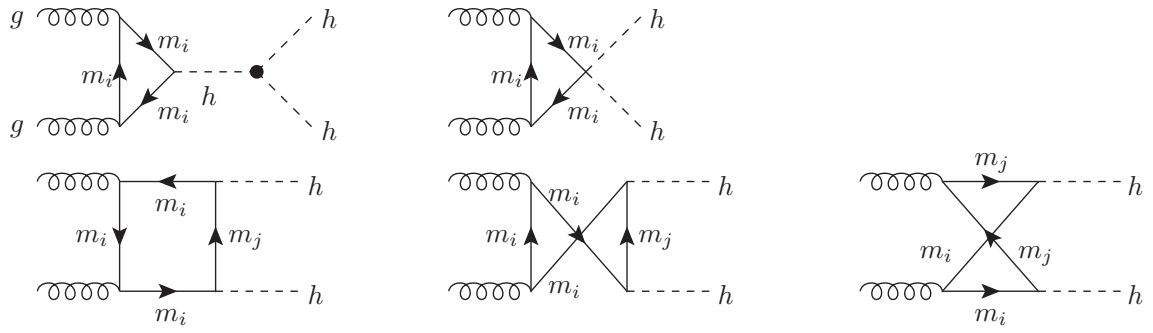

Figure 8.3.: Feynman diagrams for double Higgs production via gluon fusion with n_f novel fermionic resonances, with masses m_i $(i = 1, ..., n_f)$. The masses m_i and m_j are introduced to indicate where different fermions can contribute in the loop.

I performed the calculation of the matrix elements for the composite Higgs pair production cross section with `FeynCalc` [230]. The results can be found in Appendix G. The Lorentz structure of the matrix elements can be derived by using the Ward identity. Two different Lorentz structures arise. They are combined in such a way that they act as projectors. The triangle diagrams only contribute to the form factors corresponding to the Lorentz structure of spin $S_z = 0$ along the z-axis. The box diagrams can involve both $S_z = 0$ and $S_z = 2$ form factors. Different fermions can couple to the Higgs boson via the off-diagonal entries of the coupling matrices given in Eq. (7.20). Due to the off-diagonal matrix elements, the Higgs boson can also couple with a γ_5 to two different fermions. Diagrams including only one coupling with γ_5 disappear due to a sign flip of the coupling when the direction of the fermion line changes direction. Form factors stemming from these γ_5 contributions are denoted with a subscript '5'. The boxes then give rise to the $S_z = 0$ form factors $F_\Box$, $F_{\Box,5}$, and the $S_z = 2$ form factors $G_\Box$, $G_{\Box,5}$, whereas the triangle form factor is called $F_\triangle$. The partonic cross section is given by

$$\hat{\sigma}_{gg\to hh} = \frac{\alpha_s^2}{1024(2\pi)^3}\frac{1}{\hat{s}^2}\int_{\hat{t}_-}^{\hat{t}_+} d\hat{t}\left[\left|\sum_{i=1}^{4}\sum_{j=1}^{4}\left(g^2_{h\bar{q}_iq_j}G_\Box(m_i,m_j)+g^2_{h\bar{q}_iq_j,5}G_{\Box,5}(m_i,m_j)\right)\right|^2 + \left|\sum_{i=1}^{4}\left(C_{i,\triangle}F_\triangle(m_i)+\sum_{j=1}^{4}\left(g^2_{h\bar{q}_iq_j}F_\Box(m_i,m_j)+g^2_{h\bar{q}_iq_j,5}F_{\Box,5}(m_i,m_j)\right)\right)\right|^2\right], \tag{8.28}$$

with the integration limits

$$\hat{t}_\pm = -\frac{\hat{s}}{2}\left(1-2\frac{m_h^2}{\hat{s}}\mp\sqrt{1-\frac{4m_h^2}{\hat{s}}}\right). \tag{8.29}$$

The couplings are defined as

$$g_{h\bar{q}_iq_j} = \frac{1}{2}\left(G_{hff,ij}+G_{hff,ji}\right) \qquad g_{h\bar{q}_iq_j,5} = \frac{1}{2}\left(G_{hff,ji}-G_{hff,ij}\right), \tag{8.30}$$

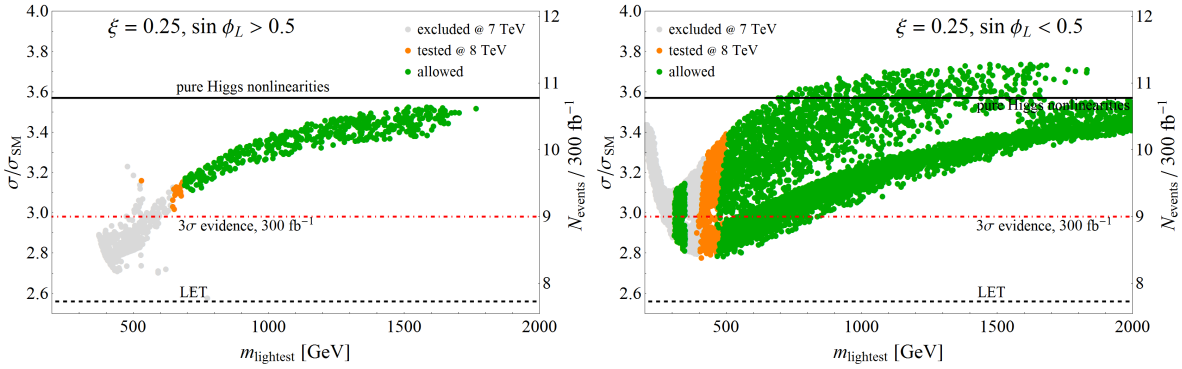

Figure 8.4.: The cross section for double Higgs production via gluon fusion normalized to the SM cross section as a function of the mass of the lightest resonance of the heavy top sector, for $m_h = 125$ GeV and $\xi = 0.25$. Green (gray) dots denote points which pass (do not pass) the constraints from EWPT and direct heavy fermion searches, whereas orange dots correspond to points that were not excluded by June 2012, but tested at LHC8 by the end of 2012. These points are excluded by now. The left plot is for $\sin\phi_L > 0.5$, the right plot for $\sin\phi_L < 0.5$. The black solid line corresponds to the result in the limit of heavy top partners keeping the full top mass dependence. The dashed line is the LET cross section normalized to the SM LET cross section. The expected number of events in the $hh \to b\bar{b}\gamma\gamma$ final state after all cuts at LHC14 with $\int \mathcal{L} = 300\,\text{fb}^{-1}$ is shown on the right side of the plots, along with the 3σ evidence threshold as red dot-dashed line. This figure is already published in Ref. [34].

and

$$g_{hh\bar{q}_i q_j} = \frac{1}{2}\left(G_{hhff,ij} + G_{hhff,ji}\right) , \tag{8.31}$$

with $G_{hff,ij}$ and $G_{hhff,ij}$ denoting the (ith, jth) matrix elements of the coupling matrices in Eq. (7.22). The triangle factor $C_{i,\triangle}$ reads

$$C_{i,\triangle} = \frac{g_{hhh}\, g_{h\bar{q}_i q_i}}{\hat{s} - m_h^2} + 2 g_{hh\bar{q}_i q_i} \quad \text{with} \quad g_{hhh} = \frac{3 m_h^2}{v}\frac{1-2\xi}{\sqrt{1-\xi}} \quad \text{in the MCHM5.} \tag{8.32}$$

The SM partonic cross section can be obtained from Eq. (8.28) for $m_i = m_j = m_t$ and taking off the sum over the top partners, replacing the couplings g_{hhh} and $g_{h\bar{q}_i q_i}$ by the SM couplings and setting $g_{hh\bar{q}_i q_i} = 0$. Of course, the contributions of $F_{\square,5}$ and $G_{\square,5}$ then get a zero prefactor and are thus irrelevant. Numerical results have been obtained by a self-written `FORTRAN` code. The SM result was cross-checked against the results given in Ref. [104]. Figure 8.4 shows the cross section divided by the SM cross section for points obtained by a scan over the parameter space for a fixed value of $\xi = 0.25$, with the mass of the lightest top partner shown on the x-axis. In Fig. 8.5 the same is shown, but for $\xi = 0.1$. The colour code of the points is the same as in Fig. 8.1. The black line shows the cross section if only the pure Higgs non-linearities are taken into account, meaning that only the mass dependence on the top quark mass is retained. The new fermionic resonances are integrated out. This corresponds to

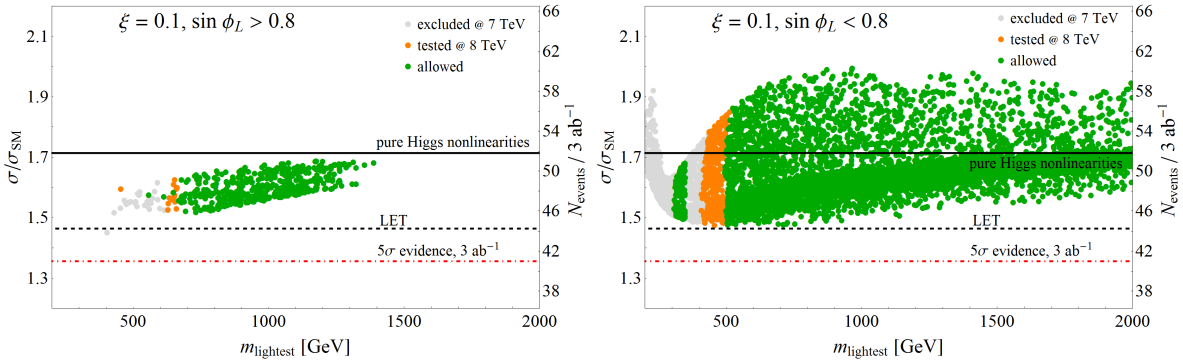

Figure 8.5.: The same as in Fig. 8.4, but for the compositeness parameter $\xi = 0.1$. The left plot here is for $\sin\phi_L > 0.8$, the right plot for $\sin\phi_L < 0.8$. On the right side of the plots the number of expected events are shown for a luminosity of $\int \mathcal{L} = 3\,\text{ab}^{-1}$. The red dashed-dotted line is the 5σ discovery line. This figure is already published in Ref. [34].

the case discussed in Ref. [366]. The cross section can be obtained from the SM cross section with the modified Higgs top couplings and taking into account the new triangle graph of Fig. 8.3 with the novel two Higgs two fermion coupling. The black dashed line corresponds to the LET approximation. It is normalized to the SM LET cross section. The labels on the right hand side of the plots give an estimate of the expected number of events at LHC14 for $\int \mathcal{L} = 300\,\text{fb}^{-1}$ for the $hh \to b\bar{b}\gamma\gamma$ final state. This final state was pointed out in Ref. [95] to be the most promising one to observe the process. The expected number of events was obtained as follows: We calculated the expected number of events based on $\sigma(pp \to hh) \times BR(hh \to b\bar{b}\gamma\gamma)$ under the assumption of a SM K-factor of 1.9. The result was multiplied by the acceptance for all cuts as derived in Ref. [95]. The number of events marked with the red dash-dotted line shows the $3\,(5)\,\sigma$ evidence line, based on the background estimate of Ref. [95] for one tagged b-jet. This is a conservative estimate as the misidentification probabilities have been improved since the appearance of Ref. [95]. Of course this is only meant to give a very rough estimate. A detailed analysis is beyond the scope of this work. As can be inferred from the plots in Figs. 8.4 and 8.5 the cross section is always enhanced with respect to the SM cross section. For $\xi = 0.25$ the enhancement is $2.7 \lesssim \sigma/\sigma_{SM} \lesssim 3.7$, for $\xi = 0.1$ it is $1.5 \lesssim \sigma/\sigma_{SM} \lesssim 2.0$. This enhancement, as discussed in detail in Ref. [366], originates mainly from the triangle graph involving an effective $hhf\bar{f}$ coupling. The other Feynman diagrams only lead to an enhancement of the cross section for $\xi > 0.75$ if only the pure Higgs non-linearities are retained. The cross section obtained in the limit of very heavy top partners, while keeping the full top mass dependence overstimates the results for $m_{lightest} \lesssim 1.5$ TeV. For larger values of $m_{lightest}$ the cross section tends to the value obtained if only the top quark loops are retained.

From the plots it can also be inferred that the cross section is quite underestimated by the LET. In order to investigate the reason for this further, we take a look at the case where the fermionic resonances can be integrated out and the only effect of the strong sector are the Higgs non-linearities, corresponding to the black line in Figs. 8.4 and 8.5.

As already mentioned, the cross section for this case can be obtained from the SM cross section by adjusting the Higgs boson couplings and adding the new triangle diagram. In the SM, the LET already underestimates the cross section by $\mathcal{O}(20\%)$ [102]. For $\xi = 0.25$ we obtained for the MCHM5 without heavy top partners $\sigma_{LET}^{MCHM5} = 37$ fb and $\sigma_{MCHM5} = 64$ fb, *i.e.* a difference of the order of 50% between the LET and the full cross section including the top mass dependence.

In order to understand why the LET does not work as well as for the single Higgs case, I calculated correction terms to the LET. They were cross-checked in a second independent calculation. They can be obtained from the full result by expanding in small external momenta before integration of the loop integrals, as described in Ref. [402]. For this purpose, we only consider here the cross section with pure Higgs non-linearities without extra fermionic resonances.[3] The propagators in the loop functions with loop momentum q can then be expanded to

$$\frac{1}{(q+p)^2 - m^2} = \frac{1}{q^2 - m^2} \frac{1}{\frac{2q\cdot p + p^2}{q^2 - m^2} + 1} \approx \frac{1}{q^2 - m^2} - \frac{2q \cdot p + p^2}{(q^2 - m^2)^2} + \dots , \tag{8.33}$$

for small external momentum p and a large mass m of the loop particles.[4] Special care needs to be taken for a consistent treatment of the orders in this expansion. The reason is that terms of the same order of p/m in the external momentum can arise in different orders of the Taylor expansion in Eq. (8.33). All terms with odd power in the loop momentum in the expansion in Eq. (8.33) drop out, as the loop integral is zero. The zeroth order results for the form factors are then given by the LET results. Going one order further gives the correction terms. The form factors then read

$$F_\triangle = \frac{\hat{s}}{m_t} \left(\frac{2}{3} + \frac{7}{180} \frac{\hat{s}}{m_t^2} \right) , \tag{8.34}$$

$$F_\square = \frac{\hat{s}}{m_t^2} \left(-\frac{2}{3} - \frac{7}{30} \frac{m_h^2}{m_t^2} \right) , \tag{8.35}$$

$$G_\square = \frac{\hat{s}}{m_t^4} \frac{11}{90} \left(\frac{m_h^4 - \hat{t}\hat{u}}{\hat{s}} \right) , \tag{8.36}$$

with $\hat{s}$, $\hat{t}$, and $\hat{u}$ denoting the partonic Mandelstam variables, see Eq. (G.1). The partonic cross section of Eq. (8.28) can be simplified to

$$\hat{\sigma}_{gg\to hh} = \frac{\alpha_s^2}{1024(2\pi)^3} \frac{1}{\hat{s}^2} \int_{\hat{t}_-}^{\hat{t}_+} d\hat{t} \left[\left| C_\triangle F_\triangle + C_\square F_\square \right|^2 + \left| C_\square G_\square \right|^2 \right] , \tag{8.37}$$

with $\hat{t}_\pm$ given by Eq. (8.29). For consistency in the orders one needs to take into account, that the form factors enter the cross section formula quadratically. Therefore

[3] After this work was finished a similar work [403] appeared with the same expansion, but taking into account also the fermionic resonances in the loop.

[4] Note that this expansion can also be performed if one of the loop masses is small, by assigning the momenta in such a way that the light fermion in the loop is without an external momentum in its propagator.

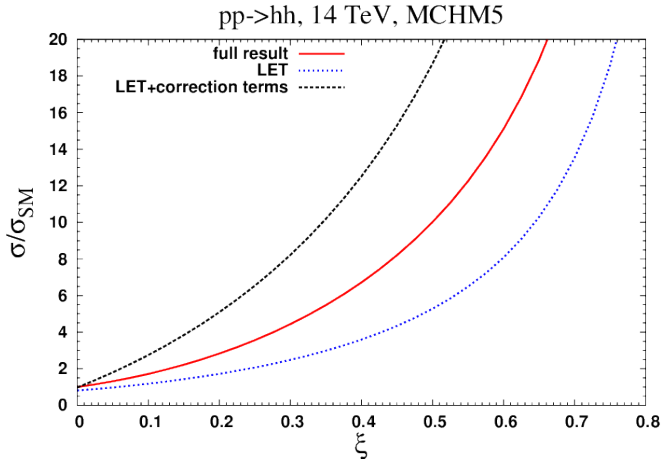

Figure 8.6.: Higgs pair production cross sections in the MCHM5 (pure Higgs non-linearities) as a function of ξ. The red solid line is the result with the full top quark mass dependence. The blue dotted line is the LET result for the cross section and the black dashed line the LET with correction terms.

only the interference terms between the result in zeroth order in p^2/m^2 and the first order result of the form factors are needed. As $G_\square$ has no zeroth order coefficient, it drops out of the first order cross section. The result then reads

$$|C_\triangle F_\triangle + C_\square F_\square|^2 + |C_\square G_\square|^2 = \frac{\hat{s}^2}{v^4}\frac{4}{9}(c_\triangle - c_\square)^2 \left[1 + \frac{1}{m_t^2(c_\triangle - c_\square)}\left(c_\triangle \frac{7}{60}\hat{s} - c_\square \frac{7}{10}m_h^2\right)\right], \tag{8.38}$$

with

$$c_\triangle = \frac{3m_h^2}{\hat{s} - m_h^2}\left(\frac{1-2\xi}{\sqrt{1-\xi}}\right)^2 - 4\xi\,, \qquad c_\square = \left(\frac{1-2\xi}{\sqrt{1-\xi}}\right)^2. \tag{8.39}$$

In Fig. 8.6 we show for the MCHM5 the full cross section (red solid line), the cross section calculated with LET (blue dotted line) and the one including the correction terms (black dashed line). The figure shows that the LET drastically underestimates the full cross section, as we already saw in Figs. 8.4 and 8.5. The correction terms improve the agreement with the full cross section only very close to the SM limit $\xi = 0$. In particular, for large values of ξ the correction terms completely fail to describe the full cross section. The reason is that, basically, the expansion in small external momenta is not valid here. For single Higgs production the expansion parameter is m_h^2/m_t^2 and the LET is the zeroth order result. For double Higgs boson production the external momenta are not small. The expansion parameters are $\hat{s}/m_t^2$, $\hat{t}/m_t^2$, $\hat{u}/m_t^2$ or m_h^2/m_t^2, but we have *e.g.* $4m_h^2 \leq \hat{s} \leq s$. This also explains that for larger ξ the disagreement of the correction terms with the full cross section becomes worse: The reason is that the diagram involving the $hhf\bar{f}$ coupling is not suppressed by an extra propagator as the triangle with the triple Higgs coupling. Therefore, the propagator cannot cure the $\hat{s}$ dependence of the correction term. The correction terms of the box diagrams are not troublesome. The correction to $G_\square$ is irrelevant, as in the squared matrix elements the leading order in $|G_\square|^2$ is one order higher as the considered order.

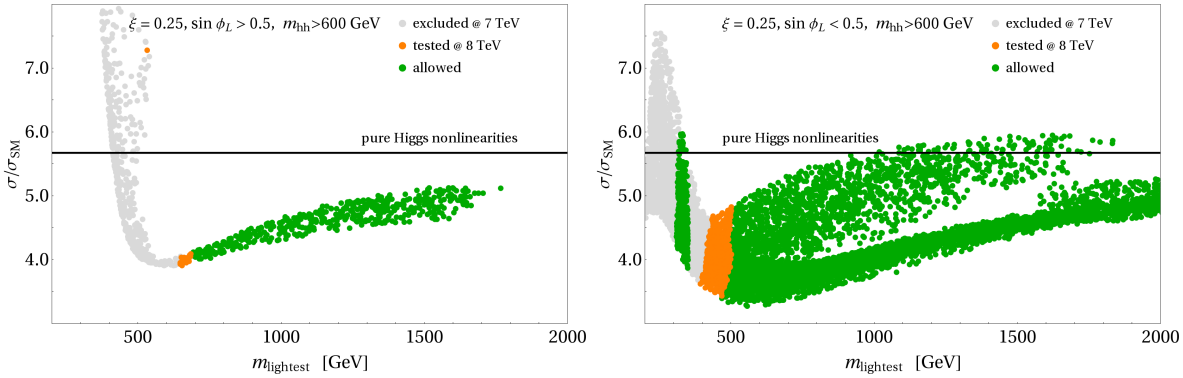

Figure 8.7.: The same as in Fig. 8.4, but with an invariant mass cut of $m_{hh} > 600$ GeV. In contrast to Fig. 8.4 neither the LET line nor the number of events is shown. This figure is already published in Ref. [34].

In $F_\square$ only the expansion parameter m_h^2/m_t^2 gets a non-zero coefficient.

Finally, we also want to study whether the application of a cut on the invariant mass m_{hh} can help to discriminate between the composite Higgs cross section and the SM cross section. Therefore, we show in Fig. 8.7 the same plots as in Fig. 8.4, but after a cut of $m_{hh} > 600$ GeV has been applied. The colour code in the plot is the same as before. We did not show the LET cross section in this plot as for kinematic distributions the LET approximation is even worse [92]. As can be seen in the plot, the invariant mass cut increases the difference between the SM cross section and the composite Higgs cross section. The cross section obtained for pure Higgs non-linearities cannot describe the full cross section with top partners accurately anymore after application of an invariant mass cut, not even for large masses of the top partners. Note that the total number of events decreases quite a bit after applying the invariant mass cut. For a measurement, this is problematic due to a small number of events. Small invariant mass cuts can, however, be useful to reduce the background, see *e.g.* Section 3.5.

8.3. NLO QCD corrections to Higgs pair production

The NLO QCD corrections to Higgs pair production in the SM have been calculated in Ref. [105] in the LET approximation. In this section we will explain how they have to be modified for Composite Higgs Models. Before that, however, a comment is in order on the LET approximation for the NLO QCD corrections. As described in the previous section, the LET is not a good approximation for Higgs pair production as the expansion in small external momenta is not valid for this process. In the NLO QCD corrections in most of the contributions, the LO cross section factors out. This is in particular true for the dominant contribution to the NLO QCD corrections given by the real radiation of a gluon. If the LO LET cross section is then replaced by the result with the full mass dependence, the final NLO result is significantly improved. As already discussed in Section 3.1 the LET approximation for the calculation of the

NLO QCD corrections is therefore expected to lead to an uncertainty on the cross section of $\mathcal{O}(10\%)$. In Fig. 8.8 the Feynman diagrams of the process at NLO QCD are shown. The blob in the figure marks the effective vertex of gluons to Higgs bosons. The Feynman diagram are divided in different categories. The first three diagrams show the virtual contributions. The other Feynman diagrams of Fig. 8.8 are the real corrections ordered by the initial states gg, gq and $q\bar{q}$. At NLO the cross section is then given by

$$\sigma_{NLO} = \sigma_{LO} + \Delta\sigma_{virt} + \Delta\sigma_{gg} + \Delta\sigma_{gq} + \Delta\sigma_{q\bar{q}}\,. \tag{8.40}$$

The real corrections $\Delta\sigma_{gg}$, $\Delta\sigma_{gq}$ and $\Delta\sigma_{q\bar{q}}$ can directly be taken over from Ref. [105] by replacing the LO cross section of the SM in the formulae by the LO cross section for Composite Higgs Models. The calculation of $\Delta\sigma_{virt}$ is a bit more involved. The first two diagrams in Fig. 8.8 are again very simple and can be taken over directly from the SM as they factorize into the LO cross section and correction terms. The only problematic diagram is the third diagram shown in Fig. 8.8. It does not factorize in that way and therefore needs to be recalculated to adjust it to the composite Higgs case. The virtual corrections are then found to be

$$\Delta\sigma_{\text{virt}} = \frac{\alpha_s(\mu_R)}{\pi}\int_{\tau_0}^{1} d\tau\ \frac{d\mathcal{L}^{gg}}{d\tau}\ \left(\frac{\alpha_s^2(\mu)G_F^2}{1024(2\pi)^3}\frac{1}{\hat{s}^2}A + \hat{\sigma}_{\text{LO},gg\to hh}\ C\right), \tag{8.41}$$

with the factorization scale denoted by μ_F and the renormalization scale by μ_R. The term with coefficient C corrsponds to the first two diagrams in Fig. 8.8, the term with coefficient A corresponds to the third diagram in Fig. 8.8. The coefficients A and C for the virtual corrections read

$$\begin{aligned} A &= \text{Re}\Bigg[\int_{\hat{t}_-}^{\hat{t}_+} d\hat{t}\Bigg\{\frac{4}{9}c_{LO}\sum_{i=1}^{n_t}\Big(C_{i,\triangle}F_{\triangle}(m_i) + \sum_{j=1}^{n_t}(g^2_{h\bar{q}_iq_j}F_{\square}(m_i,m_j) \\ &+ g^2_{h\bar{q}_iq_j,5}F_{\square,5}(m_i,m_j))\Big) - \int_{\hat{t}_-}^{\hat{t}_+} d\hat{t}\left\{\frac{4}{9}\frac{p_T^2}{2\hat{t}\hat{u}}(\hat{s}-2m_h^2)c_{LO}\sum_{i,j=1}^{n_t}(g^2_{h\bar{q}_iq_j}G_{\square}(m_i,m_j)\right\} \\ &+ g^2_{h\bar{q}_iq_j,5}G_{\square,5}(m_i,m_j))\Bigg\}\Bigg], \end{aligned} \tag{8.42}$$

$$C = \pi^2 + \frac{11}{2} + \frac{23}{6}\log\frac{\mu_R^2}{\hat{s}}\,, \tag{8.43}$$

with

$$p_T^2 = \frac{(\hat{t}-M_H^2)(\hat{u}-m_h^2)}{\hat{s}} - M_H^2\,. \tag{8.44}$$

The definitions of the couplings and the triangle form factor $C_{i,\triangle}$ can be found in Eqs. (8.30, 8.32). The form factors are given in Appendix G. The sum in the formulae runs over all n_t top partners and the top quark. The constant c_{LO} is given by

$$c_{LO} = \left(\sum_{i=1}^{n_t}\frac{g_{h\bar{q}_iq_i}v}{m_i}\right)^2. \tag{8.45}$$

I have implemented the Composite Higgs cross section with these NLO corrections into the Fortran code `HPAIR` [110]. In order to exemplify our results, we consider the

Virtual corrections:

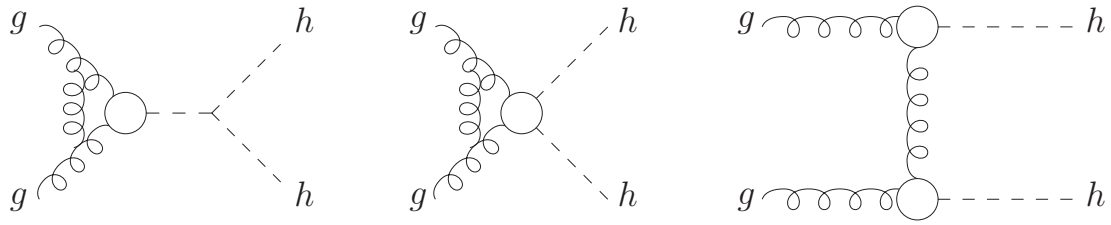

gg induced real corrections:

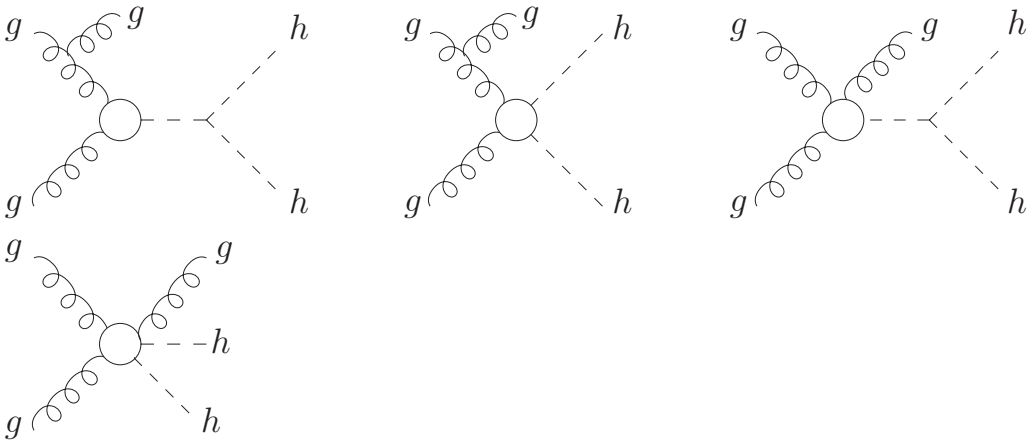

gq induced real corrections:

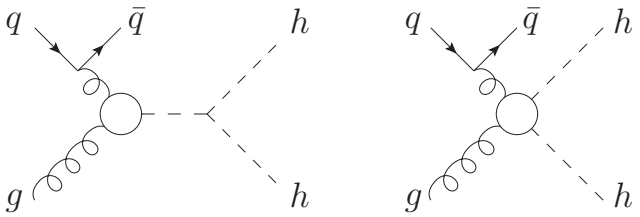

$q\bar{q}$ induced real corrections:

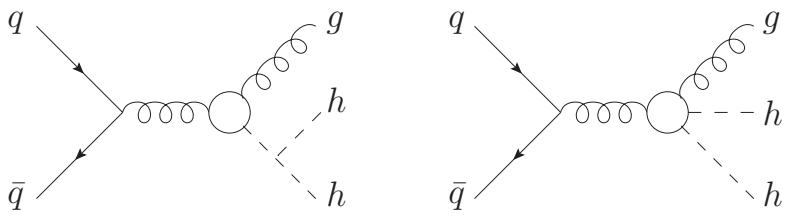

Figure 8.8.: Generic Feynman diagrams for the NLO QCD corrections to $gg \to hh$.

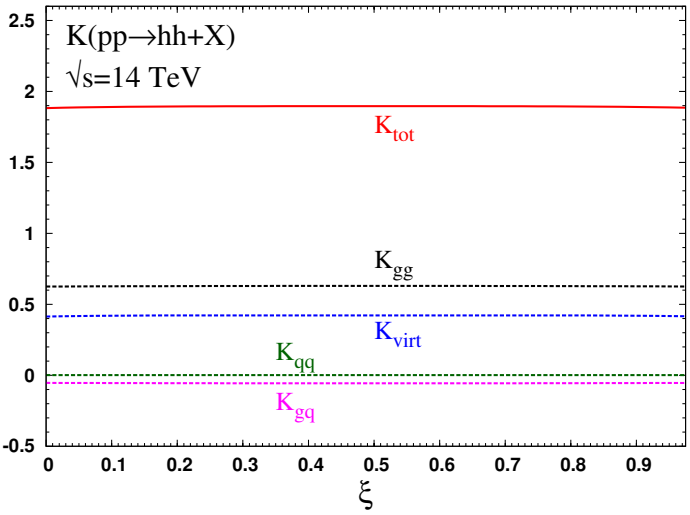

Figure 8.9.: K-factors for the $pp \to hh$ cross section as a function of ξ for the scale $\mu_F = \mu_R = M_{HH} = \sqrt{\hat{s}}$. The dashed lines show the individual contributions of the virtual contributions and the real corrections sorted by their initial states.

simpler case where only the pure Higgs non-linearities are taken into account. The constant c_{LO} then simplifies to $(1-2\xi)^2/(1-\xi)$ and the couplings reduce to $g_{h\bar{q}q,5} = 0$, $g_{h\bar{q}q} = m_q/v(1-2\xi)/\sqrt{1-\xi}$ and $g_{hh\bar{q}q} = -4\xi m_q/v^2$ with $n_t = 1$ and m_q denoting the respective quark mass. We define

$$K = \frac{\sigma_{NLO}}{\sigma_{LO}}\,, \qquad K_i = \frac{\Delta\sigma_i}{\sigma_{LO}}\,, \tag{8.46}$$

where $\Delta\sigma_i$ denotes the individual contributions to the NLO cross section. The cross section at LO is computed with the full top quark mass dependence. The cross sections are computed with the MSTW2008LO/MSTW2008NLO PDF set [111] according to the respective order of the cross section. The strong coupling constant is evaluated at the corresponding order with $\alpha_s^{NLO}(M_Z) = 0.12018$ and $\alpha_s^{LO}(M_Z) = 0.13939$. The scale is set to $\mu_F = \mu_R = M_{HH} = \sqrt{\hat{s}}$. Figure 8.9 shows the results for the K-factors for the case where the heavy top partner spectrum is integrated out as a function of ξ. The solid line shows the full K-factor, the dashed lines are the individual contributions. As can be seen from the plot, the real radiations of a gg initial state (black dashed line) are the most important contributions of the QCD corrections. They are followed by the virtual corrections (blue dashed line). The qg initiated real radiation diagrams (pink dashed line) and the $q\bar{q}$ ones (green dashed line) only lead to a very small correction. The lines basically do not depend on ξ. For the real radiation lines, the Born cross section, which shows the only dependence on ξ, factors out. out For the virtual contributions some dependence on ξ is to be expected. The C term of the virtual corrections, however, shows no dependence on ξ as it factorizes into the LO cross section. The only dependence of ξ can hence come from the A term in Eq. (8.41). It turns out, however, that the term given by C is the dominant one. This is already the case in the SM, where the A term contributes with less than 3% to $\Delta\sigma_{virt}$. This result will also hold

true for the case were the top partners are explicitly included. We thus conclude that, in good approximation, the NLO QCD corrections for Higgs pair production on the total cross section can directly be obtained by multiplying with the SM K-factor.

8.4. Summary

In this chapter we have investigated the effects of top partners on the single and double Higgs production cross sections via gluon fusion. Being both, already at LO, loop-induced processes, it is often helpful to calculate the gluon fusion cross sections via the LET approximation. In the LET approximation the loop-induced process is replaced by an effective gluon to Higgs boson coupling. In this chapter we have calculated the LET for both single and double Higgs boson production in the MCHM5 and compared to the exact cross section. For single Higgs boson production via gluon fusion, the LET very well approximates the full LO result. The full cross section depends barely on the details of the spectrum of the heavy top partners, but solely on the Higgs non-linearities expressed in terms of the parameter ξ. For double Higgs boson production via gluon fusion the LET does not provide a good approximation anymore. The full cross section shows a significant dependence on the spectrum of heavy top partners.

For the NLO QCD corrections to double Higgs boson production the LET is expected to describe the full result, if the Born cross section is taken into account with the full mass dependence. The reason is that the dominant contributions factorize into LO cross section and correction terms. Apart from the virtual corrections, which we have explicitly computed here, the corrections can be directly taken from the SM result. It turns out that the K-factor barely depends on ξ and is in good approximation given by the SM K-factor.

CHAPTER 9

Phenomenology of Bottom Partners

In the previously discussed model, with the fermions transforming in the **5** of $SO(5)$, no bottom partners with the correct quantum numbers to mix with the right-handed bottom quark were introduced. A bottom quark mass was thus not generated by the principle of partial compositeness. The bottom quark as next-heaviest fermion of the SM implies, however, a sizeable mixing with the strong sector.

Bottom partners automatically accompany top partners in the same fermionic representations. If one considers larger fermion representations than the previously discussed **5**, the top and bottom quark masses can easily be generated by a single representation. This has the advantage that no new parameters are necessary. The simplest possibility is the antisymmetric representation – a **10** of $SO(5)$. The purpose of this chapter is to show the phenomenological implications of bottom partners by means of the model of Section 7.2.2. As showed in Refs. [404–406], also partners of the lighter fermions can show an interesting phenomenology.

The chapter is organized as follows: First, in Section 9.1, the effects of bottom partners on EWPTs are discussed, followed by a discussion on direct searches of vector-like fermions and flavour physics in Section 9.2. The constraints from Higgs physics are investigated in Section 9.3, where all the results of the previous sections are taken into account to perform a χ^2 test to identify the preferred regions in parameter space. This chapter is based on Ref. [36].

9.1. Electroweak precision tests

As already shortly discussed for the top partners, New Physics models are quite constrained by the precise measurements of LEP1 of the resonant production of a Z boson. The gathered data allows, due to the very high accuracy, to probe indirectly New

Physics through loop contributions. On the theoretical side, a New Physics model can easily be checked by the calculation of the Peskin-Takeuchi parameters S, T, and U [407], which parameterize the *oblique* corrections entering through vacuum polarization diagrams of gauge boson propagators. The *non-oblique* corrections, namely vertex and box diagrams with couplings of new physics to light quarks and leptons are expected to be suppressed. The only exception is the vertex correction to the $Zb_L\bar{b}_L$ coupling, which gets sizable corrections due to New Physics. The reason is that the left-handed bottom quark is in the same $SU(2)_L$ doublet as the top quark, which can then couple in a sizable manner to new physics. We will shortly review the calculation of the S and T parameter in Composite Higgs Models. The U parameter gets contributions only from dimension-eight operators or higher. We will therefore not discuss it any further. The calculation of the vertex correction to $Zb_L\bar{b}_L$ will be discussed subsequently, with special focus on the influences of bottom partners on the calculation and the numerical results. Instead of using the S and T parameters and the shift in the $Zb_L\bar{b}_L$ coupling, we employ the parameters ϵ_1, ϵ_2, ϵ_3 and ϵ_b [408–410], as they do not depend on a reference point in the SM.

9.1.1. Contributions to ϵ_1

The T parameter – or equivalently ϵ_1 – gets a correction due to modified Higgs-vector boson couplings. They prevent a full cancellation of the UV-divergences in the T-parameter such that a logarithmically divergent part remains [376]. It is cut off by the mass of the first vector resonance m_ρ,

$$\Delta\epsilon_1^{IR} = -\frac{3\alpha(M_Z^2)}{16\pi c_W^2}\xi \log\left(\frac{m_\rho^2}{m_h^2}\right) , \tag{9.1}$$

with α the electromagnetic coupling at the scale M_Z. The cosine of the Weinberg angle is denoted by c_W. This contribution is called IR contribution as it stems from low-energy modifications due to the compositeness of the Higgs boson. Another important contribution to ϵ_1 comes from loops of fermionic partners. Explicit formulae at the one-loop order for the fermionic loop contributions can be found in Refs. [379, 411].

9.1.2. Contributions to ϵ_3

Similar to the IR contribution to ϵ_1, a UV-divergent contribution due to modified Higgs-vector boson couplings also arises for the S parameter – or ϵ_3 –,

$$\Delta\epsilon_3^{IR} = \frac{\alpha(M_Z^2)}{48\pi s_W^2}\xi \log\left(\frac{m_\rho^2}{m_h^2}\right) . \tag{9.2}$$

Additionally, at tree level there is a contribution from the mixing of elementary gauge fields with new vector and axial vector resonances [355, 412],

$$\Delta\epsilon_3^{UV} = \frac{M_W^2}{m_\rho^2}\left(1 + \frac{m_\rho^2}{m_a^2}\right) , \tag{9.3}$$

where m_a denotes the mass of the first axial vector resonance. For definiteness, we set $m_\rho/m_a \approx 3/5$ as obtained in the five-dimensional $SO(5)/SO(4)$ models of Refs. [26, 27]. We explicitly checked that varying m_ρ/m_a between 1 and 2 has only a slight effect on our numerical results.[1] The index 'UV' in Eq. (9.3) refers to the UV physics origin of this contribution.

The finite fermionic one-loop contributions to ϵ_3, which can be found in Ref. [411], are neglected, as they are small compared to the tree-level UV contributions. As pointed out in Ref. [374], there can be an additional logarithmically divergent contribution stemming from fermion loops, which is given by

$$\Delta\epsilon_3^{div} \sim \mathrm{Tr}\left[W_L^\dagger Y_L + W_R^\dagger Y_R\right] , \tag{9.4}$$

where $W_{L,R}$ are the left- and right-handed fermion couplings to W_μ^3 and $Y_{L,R}$ the corresponding hypercharges. In our case the trace in Eq. (9.4) is zero if we sum over the heavy fermion contributions including top and bottom quarks.

9.1.3. Contributions to ϵ_b

The New Physics contribution to ϵ_b is given by the shift in the $Zb_L\bar{b}_L$ coupling due to the new fermions. In this discussion, we try to stay as general as possible, such that the results can also be applied for other models. Our calculation differs from the previous works of Refs. [379, 380] by the inclusion of the mixing of the bottom quark with bottom partners.

The Lagrangian for the coupling of a Z boson to a quark Ψ_i^Q of charge Q in the mass eigenstate basis can be parameterized by

$$\mathcal{L}_Z = \frac{g_2}{2c_W} Z_\mu \bar{\Psi}_Q^i \gamma^\mu \left(X_{ij}^{QL} P_L + X_{ij}^{QR} P_R - 2s_W^2 Q\delta_{ij} \right) \Psi_Q^j , \tag{9.5}$$

where i, j run over all quarks present in the model. The matrix $X^{-1/3,L/R}$ is given by

$$X^{-1/3,L/R} = U_{L/R}^{b\,\dagger} T_L^3 U_{L/R}^b , \tag{9.6}$$

where T_L^3 is the generator defined in Eq. (E.11). For the top quark and top partners, $X^{2/3,L/R}$ is defined analogously. The amplitude of the Z boson decay into a pair of massless left-handed bottom quarks reads

$$\mathcal{M}_{Z\to b_L\bar{b}_L} = -\frac{e(g_{b_L}^{SM} + \delta g_{b_L})}{c_W s_W} \epsilon_\mu(p_Z)\bar{b}(p_{\bar{b}})\gamma^\mu P_L b(p_b) , \tag{9.7}$$

with the SM coupling $g_{b_L}^{SM}$ of the Z boson to the left-handed bottom quarks and the shift in the coupling due to New Physics δg_{b_L}. The polarization vector of the Z boson with four-momentum p_Z is denoted by ϵ_μ. We have introduced the momenta p_b and $p_{\bar{b}}$ of the bottom quark and antiquark, respectively.

[1] For a QCD like strong sector, the ratio m_ρ/m_a is roughly $1/\sqrt{2}$ [413].

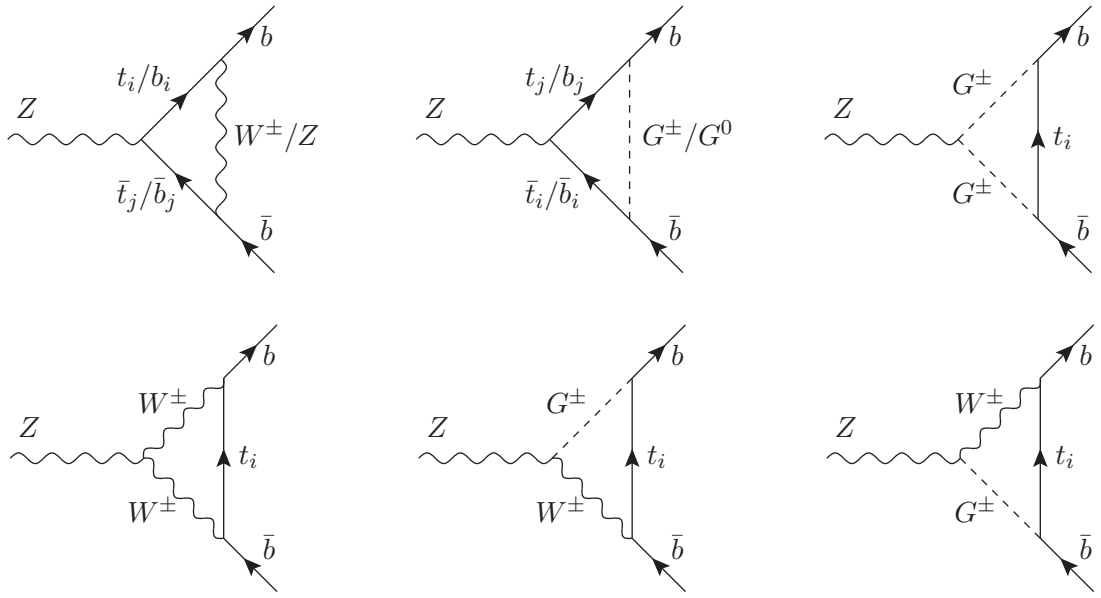

Figure 9.1.: Loop vertex diagrams for heavy fermion partner contributions to the $Zb_L\bar{b}_L$ coupling. The loops contain W bosons, Goldstone bosons and the top and bottom quark and their respective partners. The indices denote all indices occurring in the bottom and top mass matrices.

Large corrections to the $Zb_L\bar{b}_L$ coupling can occur at tree level if there is no symmetry protection. In Ref. [364] it was shown that custodial symmetry can provide such a protection of the $Zb\bar{b}$ coupling. If the $SU(2)_{L/R}$ quantum numbers obey either $T_L = T_R$ and $T_R^3 = T_L^3$ or $T_L^3 = T_R^3 = 0$, such a protection will take place.[2] The former condition is *e.g.* fulfilled if the bottom partner which mixes with the left-handed bottom quark (on Lagrangian level) is part of an $SU(2)_L \times SU(2)_R$ bidoublet, as it is the case for the $\mathbf{5_{2/3}}$ and $\mathbf{10_{2/3}}$ representations. In our case the tree-level shift in the coupling $\delta g_{Zb_L\bar{b}_L}$ is therefore tiny as we also explicitly verified numerically.

Important contributions can, however, still occur at one-loop level. We show the contributions to the one-loop corrections to the $Zb_L\bar{b}_L$ coupling in Fig. 9.1, including gauge bosons, Goldstone bosons, top and bottom quarks and their respective partners. Additionally, there are diagrams involving Higgs bosons, but they turn out to be very small. Hence we do not show them explicitly here. In order to quantify the beyond the SM effect of the heavy quarks on δg_{b_L}, the SM contribution $\mathcal{M}_{SM}^{t+b}$ of the bottom and top quarks has to be subtracted,

$$\delta g_{b_L} = \mathcal{M}^{heavy} - \mathcal{M}_{SM}^{t+b}\,, \tag{9.8}$$

where $\mathcal{M}^{heavy}$ denotes the contributions from the loops with the heavy quarks and the top and the bottom quarks. This assures that the effects of the modification of the top

[2]Note that this symmetry cannot simultaneously protect the $Zb\bar{b}$ coupling and the $Zt\bar{t}$ or $Wt\bar{b}$ couplings [364].

and bottom couplings due to the heavy new spectrum is taken into account properly. For a finite result, the $Zb_L\bar{b}_L$ vertex needs to be renormalized. We adopt an on-shell renormalization scheme similar to Ref. [414]. The wave-function renormalization constants $\delta Z^{L,R}$ relate the left- and right-handed bare fields $b_0^{L,R}$ with the renormalized ones $b^{L,R}$,

$$b_0^{L,R} = (1 + \frac{1}{2}\delta Z^{L,R})b^{L,R}\,. \tag{9.9}$$

The coupling of the Z boson to the bottom quarks involves the mixing matrices of the bottom-like quarks, see Eq. (9.6). The renormalization of the vertex hence requires their renormalization. Note that the exact definition of the generator T_L^3 in Eq. (9.6) is not relevant here, but only the fact that the mixing matrices are part of the coupling. The results can also be applied to other models as long as they have the general structure of the $Zb\bar{b}$ coupling as given in Eq. (9.6). For the renormalization of the mixing matrix U_L^b, defined in Eq. (7.32), a counterterm δu_L^b is introduced. The complete $Zb_L\bar{b}_L$ vertex including the counterterm in the mass eigenstate basis then reads

$$\begin{aligned}\mathcal{L}_{Z\bar{b}_L b_L} = -\frac{e}{s_W c_W}\bar{b}\,\gamma_\mu \left(1 + \frac{1}{2}\delta Z_L^\dagger\right)\left(1 + \delta u_L^b\right)\left(X^{-1/3,L} - 2s_W^2 Q\right) \\ \left(1 + \delta u_L^{b\,\dagger}\right)\left(1 + \frac{1}{2}\delta Z_L\right) P_L b\, Z^\mu\,.\end{aligned} \tag{9.10}$$

In Eq. (9.10) only wave-function renormalization constants and a counterterm for the mixing matrix are introduced. Counterterms for the electric charge, the Z boson field and the Weinberg angle are already included in the oblique parameters, as they are flavour-type universal. Since the light flavours do not get any New Physics corrections to the vertex, these counterterms can not lead to any new infinities compared to the SM matrix element. We can therefore expect that $\mathcal{M}^{heavy}$ is not finite with the given renormalization procedure in Eq. (9.10), but that δg_{b_L} as defined in Eq. (9.8) will be finite after the renormalization procedure.

The counterterm for the mixing matrix δu_L^b is defined antihermitian [213], to ensure the unitarity of the bare and renormalized mixing matrices,

$$\delta u_{L,ij}^b = \frac{1}{4}\left(\delta Z_{ij}^L - \delta Z_{ij}^{L\,\dagger}\right)\,. \tag{9.11}$$

For the renormalization we only need to calculate the wave-function renormalization constants δZ_{ij}^L. They are determined from Eqs. (5.15, 5.16). Note that throughout the calculation we have set $m_b = 0$, which implies that either m_i or m_j is zero in Eq. (5.15) and $m_i = 0$ in Eq. (5.16). The self-energies needed for the determination of the wave-function renormalization constants can be computed from the Feynman diagrams of Fig. 9.2.

The final results of the calculation can be found in Appendix H. Note again, that they are given as general as possible. The notation is very similar to the results given in Ref. [379]. Our results differentiate from those of Ref. [379] by the inclusion of the mixing of the bottom quarks with bottom partners, which led to a different renormalization procedure. My results of this section have been confirmed in a second independent calculation [415].

Figure 9.2.: Self-energy corrections needed for the renormalization of the vertex $Zb_L\bar{b}_L$.

9.1.4. The χ^2 test

The agreement of the model with the experimental data can be assessed by performing a χ^2 test. The experimental values for the ϵ parameters and their correlation ρ come from the LEP measurement at the Z pole mass, see Ref. [416]. We use, however, the updated values of Ref. [34], which take into account a newer value of the W boson mass [381–383]:

$$\begin{array}{rcl} \epsilon_1^{exp} &=& (5.4 \pm 1.0) \cdot 10^{-3}\,, \\ \epsilon_2^{exp} &=& (-7.9 \pm 0.90) \cdot 10^{-3}\,, \\ \epsilon_3^{exp} &=& (5.34 \pm 0.94) \cdot 10^{-3}\,, \\ \epsilon_b^{exp} &=& (-5.0 \pm 1.6) \cdot 10^{-3}\,, \end{array} \qquad \rho = \begin{pmatrix} 1 & 0.80 & 0.86 & 0.00 \\ 0.80 & 1 & 0.53 & -0.01 \\ 0.86 & 0.53 & 1 & 0.02 \\ 0.00 & -0.01 & 0.02 & 1 \end{pmatrix}. \tag{9.12}$$

The theory contributions to the parameters $\epsilon_1, \epsilon_2, \epsilon_3$ and ϵ_b are given by [34, 375],

$$\begin{array}{rcl} \epsilon_1^{th} &=& (5.66 - 0.86 \log(m_h/M_Z)) \cdot 10^{-3} + \Delta\epsilon_1^{IR} + \alpha \Delta T\,, \\ \epsilon_2^{th} &=& (-7.11 + 0.16 \log(m_h/M_Z)) \cdot 10^{-3}\,, \\ \epsilon_3^{th} &=& (5.25 + 0.54 \log(m_h/M_Z)) \cdot 10^{-3} + \Delta\epsilon_3^{IR} + \Delta\epsilon_3^{UV}\,, \\ \epsilon_b^{th} &=& -6.48 \cdot 10^{-3} + \delta g_{b_L}\,. \end{array} \tag{9.13}$$

The first summands in Eqs. (9.13) are the SM corrections. The contributions $\Delta\epsilon_i^{UV/IR}$ and δg_{b_L} have been given in Eqs. (9.1–9.3, 9.8) and ΔT is the contribution to the T parameter stemming from loops of heavy fermions as given in Ref. [379]. The covariance matrix is defined by

$$C_{ij} = \Delta\epsilon_i^{exp} \rho_{ij} \Delta\epsilon_j^{exp}\,, \tag{9.14}$$

where i, j runs over $1, 2, 3$ and b. The χ^2 test is thus defined as

$$\chi^2(\xi, M_{10}, \sin\phi_L, y) = \sum_{i,j} \left(\epsilon_i^{th} - \epsilon_i^{exp}\right) C_{ij}^{-1} \left(\epsilon_j^{th} - \epsilon_j^{exp}\right)\,. \tag{9.15}$$

We perform the χ^2 test for the four parameters ξ, M_{10}, $\sin\phi_L$ and y, as λ_t and λ_b of the Lagrangian in Eq. (7.27) are fixed by the requirement of recovering the measured values of the top and bottom quark masses. The parameter λ_q has been traded for $\sin\phi_L$. The mass of the first vector resonance m_ρ is set to its maximal value of $4\pi f$. We found that this leads for most of the parameter sets to minimal or close to minimal values of χ^2 as it minimizes $\Delta\epsilon_3^{UV}$. It also mirrors the fact that we only take the vector

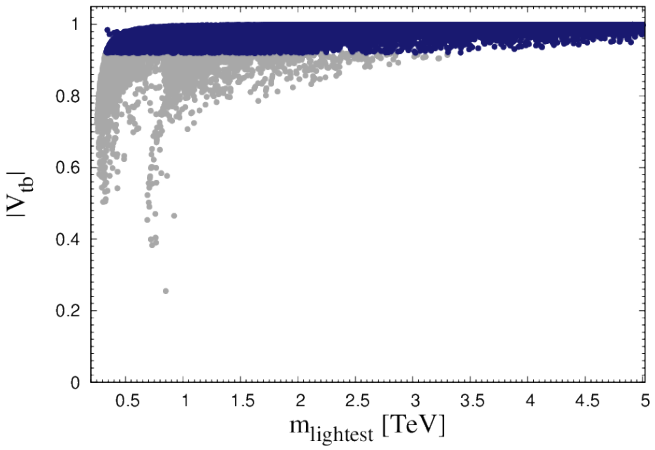

Figure 9.3.: The CKM matrix element $|V_{tb}|$ as a function of the lightest mass of the new fermions. The gray points are forbidden by the recent CMS measurement [417]. The dark blue points are allowed.

resonance indirectly into account as cut-off scale. A specific point in the parameter space fulfills the electroweak precision tests at 99% C.L. if it satisfies the criterion

$$\chi^2(\xi, M_{10}, \sin\phi_L, y) - \chi^2_{min} \leq 13.28\,, \tag{9.16}$$

where $\chi^2_{min} \approx 0.87$ is the minimum of χ^2. The latter is smaller than the SM value $\chi^2 \approx 4.71$ as expected for a model with additional parameters.

We performed a scan over the parameter space, setting the top and bottom quark masses to $m_t = 173.2$ GeV and $m_b = 4.2$ GeV, respectively, and the Higgs boson mass to $m_h = 125$ GeV. For the vector boson masses we used $M_W = 80.385$ GeV and $M_Z = 91.1876$ GeV. The model parameters have been varied in the range

$$0 \leq \xi \leq 1\,, \qquad 0 < \sin\phi_L \leq 1\,, \qquad |y| < 4\pi\,, \qquad 0 \leq M_{10} \leq 10 \text{ TeV}\,. \tag{9.17}$$

The range for y marks the perturbative regime. An additional constraint on the model is imposed by the recent measurement of the single top cross section at CMS [417], which provides a lower limit on the CKM matrix element $|V_{tb}| > 0.92$ at 95% C.L.. In our model we calculate V_{tb} from the matrix element of the W boson coupling matrix to the top and bottom quarks, $V_{tb}^{2/3,L}$, as defined in Eq. (H.1). Figure 9.3 shows $|V_{tb}|$ as a function of the lightest new fermion mass, which in our case is always a 5/3 charged fermion. The gray area shows the excluded points from the CMS constraint $|V_{tb}| > 0.92$, the dark blue points are the points which are still allowed. We only retained points which fulfill the EWPT at 99% C.L.. As can be inferred from the plot, the CMS measurement of Ref. [417] excludes quite some points, especially for small $m_{lightest}$. For $m_{lightest} \gtrsim 3.5\,\text{TeV}$ the measurement of $|V_{tb}|$ does not lead to any further constraint.

For the following discussion, we only retain points with $|V_{tb}| > 0.92$ unless stated otherwise. In Fig. 9.4 (left) we show the results of our scan in the $\sin\phi_L - \xi$ plane.

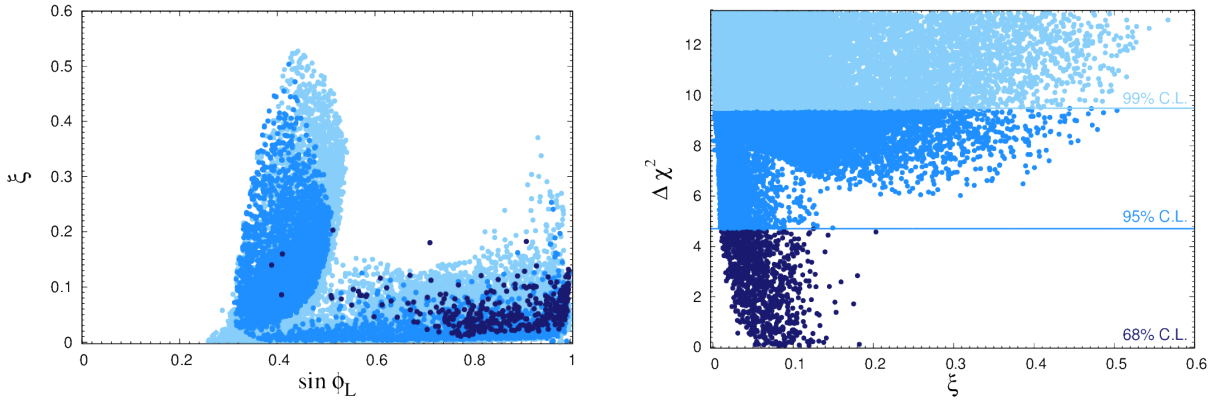

Figure 9.4.: Parameters passing the χ^2 test of electroweak precision observables, fulfilling in addition $|V_{tb}| > 0.92$, for a scan over ξ, $\sin\phi_L$, y and M_{10}. Dark blue: 68% C.L. region, medium blue: 95% C.L. region and light blue: 99% C.L. region. *Left:* the ξ-$\sin\phi_L$ plane. *Right:* $\Delta\chi^2$ versus ξ. This figure is already published in Ref. [36].

The colour code in the plot shows from darker to lighter colours the 68% C.L., the 95% C.L. and the 99% C.L. region. In the right plot of Fig. 9.4 we show $\Delta\chi^2$ versus ξ with the same colour code as in the left plot. From the two plots one can see that values up to $\xi \approx 0.2$ are still allowed by EWPT at 68% C.L.. Values up to $\xi \approx 0.55$ are allowed at 99% C.L.. For $\sin\phi_L$, there are two preferred region which allow high values of ξ: A region between $0.25 \lesssim \sin\phi_L \lesssim 0.4$ and a second one at $\sin\phi_L \approx 1$. The scan only leads to points with $\sin\phi_L \gtrsim 0.23$, otherwise the experimental top quark mass cannot be recovered, see Eq. (7.37). A similar plot to the left plot of Fig. 9.4 can be found in Ref. [380], for the fermions transforming in the fundamental representation. There, however, a maximal allowed value of $\xi \approx 0.35$ was found. Note though, that we use a different representation and instead of $m_\rho = 2.5$ TeV, we take $m_\rho = 4\pi f$, which can lower the tension with the electroweak precision observables. Note also that in both plots of Fig. 9.4 the SM limit cannot be achieved. The SM limit can be obtained for $y > 0$, by letting $\xi \to 0$ and $M_{10} \to \infty$, but we restricted ourselves to $M_{10} \leq 10$ TeV in the scan. We checked, however, explicitly that the SM limit is reached in the coupling matrices of the fermions to the Higgs boson, the Goldstone bosons and the vector bosons.

The inclusion of the bottom partners in the calculation was essential. Their inclusion not only requires the renormalization of the mixing matrix, but they also significantly influence the finite terms. We found parameters in our scan for which contributions of the bottom partner to the $Zb_L\bar{b}_L$ vertex can change $\Delta\chi^2$ by a factor of 2. For the majority of the parameter points, however, the effect is much smaller. We also explicitly calculated the Higgs boson contributions to $Zb_L\bar{b}_L$ and saw that they can maximally alter $\Delta\chi^2$ by $\pm 2.9\%$, and for most of the parameter points even less. We hence conclude that the Higgs contributions for $Zb_L\bar{b}_L$ are negligible.

A comment is in order about the approximation of zero bottom quark mass in the computation of the corrections to the $Zb_L\bar{b}_L$ vertex. Neglecting the bottom mass changes the couplings of the bottom quark and of the bottom-like quarks to the vector

bosons and Goldstone bosons. The effect, however, is small. The matrix element $X_{bb}^{-1/3,L}$, *cf.* Eq. (9.6), changes by maximally 1% and the change in the corresponding matrix element for the Goldstone coupling is $\mathcal{O}(m_b/v)$. Compared to the largest matrix elements in the Goldstone coupling matrix this is less than a percent effect.[3] A non-zero $X_{bb}^{-1/3,R}$ is induced by the bottom mass, but it is several orders of magnitude smaller than the other entries of this coupling matrix. We explicitly verified this numerically. Additional mass terms can arise in the loop corrections to the $Zb_L\bar{b}_L$ vertex. They are proportional to m_b/M_Z or higher powers, and assuming that the couplings multiplying these terms are of the same order as the ones multiplying m_t/M_Z, they would only contribute to about 3% of the total matrix element. A conservative estimate of the error done by neglecting the bottom mass is therefore 5%, obtained by adding up linearly the error due to the kinematics and an estimate of 2% for the error due to the change in the couplings. I have performed thes analysis of this section with a self-written `Mathematica` [338] code.

9.2. Constraints from direct searches and flavour physics

Further constraints on Composite Higgs Models come from direct searches of heavy vector-like fermions from Tevatron, ATLAS and CMS. The most restrictive constraints come from the ATLAS [396, 418–420] and CMS [395, 421, 422] searches for pair production of heavy new fermions. In our model, top partners can decay into W^+b, Zt and ht. If kinematically allowed, decays into a lighter new fermion accompanied by either a W, Z or h depending on the nature of the lighter fermion can occur. Bottom partners can analogously decay into W^-t, Zb and hb, or lighter new fermions. The lightest exotic fermion can only decay into W^+t or into a lighter top partner and a W boson if kinematically allowed. I have computed the theoretical predictions for the branching ratios of the new vector-like fermions. The formulae for the decay widths can be found in Appendix F.

The experimental collaborations give their newest results[4] directly in terms of branching ratios, assuming that *e.g.* for the case of a top partner

$$BR(T \to W^+b) + BR(T \to Zt) + BR(T \to ht) = 1\,. \tag{9.18}$$

Therefore, their results are strictly speaking only valid for the lightest new fermion and not necessarily for the heavier ones. In the specific model studied in this work, it turns out that the lightest new fermion is always an exotic 5/3 charged fermion. It decays to 100% into W^+t, such that the bound on the mass from the CMS analysis [395] of

$$m_\chi \geq 770 \text{ GeV}\,, \tag{9.19}$$

[3] We discuss here the Goldstone coupling and not the gauge boson coupling as this corresponds to the gauge-less limit in which *e.g.* in Ref. [380] the EWPT were calculated for the fundamental representation.

[4] Results before March 2013 were given as mass bounds under the assumption of branching ratios of 100%, see Section 8.2.1.

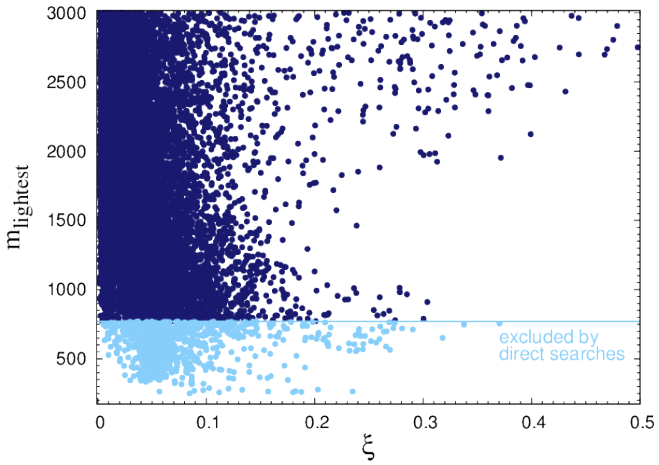

Figure 9.5.: Spectrum of the lightest composite fermion as function of ξ. The points in the plot are obtained from a scan over ξ, y, M_{10} and $\sin\phi_L$ and fulfill the EWPT at 99% C.L. and $|V_{tb}| > 0.92$. The light blue points are excluded by direct searches for vector-like fermions at 95% C.L., the dark blue points are not excluded. This plot is already published in Ref. [36].

can directly be applied to the lightest fermion. The bounds on the bottom-like quarks are less stringent, but for top-like quarks the ATLAS results extend up to 850 GeV, if the top partner decays mostly into ht [396]. This limit can be applied to the lightest top partner, since it is below the kinematic threshold of the decay $W^-\chi$, if χ has a mass larger than the limit given in Eq. (9.19). In our model, however, the search for top-like fermions never leads to stronger constraints than the searches for exotic 5/3 charged fermions. Figure 9.5 can confirm this fact, by showing the masses of the lightest partner as a function of ξ. The points in the plot fulfill the EWPT at 99% C.L. and lead to $|V_{tb}| > 0.92$. The light blue points are excluded at 95% C.L. by direct searches, the dark blue points are not excluded yet. The line marks the exclusion limit of Eq. (9.19). As can be inferred from the plot, this exclusion limit can eliminate quite some parameter space. All excluded points are, however, excluded by $m_{\chi,lightest} \geq 770$ GeV. No points above the line are excluded, confirming that the bounds on top-like fermions cannot further constrain the parameter space.

Flavour physics can lead to further constraints on Composite Higgs Models. They depend on the exact flavour structure of the model. For anarchic flavour structures very strong constraints arise from CP-violating observables in the Kaon system [423]. Implementing minimal flavour violation can, however, avoid these constraints [424]. In this case, also the light quarks are required to be composite, which can change the Higgs phenomenology [404]. While dijet searches put constraints on the New Physics coupling to up and down quarks [425, 426], the second generation quarks are practically unconstrained [427]. Alternatively, the top quark can be treated differently than the light quarks [428]. The flavour bounds can still be satisfied, and the constraints from EWPT and searches for compositeness are relaxed, as the first two generations are mostly elementary. Both the left-handed and right-handed top can be composite in this case. Bounds on the masses of the lightest fermionic resonance have been obtained

in Ref. [429] and depend on the specific flavour symmetry.[5] We do not assume a specific flavour model and therefore do not further discuss constraints from flavour physics.

9.3. Constraints from Higgs results

The recent Higgs results can further constrain the parameter space. As an input, theoretical predictions for Higgs boson production and decays are needed. They will be given in the next two subsections, followed by the numerical results of a χ^2 test with all the previously discussed constraints. The procedure to obtain the Higgs boson production and decay rates is very similar to the detailed discussion in Section 6.3.

9.3.1. Higgs boson production

Gluon fusion: Higgs boson production via gluon fusion is the dominant channel at the LHC. In the SM it is mediated by loops of top and bottom quarks. In Composite Higgs Models, as already described in Section 8.2.2, the loop contributions from the new fermions can be important. For the case of top partners we have seen in Fig. 8.1, that the cross section shows only a slight dependence on their spectrum. The cross section mainly depends on the Higgs non-linearities expressed by means of the parameter ξ. The gluon fusion cross section is therefore always reduced for $\xi < 0.75$ [430]. With bottom partners the situation changes, as the bottom quark cannot be described by the LET due to its small mass. The LET prediction for the matrix element of the bottom-like quarks, $\mathcal{M}_{bot}$, needs therefore to be modified to

$$\mathcal{M}_{bot} \approx \mathcal{M}_{LET}^{SM} \left(\frac{1-2\xi}{\sqrt{1-\xi}} - \frac{y_b}{y_b^{SM}} \right) , \tag{9.20}$$

with y_b and y_b^{SM} denoting the bottom Yukawa couplings in the Composite Higgs Model and the SM, respectively. The SM LET prediction for the matrix element is denoted by $\mathcal{M}_{LET}^{SM}$. The gluon fusion cross section hence depends on the details of the heavy bottom partner spectrum [397], encoded in the coupling y_b. The effects due to the heavy fermion spectrum are hence estimated to be of $\mathcal{O}(10\%)$ as the bottom quark effects on the gluon fusion cross section in the SM are of this size. I have implemented the process with the full fermion mass dependence into `HIGLU` [315] including the NLO QCD corrections [302–309, 326], following what has been done in the context of the 4th generation. This means that the Yukawa couplings had to be adjusted and all sums had to be extended to include the new fermions contributions. Electroweak corrections and NNLO QCD corrections have not been included. The former would require a dedicated calculation in the Composite Higgs Model. The latter is only available in the heavy top mass limit and cannot be applied to bottom quark loops. The thus obtained K-factor,

$$K = \frac{\sigma_{NLO}}{\sigma_{LO}} , \tag{9.21}$$

[5] For a mixing of the left-handed SM doublet of fermions with a $(2,2)$ under $SU(2)_L \times SU(2)_R$ and a mixing with $(1,3)$ of the right-handed fermions the mass bounds on the lightest fermion mass lie beneath the constraints from direct searches for a $U(2)^3$ flavour symmetry, see Ref. [429].

deviates by less then 2% from the SM K-factor, in accordance with Ref. [398], where the NLO and NNLO QCD corrections for Composite Higgs Models are calculated.

Vector boson fusion: The VBF cross section can be obtained from the SM cross section by multiplying with the modification factor for the Higgs boson coupling squared to vector bosons,

$$\sigma_{VBF}^{CHM} = \sigma_{VBF}^{SM}(1-\xi)\,. \tag{9.22}$$

The cross section is always reduced compared to the SM due to the reduced hVV coupling. The NLO QCD corrections are taken over from the SM [127–129, 316]. The SM cross section has been calculated with `VV2H` [110].

Higgs-strahlung off vector bosons: As for VBF, the Higgs-strahlung cross section can be obtained from the SM cross section by multiplying with the modification factor for the hVV coupling squared

$$\sigma_{VH}^{CHM} = \sigma_{VH}^{SM}(1-\xi)\,. \tag{9.23}$$

The SM cross section was taken at NLO QCD [137, 316] and calculated by means of the code `V2HV` [110].

Associated production with top quarks: The SM cross section for associated production with top quarks is quite small, roughly two orders of magnitude smaller than the gluon fusion cross section. The composite Higgs cross section can be obtained from the SM cross section by modifying accordingly the Higgs boson coupling,

$$\sigma_{ht\bar{t}}^{CHM} = \sigma_{ht\bar{t}}^{SM}\left(\frac{g_{ht\bar{t}}}{g_{ht\bar{t}}^{SM}}\right)^2\,, \tag{9.24}$$

where the coupling $g_{ht\bar{t}}$ is the matrix element of the Higgs boson coupling matrix in Eq. (7.39) associated with the top quark. In the SM, the cross section is known at NLO QCD [317–320]. We have taken the value given at the LHC Higgs cross section working group homepage [321] for $m_h = 125$ GeV.

9.3.2. Higgs boson decays

The branching ratios for the Higgs boson decays have been calculated with an adapted version of `HDECAY` [223, 322, 323]. All the decays are taken at NLO QCD if available in `HDECAY`. We have explicitly removed the electroweak corrections to the Higgs boson decays, as they can only be taken over for small deviations from the SM [431]. For the specific decay channels I have modified `HDECAY` in the following way: For the Higgs decays into fermions, the SM decay widths needed to be multiplied by modification factors for the Higgs boson couplings,

$$\Gamma_{h\to f\bar{f}}^{CHM} = \begin{cases} \left(\frac{(G_{hb\bar{b}})_{b\bar{b}}}{g_{hb\bar{b}}^{SM}}\right)^2 \Gamma_{h\to f\bar{f}}^{SM} & \text{if } f = b\,, \\ \frac{(1-2\xi)^2}{1-\xi}\Gamma_{h\to f\bar{f}}^{SM} & \text{if } f = c, s, \mu, \tau\,. \end{cases} \tag{9.25}$$

The modified coupling of the Higgs boson to a pair of bottom quarks $(G_{hb\bar{b}})_{b\bar{b}}$ is obtained from the coupling matrix $G_{hb\bar{b}}$ of Eq. (7.39) by taking the matrix element corresponding

to the mass eigenstate with the bottom quark mass. The Higgs boson to light fermion coupling is modified by a factor $(1-2\xi)/\sqrt{1-\xi}$ due to the Higgs non-linearities. For a Higgs boson of 125 GeV, decays into on-shell top quarks are kinematically forbidden. The decays into vector bosons V are obtained from the corresponding SM widths by the modification

$$\Gamma^{CHM}_{h\to VV} = (1-\xi)\,\Gamma^{SM}_{h\to VV}\,. \tag{9.26}$$

In the loop-induced decays, the loops of the top and bottom partners need to be taken into account. The widths of the Higgs boson decays into photons and gluons are given by

$$\begin{aligned}\Gamma_{\gamma\gamma} =& \frac{G_F\alpha^2 m_h^3}{128\sqrt{2}\pi^3}\left|\sum_{i=1}^{5}\frac{4}{3}\frac{v(G_{ht\bar{t}})_{ii}}{m_{t_i}}\,A^S_{1/2}(\tau_{t_i}) + \sum_{i=1}^{4}\frac{1}{3}\frac{v(G_{hb\bar{b}})_{ii}}{m_{b_i}}\,A^S_{1/2}(\tau_{b_i})\right.\\ &\left. + \frac{1-2\xi}{\sqrt{1-\xi}}\,A^S_{1/2}(\tau_\tau) + \frac{4}{3}\frac{1-2\xi}{\sqrt{1-\xi}}\,A^S_{1/2}(\tau_c) + \sqrt{1-\xi}A_1(\tau_W)\right|^2\,, \end{aligned}\tag{9.27}$$

$$\begin{aligned}\Gamma_{gg} =& \frac{G_F\alpha_s^2 m_h^3}{64\sqrt{2}\pi^3}\left|\sum_{i=1}^{5}\frac{v(G_{ht\bar{t}})_{ii}}{m_{t_i}}A^S_{1/2}(\tau_{t_i}) + \sum_{i=1}^{4}\frac{v(G_{hb\bar{b}})_{ii}}{m_{b_i}}A^S_{1/2}(\tau_{b_i})\right.\\ &\left. + \frac{1-2\xi}{\sqrt{1-\xi}}A^S_{1/2}(\tau_c)\right|^2\,, \end{aligned}\tag{9.28}$$

where we introduced the notation

$$\tau_W = \frac{4M_W^2}{m_h^2},\quad \tau_{t_i/b_i} = \frac{4m_{t_i/b_i}^2}{m_h^2},\quad \tau_c = \frac{4m_c^2}{m_h^2}\quad\text{and}\quad \tau_\tau = \frac{4m_\tau^2}{m_h^2}\,. \tag{9.29}$$

The loop functions $A^S_{1/2}$ and A_1 are given in Eqs. (6.49) and (6.59), respectively. Note, that the loop contributions of the top-like fermions in Eqs. (9.27) and (9.28) reduce to the LET contributions in the limit of heavy fermion masses, and hence only depend on the Higgs non-linearities.

We do not give any results for the Higgs boson decay into $Z\gamma$, as the current experimental results are not sensitive to this channel yet. The calculation of this decay width for our model involves the calculation of the matrix element with two different fermions in the loops, see Ref. [415]. The decay rate is, however, mostly dominated by the W boson contribution, which is reduced by $(1-\xi)$. Due to the smallness of the decay width and because it only enters in the total width in our discussion, we will not investigate it here any further. Note that in some Composite Higgs Models large deviations from the SM in $h\to Z\gamma$ are possible [432].

9.3.3. Numerical results

In order to check the compatibility of our model with EWPTs, the recent Higgs results and the measurement of V_{tb}, a χ^2 test is performed, where

$$\chi^2 = \chi^2_{EWPT} + \chi^2_{Higgs} + \chi^2_{V_{tb}}\,, \tag{9.30}$$

for the parameter points of the scan specified in Eq. (9.17). No contribution of the direct searches is included in Eq. (9.30), as no χ^2 information is available. We, however, exclude all points from the scan which do not fulfill direct searches at 95% C.L.. The contributions of the EWPTs, χ^2_{EWPT}, are defined in Eq. (9.15). For the Higgs boson results the experimental collaborations provide results in terms of the signal strength modifiers, $\mu(X)$, defined as

$$\mu(X) = \frac{\sigma(pp \to h) \cdot BR(h \to X)}{\sigma(pp \to h)_{SM} \cdot BR(h \to X)_{SM}} \,. \tag{9.31}$$

They also provide the correlation between the $ggh{+}t\bar{t}h$ and the $VBF{+}VH$ production channels. This correlation can be taken into account via a covariance matrix C defined by

$$C = \begin{pmatrix} \Delta\mu^2_{ggF+tth} & \rho\Delta\mu_{ggF+tth}\,\Delta\mu_{VBF+VH} \\ \rho\Delta\mu_{ggF+tth}\,\Delta\mu_{VBF+VH} & \Delta\mu^2_{VBF+VH} \end{pmatrix}, \quad \Delta\mu_i \equiv \sqrt{(\Delta\mu_i^{exp})^2 + \left(\Delta\mu_i^{th}\right)^2}. \tag{9.32}$$

The experimental values for the best-fit points $\Delta\mu_i$, their errors $\Delta\mu_i^{exp}$ and the correlation ρ have been extracted from the ellipse plots of Refs. [49, 433]. The thus obtained numerical values can be found in Ref. [36]. The theoretical uncertainties on μ, denoted by $\Delta\mu_i^{th}$, are obtained by calculating the uncertainties on the production cross sections due to scale dependence and PDF+α_s uncertainties. We use the relative errors on the SM cross section throughout the analysis, but explicitly checked that the errors did not change significantly in our model. The errors are consistently taken at NLO QCD. The theoretical error on μ_{VBF+VH} becomes zero because, due to the same scaling behaviour of the VBF and VH cross section, a cancellation between the SM error and the Composite Higgs cross section error can take place. With these ingredients at hand, χ^2_{Higgs} is finally defined by

$$\chi^2_{Higgs} = \sum_{channels} \sum_{i,j=1,2} (\mu_i^{exp} - \mu_i^{th}) C^{-1}_{ij} (\mu_j^{exp} - \mu_j^{th}) \,, \tag{9.33}$$

with $i,j = 1$ corresponding to the $(ggF + tth)$ production channel and $i,j = 2$ to $(VBF + VH)$. The sum over the channels takes into account the Higgs decays into $b\bar{b}$, $\tau\bar{\tau}$, $\gamma\gamma$, WW and ZZ. Note that ATLAS does not provide any information on the correlation in the $b\bar{b}$ decay mode. In this case we define the χ^2 of the $b\bar{b}$ channel as

$$\chi^2_{h\to b\bar{b}} = \frac{(\mu_b^{exp} - \mu_b^{th})^2}{(\Delta\mu_b^{exp})^2 + (\Delta\mu_b^{th})^2} \,, \tag{9.34}$$

where in the definition of μ_b, all production channels are summed up.

The χ^2 contribution from the measurement of V_{tb} reads

$$\chi^2_{V_{tb}} = \frac{(|V_{tb}^{exp}| - |V_{tb}^{th}|)^2}{(\Delta V_{tb}^{exp})^2} \,. \tag{9.35}$$

For the SM value we have assumed that $|V_{tb}^{th}| = 1$. The experimental best fit value is given by [417]

$$|V_{tb}^{exp}| = 1.02 \pm 0.046 \,, \tag{9.36}$$

Experiment	$\lvert V_{tb}\rvert > 0.92$			$\lvert V_{tb}\rvert$ in χ^2		
	ξ	χ^2/n	χ^2_n	ξ	χ^2/n	χ^2_n
ATLAS	0.105	8.06/9	0.90	0.096	12.34/10	1.23
	0	17.54/13	1.35	0	17.73/14	1.25
CMS	0.057	5.22/10	0.52	0.055	6.36/11	0.58
	0	9.90/14	0.71	0	10.09/15	0.67

Table 9.1.: Global χ^2 results for the best fit points taking into account EWPTs and the Higgs results of the ATLAS and CMS analyses, respectively: *Left:* For parameter points which fulfill $|V_{tb}| > 0.92$. *Right:* When including the measured value of $|V_{tb}|$ in the χ^2 test. The rows for $\xi = 0$ list for comparison the SM values. The number of degrees of freedom, n, are counted naively as the difference between the number of observables and the number of parameters in the model, and $\chi^2_n \equiv \chi^2/n$. This table is already published in Ref. [36].

where unitarity of the CKM matrix is not assumed. In Table 9.1, the best fit values of the scan are summarized. On the left side, the best fit values were obtained by not including $\chi^2_{V_{tb}}$ into the total χ^2 but instead requiring $|V_{tb}| > 0.92$. The right side are the best fit values if $\chi^2_{V_{tb}}$ is included into the fit. For the ATLAS Higgs results the best fit values are around $\xi \approx 0.1$, for CMS at $\xi \approx 0.055$. The best fit values are always better than the SM value, due to the larger number of free parameters. The ratio $\chi^2_n = \chi^2/n$, where n denotes the number of degrees of freedom, gives an estimate of the relative goodness of the fit. Note, however, that the counting of free parameters is not obvious, as the SM limit is reached for $y > 0$, $\xi \to 0$ and $M_{10} \to \infty$. The other parameters become meaningless in this limit.

Figure 9.6 shows $\Delta\chi^2 = \chi^2 - \chi^2_{min}$ as a function of ξ. In χ^2 the full definition of Eq. (9.30) is used including $\chi^2_{V_{tb}}$. The minimal value χ^2_{min} is the one of the best fit point. The colour distinguishes between points which do better than the SM (dark blue) and those doing worse (light blue). For the CMS results only points with $\xi \lesssim 0.1$

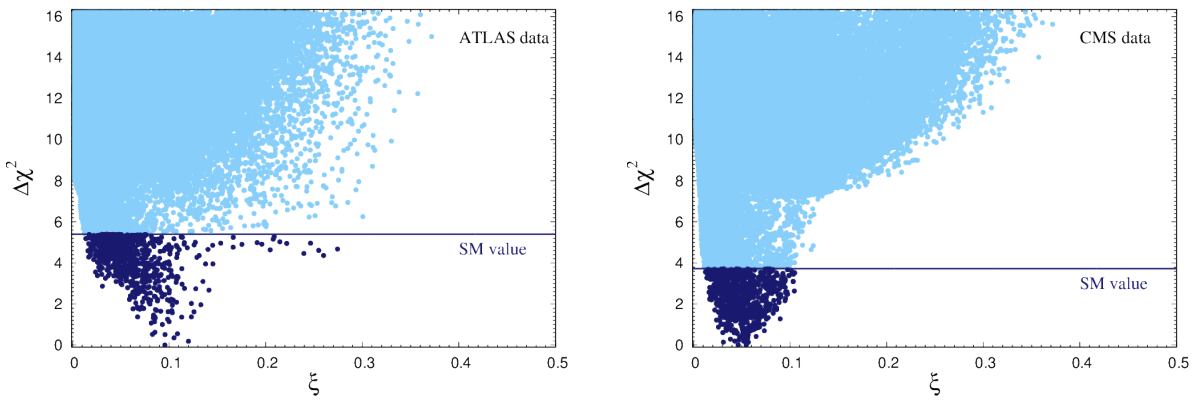

Figure 9.6.: $\Delta\chi^2 = \chi^2 - \chi^2_{min}$ taking into account the Higgs results of ATLAS (left) and CMS (right), as a function of ξ. The dark blue points do better than the SM, the light blue points have a higher $\Delta\chi^2$. This figure is already published in Ref. [36].

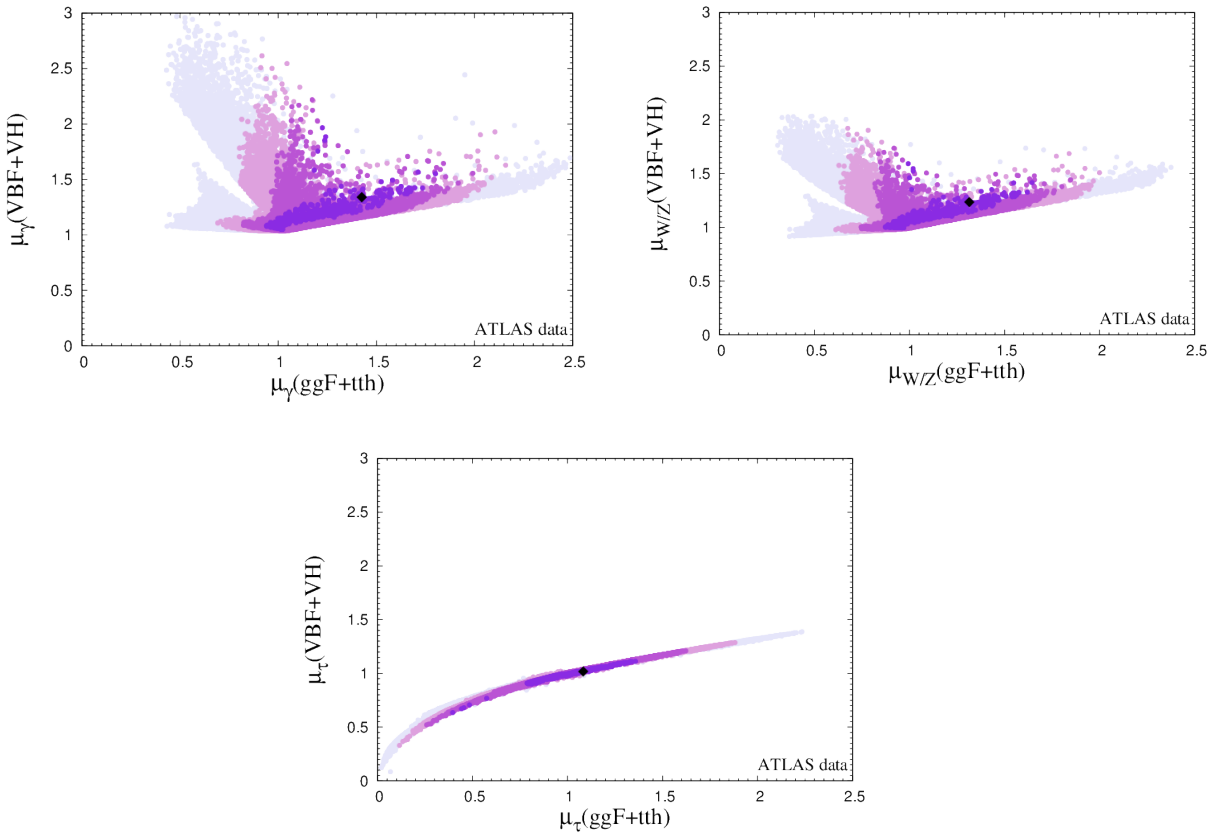

Figure 9.7.: Fit results obtained from a scan over ξ, y, $\sin\phi_L$ and M_{10} taking into account EWPTs, the measured value of $|V_{tb}|$ and the ATLAS Higgs results, shown in the $\mu_{ggF+tth} - \mu_{VBF+VH}$ plane for the channels $\gamma\gamma$ (top left), W^+W^-, ZZ (both top right) and $\tau^+\tau^-$ (bottom). The black rhombus in the plot is the best fit point. The colour code in the plots indicates from dark to light colours the 1σ, 2σ, 3σ and 5σ regions obtained from the χ^2 test with four degrees of freedom. These plots are already published in Ref. [36].

have a lower $\Delta\chi^2$ than the SM, while for the ATLAS results this is the case for points up to $\xi \lesssim 0.25$, although most of the scenarios doing better than the SM are for $\xi \lesssim 0.15$. Note that these plots can give some information on the amount of fine-tuning needed to comply with the data. The minimal amount of fine-tuning can be estimated by $\Delta = 1/\xi$, which corresponds to the inverse of the cancellation among the parameters in the Higgs potential needed in order to satisfy the EWSB condition [365]. This would *e.g.* mean for our CMS best fit point at $\xi \approx 0.05$ a tuning of $\Delta \approx 20$, and a bit less tuning for the ATLAS best fit point at $\xi \approx 0.1$ of $\Delta \approx 10$. This is only a very rough estimate. A better measure can be obtained by taking into account the explicit form of the Higgs potential, as was *e.g.* discussed in Ref. [365, 434].

In Fig. 9.7, the fit results of the scan in the $\mu_{ggF+tth} - \mu_{VBF+VH}$ plane for the Higgs decay channels into γ, W, Z and τ pairs, respectively, are shown. The black rhombus in the plot marks the best fit point obtained from the minimum value of the χ^2 test.

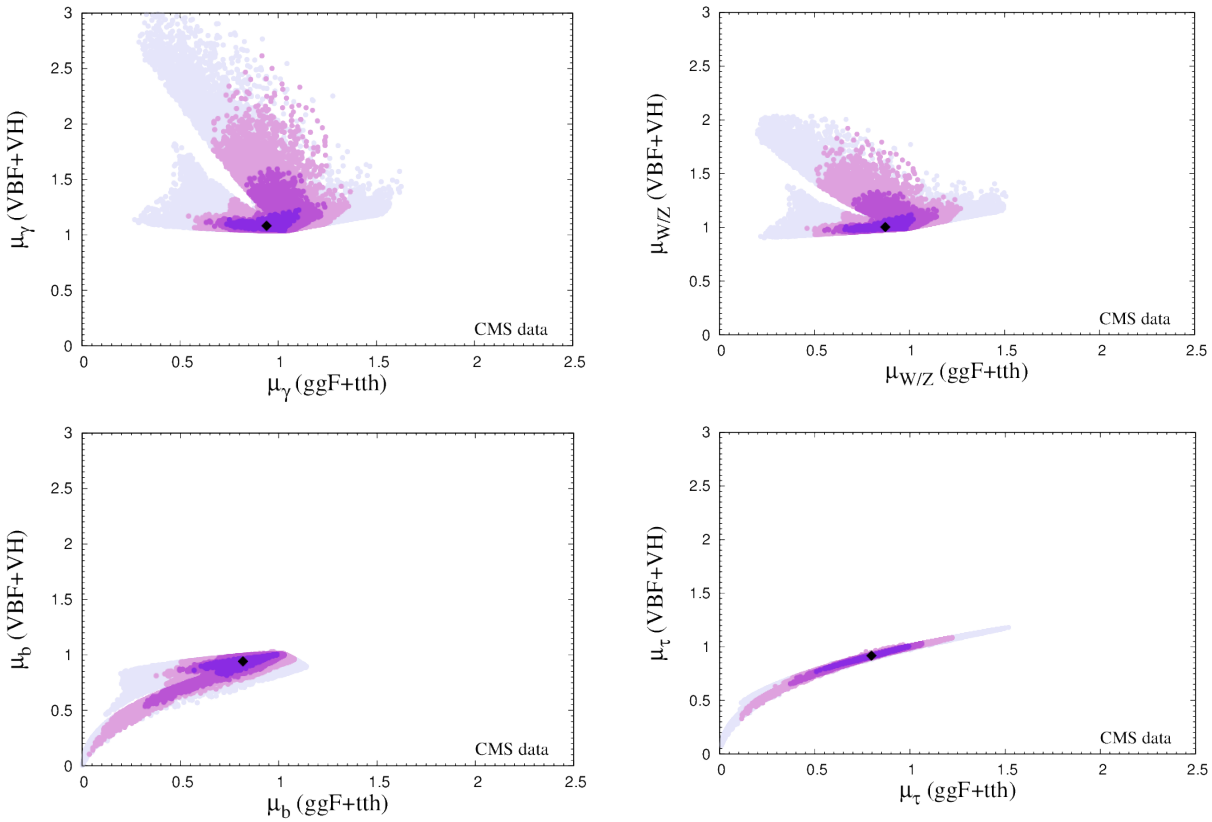

Figure 9.8.: Fit results obtained from a scan over ξ, y, $\sin\phi_L$ and M_{10} taking into account the EW precision data, the measured value of $|V_{tb}|$ and the CMS Higgs results, shown in the $\mu_{ggF+tth} - \mu_{VBF+VH}$ plane for the channels $\gamma\gamma$ (top left), W^+W^-, ZZ (both top right), $b\bar{b}$ (bottom left) and $\tau^+\tau^-$ (bottom right). The black rhombus in the plot is the best fit point. The colour code in the plots indicates from dark to light colours the 1σ, 2σ, 3σ and 5σ regions obtained from the χ^2 test with four degrees of freedom. These plots are already published in Ref. [36].

The colour code in the plots indicates from

dark to light colours the 1σ, 2σ, 3σ and 5σ regions obtained from the χ^2 test as defined in Eq. (9.30) with the experimental Higgs results of ATLAS. The fit contours for W and Z bosons are the same as their couplings are modified in the same way due to custodial symmetry. They are thus depicted in the same plot. As can be inferred from Fig. 9.7 (top left and right), the ATLAS data prefer an enhanced Higgs to $\gamma\gamma$ and Higgs to vector boson rate. The best fit point in the τ channel shows a nearly SM like rate. The same plots for the CMS Higgs results can be found in Fig. 9.8. Additionally, the $b\bar{b}$ channel is shown (bottom left), as CMS provides information about the $(VBF+VH)$ and $(ggF+tth)$ production modes and their correlation in the $b\bar{b}$ channel. The best fit points are near the SM-like rates in the $\gamma\gamma$ final state, while the rates in the W^+W^-, ZZ, $b\bar{b}$ and $\tau^+\tau^-$ channel are slightly reduced in the $(ggF+tth)$ production mode with respect to the SM value. In the $\tau\bar{\tau}$ final state the region of points passing the test is very narrow. This behaviour can already be found before

Experiment	ξ	$m_{t_{lightest}}$	χ^2
ATLAS	0.067	806 GeV	13.71
CMS	0.055	1335 GeV	7.17

Table 9.2.: Global χ^2 results for the best fit point respecting EWPT, $|V_{tb}|$ and the Higgs search results by ATLAS and CMS, respectively, with the corresponding ξ value and the mass of the lightest top partner $m_{t_{lightest}}$. In addition the constraint of Eq. (7.42) originating from the connection between a light Higgs boson and light resonances was taken into account. This table is already published in Ref. [36].

applying EWPT and $|V_{tb}|$ constraints. This means the signal strength modifiers for the different production modes $(ggF+tth)$ and $(VBF+VH)$ are correlated. This can be understood if one takes into account for a moment only the Higgs non-linearities. Then both production via gluon fusion and the decay rate $h \to \tau\bar{\tau}$ decrease with ξ proportional to $(1-2\xi)^2/(1-\xi)$. This means that the gluon fusion production cross section and the decay rate into $h \to \tau\bar{\tau}$ decrease for $\xi = 0, ..., 0.5$ and vanish completely for $\xi = 0.5$. The $(VBF+VH)$ production mode decreases with $(1-\xi)$. Due to this strong correlation between the rates from this two production channels only a small stripe remains in the $\mu_{ggF+tth} - \mu_{VBF+VH}$ plane. The effect of the imposed constraints is then merely to divide this strip into the 1σ to 5σ regions.

The region in the b-quark final state, *cf.* Fig. 9.8 (bottom left), is similarly explained. It is, however, more spread because the Higgs coupling to the bottom quarks and hence the branching ratio into the $b\bar{b}$ final state is influenced directly by the compositeness of the bottom quark. For the WW, ZZ and $\gamma\gamma$ final states there is no such strong correlation between the rates.

So far, I have not taken into account in my analysis of this section the connection between a light Higgs boson and light top partners given in Eq. (7.42). If this bound is employed, we obtain new best fit values given in Table 9.2. Additionally, we give in Table 9.2 the mass of the lightest top partner. The global χ^2 results of the new best fit values become slightly worse. Automatically, large values of ξ are eliminated, as otherwise the bound on the mass of the lightest partner would be below the exclusion from direct searches.

9.4. Summary

In this chapter the phenomenology of bottom partners has been investigated. We considered fermions transforming in the antisymmetric representation of $SO(5)$, which allowed us to introduce the bottom quark mass by the principle of partial compositeness. Being guide-lined by the principle of minimality, only the necessary operators have been introduced, leading to a minimal amount of new parameters. The constraints on such a model were investigated, with special focus on EWPTs, direct searches for new vector-like fermions, the constraint on $|V_{tb}|$ and from the current Higgs results. Compared to the previous works [378–380] computing the EWPTs in Composite Higgs

Models, we included in our calculation the loop contributions of the bottom partner to the constraint on $Zb_L\bar{b}_L$. The contributions of the bottom partners turned out to have a significant impact on the EWPTs.

Bottom partners can also have an important influence on the Higgs boson production and decay channels. As has been shown in Chapter 8, the gluon fusion Higgs production cross section can well be described by the LET approximation, which is independent of the details of the top partner spectrum. Once the bottom quark has a significant mixing with bottom partners, however, the gluon fusion cross section will show a dependence on the bottom partner spectrum, since the LET cannot be applied for the bottom quark. Hence, the full mass dependence needs to be taken into account for the calculation of the loop-induced processes. In this spirit, we evaluated here the production and decay modes of the Higgs boson and compared them to the available Higgs data.

For our final results we performed a χ^2 test, checking the compatibility of the model with EWPTs, the measurement of V_{tb} and the Higgs results. Direct searches for vector-like fermions were taken into account by excluding the affected points from the scan. ATLAS data prefers values of $\xi \approx 0.1$, with enhanced rates of the Higgs boson decaying into photons and vector bosons. CMS data prefers values of $\xi \approx 0.05$ with rather SM-like Higgs rates.

In conclusion, it was shown that the model is still in good agreement with all the investigated constraints. Bottom partners can play an important role for the viability of the model with the experimental data. The preferred values of ξ correspond to a moderate amount of fine-tuning.

CHAPTER 10

Conclusion

The discovery a Higgs boson with a mass of $\sim$ 125 GeV marks a huge success for particle physics. The next phase is the precise measurement of the properties of this last ingredient of the SM. One of the last steps to experimentally verify the mechanism of electroweak symmetry breaking of the SM is the measurement of the Higgs boson self-couplings, since they give direct access to the Higgs potential. The determination of the triple Higgs coupling provides a first step towards the experimental verification of the Higgs potential.

In the framework of this thesis, we have given predictions for the inclusive SM Higgs boson pair production cross sections via gluon fusion, vector boson fusion, Higgs-strahlung off a W or Z boson and associated production with a top quark pair. We have included in the discussion the NLO QCD corrections for gluon fusion and vector boson fusion processes. The Higgs-strahlung cross section has been given at NNLO QCD. The gluon induced subchannel of Higgs-strahlung off a Z boson, which is part of the NNLO corrections, has been calculated for the first time in the framework of this thesis. For the three processes gluon fusion, vector boson fusion and Higgs-strahlung, we have studied in detail the theoretical uncertainties. It turns out that they are of $\mathcal{O}(40\%)$ for the gluon fusion process and well below 10% for vector boson fusion and Higgs-strahlung. Our input is important for the experimental studies on the accessibility of the triple Higgs boson coupling.

The current results from LHC still leave space for physics beyond the SM. Precise predictions of the phenomenological implications of New Physics are a necessary input for the discovery of new particles or for the derivation of exclusion bounds. A particularly appealing New Physics scenario is supersymmetry. In the second part of this thesis, after giving a small introduction into supersymmetry, we have discussed the decays of a light top squark in the framework of the MSSM with flavour violation. In particular, we have been interested in the kinematic region in which the top squark can

either decay via a flavour changing decay into $(u/c)\tilde{\chi}_1^0$ or via a four-body decay. In the framework of this thesis, we have calculated the NLO QCD corrections to the $(u/c)\tilde{\chi}_1^0$ decay, allowing for the process to occur already at tree level. The corrections turn out to be $\mathcal{O}(10\% - 30\%)$. The four-body decay has been computed in this thesis with the full mass dependence of the third generation fermions including flavour-violating couplings. The flavour-violating effects are small if no flavour-violating sources other than the Yukawa couplings are introduced. The inclusion of the third generation fermion masses, however, turns out to be important.

In Chapter 6, we have studied the Higgs sector of the NMSSM with complex parameters. The five neutral Higgs bosons are then mixtures of the CP-even and CP-odd components. In this thesis, we have computed one-loop corrections to the neutral Higgs boson masses. These corrections are essential. Our analysis has shown that the Higgs boson masses can significantly depend on the phases of the complex parameters. This is in particular the case if the phases already enter the Higgs sector at tree level. Furthermore, we have given Higgs production cross sections and decay rates for the NMSSM with complex parameters.

Another interesting alternative to the SM are Composite Higgs Models. In the third part of the thesis we first gave a short introduction to such models, in which the Higgs boson is a pseudo-Goldstone Boson of a strongly-interacting sector. The Higgs mass value implies for these models the emergence of light fermionic resonances.

In Chapter 8 we have focused on fermionic resonances that can mix with the top quark. These top partners can influence Higgs boson production via gluon fusion through their loop contributions. We studied in detail the effects of the top partners on single and double Higgs boson production, also by comparing with the predictions obtained by means of the low-energy theorem. It turned out that the inclusive single Higgs boson production cross section can well be approximated by the low-energy theorem. The low-energy theorem approximation is independent of the details of the heavy spectrum, the cross section in the full mass dependence only depends slightly on the spectrum of the top partners. For double Higgs boson production the low-energy theorem prediction shows large deviations from the cross section in the full mass dependence of the fermions in the loop. The double Higgs boson production cross section including the full mass dependence of the loop particles shows a sizable dependence on the spectrum of the heavy fermions. We ended Chapter 8 with a discussion of the NLO QCD corrections to Higgs pair production via gluon fusion in the low-energy theorem approximation. In turns out, that the NLO QCD K-factor of roughly 1.9 can well be described by the SM K-factor of Ref. [105].

In Chapter 9 we studied fermionic resonances which can mix with the bottom quark. These bottom partners can show important effects on electroweak precision observables and Higgs boson production and decay rates. In the framework of this thesis, we computed the one-loop contributions of the bottom partners to the $Zb_L\bar{b}_L$ coupling. With these results at hand, we performed a χ^2 test including electroweak precision tests, the current Higgs results and the measurement of the CKM matrix element V_{tb}. We also took into account exclusions from direct searches of new heavy fermions. Our final results showed that Composite Higgs Models are still viable candidates for physics

beyond the SM.

Although with the discovery of the Higgs boson a first big success has been achieved, a lot of work still needs to be done. The true nature of this new particle yet needs to be unveiled. As we have discussed in this thesis in detail, the discovered boson can still be a particle of a New Physics scenario, as for instance one of the Higgs bosons of the MSSM or the NMSSM, or it can be a Composite Higgs boson. With the second run of the LHC we will hopefully be able to shed more light onto this exciting question.

APPENDIX A

NLO Decay Width of $\tilde{u}_1 \to c\tilde{\chi}_1^0$

In this Appendix, the results for the top squark decay width into a charm quark c and the lightest neutralino $\tilde{\chi}_1^0$ will be presented. Only the finite parts will be given, while the divergences cancel in the renormalization procedure. The full decay width is given by

$$\Gamma = \Gamma_{LO} + \Gamma_{virt} + \Gamma_{CT} + \Gamma_{real}\,, \tag{A.1}$$

with Γ_{LO} as given in Eq. (5.9). For the virtual contributions and the counterterms the scalar integrals are defined as

$$A(m_1^2) = \frac{(2\pi\mu)^{4-d}}{i\pi^2}\int \mathrm{d}^4q \frac{1}{(q^2-m_1^2)}\,, \tag{A.2}$$

$$B_i(m_1^2, m_2^2) = \frac{(2\pi\mu)^{4-d}}{i\pi^2}\int \mathrm{d}^4q \frac{1}{(q^2-m_1^2)\left((q+p_i)^2-m_2^2\right)}\,, \tag{A.3}$$

$$p_\mu B_1(p^2, m_1^2, m_2^2) = \frac{(2\pi\mu)^{4-d}}{i\pi^2}\int \mathrm{d}^4q \frac{q_\mu}{(q^2-m_1^2)\left((q+p)^2-m_2^2\right)}\,, \tag{A.4}$$

$$C_{ij}(m_1^2, m_2^2, m_3^2) = \frac{(2\pi\mu)^{4-d}}{i\pi^2}\int \mathrm{d}^4q \frac{1}{(q^2-m_1^2)\left((q+p_i)^2-m_2^2\right)\left((q+p_i+p_j)^2-m_3^2\right)}\,. \tag{A.5}$$

The indices i, j will be set to either c, $\tilde{u}_1$ or $\tilde{\chi}_1^0$ for the respective four momenta. The virtual corrections Γ_{virt} are composed of the contributions from the gluon exchange $\Gamma_{virt,g}$ and from the gluino exchange $\Gamma_{virt,\tilde{g}}$, with $\Gamma_{virt} = \Gamma_{virt,g} + \Gamma_{virt,\tilde{g}}$. The specific contributions are given by

$$\begin{aligned}\Gamma_{virt,g} =& \frac{\alpha_s(\mu)}{24\pi^2 m_{\tilde{u}_1}^3}\left((g^L)_{211}^2 + (g^R)_{211}^2\right)\mathrm{Re}\Big[B_{\tilde{\chi}_1^0}(0, m_{\tilde{u}_1}^2)(2m_{\tilde{\chi}_1^0}^4 - 2m_{\tilde{\chi}_1^0}^2 m_{\tilde{u}_1}^2)\\ &-2B_c(0,0)(m_{\tilde{\chi}_1^0}^2 - m_{\tilde{u}_1}^2)^2 - B_{\tilde{u}}(0, m_{\tilde{u}_1}^2)(m_{\tilde{\chi}_1^0}^4 - m_{\tilde{u}_1}^4)\end{aligned}$$

$$+ 2C_{c,\tilde{\chi}_1^0}(0,0,m^2_{\tilde{u}_1})(m^4_{\tilde{\chi}_1^0} - 2m^2_{\tilde{\chi}_1^0}m^2_{\tilde{u}_1} + m^4_{\tilde{u}_1})(m^2_{\tilde{\chi}_1^0} - m^2_{\tilde{u}_1})\Big] \,, \tag{A.6}$$

$$\begin{aligned}
\Gamma_{virt,\tilde{g}} =& \frac{\alpha_s(\mu)}{12\pi^2\, m_{\tilde{u}_1}} \left(1 - \frac{m^2_{\tilde{\chi}_1^0}}{m^2_{\tilde{u}_1}}\right) \sum_{i=1}^{3}\sum_{s=1}^{6} \mathrm{Re}\Big[m_{\tilde{\chi}_1^0} B_{\tilde{\chi}_0}(m_{u_i}, m_{\tilde{u}_s})\,[\\
&- W^{\tilde{u}*}_{1i} W^{\tilde{u}*}_{s5} \left(g^L_{211} g^L_{is1} m_{u_i} + g^L_{211} g^R_{is1} m_{\tilde{\chi}_1^0}\right) - W^{\tilde{u}*}_{1\,i+3} W^{\tilde{u}*}_{s2} \left(g^R_{211} g^R_{is1} m_{u_i} + g^R_{211} g^L_{is1} m_{\tilde{\chi}_1^0}\right) \\
&+ W^{\tilde{u}*}_{1i} W^{\tilde{u}*}_{s2}\, g^R_{211} g^R_{is1} m_{\tilde{g}} + W^{\tilde{u}*}_{1\,i+3} W^{\tilde{u}*}_{s5}\, g^L_{211} g^L_{is1} m_{\tilde{g}}\Big] \\
&+ B_{\tilde{u}}(m^2_{u_i}, m^2_{\tilde{g}}) \Big[W^{\tilde{u}*}_{1i} W^{\tilde{u}*}_{s5} \left(g^L_{211} g^L_{is1} m_{\tilde{\chi}_1^0} m_{u_i} + g^L_{211} g^R_{is1} m^2_{\tilde{u}_1}\right) \\
&+ W^{\tilde{u}*}_{1\,i+3} W^{\tilde{u}*}_{s2} \left(g^R_{211} g^R_{is1} m_{\tilde{\chi}_1^0} m_{u_i} + g^R_{211} g^L_{is1} m^2_{\tilde{u}_1}\right) \\
&- W^{\tilde{u}*}_{1\,i+3} W^{\tilde{u}*}_{s5}\, g^L_{211} g^L_{is1} m_{\tilde{\chi}_1^0} m_{\tilde{g}} - W^{\tilde{u}*}_{1i} W^{\tilde{u}*}_{s2}\, g^R_{211} g^R_{is1} m_{\tilde{\chi}_1^0} m_{\tilde{g}}\Big] \\
&+ C_{c,\tilde{\chi}_1^0}(m^2_{\tilde{g}}, m^2_{\tilde{u}_s}, m^2_{u_i}) \Big[-W^{\tilde{u}*}_{1i} W^{\tilde{u}*}_{s5} \left(g^L_{211} g^L_{is1} m_{u_i} m_{\tilde{\chi}_1^0}(m^2_{\tilde{g}} - m^2_{\tilde{u}_s})\right. \\
&\left. + g^L_{211} g^R_{is1}(m^2_{\tilde{\chi}_0} m^2_{\tilde{g}} - m^2_{\tilde{u}_1} m^2_{\tilde{u}_s})\right) - W^{\tilde{u}*}_{1\,i+3} W^{\tilde{u}*}_{s2} \left(g^R_{211} g^R_{is1} m_{u_i} m_{\tilde{\chi}_1^0}(m^2_{\tilde{g}} - m^2_{\tilde{u}_s})\right. \\
&\left. + g^R_{211} g^L_{is1}(m^2_{\tilde{\chi}_0} m^2_{\tilde{g}} - m^2_{\tilde{u}_1} m^2_{\tilde{u}_s})\right) + W^{\tilde{u}*}_{s5} W^{\tilde{u}*}_{1\,i+3} \left(g^L_{211} g^L_{is1} m_{\tilde{\chi}_1^0} m_{\tilde{g}}(m^2_{\tilde{\chi}_1^0} + m^2_{\tilde{g}}\right. \\
&\left. - m^2_{\tilde{u}_1} - m^2_{\tilde{u}_s}) + g^L_{211} g^R_{is1} m_{\tilde{g}} m_{u_i}(m^2_{\tilde{\chi}_1^0} - m^2_{\tilde{u}_1})\right) + W^{\tilde{u}*}_{s2} W^{\tilde{u}*}_{1i} \left(g^R_{211} g^R_{is1} m_{\tilde{\chi}_1^0} m_{\tilde{g}}\right. \\
&\left. (m^2_{\tilde{\chi}_1^0} + m^2_{\tilde{g}} - m^2_{\tilde{u}_1} - m^2_{\tilde{u}_s}) + g^R_{211} g^L_{is1} m_{\tilde{g}} m_{u_i}(m^2_{\tilde{\chi}_1^0} - m^2_{\tilde{u}_1})\right)\Big]\Big] \,.
\end{aligned} \tag{A.7}$$

The gluino mass is denoted by $m_{\tilde{g}}$ and μ denotes the renormalization scale. All other notations correspond to those introduced in Chapter 5. The part of the decay width corresponding to the counterterms Γ_{CT} is given by

$$\Gamma_{CT} = \frac{1}{8\pi} m_{\tilde{u}_1} \left(1 - \frac{m^2_{\tilde{\chi}_1^0}}{m^2_{\tilde{u}_1}}\right)^2 \left(\delta g^L_{211} g^L_{211} + \delta g^R_{211} g^R_{211}\right) \,, \tag{A.8}$$

with $\delta g^{L/R}$ as defined in Eqs. (5.24) and (5.25). The specific counterterms were derived in Section 5.2.2. Only the self-energies have not been given yet. The squark self-energy reads (with $s, t = 1, ..., 6$)

$$\begin{aligned}
\tilde{\Sigma}_{st}(p^2) =& \frac{\alpha_s(\mu)}{3\pi} \sum_{r=1}^{6} \left[A(m^2_{\tilde{u}_r}) \sum_{v=1}^{6}\sum_{w=1}^{6} W^{\tilde{u}*}_{sv} W^{\tilde{u}}_{rv} W^{\tilde{u}*}_{rw} W^{\tilde{u}}_{tw}\right] \\
&- \frac{2\alpha_s(\mu)}{3\pi} \sum_{i=1}^{3} \Big[A(m^2_{u_i})(W^{\tilde{u}*}_{s\,,i+3} W^{\tilde{u}}_{t\,i+3} + W^{\tilde{u}*}_{si} W^{\tilde{u}}_{ti}) + \\
&\qquad A(m^2_{\tilde{g}})(W^{\tilde{u}*}_{s\,i+3} W^{\tilde{u}}_{t\,i+3} + W^{\tilde{u}*}_{si} W^{\tilde{u}}_{ti}) + \\
&\qquad B_{p^2}(m^2_{u_i}, m^2_{\tilde{g}}) \left((m^2_{u_i} + m^2_{\tilde{g}} - p^2)(W^{\tilde{u}*}_{si} W^{\tilde{u}}_{ti} + W^{\tilde{u}*}_{s\,i+3} W^{\tilde{u}}_{t\,i+3})\right. \\
&\qquad \left. -2m_{u_i} m_{\tilde{g}}(W^{\tilde{u}*}_{si} W^{\tilde{u}}_{t\,i+3} + W^{\tilde{u}*}_{s\,i+3} W^{\tilde{u}}_{ti})\right)\Big] \\
&+ \frac{2\alpha_s(\mu)}{3\pi} \delta_{st} \left[A(m^2_{\tilde{u}_s}) - 2(p^2 + m^2_{\tilde{u}_s}) B_{p^2}(0, m^2_{\tilde{u}_s})\right] \,.
\end{aligned} \tag{A.9}$$

The symbol B_{p^2} is defined in analogy to Eq. (A.3), with undetermined momentum p^2. The quark self-energies are

$$\Sigma^L_{ij} = -\frac{2\alpha_s(\mu)}{3\pi}\sum_{s=1}^{6} B_1(p^2, m^2_{\tilde{g}}, m^2_{\tilde{u}_s}) W^{\tilde{u}}_{si} W^{\tilde{u}*}_{sj}\,, \tag{A.10}$$

$$\Sigma^R_{ij} = -\frac{2\alpha_s(\mu)}{3\pi}\sum_{s=1}^{6} B_1(p^2, m^2_{\tilde{g}}, m^2_{\tilde{u}_s}) W^{\tilde{u}}_{s\,i+3} W^{\tilde{u}*}_{s\,j+3}\,, \tag{A.11}$$

$$\Sigma^l_{ij} = -\frac{2\alpha_s(\mu)}{3\pi}\sum_{s=1}^{6} m_{\tilde{g}} B_{p^2}(m^2_{\tilde{g}}, m^2_{\tilde{u}_s}) W^{\tilde{u}*}_{s\,i+3} W^{\tilde{u}}_{s\,j}\,, \tag{A.12}$$

$$\Sigma^r_{ij} = -\frac{2\alpha_s(\mu)}{3\pi}\sum_{s=1}^{6} m_{\tilde{g}} B_{p^2}(m^2_{\tilde{g}}, m^2_{\tilde{u}_s}) W^{\tilde{u}}_{s\,j+3} W^{\tilde{u}*}_{s\,i}\,. \tag{A.13}$$

We finally give also the real corrections Γ_{real}. They read

$$\begin{aligned}
\Gamma_{real} = -\frac{\alpha_s(\mu)}{288\pi^2} m_{\tilde{u}_1} ((g^L_{211})^2 + (g^R_{211})^2) \Big[& 10\pi^2 - 99 + 204r^2 - 20\pi^2 r^2 \\
& - 105r^4 + 10\pi^2 r^4 - 6(-1+r^2)^2 \log^2\left(\frac{m^2_{\tilde{u}_1}}{\mu^2}\right) + 24r^2\log(r^2) - 18r^4\log(r^2) \\
& + 60\log(1-r^2) - 120r^2\log(1-r^2) + 60r^4\log(1-r^2) - 24\log(1-r^2)^2 \\
& + 48r^2\log^2(1-r^2) - 24r^4\log^2(1-r^2) - 6(-1+r^2)^2\log\left(\frac{m^2_{\tilde{u}_1}}{\mu^2}\right) \\
& \Big(-5 + 4\log(1-r^2)\Big) - 24(-1+r^2)^2 Li_2(1-r^2)\Big]\,,
\end{aligned} \tag{A.14}$$

with r defined in Eq. (5.29) and

$$Li_2(z) = -\int_0^z du \frac{\log(1-u)}{u} \qquad\qquad z \in \mathbb{C} \setminus [1, \infty)\,. \tag{A.15}$$

APPENDIX B

Relations between the original and the physical parameters

For the transformation of the Lagrangian from the original parameters to the physical ones the following relations are used:

$$m^2_{H_d} = \frac{e}{2c_\beta M_W s_W} t_{h_d} - \Big[\frac{M_Z^2 c_{2\beta}}{2} - v_s t_\beta |\lambda| \left(\frac{|A_\lambda|}{\sqrt{2}} c_{\varphi_x} + |\kappa| \frac{v_s}{2} c_{\varphi_y}\right) + |\lambda|^2 \left(\frac{2 s_\beta^2 M_W^2 s_W^2}{e^2} + \frac{v_s^2}{2}\right)\Big] \,, \tag{B.1}$$

$$m^2_{H_u} = \frac{e}{2s_\beta M_W s_W} t_{h_u} + \Big[\frac{M_Z^2 c_{2\beta}}{2} + \frac{|\lambda| v_s}{t_\beta} \left(\frac{|A_\lambda|}{\sqrt{2}} c_{\varphi_x} + |\kappa| \frac{v_s}{2} c_{\varphi_y}\right) - |\lambda|^2 \left(\frac{2 c_\beta^2 M_W^2 s_W^2}{e^2} + \frac{v_s^2}{2}\right)\Big] \,, \tag{B.2}$$

$$m^2_S = \frac{t_{h_s}}{v_s} + \Big[s_{2\beta}|\lambda| \left(\frac{|A_\lambda|}{\sqrt{2}} c_{\varphi_x} + |\kappa| v_s c_{\varphi_y}\right) - |\lambda|^2 v_s\Big] \frac{2 M_W^2 s_W^2}{e^2 v_s} - |\kappa|^2 v_s^2 - \frac{1}{\sqrt{2}} |A_\kappa| |\kappa| v_s c_{\varphi_z} \,, \tag{B.3}$$

$$\varphi_{A_\lambda} = \mathrm{sign}_x \Big[n_x \pi + (-1)^{n_x} \Big| \arcsin\Big(\frac{e}{\sqrt{2}|A_\lambda| M_W s_W s_\beta |\lambda| v_s} t_{a_d} + \frac{|\kappa| v_s}{\sqrt{2}|A_\lambda|} s_{\varphi_y}\Big)\Big|\Big] - \varphi_\lambda - \varphi_s - \varphi_u \,, \tag{B.4}$$

$$\varphi_{A_\kappa} = \mathrm{sign}_z \Big[n_z \pi + (-1)^{n_z} \Big| \arcsin\Big(\frac{\sqrt{2}}{|A_\kappa| v_s} \Big[\frac{2 M_W s_W c_\beta}{e |\kappa| v_s^2} t_{a_d} + \frac{3 M_W^2 s_W^2 s_{2\beta} |\lambda|}{e^2} s_{\varphi_y} - \frac{1}{|\kappa| v_s} t_{a_s}\Big]\Big)\Big|\Big] - \varphi_\kappa - 3\varphi_s \,, \tag{B.5}$$

$$|A_\lambda| = \frac{s_{2\beta}}{\sqrt{2}c_{\varphi_x}|\lambda|v_s c^2_{\Delta\beta}}\Bigg[M^2_{H^\pm} - M^2_W c^2_{\Delta\beta} - |\kappa||\lambda|v_s^2\frac{c^2_{\Delta\beta}}{s_{2\beta}}c_{\varphi_y} + \frac{2M^2_W s^2_W c^2_{\Delta\beta}}{e^2}|\lambda|^2$$
$$- \frac{e}{2M_W s_W}\left[t_{h_u}\frac{c^2_{\beta_c}}{s_\beta} + t_{h_d}\frac{s^2_{\beta_c}}{c_\beta}\right]\Bigg] , \tag{B.6}$$

$$v_u = \frac{2M_W s_W s_\beta}{e} , \quad v_d = \frac{2M_W s_W c_\beta}{e} , \tag{B.7}$$

$$g_1 = \frac{e}{c_W} , \quad g_2 = \frac{e}{s_W} \quad \text{with} \quad c_W = \frac{M_W}{M_Z} \quad \text{and} \quad s^2_W = 1 - c^2_W , \tag{B.8}$$

with n_x and n_z zero or one if there exist two solutions of the tadpole conditions in Eqs. (6.13) and (6.15) and zero if there exists only one solution. The single solutions correspond to $\varphi_x, \varphi_z = \pm\pi/2$. Here, $\text{sign}_{x/z}$ are the signs of the corresponding arcsine evaluated in the interval $[-\pi, \pi)$. We have defined $\Delta\beta = \beta - \beta_B$ and $\beta_B \equiv \beta_n = \beta_c$.

APPENDIX C

Higgs boson mass matrix at tree level in the complex NMSSM

In this Appendix, the tree-level Higgs boson mass matrix will be given directly in terms of the parameters used as the input parameters in the renormalization procedure. The consistency in the parameter choice is essential in order to obtain the correct counterterm matrix. Therefore, the mass matrix is expressed in the the parameters $|\lambda|,\ |\kappa|,\ |A_\kappa|,\ v_s,\ \varphi_\lambda,\ \varphi_\kappa,\ \varphi_s$, and φ_u, the tadpoles t_ϕ as defined in Eqs. (6.10-6.14), the gauge couplings and the VEVs have been replaced by the electric charge e, the W boson mass M_W, the Z boson mass M_Z and t_β, and the parameter A_λ has been treated for the charged Higgs boson mass $M_{H^\pm}$. The sine of the Weinberg angle is given by $s_W = (1 - M_W^2/M_Z^2)^{1/2}$ and still needs to be replaced in the following equations before the renormalization procedure is applied. In addition, the parameter A_λ is replaced by the charged Higgs boson mass $M_{H^\pm}$. The Higgs boson mass matrix, in the basis $\Phi = (h_d, h_u, h_s, A, a_s, G)^T$, then reads

$$
\begin{aligned}
M_{h_d h_d} = &\left[\frac{M_{H^\pm}^2}{c_{\Delta\beta}^2} - M_W^2\right] s_\beta^2 + M_Z^2 c_\beta^2 + \frac{e c_\beta c_{\beta_B}^2}{2 M_W s_W c_{\Delta\beta}^2}\Big[(1 + 2 t_\beta t_{\beta_B}) t_{h_d} - t_\beta t_{h_u}\Big] \\
&+ 2|\lambda|^2 M_W^2 \frac{s_W^2}{e^2} s_\beta^2 \ , \qquad \text{(C.1)} \\
M_{h_d h_u} = &-\left[\frac{M_{H^\pm}^2}{c_{\Delta\beta}^2} - M_W^2 + M_Z^2\right] s_\beta c_\beta + \frac{e c_\beta c_{\beta_B}^2}{2 M_W s_W c_{\Delta\beta}^2}\Big[t_{h_u} + t_\beta t_{\beta_B}^2 t_{h_d}\Big] \\
&+ |\lambda|^2 M_W^2 \frac{s_W^2}{e^2} s_{2\beta} \ , \qquad \text{(C.2)} \\
M_{h_u h_u} = &\left[\frac{M_{H^\pm}^2}{c_{\Delta\beta}^2} - M_W^2\right] c_\beta^2 + M_Z^2 s_\beta^2 + \frac{e c_\beta s_{2\beta_B}}{4 M_W s_W c_{\Delta\beta}^2}\Big[(2 + t_\beta t_{\beta_B}) t_{h_u} - t_{\beta_B} t_{h_d}\Big] \\
&+ 2|\lambda|^2 M_W^2 \frac{s_W^2}{e^2} c_\beta^2 \ , \qquad \text{(C.3)}
\end{aligned}
$$

$$M_{h_d h_s} = -\left[\frac{M_{H^\pm}^2}{c_{\Delta\beta}^2} - M_W^2\right]\frac{M_W s_W s_\beta s_{2\beta}}{e v_s} + \frac{s_\beta c_\beta c_{\beta_B}^2}{v_s c_{\Delta\beta}^2}\Big[t_{h_u} + t_\beta t_{\beta_B}^2 t_{h_d}\Big]$$
$$+ |\lambda| M_W \frac{s_W}{e} v_s \Big[2|\lambda| c_\beta - |\kappa| s_\beta c_{\varphi_y}\Big] - \frac{4|\lambda|^2 M_W^3 s_W^3 s_\beta^2 c_\beta}{e^3 v_s} \ , \tag{C.4}$$

$$M_{h_u h_s} = -\left[\frac{M_{H^\pm}^2}{c_{\Delta\beta}^2} - M_W^2\right]\frac{M_W s_W c_\beta s_{2\beta}}{e v_s} + \frac{c_\beta^2 c_{\beta_B}^2}{v_s c_{\Delta\beta}^2}\Big[t_{h_u} + t_\beta t_{\beta_B}^2 t_{h_d}\Big]$$
$$+ |\lambda| M_W \frac{s_W}{e} v_s \Big[2|\lambda| s_\beta - |\kappa| c_\beta c_{\varphi_y}\Big] - \frac{4|\lambda|^2 M_W^3 s_W^3 s_\beta c_\beta^2}{e^3 v_s} \ , \tag{C.5}$$

$$M_{h_s h_s} = \left[\frac{M_{H^\pm}^2}{c_{\Delta\beta}^2} - M_W^2\right]\frac{M_W^2 s_W^2 s_{2\beta}^2}{e^2 v_s^2} - \frac{M_W s_W s_{2\beta} c_\beta c_{\beta_B}^2}{e v_s^2 c_{\Delta\beta}^2}\Big[t_{h_u} + t_\beta t_{\beta_B}^2 t_{h_d}\Big] + \frac{t_{h_s}}{v_s}$$
$$+ |\lambda| M_W^2 \frac{s_W^2 s_{2\beta}}{e^2 v_s^2}\Big[2|\lambda| M_W^2 \frac{s_W^2}{e^2} s_{2\beta} - |\kappa| v_s^2 c_{\varphi_y}\Big]$$
$$+ 2|\kappa|^2 v_s^2 + \frac{1}{\sqrt{2}}|A_\kappa||\kappa| v_s c_{\varphi_z} \ , \tag{C.6}$$

$$M_{AA} = M_{H^\pm}^2 - M_W^2 c_{\Delta\beta}^2 + 2|\lambda|^2 M_W^2 \frac{s_W^2}{e^2} c_{\Delta\beta}^2 \ , \tag{C.7}$$

$$M_{A a_s} = \Big[M_{H^\pm}^2 - M_W^2 c_{\Delta\beta}^2\Big]\frac{M_W s_W s_{2\beta}}{e v_s c_{\Delta\beta}} - \frac{c_\beta c_{\beta_B}^2}{v_s c_{\Delta\beta}}\Big[t_{h_u} + t_\beta t_{\beta_B}^2 t_{h_d}\Big]$$
$$+ |\lambda| M_W \frac{s_W c_{\Delta\beta}}{e v_s}\Big[2|\lambda| M_W^2 \frac{s_W^2}{e^2} s_{2\beta} - 3|\kappa| v_s^2 c_{\varphi_y}\Big] \ , \tag{C.8}$$

$$M_{a_s a_s} = \Big[M_{H^\pm}^2 - M_W^2 c_{\Delta\beta}^2\Big]\frac{M_W^2 s_W^2 s_{2\beta}^2}{e^2 v_s^2 c_{\Delta\beta}^2} - \frac{M_W s_W s_{2\beta} c_\beta c_{\beta_B}^2}{e v_s^2 c_{\Delta\beta}^2}\Big[t_{h_u} + t_\beta t_{\beta_B}^2 t_{h_d}\Big] + \frac{t_{h_s}}{v_s}$$
$$+ |\lambda| M_W^2 \frac{s_{\theta_W}^2 s_{2\beta}}{e^2 v_s^2}\Big[2|\lambda| M_W^2 \frac{s_W^2}{e^2} s_{2\beta} + 3|\kappa| v_s^2 c_{\varphi_y}\Big] - \frac{3}{\sqrt{2}}|A_\kappa||\kappa| v_s c_{\varphi_z} \ , \tag{C.9}$$

$$M_{AG} = \Big[M_{H^\pm}^2 - M_W^2 c_{\Delta\beta}^2\Big] t_{\Delta\beta} + \frac{e c_{\beta_B}}{2 M_W s_W c_{\Delta\beta}}\Big[t_{\beta_B} t_{h_d} - t_{h_u}\Big] + |\lambda|^2 M_W^2 \frac{s_W^2}{e^2} s_{2\Delta\beta} \ , \tag{C.10}$$

$$M_{a_s G} = \Big[M_{H^\pm}^2 - M_W^2 c_{\Delta\beta}^2\Big]\frac{M_W s_W s_{2\beta} s_{\Delta\beta}}{e v_s c_{\Delta\beta}^2} - \frac{c_\beta c_{\beta_B}^2 s_{\Delta\beta}}{v_s c_{\Delta\beta}^2}\Big[t_{h_u} + t_\beta t_{\beta_B}^2 t_{h_d}\Big]$$
$$+ |\lambda| M_W \frac{s_W s_{\Delta\beta}}{e v_s}\Big[2|\lambda| M_W^2 \frac{s_W^2}{e^2} s_{2\beta} - 3|\kappa| v_s^2 c_{\varphi_y}\Big] \ , \tag{C.11}$$

$$M_{GG} = \Big[M_{H^\pm}^2 - M_W^2 c_{\Delta\beta}^2\Big] t_{\Delta\beta}^2 + \frac{e c_{\beta - 2\beta_B}}{2 M_W s_W c_{\Delta\beta}^2}\Big[t_{h_d} - t_{\beta - 2\beta_B} t_{h_u}\Big] + 2|\lambda|^2 M_W^2 \frac{s_W^2}{e^2} s_{\Delta\beta}^2 \ . \tag{C.12}$$

with the mixing between CP-even and CP-odd components given by

$$M_{ha}\mathcal{G}^T = \begin{pmatrix} \frac{e c_{\beta_B}}{2 M_W s_W s_\beta} t_{a_d} & \frac{1}{v_s} t_{a_d} + 3|\kappa||\lambda| M_W \frac{s_W}{e} v_s s_\beta s_{\varphi_y} & -\frac{e s_{\beta_B}}{2 M_W s_W s_\beta} t_{a_d} \\ \frac{e s_{\beta_B}}{2 M_W s_W s_\beta} t_{a_d} & \frac{1}{v_s t_\beta} t_{a_d} + 3|\kappa||\lambda| M_W \frac{s_W}{e} v_s c_\beta s_{\varphi_y} & \frac{e c_{\beta_B}}{2 M_W s_W s_\beta} t_{a_d} \\ M_{h_s A} & M_{h_s a_s} & M_{h_s G} \end{pmatrix} \tag{C.13}$$

with $\mathcal{G}$ as defined in Eq. (6.18) and

$$M_{h_s A} = \frac{c_{\Delta\beta}}{v_s s_\beta} t_{a_d} - |\kappa||\lambda| M_W \frac{s_W}{e} v_s c_{\Delta\beta} s_{\varphi_y} \ , \tag{C.14}$$

$$M_{h_s a_s} = \frac{2}{v_s} t_{a_s} - \frac{4 M_W s_W}{e} \left[\frac{c_\beta}{v_s^2} t_{a_d} + |\kappa||\lambda| M_W \frac{s_W}{e} s_{2\beta} s_{\varphi_y} \right] , \tag{C.15}$$

$$M_{h_s G} = \frac{s_{\Delta\beta}}{v_s s_\beta} t_{a_d} - |\kappa||\lambda| M_W \frac{s_W}{e} v_s s_{\Delta\beta} s_{\varphi_y} \ . \tag{C.16}$$

For $\phi_y = n\pi$ with $n \in \mathbb{Z}$ the entries of M_{ha} vanish and their is no mixing between CP-even and CP-odd components. We have introduced $\Delta\beta$ defined as $\Delta\beta = \beta - \beta_B$. At tree level the relation $\beta_B = \beta_c = \beta_n = \beta$ holds. At one loop these angles need to be distinguished, as the mixing matrices of the charged and neutral Higgs bosons are not renormalized. Therefore β_B, β_c and β_n do not get a counterterm, whereas β is renormalized with the counterterm $\delta\beta = c_\beta^2 \delta t_\beta$.

APPENDIX D

Conventions for the Higgs boson couplings in the complex NMSSM

In this Appendix the coupling factors appearing in the formulae for the production and decay rates of the NMSSM Higgs bosons in Section 6.3 are defined. The full coupling in this section is denoted by C with the appropriate subscript. The reduced coupling constants g (with subscript) can be obtained from the full couplings C by means of the following formulae.

The Higgs boson to fermion couplings are given by ($i = 1, ..., 5$)

$$C_{H_i f\bar{f}} = -\frac{i g_2 m_f}{2 M_W} \left[g^S_{H_i f\bar{f}} - i\gamma_5 \, g^P_{H_i f\bar{f}} \right] , \tag{D.1}$$

with

$$g^S_{H_i f\bar{f}} = \begin{cases} \frac{\mathcal{R}_{i2}}{\sin\beta} & \text{for } f = \text{ up-type} \\ \frac{\mathcal{R}_{i1}}{\cos\beta} & \text{for } f = \text{ down-type} \end{cases} \tag{D.2}$$

and

$$g^P_{H_i f\bar{f}} = \begin{cases} \frac{\mathcal{R}_{i4}}{\tan\beta} & \text{for } f = \text{ up-type} \\ \mathcal{R}_{i4} \tan\beta & \text{for } f = \text{ down-type} . \end{cases} \tag{D.3}$$

The Higgs boson squark couplings are defined as

$$C_{H_i \tilde{f} \tilde{f}^*} = -i g_2 \frac{M_Z^2}{M_W} g_{H_i \tilde{f} \tilde{f}} . \tag{D.4}$$

The formula for $g_{H_i \tilde{f} \tilde{f}}$ is lengthy and therefore we refer to the program code of `NMSSMCALC` [37] and Ref. [292] for detailed expressions. For the neutral Higgs boson decays the Higgs couplings to W bosons are necessary. They are given by

$$C_{H_i VV} = i g_2 M_V g_{H_i VV} , \qquad \text{with} \qquad g_{H_i VV} = \mathcal{R}_{i1} \cos\beta + \mathcal{R}_{i2} \sin\beta , \tag{D.5}$$

with $V = W$, Z. Furthermore, the convention for the Higgs boson couplings to charged Higgs bosons is

$$C_{H_i H^+ H^-} = -\frac{i g_2 M_Z^2}{2 M_W} g_{H_i H^+ H^-} \ . \tag{D.6}$$

For the Higgs boson couplings to charginos we used the convention ($j, k = 1, 2$)

$$C_{H_i \tilde{\chi}_j^+ \tilde{\chi}_k^-} = -i \frac{g_2}{2} \left[g^S_{H_i \tilde{\chi}_j^+ \tilde{\chi}_k^-} - i\gamma_5 \, g^P_{H_i \tilde{\chi}_j^+ \tilde{\chi}_k^-} \right] \ . \tag{D.7}$$

For all the discussed decays we, however, only need the case $j = k$. The full expressions for $g_{H_i H^+ H^-}$ and $g^{S/P}_{H_i \tilde{\chi}_j^+ \tilde{\chi}_j^-}$ can be found in the program code of `NMSSMCALC` [37] or in Ref. [292].

APPENDIX E

The special orthogonal group

In this Appendix, we will give some basics results and formulae regarding $SO(N)$ groups, in particular for $SO(5)$. The special orthogonal group $SO(N)$ is defined by

$$O^T O = 1 \tag{E.1}$$

and

$$\det O = 1\,, \tag{E.2}$$

with $O \in SO(N)$ and describes rotations in the N-dimensional Euclidean space. Its fundamental representation is given by an N component vector ϕ, with transformation properties given by

$$\phi_i \to \phi_i' = O_{ij}\phi_j \tag{E.3}$$

with $i, j = 1, ..., N$. Sometimes it can be useful, to write the representation in terms of a two-indexed object, in particular for the symmetric and antisymmetric representation, as is discussed in Chapter 7. The transformation rule then reads

$$\phi_{ij} \to \phi_{ij}' = O_{ik}O_{jn}\phi_{kn}\,. \tag{E.4}$$

The $SO(N)$ element O is given by

$$O = e^{i\frac{T^a\theta^a}{2}} \approx 1 + \frac{i}{2}T^a\theta^a\,, \tag{E.5}$$

with T^a the generators of $SO(N)$ and θ the infinitesimal parameter associated with the rotation. Using the defining property in Eq. (E.1), the transposed generator can be calculated

$$O^T O = 1 + \frac{i}{2}\left((T^a)^T + T^a\right)\theta^a \stackrel{!}{=} 1 \quad \Rightarrow \quad T^T = -T\,. \tag{E.6}$$

With Eq. (E.6) at hand, Eq. (E.4) becomes

$$\phi'_{ij} = (O\phi O^T)_{ij} \approx \phi_{ij} + \frac{i}{2}\theta^a \left(T^a\phi + \phi(T^a)^T\right)_{ij} = \phi_{ij} + \frac{i}{2}\theta^a [T^a, \phi]_{ij} \,. \tag{E.7}$$

Hence the action of the generator on a two-indexed representation is given by the commutator with the generator in the fundamental representation. We just need to verify, that the antisymmetric/symmetric representation can indeed be described as two-indexed representations. The antisymmetric/symmetric representations are defined by

$$\phi^T = \begin{cases} -\phi, & \text{for antisymmetric representation} \\ \phi & \text{for symmetric representation} \,. \end{cases} \tag{E.8}$$

Hence the transpose of the transformed representation as given in Eq. (E.4) can be calculated to prove that it is still antisymmetric/symmetric. Indeed,

$$(\phi')^T_{ij} = \phi^T_{ij} + \frac{i}{2}\theta^a [T^a, \phi]^T_{ij} = \phi^T_{ij} + \frac{i}{2}\theta^a [T^a, \phi^T]_{ij} \tag{E.9}$$

is symmetric/antisymmetric if ϕ is symmetric/antisymmetric. Note that in general in $SO(N)$ groups, the antisymmetric representation corresponds to the adjoint representation.

By now, all the properties are in general valid for $SO(N)$ models. We are, however, in particular interested in the $SO(5)$. Thus, we finally give an explicit form for the generators of $SO(5)$ in a suitable basis. The generators of $SO(5)/SO(4)$ are given by

$$(T^{\hat{a}})_{ij} = -\frac{i}{\sqrt{2}} \left(\delta^{\hat{a}}_i \delta^5_j - \delta^{\hat{a}}_j \delta^5_i\right) \,, \tag{E.10}$$

with ($\hat{a} = 1, ..., 4$). Together with the ones of $SU(2)_{L,R}$ ($a, b, c = 1, 2, 3$, $i, j = 1, ..., 5$),

$$(T^a_L)_{ij} = -\frac{i}{2}\left[\frac{1}{2}\epsilon^{abc}(\delta^b_i\delta^c_j - \delta^b_j\delta^c_i) + \delta^a_i\delta^4_j - \delta^4_i\delta^a_j\right] \,, \tag{E.11}$$

$$(T^a_R)_{ij} = -\frac{i}{2}\left[\frac{1}{2}\epsilon^{abc}(\delta^b_i\delta^c_j - \delta^b_j\delta^c_i) - \delta^a_i\delta^4_j + \delta^4_i\delta^a_j\right] \,, \tag{E.12}$$

they form the complete set of generators in the fundamental representation of $SO(5)$. Of course, the $SU(2)_{L,R}$ generators fulfill the $SU(2)$ algebra $[T^i, T^j] = i\epsilon^{ijk}T^k$.

APPENDIX F

Decay widths for vector-like fermions

In this Appendix, the decay widths for vector-like fermions will be given in a general form, such that they can be applied for other models. The decay width of a fermion F with mass M_F into a vector boson V with mass M_V and a lighter fermion f with mass m_f and the Lagrangian

$$\mathcal{L} = \bar{F}\gamma^\mu(g_L^V P_L + g_R^V P_R) f V_\mu + h.c.\,, \tag{F.1}$$

where g_L^V and g_R^V are generic coupling constants, is given by

$$\begin{aligned}\Gamma(F \to Vf) = \frac{M_F}{32\pi}\sqrt{\lambda(M_F, m_f, M_V)}\Bigg\{&(|g_L^V|^2 + |g_R^V|^2)\left(\frac{M_F^2}{M_V^2}\right) \\ &\left[\frac{M_V^2(M_F^2 + m_f^2) + (M_F^2 - m_f^2)^2 - 2M_V^4}{M_F^4}\right] - 12\,\frac{m_f}{M_F}\mathrm{Re}(g_L^V g_R^{V*})\Bigg\}\,.\end{aligned} \tag{F.2}$$

We have defined

$$\lambda(M, m_1, m_2) = 1 - 2\frac{m_1^2 + m_2^2}{M^2} + \frac{(m_1^2 - m_2^2)^2}{M^4}\,. \tag{F.3}$$

For the decay into a Higgs boson h and a fermion f the Lagrangian is given by

$$\mathcal{L} = \bar{F}(g_L^S P_L + g_R^S P_R) f h + h.c.\,. \tag{F.4}$$

The partial decay width then reads

$$\begin{aligned}\Gamma(F \to hf) =&\frac{M_F}{32\pi}\sqrt{\lambda(M_F, m_f, m_h)} \\ &\left[(|g_L^S|^2 + |g_R^S|^2)\left(1 + \frac{m_f^2}{M_F^2} - \frac{m_h^2}{M_F^2}\right) + 4\frac{m_f}{M_F}\mathrm{Re}(g_L^S g_R^{S*})\right].\end{aligned} \tag{F.5}$$

My results for the decay widths were compared with the work of a second computation [435], and in a limit were some of the couplings are set to zero with Ref. [436].

APPENDIX G

Triangle and box form factors for double Higgs boson production

In this Appendix the analytic results for the triangle and box form factors for Higgs pair production in a Composite Higgs Model are given. They can also be found in Ref. [34, 437, 438].[1]

G.1. Notation

The four-momenta of the gluons are denoted by p_1 and p_2, the four-momenta of the Higgs bosons by p_3 and p_4 with all momenta incoming. The Mandelstam variables $\hat{s}$, $\hat{t}$, $\hat{u}$ are hence given by

$$\hat{s} = (p_1 + p_2)^2 \ , \qquad \hat{t} = (p_1 + p_3)^2 \ , \qquad \hat{u} = (p_2 + p_3)^2 \ . \tag{G.1}$$

The scalar integrals are defined as

$$\begin{aligned} &C_{ij}(m_1^2, m_2^2, m_3^2) = \\ &\quad \int \frac{\mathrm{d}^4 q}{i\pi^2} \frac{1}{(q^2 - m_1^2)\left((q+p_i)^2 - m_2^2\right)\left((q+p_i+p_j)^2 - m_3^2\right)} \\ &D_{ijk}(m_1^2, m_2^2, m_3^2, m_4^2) = \\ &\quad \int \frac{\mathrm{d}^4 q}{i\pi^2} \frac{1}{(q^2 - m_1^2)\left((q+p_i)^2 - m_2^2\right)\left((q+p_i+p_j)^2 - m_3^2\right)\left((q+p_i+p_j+p_k)^2 - m_4^2\right)} \ . \end{aligned} \tag{G.2}$$

They have been evaluated numerically in a self-written code with the help of `LoopTools` [148, 149]. We introduce the following abbreviations for the scalar inte-

[1] Compared to Ref. [34] a typo was corrected in this thesis.

grals, to give the results for the form factors in a compact way

$$\begin{aligned} C_{12} &\equiv C_{12}(m_1^2, m_1^2, m_1^2)\,, & C_{13} &\equiv C_{13}(m_1^2, m_1^2, m_2^2)\,, \\ C_{14} &\equiv C_{14}(m_1^2, m_1^2, m_2^2)\,, & C_{23} &\equiv C_{23}(m_1^2, m_1^2, m_2^2)\,, \\ C_{24} &\equiv C_{24}(m_1^2, m_1^2, m_2^2)\,, & C_{34} &\equiv C_{34}(m_1^2, m_2^2, m_1^2)\,, \\ D_{123} &\equiv D_{123}(m_1^2, m_1^2, m_1^2, m_2^2)\,, & D_{132} &\equiv D_{132}(m_1^2, m_1^2, m_2^2, m_2^2)\,, \\ D_{213} &\equiv D_{213}(m_1^2, m_1^2, m_1^2, m_2^2)\,. \end{aligned} \tag{G.3}$$

G.2. Tensor basis and projectors

The tensor basis reads

$$A_1^{\mu\nu} = g^{\mu\nu} - \frac{p_1^\nu\, p_2^\mu}{(p_1 \cdot p_2)} \tag{G.4}$$

$$A_2^{\mu\nu} = g^{\mu\nu} + \frac{p_3^2\, p_1^\nu\, p_2^\mu}{p_T^2\,(p_1 \cdot p_2)} - \frac{2\,(p_3 \cdot p_2)\, p_1^\nu\, p_3^\mu}{p_T^2\,(p_1 \cdot p_2)} - \frac{2\,(p_3 \cdot p_1)\, p_3^\nu\, p_2^\mu}{p_T^2\,(p_1 \cdot p_2)} + \frac{2 p_3^\mu\, p_3^\nu}{p_T^2} \tag{G.5}$$

with

$$p_T^2 = 2\frac{(p_1 \cdot p_3)\,(p_2 \cdot p_3)}{(p_1 \cdot p_2)} - p_3^2\,,$$

$$A_1 \cdot A_2 = 0 \qquad \text{and} \qquad A_1 \cdot A_1 = A_2 \cdot A_2 = 2\,. \tag{G.6}$$

The Lorentz structure $A_1^{\mu\nu}$ corresponds to $S_z = 0$, and $A_2^{\mu\nu}$ to $S_z = 2$.

G.3. Form factor

Triangle:

$$F_\triangle(m) = 2\left[2m + \left(4m^3 - \hat{s}\,m\right) C_{12}\right]\,. \tag{G.7}$$

Box form factors

$$\begin{aligned} F_\square(m_i, m_j) &= \frac{2}{\hat{s}}\Big[2\hat{s} + 4m_i^2\hat{s}\,C_{12} + \hat{s}((m_i + m_j)(2m_i^2(m_i + m_j) - m_i\hat{s}) \\ &- m_i^2(\hat{t} + \hat{u}))(D_{123} + D_{132} + D_{213}) \\ &+ (m_h^2 - (m_i + m_j)^2)\Big[(\hat{t} - m_h^2)(C_{13} + C_{24}) + (\hat{u} - m_h^2)(C_{23} + C_{14}) \\ &- (\hat{t}\hat{u} - m_h^4 + \hat{s}(m_j^2 - m_i^2))D_{132}\Big]\Big] \end{aligned} \tag{G.8}$$

$$
\begin{aligned}
&G_{\Box}(m_i, m_j) \\
&= \frac{1}{\hat{t}\hat{u} - m_h^4}\Big[(\hat{t}^2 + \hat{u}^2 - (4m_j^2 + 4m_i m_j)(\hat{t} + \hat{u}) + 4(m_j - m_i)(m_i + m_j)^3 + 2m_h^4)\hat{s}C_{12} \\
&+ (m_h^4 + \hat{t}^2 - 2\hat{t}(m_i + m_j)^2)((\hat{t} - m_h^2)(C_{13} + C_{24}) - \hat{s}\hat{t}D_{213}) \\
&+ (m_h^4 + \hat{u}^2 - 2\hat{u}(m_i + m_j)^2)((\hat{u} - m_h^2)(C_{23} + C_{14}) - \hat{s}\hat{u}D_{123}) \qquad \text{(G.9)} \\
&- (\hat{t}^2 + \hat{u}^2 - 2m_h^4)(\hat{t} + \hat{u} - 2(m_i + m_j)^2)C_{34} \\
&- (\hat{t} + \hat{u} - 2(m_i + m_j)^2)((\hat{t}\hat{u} - m_h^4)(m_i^2 + m_j^2) + \hat{s}(m_i^2 - m_j^2)^2)(D_{123} + D_{132} + D_{213})\Big]
\end{aligned}
$$

and

$$
F_{\Box,5}(m_i, m_j) = -F_{\Box}(m_i, -m_j), \qquad G_{\Box,5}(m_i, m_j) = -G_{\Box}(m_i, -m_j). \qquad \text{(G.10)}
$$

APPENDIX H

Results for the vertex correction to $Zb_L\bar{b}_L$

The results for the corrections to the vertex $Zb_L\bar{b}_L$ will be presented in this Appendix. In order to give them in a general way, the Lagrangians for the specific couplings of the W bosons, the Z bosons, the charged Goldstone bosons $G^{\pm}$ and the neutral Goldstone boson G^0 to the quarks Ψ of charge Q and $Q-1$ are parameterized as follows

$$\mathcal{L}_W = \frac{g_2}{\sqrt{2}} W_\mu^+ \bar{\Psi}_Q^i \gamma^\mu \left(V_{ij}^{QL} P_L + V_{ij}^{QR} P_R \right) \Psi_{(Q-1)}^j + h.c.\,, \tag{H.1}$$

$$\mathcal{L}_Z = \frac{g_2}{2c_W} Z_\mu \bar{\Psi}_Q^i \gamma^\mu \left(X_{ij}^{QL} P_L + X_{ij}^{QR} P_R - 2s_W^2 Q \delta_{ij} \right) \Psi_Q^j\,, \tag{H.2}$$

$$\mathcal{L}_{G^\pm} = \frac{g_2}{\sqrt{2}} G^+ \bar{\Psi}_Q^i \left(W_{ij}^{QL} P_L + W_{ij}^{QR} P_R \right) \Psi_{(Q-1)}^j \quad + h.c\,, \tag{H.3}$$

$$\mathcal{L}_{G^0} = \frac{g_2}{2c_W} G^0 \bar{\Psi}_Q^i \left(Y_{ij}^{QL} P_L + Y_{ij}^{QR} P_R \right) \Psi_Q^j\,. \tag{H.4}$$

The indices i and j run over all the quarks present in the model, $V^{QL/R}$, $W^{QL/R}$, $X^{QL/R}$ and $Y^{QL/R}$ denote the coupling matrices. Additionally, we define

$$\tilde{X}_{ij}^{Q(L/R)} = X_{ij}^{Q(L/R)} - 2s_W^2 Q \delta_{ij}\,. \tag{H.5}$$

The decay amplitude $\mathcal{M}^{heavy}$, as defined in Eq. (9.8), gets loop contributions from the top quark and its partners, $\mathcal{M}_t^{heavy}$, from the bottom quark and its partners, $\mathcal{M}_b^{heavy}$, and from Higgs bosons in the loops, $\mathcal{M}_{Higgs}^{heavy}$. Hence, we denote collectively

$$\mathcal{M}^{heavy} = \mathcal{M}_t^{heavy} + \mathcal{M}_b^{heavy} + \mathcal{M}_{Higgs}^{heavy}\,. \tag{H.6}$$

We introduce the reduced masses

$$y_i = \frac{m_i^2}{M_Z^2}, \qquad y_W = \frac{M_W^2}{M_Z^2} \qquad \text{and} \qquad y_\beta^b = \frac{m_{b\beta}^2}{M_Z^2}\,, \tag{H.7}$$

where m_i is the mass of one of the top-like quarks denoted by the index i and $m_{b\beta}$ the mass of one of the bottom-type quarks, denoted by the index β. With the definitions of the gauge and Goldstone boson couplings as in Eqs. (H.1–H.4) the contributions from the top quark and the heavy top partners ($Q = 2/3$) read,

$$\begin{aligned}
\mathcal{M}_t^{heavy} = &-\frac{\alpha}{8\pi s_W^2}\sum_i\Bigg[\sum_j V_{jb}^{QL}V_{ib}^{QL\star}(2\tilde{X}_{ij}^{QR}E_1^{ij}+\tilde{X}_{ij}^{QL}E_2^{ij})\\
&+W_{jb}^{QL}W_{ib}^{QL\star}(\tilde{X}_{ij}^{QL}E_1^{ij}+\tilde{X}_{ij}^{QR}E_3^{ij})\Big]\\
&+\Bigg[\sum_\beta \tilde{X}_{b\beta}^{-1/3,L}\left(\frac{1}{2}\left(V_{i\beta}^{QL\star}V_{ib}^{QL}+V_{i\beta}^{QL}V_{ib}^{QL\star}\right)(2E_4^{i\beta}-1)\right.\\
&\left.+\frac{1}{2}\left(W_{i\beta}^{QL\star}W_{ib}^{QL}+W_{i\beta}^{QL}W_{ib}^{QL\star}\right)E_4^{i\beta}\right)\Bigg]\\
&+(2s_W^2-1)\left|W_{ib}^{QL}\right|^2E_5^i-2c_W^2\left|V_{ib}^{QL}\right|^2E_6^i+4s_W^2\,\mathrm{Re}(V_{ib}^{QL\star}W_{ib}^{QL})E_7^i\\
&-\sum_\beta \tilde{X}_{\beta b}^{-1/3,L}(W_{ib}^{QR\star}W_{i\beta}^{QL}-4V_{ib}^{QR}V_{i\beta}^{QL\star})E_8^{i\beta}\,,
\end{aligned}\tag{H.8}$$

where the summation in i, j runs over all indices appearing in the top mass matrix and the summation in β over all indices appearing in the bottom mass matrix. The index b stands for the mass eigenstate with the bottom quark mass. The abbreviations introduced in the above formula are given by

$$E_1^{ij} = \sqrt{y_iy_j}\,I_1(y_i,y_W,y_j)\,,\tag{H.9}$$

$$\begin{aligned}
E_2^{ij} = &\,\mathrm{Div}-2+y_i+y_j-2y_W+2I_1(y_i,y_W,y_j)\,(y_i-y_W-1)\,(y_j-y_W-1)\\
&-I_2(y_i,y_j)\,(y_i+y_j-2y_W-3)+\log(y_i)\left(\frac{2y_i}{y_i-y_W}-y_i\right)\\
&+\log(y_j)\left(\frac{2y_j}{y_j-y_W}-y_j\right)+2y_W\log(y_W)\left(1-\frac{y_i+y_j-2y_W}{(y_i-y_W)(y_j-y_W)}\right)\,,
\end{aligned}\tag{H.10}$$

$$\begin{aligned}
E_3^{ij} = &\,\frac{1}{2}\Big[\mathrm{Div}+1+y_i+y_j-2y_W+2I_1(y_i,y_W,y_j)\,(y_i-y_W)\,(y_j-y_W)\\
&-I_2(y_i,y_j)\,(y_i+y_j-2y_W+1)-y_i\log(y_i)-y_j\log(y_j)+2y_W\log(y_W)\Big]\,,
\end{aligned}\tag{H.11}$$

$$E_4^{i\beta} = \frac{1}{2}\begin{cases}
\mathrm{Re}\Big[-\mathrm{Div}+2-\log(y_W)-\frac{y_W-y_i}{y_i}\sqrt{\frac{y_\beta^b}{y_i}}E_8^{i\beta}\\
+x_+(y_\beta^b,y_W,y_i)\log(1-1/x_+(y_\beta^b,y_W,y_i))\\
+x_-(y_\beta^b,y_W,y_i)\log(1-1/x_-(y_\beta^b,y_W,y_i))\Big] & \text{for } y_\beta^b\neq 0\,,\\
\\
-\mathrm{Div}+1-\frac{y_i}{y_i-y_W}\log(y_i)-\frac{y_W}{y_W-y_i}\log(y_W)\\
+\frac{y_i+y_W}{2(y_i-y_w)}-\frac{y_iy_W}{(y_i-y_W)^2}\log(y_i/y_W) & \text{for } y_\beta^b=0\,,
\end{cases}\tag{H.12}$$

$$
\begin{aligned}
E_5^i &= \frac{\text{Div}}{2} - \frac{1}{2} + y_i - y_W - y_i \log(y_i) + y_W \log(y_W) \\
&\quad -I_1(y_W, y_i, y_W)\left((y_i - y_W)^2 + y_i\right) \\
&\quad -I_2(y_W, y_W)\left(y_i - y_W + \frac{1}{2}\right), \qquad \text{(H.13)} \\
E_6^i &= 3\ \text{Div} - 4 + 2\,(y_i - y_W) - 2I_1(y_W, y_i, y_W)\left((y_i - y_W)^2 + 2y_W\right) \\
&\quad -I_2(y_W, y_W)\,(2y_i - 2y_W - 1) \\
&\quad +2\log(y_i)\left(\frac{2y_i}{y_i - y_W} - y_i\right) + 2\log(y_W)\left(-\frac{2y_W}{y_i - y_W} + y_W\right), \qquad \text{(H.14)} \\
E_7^i &= \sqrt{y_W y_i}\, I_1(y_W, y_i, y_W), \qquad \text{(H.15)}
\end{aligned}
$$

and

$$
E_8^{i\beta} = \begin{cases} \sqrt{\frac{y_i}{y_\beta^b}}\text{Re}\left[1 + \frac{y_i}{y_W - y_i}\log\left(\frac{y_W}{y_i}\right)\right. & \\ \left. +x_+(y_\beta^b, y_W, y_i)\log(1 - 1/x_+(y_\beta^b, y_W, y_i)) \right. & \\ \left. +x_-(y_\beta^b, y_W, y_i)\log(1 - 1/x_-(y_\beta^b, y_W, y_i))\right] & \text{for } y_\beta^b \neq 0, \\ & \\ 0 & \text{for } y_\beta^b = 0, \end{cases} \qquad \text{(H.16)}
$$

with

$$
x_\pm(y_1, y_2, y_3) = \frac{1}{2}\left(1 + \frac{y_3 - y_2}{y_1} \pm \sqrt{\left(1 + \frac{y_3 - y_2}{y_1}\right)^2 - \frac{4y_3}{y_1}}\right), \qquad \text{(H.17)}
$$

$$
\begin{aligned}
I_1(y_1, y_2, y_3) &= -\int_0^1 dx \frac{1}{x + y_2 - y_3} \log\left[\frac{xy_1 + (1-x)y_2}{xy_1 + (1-x)y_3 - x(1-x)}\right], \qquad \text{(H.18)} \\
I_2(y_1, y_2) &= -\int_0^1 dx \log[xy_1 + (1-x)y_2 - x(1-x)]. \qquad \text{(H.19)}
\end{aligned}
$$

The symbol "Div" in the formulae stands for the divergent part and has to cancel in the end. The expressions E_1, E_2, E_3, E_5, E_6 and E_7 are the same as the ones obtained in Ref. [379], whereas, due to the mixing matrix renormalization, expression E_4 differs from Ref. [379] and an additional contribution, corresponding to the E_8 term was added. Note that the gauge boson self-interactions and the interactions of the Goldstone bosons with the gauge bosons for the derivation of the result for $\mathcal{M}_t^{heavy}$ are those of the SM and are defined as in Ref. [379].

In case the fermions in the loop are the bottom quark and its partners, the amplitude $\mathcal{M}_b^{heavy}$ is obtained from Eq. (H.8) for $Q = -1/3$ by taking the first three lines and the last line with the replacements

$$
y_W \to 1, \quad y_{i,j} \to y_{i,j}^b, \quad V_{ij}^{Q(L,R)} \to \frac{1}{\sqrt{2}c_W}\widetilde{X}_{ij}^{Q(L,R)} \quad \text{and} \quad W_{ij}^{Q(L,R)} \to \frac{1}{\sqrt{2}c_W} Y_{ij}^{Q(L,R)}. \qquad \text{(H.20)}
$$

Additionally, for bottom partners in the loop there are also Higgs contributions. They read

$$\begin{aligned}\mathcal{M}^{heavy}_{Higgs} = &-\frac{1}{16\pi^2}\sum_i\Bigg[\sum_j G^{hbb\star}_{bj}G^{hbb}_{bi}(\tilde{X}^{-1/3,L}_{ij}E^{ij}_1+\tilde{X}^{-1/3,R}_{ij}E^{ij}_3)\\ &-\tilde{X}^{-1/3,L}_{jb}(G^{hbb\star}_{ib}G^{hbb\star}_{ji})E^{ij}_8+\tilde{X}^{-1/3,L}_{bj}\frac{E^{ij}_4}{2}\left(G^{hbb}_{ji}G^{hbb\star}_{bi}+G^{hbb\star}_{ji}G^{hbb}_{bi}\right)\Bigg]\\ &+\frac{2es_W}{c_W}\,\mathrm{Re}(G^{hbb\star}_{bi}X^{-1/3,L\star}_{ib})E^i_7\,,\end{aligned} \tag{H.21}$$

where in the E_i expressions, as given by Eqs. (H.9–H.16), the replacements $y_W \to m_h^2/M_Z^2$ and $y_i \to y_i^b$ are needed. All summations over i and j are understood as summations over the bottom indices. The Higgs boson coupling matrices $G_{hb\bar{b}}$ were defined in Eq. (7.39). For the SM result $\mathcal{M}^{t+b}_{SM}$, the top-loop contribution $\mathcal{M}^{t}_{SM}$ has been calculated from Eq. (H.8) by replacing the couplings with the corresponding SM couplings and by taking into account only top contributions, *i.e.* no summation over the heavy top partner contributions is performed. Analogously, the bottom-loop contribution $\mathcal{M}^{b}_{SM}$ is obtained from the first three lines of Eq. (H.8) after the replacements in Eq. (H.20) and by substituting the corresponding SM couplings where necessary and not taking into account any heavy bottom partner loop.

Bibliography

[1] **ATLAS** Collaboration, G. Aad *et al.*, *Observation of a new particle in the search for the Standard Model Higgs boson with the ATLAS detector at the LHC*. Phys. Lett. **B716** (2012) 1–29, arXiv:1207.7214 [hep-ex].

[2] **CMS** Collaboration, S. Chatrchyan *et al.*, *Observation of a new boson at a mass of 125 GeV with the CMS experiment at the LHC*. Phys. Lett. **B716** (2012) 30–61, arXiv:1207.7235 [hep-ex].

[3] S. Weinberg, *A Model of Leptons*. Phys. Rev. Lett. **19** (1967) 1264–1266.

[4] A. Salam. Proceedings of the 8th Nobel Symposium p. 367.

[5] S. Glashow, *Partial Symmetries of Weak Interactions*. Nucl. Phys. **22** (1961) 579–588.

[6] P. W. Higgs, *Broken Symmetries and the Masses of Gauge Bosons*. Phys. Rev. Lett. **13** (1964) 508–509.

[7] P. Higgs, *Broken symmetries, massless particlees and gauge fields*. Physics Letters **12** (1964) 132 – 133.

[8] F. Englert and R. Brout, *Broken symmetry and the mass of gauge vector mesons*. Phys. Rev. Lett. **13** (1964) 321–322.

[9] G. S. Guralnik, C. R. Hagen, and T. W. B. Kibble, *Global Conservation Laws and Massless Particles*. Phys. Rev. Lett. **13** (1964) 585–587.

[10] T. Kibble, *Symmetry breaking in non Abelian gauge theories*. Phys. Rev. **155** (1967) 1554–1561.

[11] D. Volkov and V. Akulov, *Is the neutrino a goldstone particle?* Physics Letters B **46** (1973) 109 – 110.

[12] J. Wess and B. Zumino, *Supergauge transformations in four dimensions*. Nucl. Phys. B **70** (1974) 39 – 50.

[13] H. P. Nilles, *Supersymmetry, supergravity and particle physics*. Physics Reports **110** (1984) 1 – 162.

[14] H. E. Haber and G. L. Kane, *The search for supersymmetry: Probing physics beyond the standard model*. Physics Reports **117** (1985) 75 – 263.

[15] M. F. Sohnius, *Introducing supersymmetry*. Physics Reports **128** (1985) 39 – 204.

[16] J. F. Gunion and H. E. Haber, *Higgs bosons in supersymmetric models (I)*. Nucl. Phys. B **272** (1986) 1 – 76.

[17] J. F. Gunion and H. E. Haber, *Higgs bosons in supersymmetric models (II). Implications for phenomenology*. Nucl. Phys. B **278** (1986) 449 – 492.

[18] S. P. Martin, *A Supersymmetry primer*. arXiv:hep-ph/9709356 [hep-ph].

[19] S. Dimopoulos and J. Preskill, *Massless composites with massive constituents*. Nucl. Phys. B **199** (1982) 206 – 222.

[20] D. B. Kaplan and H. Georgi, *SU(2) x U(1) breaking by vacuum misalignment*. Phys. Lett. **B136** (1984) 183–186.

[21] M. J. Dugan, H. Georgi, and D. B. Kaplan, *Anatomy of a composite Higgs model*. Nucl. Phys. **B254** (1984) 299–326.

[22] B. Kaplan, David H. Georgi, and S. Dimopoulos, *Composite Higgs Scalars*. Phys. Lett. **B136** (1984) 187–190.

[23] T. Banks, *Constraints on $SU2 \times U1$ breaking by vacuum misalignment*. Nucl. Phys. B **243** (1984) 125 – 130.

[24] H. Georgi, D. B. Kaplan, and P. Galison, *Calculation of the composite Higgs mass*. Physics Letters B **143** (1984) no. 1-3, 152 – 154.

[25] H. Georgi and D. B. Kaplan, *Composite Higgs and custodial SU(2)*. Physics Letters B **145** (1984) 216 – 220.

[26] K. Agashe, R. Contino, and A. Pomarol, *The Minimal composite Higgs model*. Nucl. Phys. **B719** (2005) 165–187, arXiv:hep-ph/0412089 [hep-ph].

[27] R. Contino, L. Da Rold, and A. Pomarol, *Light custodians in natural composite Higgs models*. Phys. Rev. **D75** (2007) 055014, arXiv:hep-ph/0612048 [hep-ph].

[28] O. Matsedonskyi, G. Panico, and A. Wulzer, *Light Top Partners for a Light Composite Higgs*. JHEP **1301** (2013) 164, arXiv:1204.6333 [hep-ph].

[29] M. Redi and A. Tesi, *Implications of a Light Higgs in Composite Models*. JHEP **1210** (2012) 166, arXiv:1205.0232 [hep-ph].

[30] D. Marzocca, M. Serone, and J. Shu, *General Composite Higgs Models*. JHEP **1208** (2012) 013, arXiv:1205.0770 [hep-ph].

[31] A. Pomarol and F. Riva, *The Composite Higgs and Light Resonance Connection*. JHEP **1208** (2012) 135, arXiv:1205.6434 [hep-ph].

[32] D. Pappadopulo, A. Thamm, and R. Torre, *A minimally tuned composite Higgs model from an extra dimension*. JHEP **1307** (2013) 058, arXiv:1303.3062 [hep-ph].

[33] T. Graf, R. Grober, M. Muhlleitner, H. Rzehak, and K. Walz, *Higgs Boson Masses in the Complex NMSSM at One-Loop Level*. JHEP **1210** (2012) 122, arXiv:1206.6806 [hep-ph].

[34] M. Gillioz, R. Grober, C. Grojean, M. Muhlleitner, and E. Salvioni, *Higgs Low-Energy Theorem (and its corrections) in Composite Models*. JHEP **1210** (2012) 004, arXiv:1206.7120 [hep-ph].

[35] J. Baglio, A. Djouadi, R. Grober, M. Muhlleitner, J. Quevillon, and M. Spira, *The measurement of the Higgs self-coupling at the LHC: theoretical status*. JHEP **1304** (2013) 151, arXiv:1212.5581 [hep-ph].

[36] M. Gillioz, R. Grober, A. Kapuvari, and M. Muhlleitner, *Vector-like Bottom Quarks in Composite Higgs Models*. JHEP **1403** (2014) 037, arXiv:1311.4453 [hep-ph].

[37] J. Baglio, R. Grober, M. Muhlleitner, D. Nhung, H. Rzehak, *et al.*, *NMSSMCALC: A Program Package for the Calculation of Loop-Corrected Higgs Boson Masses and Decay Widths in the (Complex) NMSSM*. arXiv:1312.4788 [hep-ph].

[38] A. Djouadi, W. Kilian, M. Muhlleitner, and P. Zerwas, *Testing Higgs selfcouplings at e+ e- linear colliders*. Eur. Phys. J. **C10** (1999) 27–43, arXiv:hep-ph/9903229 [hep-ph].

[39] A. Djouadi, W. Kilian, M. Muhlleitner, and P. Zerwas, *Production of neutral Higgs boson pairs at LHC*. Eur. Phys. J. **C10** (1999) 45–49, arXiv:hep-ph/9904287 [hep-ph].

[40] M. M. Muhlleitner, *Higgs particles in the standard model and supersymmetric theories*. arXiv:hep-ph/0008127 [hep-ph].

[41] S. Dimopoulos and G. Giudice, *Naturalness constraints in supersymmetric theories with nonuniversal soft terms*. Phys. Lett. **B357** (1995) 573–578, arXiv:hep-ph/9507282 [hep-ph].

[42] P. Fayet, *Supergauge Invariant Extension of the Higgs Mechanism and a Model for the electron and Its Neutrino*. Nucl. Phys. **B90** (1975) 104–124.

[43] R. K. Kaul and P. Majumdar, *Cancellation of Quadratically Divergent Mass Corrections in Globally Supersymmetric Spontaneously Broken Gauge Theories*. Nucl. Phys. **B199** (1982) 36.

[44] R. Barbieri, S. Ferrara, and C. A. Savoy, *Gauge Models with Spontaneously Broken Local Supersymmetry*. Phys. Lett. **B119** (1982) 343.

[45] H. P. Nilles, M. Srednicki, and D. Wyler, *Weak Interaction Breakdown Induced by Supergravity*. Phys. Lett. **B120** (1983) 346.

[46] J. Frere, D. Jones, and S. Raby, *Fermion Masses and Induction of the Weak Scale by Supergravity*. Nucl. Phys. **B222** (1983) 11.

[47] J. Derendinger and C. A. Savoy, *Quantum Effects and SU(2) x U(1) Breaking in Supergravity Gauge Theories*. Nucl. Phys. **B237** (1984) 307.

[48] **ATLAS** Collaboration, *Combined measurements of the mass and signal strength of the Higgs-like boson with the ATLAS detector using up to 25 fb^{-1} of proton-proton collision data* Tech. Rep. ATLAS-CONF-2013-014, CERN, Geneva, Mar, 2013.

[49] **CMS** Collaboration, *Combination of standard model Higgs boson searches and measurements of the properties of the new boson with a mass near 125 GeV* Tech. Rep. CMS-PAS-HIG-13-005, CERN, Geneva, 2013.

[50] F. Bezrukov, M. Y. Kalmykov, B. A. Kniehl, and M. Shaposhnikov, *Higgs Boson Mass and New Physics*. JHEP **1210** (2012) 140, `arXiv:1205.2893 [hep-ph]`.

[51] G. Degrassi, S. Di Vita, J. Elias-Miro, J. R. Espinosa, G. F. Giudice, *et al.*, *Higgs mass and vacuum stability in the Standard Model at NNLO*. JHEP **1208** (2012) 098, `arXiv:1205.6497 [hep-ph]`.

[52] D. Buttazzo, G. Degrassi, P. P. Giardino, G. F. Giudice, F. Sala, *et al.*, *Investigating the near-criticality of the Higgs boson*. `arXiv:1307.3536 [hep-ph]`.

[53] M. S. Chanowitz, M. Furman, and I. Hinchliffe, *Weak Interactions of Ultraheavy Fermions*. Phys. Lett. **B78** (1978) 285.

[54] N. Cabibbo, L. Maiani, G. Parisi, and R. Petronzio, *Bounds on the Fermions and Higgs Boson Masses in Grand Unified Theories*. Nucl. Phys. **B158** (1979) 295–305.

[55] R. A. Flores and M. Sher, *Upper Limits to Fermion Masses in the Glashow-Weinberg-Salam Model*. Phys. Rev. **D27** (1983) 1679.

[56] M. Lindner, *Implications of Triviality for the Standard Model*. Z. Phys. **C31** (1986) 295.

[57] A. Hasenfratz, K. Jansen, C. B. Lang, T. Neuhaus, and H. Yoneyama, *The Triviality Bound of the Four Component phi**4 Model*. Phys. Lett. **B199** (1987) 531.

[58] J. Kuti, L. Lin, and Y. Shen, *Upper Bound on the Higgs Mass in the Standard Model*. Phys. Rev. Lett. **61** (1988) 678.

[59] M. Sher, *Electroweak Higgs Potentials and Vacuum Stability*. Phys. Rept. **179** (1989) 273–418.

[60] M. Luscher and P. Weisz, *Scaling Laws and Triviality Bounds in the Lattice phi**4 Theory. 3. N Component Model*. Nucl. Phys. **B318** (1989) 705.

[61] M. Sher, *Precise vacuum stability bound in the standard model*. Phys. Lett. **B317** (1993) 159–163, arXiv:hep-ph/9307342 [hep-ph].

[62] G. Altarelli and G. Isidori, *Lower limit on the Higgs mass in the standard model: An Update*. Phys. Lett. **B337** (1994) 141–144.

[63] J. Casas, J. Espinosa, and M. Quiros, *Improved Higgs mass stability bound in the standard model and implications for supersymmetry*. Phys. Lett. **B342** (1995) 171–179, arXiv:hep-ph/9409458 [hep-ph].

[64] J. Espinosa and M. Quiros, *Improved metastability bounds on the standard model Higgs mass*. Phys. Lett. **B353** (1995) 257–266, arXiv:hep-ph/9504241 [hep-ph].

[65] B. W. Lee, C. Quigg, and H. B. Thacker, *Weak Interactions at Very High-Energies: The Role of the Higgs Boson Mass*. Phys. Rev. **D16** (1977) 1519.

[66] B. Cleveland, T. Daily, J. Davis, Raymond, J. R. Distel, K. Lande, *et al.*, *Measurement of the solar electron neutrino flux with the Homestake chlorine detector*. Astrophys. J. **496** (1998) 505–526.

[67] **Super-Kamiokande** Collaboration, S. Fukuda *et al.*, *Solar B-8 and hep neutrino measurements from 1258 days of Super-Kamiokande data*. Phys. Rev. Lett. **86** (2001) 5651–5655, arXiv:hep-ex/0103032 [hep-ex].

[68] **SNO** Collaboration, B. Aharmim *et al.*, *Electron energy spectra, fluxes, and day-night asymmetries of B-8 solar neutrinos from measurements with NaCl dissolved in the heavy-water detector at the Sudbury Neutrino Observatory*. Phys. Rev. **C72** (2005) 055502, arXiv:nucl-ex/0502021 [nucl-ex].

[69] **KamLAND** Collaboration, K. Eguchi *et al.*, *First results from KamLAND: Evidence for reactor anti-neutrino disappearance*. Phys. Rev. Lett. **90** (2003) 021802, arXiv:hep-ex/0212021 [hep-ex].

[70] B. Pontecorvo, *Mesonium and anti-mesonium*. Sov. Phys. JETP **6** (1957) 429.

[71] **Particle Data Group** Collaboration, J. Beringer *et al.*, *Review of Particle Physics (RPP)*. Phys. Rev. **D86** (2012) 010001.

[72] P. Minkowski, *mu –> e gamma at a Rate of One Out of 1-Billion Muon Decays?* Phys. Lett. **B67** (1977) 421.

[73] M. Gell-Mann, P. Ramond, and R. Slansky, *Complex Spinors and Unified Theories*. Conf. Proc. **C790927** (1979) 315–321, arXiv:1306.4669 [hep-th].

[74] R. N. Mohapatra and G. Senjanovic, *Neutrino Mass and Spontaneous Parity Violation*. Phys. Rev. Lett. **44** (1980) 912.

[75] D. Clowe, M. Bradac, A. H. Gonzalez, M. Markevitch, S. W. Randall, *et al.*, *A direct empirical proof of the existence of dark matter*. Astrophys. J. **648** (2006) L109–L113, arXiv:astro-ph/0608407 [astro-ph].

[76] **WMAP** Collaboration, D. Spergel *et al.*, *Wilkinson Microwave Anisotropy Probe (WMAP) three year results: implications for cosmology*. Astrophys. J. Suppl. **170** (2007) 377, arXiv:astro-ph/0603449 [astro-ph].

[77] **Planck** Collaboration, P. Ade *et al.*, *Planck 2013 results. XVI. Cosmological parameters*. arXiv:1303.5076 [astro-ph.CO].

[78] G. Steigman and M. S. Turner, *Cosmological Constraints on the Properties of Weakly Interacting Massive Particles*. Nucl. Phys. **B253** (1985) 375.

[79] **Supernova Search Team** Collaboration, A. G. Riess *et al.*, *Observational evidence from supernovae for an accelerating universe and a cosmological constant*. Astron. J. **116** (1998) 1009–1038, arXiv:astro-ph/9805201 [astro-ph].

[80] **Supernova Cosmology Project** Collaboration, S. Perlmutter *et al.*, *Measurements of Omega and Lambda from 42 high redshift supernovae*. Astrophys. J. **517** (1999) 565–586, arXiv:astro-ph/9812133 [astro-ph].

[81] M. Li, X.-D. Li, S. Wang, and Y. Wang, *Dark Energy: A Brief Review*. Front. Phys. China. **8** (2013) 828–846, arXiv:1209.0922 [astro-ph.CO].

[82] A. D. Sakharov, *Violation of CP in variance, C asymmetry, and baryon asymmetry of the universe*. Journal of Experimental and Theoretical Physics **5** (1967) 24–27.

[83] G. 't Hooft, *Recent developments in gauge theories*. in Proc. of 1979 Cargèse Institute. Plenum Press, New York, 1980.

[84] A. Djouadi, *The Anatomy of electro-weak symmetry breaking. I: The Higgs boson in the standard model*. Phys. Rept. **457** (2008) 1–216, arXiv:hep-ph/0503172 [hep-ph].

[85] G. 't Hooft, *Naturalness, chiral symmetry, and spontaneous chiral symmetry breaking*. NATO Adv. Study Inst. Ser. B Phys. **59** (1980) 135.

[86] T. Asaka and M. Shaposhnikov, *The nuMSM, dark matter and baryon asymmetry of the universe*. Phys. Lett. **B620** (2005) 17–26, arXiv:hep-ph/0505013 [hep-ph].

[87] S. Weinberg, *Anthropic Bound on the Cosmological Constant*. Phys. Rev. Lett. **59** (1987) 2607–2610.

[88] T. Plehn and M. Rauch, *The quartic higgs coupling at hadron colliders*. Phys. Rev. **D72** (2005) 053008, arXiv:hep-ph/0507321 [hep-ph].

[89] G. Cynolter, E. Lendvai, and G. Pocsik, *Resonance production of three neutral supersymmetric Higgs bosons at LHC*. Acta Phys.Polon. **B31** (2000) 1749–1757, arXiv:hep-ph/0003008 [hep-ph].

[90] T. Binoth, S. Karg, N. Kauer, and R. Ruckl, *Multi-Higgs boson production in the Standard Model and beyond*. Phys. Rev. **D74** (2006) 113008, arXiv:hep-ph/0608057 [hep-ph].

[91] **CLIC Physics Working Group** Collaboration, E. Accomando *et al.*, *Physics at the CLIC multi-TeV linear collider*. arXiv:hep-ph/0412251 [hep-ph].

[92] U. Baur, T. Plehn, and D. L. Rainwater, *Measuring the Higgs boson self coupling at the LHC and finite top mass matrix elements*. Phys. Rev. Lett. **89** (2002) 151801, arXiv:hep-ph/0206024 [hep-ph].

[93] U. Baur, T. Plehn, and D. L. Rainwater, *Determining the Higgs boson selfcoupling at hadron colliders*. Phys. Rev. **D67** (2003) 033003, arXiv:hep-ph/0211224 [hep-ph].

[94] U. Baur, T. Plehn, and D. L. Rainwater, *Examining the Higgs boson potential at lepton and hadron colliders: A Comparative analysis*. Phys. Rev. **D68** (2003) 033001, arXiv:hep-ph/0304015 [hep-ph].

[95] U. Baur, T. Plehn, and D. L. Rainwater, *Probing the Higgs selfcoupling at hadron colliders using rare decays*. Phys. Rev. **D69** (2004) 053004, arXiv:hep-ph/0310056 [hep-ph].

[96] M. J. Dolan, C. Englert, and M. Spannowsky, *Higgs self-coupling measurements at the LHC*. JHEP **1210** (2012) 112, arXiv:1206.5001 [hep-ph].

[97] A. Papaefstathiou, L. L. Yang, and J. Zurita, *Higgs boson pair production at the LHC in the $b\bar{b}W^+W^-$ channel*. Phys. Rev. **D87** (2013) 011301, arXiv:1209.1489 [hep-ph].

[98] F. Goertz, A. Papaefstathiou, L. L. Yang, and J. Zurita, *Higgs Boson self-coupling measurements using ratios of cross sections*. JHEP **1306** (2013) 016, arXiv:1301.3492 [hep-ph].

[99] W. Yao, *Studies of measuring Higgs self-coupling with $HH \to b\bar{b}\gamma\gamma$ at the future hadron colliders*. arXiv:1308.6302 [hep-ph].

[100] V. Barger, L. L. Everett, C. Jackson, and G. Shaughnessy, *Higgs-Pair Production and Measurement of the Triscalar Coupling at LHC(8,14)*. Phys. Lett. **B728** (2014) 433–436, arXiv:1311.2931 [hep-ph].

[101] O. J. Eboli, G. Marques, S. Novaes, and A. Natale, *Twin Higgs boson production*. Phys. Lett. **B197** (1987) 269.

[102] E. N. Glover and J. van der Bij, *Higgs boson pair production via gluon fusion*. Nucl. Phys. **B309** (1988) 282.

[103] D. A. Dicus, C. Kao, and S. S. Willenbrock, *Higgs Boson Pair Production From Gluon Fusion*. Phys. Lett. **B203** (1988) 457.

[104] T. Plehn, M. Spira, and P. Zerwas, *Pair production of neutral Higgs particles in gluon-gluon collisions*. Nucl. Phys. **B479** (1996) 46–64, arXiv:hep-ph/9603205 [hep-ph].

[105] S. Dawson, S. Dittmaier, and M. Spira, *Neutral Higgs boson pair production at hadron colliders: QCD corrections*. Phys. Rev. **D58** (1998) 115012, arXiv:hep-ph/9805244 [hep-ph].

[106] J. Grigo, J. Hoff, K. Melnikov, and M. Steinhauser, *On the Higgs boson pair production at the LHC*. Nucl. Phys. **B875** (2013) 1–17, arXiv:1305.7340 [hep-ph].

[107] R. Frederix, S. Frixione, V. Hirschi, F. Maltoni, O. Mattelaer, *et al.*, *Higgs pair production at the LHC with NLO and parton-shower effects*. arXiv:1401.7340 [hep-ph].

[108] D. de Florian and J. Mazzitelli, *Higgs Boson Pair Production at Next-to-Next-to-Leading Order in QCD*. Phys. Rev. Lett. **111** (2013) 201801, arXiv:1309.6594 [hep-ph].

[109] D. Y. Shao, C. S. Li, H. T. Li, and J. Wang, *Threshold resummation effects in Higgs boson pair production at the LHC*. JHEP **1307** (2013) 169, arXiv:1301.1245 [hep-ph].

[110] *See M. Spira's website*. http://people.web.psi.ch/spira/proglist.html.

[111] A. Martin, W. Stirling, R. Thorne, and G. Watt, *Parton distributions for the LHC*. Eur. Phys. J. **C63** (2009) 189–285, arXiv:0901.0002 [hep-ph].

[112] Y. L. Dokshitzer, *Calculation of the Structure Functions for Deep Inelastic Scattering and e+ e- Annihilation by Perturbation Theory in Quantum Chromodynamics*. Sov. Phys. JETP **46** (1977) 641–653.

[113] V. Gribov and L. Lipatov, *Deep inelastic e p scattering in perturbation theory*. Sov. J. Nucl. Phys. **15** (1972) 438–450.

[114] G. Altarelli and G. Parisi, *Asymptotic Freedom in Parton Language*. Nucl. Phys. **B126** (1977) 298.

[115] **LHC Higgs Cross Section Working Group** Collaboration, S. Dittmaier *et al.*, *Handbook of LHC Higgs Cross Sections: 1. Inclusive Observables*. arXiv:1101.0593 [hep-ph].

[116] J. Baglio and A. Djouadi, *Higgs production at the lHC*. JHEP **1103** (2011) 055, arXiv:1012.0530 [hep-ph].

[117] H.-L. Lai, J. Huston, Z. Li, P. Nadolsky, J. Pumplin, *et al.*, *Uncertainty induced by QCD coupling in the CTEQ global analysis of parton distributions*. Phys. Rev. **D82** (2010) 054021, arXiv:1004.4624 [hep-ph].

[118] S. Alekhin, J. Blumlein, and S. Moch, *Parton Distribution Functions and Benchmark Cross Sections at NNLO*. Phys. Rev. **D86** (2012) 054009, arXiv:1202.2281 [hep-ph].

[119] M. Gluck, P. Jimenez-Delgado, E. Reya, and C. Schuck, *On the role of heavy flavor parton distributions at high energy colliders*. Phys. Lett. **B664** (2008) 133–138, arXiv:0801.3618 [hep-ph].

[120] **H1 and ZEUS** Collaboration, V. Radescu, *Hera Precision Measurements and Impact for LHC Predictions*. arXiv:1107.4193 [hep-ex].

[121] **NNPDF** Collaboration, A. Guffanti, *NNPDF2.1: Including heavy quark mass effects in NNPDF fits*. AIP Conf. Proc. **1369** (2011) 21–28.

[122] A. Martin, W. Stirling, R. Thorne, and G. Watt, *Uncertainties on alpha(S) in global PDF analyses and implications for predicted hadronic cross sections*. Eur. Phys. J. **C64** (2009) 653–680, arXiv:0905.3531 [hep-ph].

[123] J. R. Ellis, M. K. Gaillard, and D. V. Nanopoulos, *A Phenomenological Profile of the Higgs Boson*. Nucl. Phys. **B106** (1976) 292.

[124] M. A. Shifman, A. Vainshtein, M. Voloshin, and V. I. Zakharov, *Low-Energy Theorems for Higgs Boson Couplings to Photons*. Sov. J. Nucl. Phys. **30** (1979) 711–716.

[125] B. A. Kniehl and M. Spira, *Low-energy theorems in Higgs physics*. Z. Phys. **C69** (1995) 77–88, arXiv:hep-ph/9505225 [hep-ph].

[126] J. Baglio and A. Djouadi, *Predictions for Higgs production at the Tevatron and the associated uncertainties*. JHEP **1010** (2010) 064, arXiv:1003.4266 [hep-ph].

[127] T. Han, G. Valencia, and S. Willenbrock, *Structure function approach to vector boson scattering in p p collisions*. Phys. Rev. Lett. **69** (1992) 3274–3277, arXiv:hep-ph/9206246 [hep-ph].

[128] T. Figy, C. Oleari, and D. Zeppenfeld, *Next-to-leading order jet distributions for Higgs boson production via weak boson fusion*. Phys. Rev. **D68** (2003) 073005, arXiv:hep-ph/0306109 [hep-ph].

[129] E. L. Berger and J. M. Campbell, *Higgs boson production in weak boson fusion at next-to-leading order*. Phys. Rev. **D70** (2004) 073011, arXiv:hep-ph/0403194 [hep-ph].

[130] K. Arnold, M. Bahr, G. Bozzi, F. Campanario, C. Englert, *et al.*, *VBFNLO: A Parton level Monte Carlo for processes with electroweak bosons*. Comput. Phys. Commun. **180** (2009) 1661–1670, arXiv:0811.4559 [hep-ph].

[131] K. Arnold, J. Bellm, G. Bozzi, F. Campanario, C. Englert, *et al.*, *Release Note – Vbfnlo-2.6.0*. arXiv:1207.4975 [hep-ph].

[132] T. Figy, *Next-to-leading order QCD corrections to light Higgs Pair production via vector boson fusion*. Mod. Phys. Lett. **A23** (2008) 1961–1973, arXiv:0806.2200 [hep-ph].

[133] L. Liu-Sheng, Z. Ren-You, M. Wen-Gan, G. Lei, L. Wei-Hua, *et al.*, *NNLO QCD corrections to Higgs pair production via vector boson fusion at hadron colliders*. arXiv:1401.7754 [hep-ph].

[134] V. D. Barger, T. Han, and R. Phillips, *Double Higgs Boson Bremsstrahlung From W and Z Bosons at Supercolliders*. Phys. Rev. **D38** (1988) 2766.

[135] G. Altarelli, R. K. Ellis, and G. Martinelli, *Large Perturbative Corrections to the Drell-Yan Process in QCD*. Nucl. Phys. **B157** (1979) 461.

[136] J. Kubar-Andre and F. E. Paige, *Gluon Corrections to the Drell-Yan Model*. Phys. Rev. **D19** (1979) 221.

[137] T. Han and S. Willenbrock, *QCD correction to the p p —> W H and Z H total cross-sections*. Phys. Lett. **B273** (1991) 167–172.

[138] R. V. Harlander and W. B. Kilgore, *Next-to-next-to-leading order Higgs production at hadron colliders*. Phys. Rev. Lett. **88** (2002) 201801, arXiv:hep-ph/0201206 [hep-ph].

[139] R. Hamberg, W. van Neerven, and T. Matsuura, *A Complete calculation of the order α_s^2 correction to the Drell-Yan K factor*. Nucl. Phys. **B359** (1991) 343–405.

[140] O. Brein, A. Djouadi, and R. Harlander, *NNLO QCD corrections to the Higgs-strahlung processes at hadron colliders*. Phys. Lett. **B579** (2004) 149–156, arXiv:hep-ph/0307206 [hep-ph].

[141] D. A. Dicus and C. Kao, *Higgs Boson - Z^0 Production From Gluon Fusion*. Phys. Rev. **D38** (1988) 1008.

[142] B. A. Kniehl, *Associated Production of Higgs and Z Bosons From Gluon Fusion in Hadron Collisions*. Phys. Rev. **D42** (1990) 2253–2258.

[143] D. A. Dicus and S. S. Willenbrock, *Radiative Corrections to the Ratio of Z and W Boson Production*. Phys. Rev. **D34** (1986) 148.

[144] K.-i. Hikasa, *Counting neutrino species at high-energy proton - anti-proton collisions*. Phys. Rev. **D29** (1984) 1939.

[145] R. J. Gonsalves, C.-M. Hung, and J. Pawlowski, *Heavy quark triangle diagram contributions to Z boson production in hadron collisions*. Phys. Rev. **D46** (1992) 4930–4942.

[146] P. Rijken and W. van Neerven, *Heavy flavor contributions to the Drell-Yan cross-section*. Phys. Rev. **D52** (1995) 149–161, arXiv:hep-ph/9501373 [hep-ph].

[147] T. Hahn, *Generating Feynman diagrams and amplitudes with FeynArts 3*. Comput. Phys. Commun. **140** (2001) 418–431, arXiv:hep-ph/0012260 [hep-ph].

[148] T. Hahn and M. Perez-Victoria, *Automatized one loop calculations in four-dimensions and D-dimensions*. Comput. Phys. Commun. **118** (1999) 153–165, arXiv:hep-ph/9807565 [hep-ph].

[149] T. Hahn and M. Rauch, *News from FormCalc and LoopTools*. Nucl. Phys. Proc. Suppl. **157** (2006) 236–240, arXiv:hep-ph/0601248 [hep-ph].

[150] T. Hahn, *A Mathematica interface for FormCalc-generated code*. Comput. Phys. Commun. **178** (2008) 217–221, arXiv:hep-ph/0611273 [hep-ph].

[151] J. Alwall, P. Demin, S. de Visscher, R. Frederix, M. Herquet, *et al.*, *MadGraph/MadEvent v4: The New Web Generation*. JHEP **0709** (2007) 028, arXiv:0706.2334 [hep-ph].

[152] J. Alwall, M. Herquet, F. Maltoni, O. Mattelaer, and T. Stelzer, *MadGraph 5 : Going Beyond*. JHEP **1106** (2011) 128, arXiv:1106.0522 [hep-ph].

[153] M. Moretti, S. Moretti, F. Piccinini, R. Pittau, and A. Polosa, *Higgs boson self-couplings at the LHC as a probe of extended Higgs sectors*. JHEP **0502** (2005) 024, arXiv:hep-ph/0410334 [hep-ph].

[154] T. Sjostrand, S. Mrenna, and P. Z. Skands, *PYTHIA 6.4 Physics and Manual*. JHEP **0605** (2006) 026, arXiv:hep-ph/0603175 [hep-ph].

[155] J. Quevillon, *Higgs Physics Beyond the Standard Model*. Dissertation, 2014.

[156] **ATLAS** Collaboration, *Performance of the Reconstruction and Identification of Hadronic Tau Decays in ATLAS with 2011 Data* Tech. Rep. ATLAS-CONF-2012-142, CERN, Geneva, Oct, 2012.

[157] **CMS** Collaboration, S. Chatrchyan *et al.*, *Performance of τ-lepton reconstruction and identification in CMS* J. Instrum. **7** (Sep, 2011) P01001 33 p.

[158] S. R. Coleman and J. Mandula, *All Possible Symmetries of the S Matrix*. Phys. Rev. **159** (1967) 1251–1256.

[159] R. Haag, J. T. Lopuszanski, and M. Sohnius, *All Possible Generators of Supersymmetries of the s Matrix*. Nucl. Phys. **B88** (1975) 257.

[160] Y. Golfand and E. Likhtman, *Extension of the Algebra of Poincare Group Generators and Violation of p Invariance*. JETP Lett. **13** (1971) 323–326.

[161] M. Drees, R. Godbole, and P. Roy, *Theory and phenomenology of sparticles : an account of four-dimensional N = 1 supersymmetry in high energy physics*. World Scientific, Singapore [u.a.], repr. ed., 2005.

[162] A. Salam and J. Strathdee, *Supergauge Transformations*. Nucl. Phys. **B76** (1974) 477–482.

[163] J. Wess and B. Zumino, *Supergauge Invariant Extension of Quantum Electrodynamics*. Nucl. Phys. **B78** (1974) 1.

[164] J. Terning, *Modern supersymmetry : dynamics and duality*. International series of monographs on physics ; 132. Oxford Univ. Press, 1. publ. ed., 2006.

[165] L. J. Hall, V. A. Kostelecky, and S. Raby, *New Flavor Violations in Supergravity Models*. Nucl. Phys. **B267** (1986) 415.

[166] F. Brummer, S. Kraml, and S. Kulkarni, *Anatomy of maximal stop mixing in the MSSM*. JHEP **1208** (2012) 089, `arXiv:1204.5977 [hep-ph]`.

[167] C. Wymant, *Optimising Stop Naturalness*. Phys. Rev. **D86** (2012) 115023, `arXiv:1208.1737 [hep-ph]`.

[168] C. Boehm, A. Djouadi, and M. Drees, *Light scalar top quarks and supersymmetric dark matter*. Phys. Rev. **D62** (2000) 035012, `arXiv:hep-ph/9911496 [hep-ph]`.

[169] J. R. Ellis, K. A. Olive, and Y. Santoso, *Calculations of neutralino stop coannihilation in the CMSSM*. Astropart. Phys. **18** (2003) 395–432, `arXiv:hep-ph/0112113 [hep-ph]`.

[170] C. Balazs, M. S. Carena, and C. Wagner, *Dark matter, light stops and electroweak baryogenesis*. Phys. Rev. **D70** (2004) 015007, `arXiv:hep-ph/0403224 [hep-ph]`.

[171] C. Balazs, M. S. Carena, A. Menon, D. Morrissey, and C. Wagner, *The Supersymmetric origin of matter*. Phys. Rev. **D71** (2005) 075002, arXiv:hep-ph/0412264 [hep-ph].

[172] M. S. Carena, M. Quiros, and C. Wagner, *Opening the window for electroweak baryogenesis*. Phys. Lett. **B380** (1996) 81–91, arXiv:hep-ph/9603420 [hep-ph].

[173] M. S. Carena, M. Quiros, and C. Wagner, *Electroweak baryogenesis and Higgs and stop searches at LEP and the Tevatron*. Nucl. Phys. **B524** (1998) 3–22, arXiv:hep-ph/9710401 [hep-ph].

[174] D. Delepine, J. Gerard, R. Gonzalez Felipe, and J. Weyers, *A Light stop and electroweak baryogenesis*. Phys. Lett. **B386** (1996) 183–188, arXiv:hep-ph/9604440 [hep-ph].

[175] M. Carena, G. Nardini, M. Quiros, and C. Wagner, *The Baryogenesis Window in the MSSM*. Nucl. Phys. **B812** (2009) 243–263, arXiv:0809.3760 [hep-ph].

[176] M. Carena, G. Nardini, M. Quiros, and C. E. Wagner, *The Effective Theory of the Light Stop Scenario*. JHEP **0810** (2008) 062, arXiv:0806.4297 [hep-ph].

[177] M. Laine, G. Nardini, and K. Rummukainen, *Lattice study of an electroweak phase transition at $m_h \sim$ 126 GeV*. JCAP **1301** (2013) 011, arXiv:1211.7344 [hep-ph].

[178] **ATLAS** Collaboration, *Search for pair-produced top squarks decaying into a charm quark and the lightest neutralinos with 20.3 fb^{-1} of pp collisions at $\sqrt{s} = 8$ TeV with the ATLAS detector at the LHC* Tech. Rep. ATLAS-CONF-2013-068, CERN, Geneva, Jul, 2013.

[179] K.-i. Hikasa and M. Kobayashi, *Light Scalar Top at e+ e- Colliders*. Phys. Rev. **D36** (1987) 724.

[180] M. Muhlleitner and E. Popenda, *Light Stop Decay in the MSSM with Minimal Flavour Violation*. JHEP **1104** (2011) 095, arXiv:1102.5712 [hep-ph].

[181] E. Popenda, *Higher Order Corrections to Supersymmetric Production and Decay Processes*. Dissertation, 2012.

[182] C. Boehm, A. Djouadi, and Y. Mambrini, *Decays of the lightest top squark*. Phys. Rev. **D61** (2000) 095006, arXiv:hep-ph/9907428 [hep-ph].

[183] **CMS** Collaboration, *Search for top squarks decaying to a charm quark and a neutralino in events with a jet and missing transverse momentum* Tech. Rep. CMS-PAS-SUS-13-009, CERN, Geneva, 2014.

[184] **D0** Collaboration, V. Abazov *et al.*, *Search for scalar top quarks in the acoplanar charm jets and missing transverse energy final state in $p\bar{p}$ collisions at $\sqrt{s}$ = 1.96-TeV*. Phys. Lett. **B665** (2008) 1–8, arXiv:0803.2263 [hep-ex].

[185] **CDF** Collaboration, T. Aaltonen *et al.*, *Search for Scalar Top Quark Production in $p\bar{p}$ Collisions at $\sqrt{s} = 1.96$ TeV*. JHEP **1210** (2012) 158, arXiv:1203.4171 [hep-ex].

[186] **OPAL** Collaboration, G. Abbiendi *et al.*, *Search for scalar top and scalar bottom quarks at S**(1/2) = 189-GeV at LEP*. Phys. Lett. **B456** (1999) 95–106, arXiv:hep-ex/9903070 [hep-ex].

[187] **OPAL** Collaboration, G. Abbiendi *et al.*, *Search for scalar top and scalar bottom quarks at LEP*. Phys. Lett. **B545** (2002) 272–284, arXiv:hep-ex/0209026 [hep-ex].

[188] A. Delgado, G. F. Giudice, G. Isidori, M. Pierini, and A. Strumia, *The light stop window*. Eur. Phys. J. **C73** (2013) 2370, arXiv:1212.6847 [hep-ph].

[189] **CMS** Collaboration, S. Chatrchyan *et al.*, *Search for dark matter and large extra dimensions in monojet events in pp collisions at $\sqrt{s} = 7$ TeV*. JHEP **1209** (2012) 094, arXiv:1206.5663 [hep-ex].

[190] **ATLAS** Collaboration, G. Aad *et al.*, *Search for dark matter candidates and large extra dimensions in events with a jet and missing transverse momentum with the ATLAS detector*. JHEP **1304** (2013) 075, arXiv:1210.4491 [hep-ex].

[191] **ATLAS** Collaboration, G. Aad *et al.*, *Search for squarks and gluinos using final states with jets and missing transverse momentum with the ATLAS detector in $\sqrt{s} = 7$ TeV proton-proton collisions*. Phys. Lett. **B710** (2012) 67–85, arXiv:1109.6572 [hep-ex].

[192] **CMS** Collaboration, S. Chatrchyan *et al.*, *Search for supersymmetry in final states with missing transverse energy and 0, 1, 2, or at least 3 b-quark jets in 7 TeV pp collisions using the variable alphaT*. JHEP **1301** (2013) 077, arXiv:1210.8115 [hep-ex].

[193] C. Rogan, *Kinematical variables towards new dynamics at the LHC*. arXiv:1006.2727 [hep-ph].

[194] R. S. Chivukula and H. Georgi, *Composite Technicolor Standard Model*. Phys. Lett. **B188** (1987) 99.

[195] L. Hall and L. Randall, *Weak scale effective supersymmetry*. Phys. Rev. Lett. **65** (1990) 2939–2942.

[196] G. D'Ambrosio, G. Giudice, G. Isidori, and A. Strumia, *Minimal flavor violation: An Effective field theory approach*. Nucl. Phys. **B645** (2002) 155–187, arXiv:hep-ph/0207036 [hep-ph].

[197] N. Cabibbo, *Unitary Symmetry and Leptonic Decays*. Phys. Rev. Lett. **10** (1963) 531–533.

[198] M. Kobayashi and T. Maskawa, *CP Violation in the Renormalizable Theory of Weak Interaction*. Prog.Theor.Phys. **49** (1973) 652–657.

[199] G. Arcadi, L. Di Luzio, and M. Nardecchia, *Minimal Flavour Violation and Neutrino Masses without R-parity*. JHEP **1205** (2012) 048, arXiv:1111.3941 [hep-ph].

[200] G. Colangelo, E. Nikolidakis, and C. Smith, *Supersymmetric models with minimal flavour violation and their running*. Eur. Phys. J. **C59** (2009) 75–98, arXiv:0807.0801 [hep-ph].

[201] R. Barbieri, G. Dvali, and L. J. Hall, *Predictions from a U(2) flavor symmetry in supersymmetric theories*. Phys. Lett. **B377** (1996) 76–82, arXiv:hep-ph/9512388 [hep-ph].

[202] R. Barbieri, D. Buttazzo, F. Sala, and D. M. Straub, *Flavour physics and flavour symmetries after the first LHC phase*. arXiv:1402.6677 [hep-ph].

[203] M. Drees and M. M. Nojiri, *The Neutralino relic density in minimal $N = 1$ supergravity*. Phys. Rev. **D47** (1993) 376–408, arXiv:hep-ph/9207234 [hep-ph].

[204] **CMS** Collaboration, *Search for electroweak production of charginos, neutralinos, and sleptons using leptonic final states in pp collisions at 8 TeV* Tech. Rep. CMS-PAS-SUS-13-006, CERN, Geneva, 2013.

[205] **ATLAS** Collaboration, *Search for direct production of charginos and neutralinos in events with three leptons and missing transverse momentum in 21 fb^{-1} of pp collisions at $\sqrt{s} = 8$ TeV with the ATLAS detector* Tech. Rep. ATLAS-CONF-2013-035, CERN, Geneva, Mar, 2013.

[206] S. Kraml, H. Eberl, A. Bartl, W. Majerotto, and W. Porod, *SUSY QCD corrections to scalar quark decays into charginos and neutralinos*. Phys. Lett. **B386** (1996) 175–182, arXiv:hep-ph/9605412 [hep-ph].

[207] A. Djouadi, W. Hollik, and C. Junger, *QCD corrections to scalar quark decays*. Phys. Rev. **D55** (1997) 6975–6985, arXiv:hep-ph/9609419 [hep-ph].

[208] W. Hollik, J. M. Lindert, and D. Pagani, *NLO corrections to squark-squark production and decay at the LHC*. JHEP **1303** (2013) 139, arXiv:1207.1071 [hep-ph].

[209] T. Kinoshita, *Mass singularities of Feynman amplitudes*. J. Math. Phys. **3** (1962) 650–677.

[210] T. Lee and M. Nauenberg, *Degenerate Systems and Mass Singularities*. Phys. Rev. **133** (1964) B1549–B1562.

[211] W. Siegel, *Supersymmetric Dimensional Regularization via Dimensional Reduction*. Phys. Lett. **B84** (1979) 193.

[212] D. Capper, D. Jones, and P. van Nieuwenhuizen, *Regularization by Dimensional Reduction of Supersymmetric and Nonsupersymmetric Gauge Theories*. Nucl. Phys. **B167** (1980) 479.

[213] A. Denner and T. Sack, *Renormalization of the Quark Mixing Matrix*. Nucl. Phys. **B347** (1990) 203–216.

[214] P. Gambino, P. Grassi, and F. Madricardo, *Fermion mixing renormalization and gauge invariance*. Phys. Lett. **B454** (1999) 98–104, arXiv:hep-ph/9811470 [hep-ph].

[215] B. A. Kniehl, F. Madricardo, and M. Steinhauser, *Gauge independent W boson partial decay widths*. Phys. Rev. **D62** (2000) 073010, arXiv:hep-ph/0005060 [hep-ph].

[216] A. Barroso, L. Brucher, and R. Santos, *Renormalization of the Cabibbo-Kobayashi-Maskawa matrix*. Phys. Rev. **D62** (2000) 096003, arXiv:hep-ph/0004136 [hep-ph].

[217] Y. Yamada, *Gauge dependence of the on-shell renormalized mixing matrices*. Phys. Rev. **D64** (2001) 036008, arXiv:hep-ph/0103046 [hep-ph].

[218] A. Crivellin, L. Hofer, U. Nierste, and D. Scherer, *Phenomenological consequences of radiative flavor violation in the MSSM*. Phys. Rev. **D84** (2011) 035030, arXiv:1105.2818 [hep-ph].

[219] H. Eberl, K. Hidaka, S. Kraml, W. Majerotto, and Y. Yamada, *Improved SUSY QCD corrections to Higgs boson decays into quarks and squarks*. Phys. Rev. **D62** (2000) 055006, arXiv:hep-ph/9912463 [hep-ph].

[220] J. M. Campbell, R. K. Ellis, and F. Tramontano, *Single top production and decay at next-to-leading order*. Phys. Rev. **D70** (2004) 094012, arXiv:hep-ph/0408158 [hep-ph].

[221] A. Wlotzka, *Decays of the lightest squark in the MSSM with Flavour Violation*, 2014. Master thesis, KIT.

[222] M. Muhlleitner, A. Djouadi, and Y. Mambrini, *SDECAY: A Fortran code for the decays of the supersymmetric particles in the MSSM*. Comput. Phys. Commun. **168** (2005) 46–70, arXiv:hep-ph/0311167 [hep-ph].

[223] A. Djouadi, M. Muhlleitner, and M. Spira, *Decays of supersymmetric particles: The Program SUSY-HIT (SUspect-SdecaY-Hdecay-InTerface)*. Acta Phys.Polon. **B38** (2007) 635–644, arXiv:hep-ph/0609292 [hep-ph].

[224] B. Allanach, C. Balazs, G. Belanger, M. Bernhardt, F. Boudjema, *et al.*, *SUSY Les Houches Accord 2*. Comput. Phys. Commun. **180** (2009) 8–25, arXiv:0801.0045 [hep-ph].

[225] A. Denner, H. Eck, O. Hahn, and J. Kublbeck, *Feynman rules for fermion number violating interactions*. Nucl. Phys. **B387** (1992) 467–484.

[226] S. Jones and C. Llewellyn Smith, *Leptoproduction of Supersymmetric Particles*. Nucl. Phys. **B217** (1983) 145.

[227] H. E. Haber and G. L. Kane, *The Search for Supersymmetry: Probing Physics Beyond the Standard Model*. Phys. Rept. **117** (1985) 75–263.

[228] E. I. Gates and K. L. Kowalski, *Majorana Feynman rules*. Phys. Rev. **D37** (1988) 938.

[229] J. Gluza and M. Zralek, *Feynman rules for Majorana neutrino interactions*. Phys. Rev. **D45** (1992) 1693–1700.

[230] R. Mertig, M. Bohm, and A. Denner, *FEYN CALC: Computer algebraic calculation of Feynman amplitudes*. Comput. Phys. Commun. **64** (1991) 345–359.

[231] R. Kleiss, W. J. Stirling, and S. Ellis, *A New Monte Carlo Treatment of Multiparticle Phase Space at High-energies*. Comput. Phys. Commun. **40** (1986) 359.

[232] W. Porod, *SPheno, a program for calculating supersymmetric spectra, SUSY particle decays and SUSY particle production at e+ e- colliders*. Comput. Phys. Commun. **153** (2003) 275–315, arXiv:hep-ph/0301101 [hep-ph].

[233] W. Porod and F. Staub, *SPheno 3.1: Extensions including flavour, CP-phases and models beyond the MSSM*. Comput. Phys. Commun. **183** (2012) 2458–2469, arXiv:1104.1573 [hep-ph].

[234] B. Allanach, *SOFTSUSY: a program for calculating supersymmetric spectra*. Comput. Phys. Commun. **143** (2002) 305–331, arXiv:hep-ph/0104145 [hep-ph].

[235] B. Allanach, S. Kraml, and W. Porod, *Comparison of SUSY mass spectrum calculations*. arXiv:hep-ph/0207314 [hep-ph].

[236] B. Allanach, S. Kraml, and W. Porod, *Theoretical uncertainties in sparticle mass predictions from computational tools*. JHEP **0303** (2003) 016, arXiv:hep-ph/0302102 [hep-ph].

[237] L. Wolfenstein, *Parametrization of the Kobayashi-Maskawa Matrix*. Phys. Rev. Lett. **51** (1983) 1945.

[238] **Particle Data Group** Collaboration, C. Amsler *et al.*, *Review of Particle Physics*. Phys. Lett. **B667** (2008) 1–1340.

[239] **ATLAS** Collaboration, *Search for squarks and gluinos with the ATLAS detector in final states with jets and missing transverse momentum and 20.3 fb^{-1} of $\sqrt{s} = 8$ TeV proton-proton collision data* Tech. Rep. ATLAS-CONF-2013-047, CERN, Geneva, May, 2013.

[240] **ATLAS** Collaboration, *Search for strong production of supersymmetric particles in final states with missing transverse momentum and at least three b-jets using 20.1 fbâ1 of pp collisions at sqrt(s) = 8 TeV with the ATLAS Detector.* Tech. Rep. ATLAS-CONF-2013-061, CERN, Geneva, Jun, 2013.

[241] **CMS** Collaboration, *Search for supersymmetry using razor variables in events with b-jets in pp collisions at 8 TeV* Tech. Rep. CMS-PAS-SUS-13-004, CERN, Geneva, 2013.

[242] **CMS** Collaboration, S. Chatrchyan *et al.*, *Search for new physics in the multijet and missing transverse momentum final state in proton-proton collisions at sqrt(s) = 8 TeV.* arXiv:1402.4770 [hep-ex].

[243] **ATLAS** Collaboration, *Search for direct-slepton and direct-chargino production in final states with two opposite-sign leptons, missing transverse momentum and no jets in 20/fb of pp collisions at sqrt(s) = 8 TeV with the ATLAS detector* Tech. Rep. ATLAS-CONF-2013-049, CERN, Geneva, May, 2013.

[244] P. Bechtle, O. Brein, S. Heinemeyer, G. Weiglein, and K. E. Williams, *HiggsBounds: Confronting Arbitrary Higgs Sectors with Exclusion Bounds from LEP and the Tevatron.* Comput. Phys. Commun. **181** (2010) 138–167, arXiv:0811.4169 [hep-ph].

[245] P. Bechtle, O. Brein, S. Heinemeyer, O. Stål, T. Stefaniak, *et al.*, *HiggsBounds-4: Improved Tests of Extended Higgs Sectors against Exclusion Bounds from LEP, the Tevatron and the LHC.* Eur. Phys. J. **C74** (2014) 2693, arXiv:1311.0055 [hep-ph].

[246] P. Bechtle, S. Heinemeyer, O. Stål, T. Stefaniak, and G. Weiglein, *HiggsSignals: Confronting arbitrary Higgs sectors with measurements at the Tevatron and the LHC.* Eur. Phys. J. **C74** (2014) 2711, arXiv:1305.1933 [hep-ph].

[247] **CMS and LHCb** Collaboration, *Combination of results on the rare decays $B^0_{(s)} \to \mu^+\mu^-$ from the CMS and LHCb experiments* Tech. Rep. CMS-PAS-BPH-13-007. CERN-LHCb-CONF-2013-012, CERN, Geneva, Jul, 2013.

[248] **ATLAS, CDF, CMS, D0 and LHCb** Collaboration, P. Eerola, *Rare $B^0_{(s)} \to \mu^+\mu^-$ decays.* arXiv:1209.3440 [hep-ex].

[249] **Belle** Collaboration, J. Brodzicka *et al.*, *Physics Achievements from the Belle Experiment.* PTEP **2012** (2012) 04D001, arXiv:1212.5342 [hep-ex].

[250] **BaBar** Collaboration, J. Lees *et al.*, *Evidence of $B \to \tau\nu$ decays with hadronic B tags*. Phys. Rev. **D88** (2013) 031102, arXiv:1207.0698 [hep-ex].

[251] **BaBar** Collaboration, J. Lees *et al.*, *Measurement of $B(B \to X_s\gamma)$, the $B \to X_s\gamma$ photon energy spectrum, and the direct CP asymmetry in $B \to X_{s+d}\gamma$ decays*. Phys. Rev. **D86** (2012) 112008, arXiv:1207.5772 [hep-ex].

[252] F. Mahmoudi, *SuperIso: A Program for calculating the isospin asymmetry of B —> K* gamma in the MSSM*. Comput. Phys. Commun. **178** (2008) 745–754, arXiv:0710.2067 [hep-ph].

[253] F. Mahmoudi, *SuperIso v2.3: A Program for calculating flavor physics observables in Supersymmetry*. Comput. Phys. Commun. **180** (2009) 1579–1613, arXiv:0808.3144 [hep-ph].

[254] A. Arbey and F. Mahmoudi, *SuperIso Relic: A Program for calculating relic density and flavor physics observables in Supersymmetry*. Comput. Phys. Commun. **181** (2010) 1277–1292, arXiv:0906.0369 [hep-ph].

[255] **WMAP** Collaboration, C. Bennett *et al.*, *Nine-Year Wilkinson Microwave Anisotropy Probe (WMAP) Observations: Final Maps and Results*. Astrophys. J. Suppl. **208** (2013) 20, arXiv:1212.5225 [astro-ph.CO].

[256] M. Fairbairn, A. Kraan, D. Milstead, T. Sjostrand, P. Z. Skands, *et al.*, *Stable massive particles at colliders*. Phys. Rept. **438** (2007) 1–63, arXiv:hep-ph/0611040 [hep-ph].

[257] G. Hiller and Y. Nir, *Measuring Flavor Mixing with Minimal Flavor Violation at the LHC*. JHEP **0803** (2008) 046, arXiv:0802.0916 [hep-ph].

[258] *Search for massive particles in multijet signatures with the ATLAS detector in $\sqrt{s} = 8$ TeV pp collisions at the LHC* Tech. Rep. ATLAS-CONF-2013-091, CERN, Geneva, Aug, 2013.

[259] *Search for long-lived, heavy particles in final states with a muon and a multi-track displaced vertex in proton-proton collisions at sqrt(s) = 8TeV with the ATLAS detector.* Tech. Rep. ATLAS-CONF-2013-092, CERN, Geneva, Aug, 2013.

[260] T. Hurth, *Present status of inclusive rare B decays*. Rev. Mod. Phys. **75** (2003) 1159–1199, arXiv:hep-ph/0212304 [hep-ph].

[261] J. F. Donoghue and A. A. Petrov, *Is B –> X(s) gamma equal to b –> s gamma? Spectator contributions to rare inclusive B decays*. Phys. Rev. **D53** (1996) 3664–3671, arXiv:hep-ph/9510227 [hep-ph].

[262] G. Paz, *Theory of Inclusive Radiative B Decays*. arXiv:1011.4953 [hep-ph].

[263] J. E. Kim and H. P. Nilles, *The mu Problem and the Strong CP Problem*. Phys. Lett. **B138** (1984) 150.

[264] U. Ellwanger, C. Hugonie, and A. M. Teixeira, *The Next-to-Minimal Supersymmetric Standard Model*. Phys. Rept. **496** (2010) 1–77, arXiv:0910.1785 [hep-ph].

[265] **ACME** Collaboration, J. Baron *et al.*, *Order of Magnitude Smaller Limit on the Electric Dipole Moment of the Electron*. Science **343** (2014) no. 6168, 269–272, arXiv:1310.7534 [physics.atom-ph].

[266] B. Regan, E. Commins, C. Schmidt, and D. DeMille, *New limit on the electron electric dipole moment*. Phys. Rev. Lett. **88** (2002) 071805.

[267] C. Baker, D. Doyle, P. Geltenbort, K. Green, M. van der Grinten, *et al.*, *An Improved experimental limit on the electric dipole moment of the neutron*. Phys. Rev. Lett. **97** (2006) 131801, arXiv:hep-ex/0602020 [hep-ex].

[268] W. Griffith, M. Swallows, T. Loftus, M. Romalis, B. Heckel, *et al.*, *Improved Limit on the Permanent Electric Dipole Moment of Hg-199*. Phys. Rev. Lett. **102** (2009) 101601.

[269] M. Matsuda and M. Tanimoto, *Explicit CP violation of the Higgs sector in the next-to-minimal supersymmetric standard model*. Phys. Rev. **D52** (1995) 3100–3107, arXiv:hep-ph/9504260 [hep-ph].

[270] N. Haba, *Explicit CP violation in the Higgs sector of the next-to-minimal supersymmetric standard model*. Prog. Theor. Phys. **97** (1997) 301–310, arXiv:hep-ph/9608357 [hep-ph].

[271] T. Ibrahim and P. Nath, *The Neutron and the lepton EDMs in MSSM, large CP violating phases, and the cancellation mechanism*. Phys. Rev. **D58** (1998) 111301, arXiv:hep-ph/9807501 [hep-ph].

[272] J. R. Ellis, J. S. Lee, and A. Pilaftsis, *Electric Dipole Moments in the MSSM Reloaded*. JHEP **0810** (2008) 049, arXiv:0808.1819 [hep-ph].

[273] M. Boz, *The Higgs sector and electron electric dipole moment in next-to-minimal supersymmetry with explicit CP violation*. Mod. Phys. Lett. **A21** (2006) 243–264, arXiv:hep-ph/0511072 [hep-ph].

[274] K. Cheung, T.-J. Hou, J. S. Lee, and E. Senaha, *Higgs Mediated EDMs in the Next-to-MSSM: An Application to Electroweak Baryogenesis*. Phys. Rev. **D84** (2011) 015002, arXiv:1102.5679 [hep-ph].

[275] U. Ellwanger, *Radiative corrections to the neutral Higgs spectrum in supersymmetry with a gauge singlet*. Phys. Lett. **B303** (1993) 271–276, arXiv:hep-ph/9302224 [hep-ph].

[276] T. Elliott, S. King, and P. White, *Supersymmetric Higgs bosons at the limit*. Phys. Lett. **B305** (1993) 71–77, arXiv:hep-ph/9302202 [hep-ph].

[277] T. Elliott, S. King, and P. White, *Squark contributions to Higgs boson masses in the next-to-minimal supersymmetric standard model*. Phys. Lett. **B314** (1993) 56–63, arXiv:hep-ph/9305282 [hep-ph].

[278] T. Elliott, S. King, and P. White, *Radiative corrections to Higgs boson masses in the next-to-minimal supersymmetric Standard Model*. Phys. Rev. **D49** (1994) 2435–2456, arXiv:hep-ph/9308309 [hep-ph].

[279] P. Pandita, *Radiative corrections to the scalar Higgs masses in a nonminimal supersymmetric Standard Model*. Z. Phys. **C59** (1993) 575–584.

[280] P. Pandita, *One loop radiative corrections to the lightest Higgs scalar mass in nonminimal supersymmetric Standard Model*. Phys. Lett. **B318** (1993) 338–346.

[281] U. Ellwanger and C. Hugonie, *Yukawa induced radiative corrections to the lightest Higgs boson mass in the NMSSM*. Phys. Lett. **B623** (2005) 93–103, arXiv:hep-ph/0504269 [hep-ph].

[282] G. Degrassi and P. Slavich, *On the radiative corrections to the neutral Higgs boson masses in the NMSSM*. Nucl. Phys. **B825** (2010) 119–150, arXiv:0907.4682 [hep-ph].

[283] F. Staub, W. Porod, and B. Herrmann, *The Electroweak sector of the NMSSM at the one-loop level*. JHEP **1010** (2010) 040, arXiv:1007.4049 [hep-ph].

[284] S. Ham, J. Kim, S. Oh, and D. Son, *The Charged Higgs boson in the next-to-minimal supersymmetric standard model with explicit CP violation*. Phys. Rev. **D64** (2001) 035007, arXiv:hep-ph/0104144 [hep-ph].

[285] S. Ham, S. Oh, and D. Son, *Neutral Higgs sector of the next-to-minimal supersymmetric standard model with explicit CP violation*. Phys. Rev. **D65** (2002) 075004, arXiv:hep-ph/0110052 [hep-ph].

[286] S. Ham, Y. Jeong, and S. Oh, *Radiative CP violation in the Higgs sector of the next-to-minimal supersymmetric model*. arXiv:hep-ph/0308264 [hep-ph].

[287] K. Funakubo and S. Tao, *The Higgs sector in the next-to-MSSM*. Prog. Theor. Phys. **113** (2005) 821–842, arXiv:hep-ph/0409294 [hep-ph].

[288] S. Ham, S. Kim, S. Oh, and D. Son, *Higgs bosons of the NMSSM with explicit CP violation at the ILC*. Phys. Rev. **D76** (2007) 115013, arXiv:0708.2755 [hep-ph].

[289] K. Cheung, T.-J. Hou, J. S. Lee, and E. Senaha, *The Higgs Boson Sector of the Next-to-MSSM with CP Violation*. Phys. Rev. **D82** (2010) 075007, arXiv:1006.1458 [hep-ph].

[290] K. Ender, T. Graf, M. Muhlleitner, and H. Rzehak, *Analysis of the NMSSM Higgs Boson Masses at One-Loop Level*. Phys. Rev. **D85** (2012) 075024, arXiv:1111.4952 [hep-ph].

[291] J. Baglio, T. Dao, R. Gröber, M. Mühlleitner, H. Rzehak, *et al.*, *A new implementation of the NMSSM Higgs boson decays*. EPJ Web Conf. **49** (2013) 12001.

[292] M. Maniatis, *The Next-to-Minimal Supersymmetric extension of the Standard Model reviewed*. Int. J. Mod. Phys. **A25** (2010) 3505–3602, arXiv:0906.0777 [hep-ph].

[293] D. Stöckinger, *Ein-Schleifen-Beiträge zu schwachen Dipolmomenten und Quark/Squark-Zerfällen im MSSM*, 1998. Diploma thesis, Universität Karlsruhe.

[294] C. Schappacher, *Fermion-Paarerzeugung in e^+e^--und Hadron- Kollisionen im Standard Model und im Minimalen Supersymmetrischen Standardmodell mit expliziter CP-Verletzung*. Dissertation, 2002.

[295] M. Frank, *Strahlungskorrekturen im Higgs-Sektor des Minimalen Supersymmetrischen Standardmodells mit CP-Verletzung*. Dissertation, 2003.

[296] M. Frank, T. Hahn, S. Heinemeyer, W. Hollik, H. Rzehak, *et al.*, *The Higgs Boson Masses and Mixings of the Complex MSSM in the Feynman-Diagrammatic Approach*. JHEP **0702** (2007) 047, arXiv:hep-ph/0611326 [hep-ph].

[297] H. A. Rzehak, *Two-loop contributions to the supersymmetric Higgs sector*. Dissertation, 2005.

[298] A. Freitas and D. Stockinger, *Gauge dependence and renormalization of tan beta in the MSSM*. Phys. Rev. **D66** (2002) 095014, arXiv:hep-ph/0205281 [hep-ph].

[299] A. Bharucha, A. Fowler, G. Moortgat-Pick, and G. Weiglein, *Consistent on shell renormalisation of electroweakinos in the complex MSSM: LHC and LC predictions*. JHEP **1305** (2013) 053, arXiv:1211.3134 [hep-ph].

[300] K. Walz, *Analysis of the Higgs boson masses at One-Loop level in the Complex NMSSM*, 2011. Diploma thesis, KIT.

[301] W. Hollik, E. Kraus, M. Roth, C. Rupp, K. Sibold, *et al.*, *Renormalization of the minimal supersymmetric standard model*. Nucl. Phys. **B639** (2002) 3–65, arXiv:hep-ph/0204350 [hep-ph].

[302] A. Djouadi, M. Spira, and P. Zerwas, *Production of Higgs bosons in proton colliders: QCD corrections*. Phys. Lett. **B264** (1991) 440–446.

[303] S. Dawson, *Radiative corrections to Higgs boson production*. Nucl. Phys. **B359** (1991) 283–300.

[304] R. P. Kauffman and W. Schaffer, *QCD corrections to production of Higgs pseudoscalars*. Phys. Rev. **D49** (1994) 551–554, arXiv:hep-ph/9305279 [hep-ph].

[305] S. Dawson and R. Kauffman, *QCD corrections to Higgs boson production: nonleading terms in the heavy quark limit*. Phys. Rev. **D49** (1994) 2298–2309, arXiv:hep-ph/9310281 [hep-ph].

[306] M. Kramer, E. Laenen, and M. Spira, *Soft gluon radiation in Higgs boson production at the LHC*. Nucl. Phys. **B511** (1998) 523–549, arXiv:hep-ph/9611272 [hep-ph].

[307] D. Graudenz, M. Spira, and P. Zerwas, *QCD corrections to Higgs boson production at proton proton colliders*. Phys. Rev. Lett. **70** (1993) 1372–1375.

[308] M. Spira, A. Djouadi, D. Graudenz, and P. Zerwas, *SUSY Higgs production at proton colliders*. Phys. Lett. **B318** (1993) 347–353.

[309] R. Harlander and P. Kant, *Higgs production and decay: Analytic results at next-to-leading order QCD*. JHEP **0512** (2005) 015, arXiv:hep-ph/0509189 [hep-ph].

[310] M. Muhlleitner and M. Spira, *Higgs Boson Production via Gluon Fusion: Squark Loops at NLO QCD*. Nucl. Phys. **B790** (2008) 1–27, arXiv:hep-ph/0612254 [hep-ph].

[311] C. Anastasiou and K. Melnikov, *Higgs boson production at hadron colliders in NNLO QCD*. Nucl. Phys. **B646** (2002) 220–256, arXiv:hep-ph/0207004 [hep-ph].

[312] R. V. Harlander and W. B. Kilgore, *Production of a pseudoscalar Higgs boson at hadron colliders at next-to-next-to leading order*. JHEP **0210** (2002) 017, arXiv:hep-ph/0208096 [hep-ph].

[313] V. Ravindran, J. Smith, and W. L. van Neerven, *NNLO corrections to the total cross-section for Higgs boson production in hadron hadron collisions*. Nucl. Phys. **B665** (2003) 325–366, arXiv:hep-ph/0302135 [hep-ph].

[314] C. Anastasiou and K. Melnikov, *Pseudoscalar Higgs boson production at hadron colliders in NNLO QCD*. Phys. Rev. **D67** (2003) 037501, arXiv:hep-ph/0208115 [hep-ph].

[315] M. Spira, *HIGLU: A program for the calculation of the total Higgs production cross-section at hadron colliders via gluon fusion including QCD corrections*. arXiv:hep-ph/9510347 [hep-ph].

[316] M. Spira, *QCD effects in Higgs physics*. Fortsch. Phys. **46** (1998) 203–284, arXiv:hep-ph/9705337 [hep-ph].

[317] W. Beenakker, S. Dittmaier, M. Kramer, B. Plumper, M. Spira, *et al.*, *Higgs radiation off top quarks at the Tevatron and the LHC*. Phys. Rev. Lett. **87** (2001) 201805, arXiv:hep-ph/0107081 [hep-ph].

[318] L. Reina and S. Dawson, *Next-to-leading order results for t anti-t h production at the Tevatron*. Phys. Rev. Lett. **87** (2001) 201804, arXiv:hep-ph/0107101 [hep-ph].

[319] W. Beenakker, S. Dittmaier, M. Kramer, B. Plumper, M. Spira, *et al.*, *NLO QCD corrections to t anti-t H production in hadron collisions*. Nucl. Phys. **B653** (2003) 151–203, arXiv:hep-ph/0211352 [hep-ph].

[320] S. Dawson, L. Orr, L. Reina, and D. Wackeroth, *Associated top quark Higgs boson production at the LHC*. Phys. Rev. **D67** (2003) 071503, arXiv:hep-ph/0211438 [hep-ph].

[321] *See the website of the LHC Higgs cross section working group*. https://twiki.cern.ch/twiki/bin/view/LHCPhysics/CrossSections.

[322] A. Djouadi, J. Kalinowski, and M. Spira, *HDECAY: A Program for Higgs boson decays in the standard model and its supersymmetric extension*. Comput. Phys. Commun. **108** (1998) 56–74, arXiv:hep-ph/9704448 [hep-ph].

[323] J. Butterworth, A. Arbey, L. Basso, S. Belov, A. Bharucha, *et al.*, *The Tools and Monte Carlo working group Summary Report*. arXiv:1003.1643 [hep-ph].

[324] K. Chetyrkin, B. A. Kniehl, and M. Steinhauser, *Decoupling relations to O (α_s^3) and their connection to low-energy theorems*. Nucl. Phys. **B510** (1998) 61–87, arXiv:hep-ph/9708255 [hep-ph].

[325] T. Inami, T. Kubota, and Y. Okada, *Effective Gauge Theory and the Effect of Heavy Quarks in Higgs Boson Decays*. Z. Phys. **C18** (1983) 69.

[326] M. Spira, A. Djouadi, D. Graudenz, and P. Zerwas, *Higgs boson production at the LHC*. Nucl. Phys. **B453** (1995) 17–82, arXiv:hep-ph/9504378 [hep-ph].

[327] K. Chetyrkin, B. A. Kniehl, and M. Steinhauser, *Hadronic Higgs decay to order α_s^4*. Phys. Rev. Lett. **79** (1997) 353–356, arXiv:hep-ph/9705240 [hep-ph].

[328] Y. Schroder and M. Steinhauser, *Four-loop decoupling relations for the strong coupling*. JHEP **0601** (2006) 051, arXiv:hep-ph/0512058 [hep-ph].

[329] K. Chetyrkin, J. H. Kuhn, and C. Sturm, *QCD decoupling at four loops*. Nucl. Phys. **B744** (2006) 121–135, arXiv:hep-ph/0512060 [hep-ph].

[330] P. Baikov and K. Chetyrkin, *Top Quark Mediated Higgs Boson Decay into Hadrons to Order α_s^5*. Phys. Rev. Lett. **97** (2006) 061803, arXiv:hep-ph/0604194 [hep-ph].

[331] S. Dawson, A. Djouadi, and M. Spira, *QCD corrections to SUSY Higgs production: The Role of squark loops*. Phys. Rev. Lett. **77** (1996) 16–19, arXiv:hep-ph/9603423 [hep-ph].

[332] H.-Q. Zheng and D.-D. Wu, *First order QCD corrections to the decay of the Higgs boson into two photons*. Phys. Rev. **D42** (1990) 3760–3763.

[333] A. Djouadi, M. Spira, J. van der Bij, and P. Zerwas, *QCD corrections to gamma gamma decays of Higgs particles in the intermediate mass range*. Phys. Lett. **B257** (1991) 187–190.

[334] S. Dawson and R. Kauffman, *QCD corrections to H —> gamma gamma*. Phys. Rev. **D47** (1993) 1264–1267.

[335] A. Djouadi, M. Spira, and P. Zerwas, *Two photon decay widths of Higgs particles*. Phys. Lett. **B311** (1993) 255–260, arXiv:hep-ph/9305335 [hep-ph].

[336] K. Melnikov and O. I. Yakovlev, *Higgs —> two photon decay: QCD radiative correction*. Phys. Lett. **B312** (1993) 179–183, arXiv:hep-ph/9302281 [hep-ph].

[337] M. Inoue, R. Najima, T. Oka, and J. Saito, *QCD corrections to two photon decay of the Higgs boson and its reverse process*. Mod. Phys. Lett. **A9** (1994) 1189–1194.

[338] *Mathematica Edition: Version 7.0*. Wolfram Research, Inc., Champaign, Illinois, 2008.

[339] P. Z. Skands, B. Allanach, H. Baer, C. Balazs, G. Belanger, *et al.*, *SUSY Les Houches accord: Interfacing SUSY spectrum calculators, decay packages, and event generators*. JHEP **0407** (2004) 036, arXiv:hep-ph/0311123 [hep-ph].

[340] U. Ellwanger, J. F. Gunion, and C. Hugonie, *NMHDECAY: A Fortran code for the Higgs masses, couplings and decay widths in the NMSSM*. JHEP **0502** (2005) 066, arXiv:hep-ph/0406215 [hep-ph].

[341] U. Ellwanger and C. Hugonie, *NMHDECAY 2.0: An Updated program for sparticle masses, Higgs masses, couplings and decay widths in the NMSSM*. Comput. Phys. Commun. **175** (2006) 290–303, arXiv:hep-ph/0508022 [hep-ph].

[342] G. Belanger, F. Boudjema, C. Hugonie, A. Pukhov, and A. Semenov, *Relic density of dark matter in the NMSSM*. JCAP **0509** (2005) 001, arXiv:hep-ph/0505142 [hep-ph].

[343] **LEP Working Group for Higgs boson searches, ALEPH, DELPHI, L3 and OPAL** Collaboration, R. Barate *et al.*, *Search for the standard model Higgs boson at LEP*. Phys. Lett. **B565** (2003) 61–75, arXiv:hep-ex/0306033 [hep-ex].

[344] **ALEPH, DELPHI, L3, OPAL and LEP Working Group for Higgs Boson Searches** Collaboration, S. Schael *et al.*, *Search for neutral MSSM Higgs bosons at LEP*. Eur. Phys. J. **C47** (2006) 547–587, arXiv:hep-ex/0602042 [hep-ex].

[345] **TEVNPH (Tevatron New Phenomina and Higgs Working Group), CDF and D0** Collaboration, *Combined CDF and D0 Search for Standard Model Higgs Boson Production with up to 10.0 fb^{-1} of Data*. arXiv:1203.3774 [hep-ex].

[346] P. Bechtle, O. Brein, S. Heinemeyer, G. Weiglein, and K. E. Williams, *HiggsBounds: Confronting Arbitrary Higgs Sectors with Exclusion Bounds from LEP and the Tevatron*. Comput. Phys. Commun. **181** (2010) 138–167, arXiv:0811.4169 [hep-ph].

[347] P. Bechtle, O. Brein, S. Heinemeyer, G. Weiglein, and K. E. Williams, *HiggsBounds 2.0.0: Confronting Neutral and Charged Higgs Sector Predictions with Exclusion Bounds from LEP and the Tevatron*. Comput. Phys. Commun. **182** (2011) 2605–2631, arXiv:1102.1898 [hep-ph].

[348] S. King, M. Muhlleitner, and R. Nevzorov, *NMSSM Higgs Benchmarks Near 125 GeV*. Nucl. Phys. **B860** (2012) 207–244, arXiv:1201.2671 [hep-ph].

[349] D. Miller, R. Nevzorov, and P. Zerwas, *The Higgs sector of the next-to-minimal supersymmetric standard model*. Nucl. Phys. **B681** (2004) 3–30, arXiv:hep-ph/0304049 [hep-ph].

[350] **ATLAS** Collaboration, *Search for direct top squark pair production in final states with one isolated lepton, jets, and missing transverse momentum in $sqrts = 8, TeV$ pp collisions using 21 fb^{-1} of ATLAS data* Tech. Rep. ATLAS-CONF-2013-037, CERN, Geneva, Mar, 2013.

[351] **CMS** Collaboration, *Search for top squarks in multijet events with large missing momentum in proton-proton collisions at 8 TeV* Tech. Rep. CMS-PAS-SUS-13-015, CERN, Geneva, 2013.

[352] S. Weinberg, *Implications of Dynamical Symmetry Breaking*. Phys. Rev. **D13** (1976) 974–996.

[353] L. Susskind, *Dynamics of Spontaneous Symmetry Breaking in the Weinberg-Salam Theory*. Phys. Rev. **D20** (1979) 2619–2625.

[354] R. Contino, Y. Nomura, and A. Pomarol, *Higgs as a holographic pseudoGoldstone boson*. Nucl. Phys. **B671** (2003) 148–174, arXiv:hep-ph/0306259 [hep-ph].

[355] G. Giudice, C. Grojean, A. Pomarol, and R. Rattazzi, *The Strongly-Interacting Light Higgs*. JHEP **0706** (2007) 045, arXiv:hep-ph/0703164 [hep-ph].

[356] S. Weinberg, *Baryon and Lepton Nonconserving Processes*. Phys. Rev. Lett. **43** (1979) 1566–1570.

[357] A. Azatov, R. Contino, and J. Galloway, *Model-Independent Bounds on a Light Higgs*. JHEP **1204** (2012) 127, arXiv:1202.3415 [hep-ph]. Erratum-ibid. **1304** (2012) 140.

[358] R. Contino, C. Grojean, M. Moretti, F. Piccinini, and R. Rattazzi, *Strong Double Higgs Production at the LHC*. JHEP **1005** (2010) 089, arXiv:1002.1011 [hep-ph].

[359] R. Slansky, *Group Theory for Unified Model Building*. Phys. Rept. **79** (1981) 1–128.

[360] B. Gripaios, A. Pomarol, F. Riva, and J. Serra, *Beyond the Minimal Composite Higgs Model*. JHEP **0904** (2009) 070, arXiv:0902.1483 [hep-ph].

[361] J. R. Espinosa, B. Gripaios, T. Konstandin, and F. Riva, *Electroweak Baryogenesis in Non-minimal Composite Higgs Models*. JCAP **1201** (2012) 012, arXiv:1110.2876 [hep-ph].

[362] J. Mrazek, A. Pomarol, R. Rattazzi, M. Redi, J. Serra, *et al.*, *The Other Natural Two Higgs Doublet Model*. Nucl. Phys. **B853** (2011) 1–48, arXiv:1105.5403 [hep-ph].

[363] R. Contino, D. Marzocca, D. Pappadopulo, and R. Rattazzi, *On the effect of resonances in composite Higgs phenomenology*. JHEP **1110** (2011) 081, arXiv:1109.1570 [hep-ph].

[364] K. Agashe, R. Contino, L. Da Rold, and A. Pomarol, *A Custodial symmetry for Zb anti-b*. Phys. Lett. **B641** (2006) 62–66, arXiv:hep-ph/0605341 [hep-ph].

[365] G. Panico, M. Redi, A. Tesi, and A. Wulzer, *On the Tuning and the Mass of the Composite Higgs*. JHEP **1303** (2013) 051, arXiv:1210.7114 [hep-ph].

[366] R. Grober and M. Muhlleitner, *Composite Higgs Boson Pair Production at the LHC*. JHEP **1106** (2011) 020, arXiv:1012.1562 [hep-ph].

[367] J. Barnard, T. Gherghetta, A. Medina, and T. S. Ray, *Radiative corrections to the composite Higgs mass from a gluon partner*. JHEP **1310** (2013) 055, arXiv:1307.4778 [hep-ph].

[368] B. Bellazzini, C. Csáki, and J. Serra, *Composite Higgses*. arXiv:1401.2457 [hep-ph].

[369] F. Caracciolo, A. Parolini, and M. Serone, *UV Completions of Composite Higgs Models with Partial Compositeness*. JHEP **1302** (2013) 066, arXiv:1211.7290 [hep-ph].

[370] D. Marzocca, A. Parolini, and M. Serone, *Supersymmetry with a pNGB Higgs and Partial Compositeness*. arXiv:1312.5664 [hep-ph].

[371] J. Barnard, T. Gherghetta, and T. S. Ray, *UV descriptions of composite Higgs models without elementary scalars*. arXiv:1311.6562 [hep-ph].

[372] G. Cacciapaglia and F. Sannino, *Fundamental Composite (Goldstone) Higgs Dynamics*. arXiv:1402.0233 [hep-ph].

[373] A. Pierce, J. Thaler, and L.-T. Wang, *Disentangling Dimension Six Operators through Di-Higgs Boson Production*. JHEP **0705** (2007) 070, arXiv:hep-ph/0609049 [hep-ph].

[374] C. Grojean, O. Matsedonskyi, and G. Panico, *Light top partners and precision physics*. JHEP **1310** (2013) 160, arXiv:1306.4655 [hep-ph].

[375] K. Agashe and R. Contino, *The Minimal composite Higgs model and electroweak precision tests*. Nucl. Phys. **B742** (2006) 59–85, arXiv:hep-ph/0510164 [hep-ph].

[376] R. Barbieri, B. Bellazzini, V. S. Rychkov, and A. Varagnolo, *The Higgs boson from an extended symmetry*. Phys. Rev. **D76** (2007) 115008, arXiv:0706.0432 [hep-ph].

[377] A. Pomarol and J. Serra, *Top Quark Compositeness: Feasibility and Implications*. Phys. Rev. **D78** (2008) 074026, arXiv:0806.3247 [hep-ph].

[378] P. Lodone, *Vector-like quarks in a 'composite' Higgs model*. JHEP **0812** (2008) 029, arXiv:0806.1472 [hep-ph].

[379] C. Anastasiou, E. Furlan, and J. Santiago, *Realistic Composite Higgs Models*. Phys. Rev. **D79** (2009) 075003, arXiv:0901.2117 [hep-ph].

[380] M. Gillioz, *A Light composite Higgs boson facing electroweak precision tests*. Phys. Rev. **D80** (2009) 055003, arXiv:0806.3450 [hep-ph].

[381] **CDF** Collaboration, T. Aaltonen *et al.*, *Precise measurement of the W-boson mass with the CDF II detector*. Phys. Rev. Lett. **108** (2012) 151803, arXiv:1203.0275 [hep-ex].

[382] **D0** Collaboration, V. M. Abazov *et al.*, *Measurement of the W Boson Mass with the D0 Detector*. Phys. Rev. Lett. **108** (2012) 151804, arXiv:1203.0293 [hep-ex].

[383] **CDF and D0** Collaboration, T. E. W. Group, *2012 Update of the Combination of CDF and D0 Results for the Mass of the W Boson*. arXiv:1204.0042 [hep-ex].

[384] **CMS** Collaboration, S. Chatrchyan *et al.*, *Search for pair produced fourth-generation up-type quarks in pp collisions at $\sqrt{s} = 7$ TeV with a lepton in the final state*. Phys. Lett. **B718** (2012) 307–328, arXiv:1209.0471 [hep-ex].

[385] **CMS** Collaboration, S. Chatrchyan *et al.*, *Search for heavy, top-like quark pair production in the dilepton final state in pp collisions at $\sqrt{s} = 7$ TeV*. Phys. Lett. **B716** (2012) 103–121, arXiv:1203.5410 [hep-ex].

[386] **CMS** Collaboration, S. Chatrchyan *et al.*, *Search for heavy bottom-like quarks in 4.9 inverse femtobarns of pp collisions at $\sqrt{s} = 7$ TeV*. JHEP **1205** (2012) 123, arXiv:1204.1088 [hep-ex].

[387] **CMS** Collaboration, S. Chatrchyan *et al.*, *Search for a Vector-like Quark with Charge 2/3 in t + Z Events from pp Collisions at $\sqrt{s} = 7$ TeV*. Phys. Rev. Lett. **107** (2011) 271802, arXiv:1109.4985 [hep-ex].

[388] **ATLAS** Collaboration, G. Aad *et al.*, *Search for pair production of a heavy up-type quark decaying to a W boson and a b quark in the lepton+jets channel with the ATLAS detector*. Phys. Rev. Lett. **108** (2012) 261802, arXiv:1202.3076 [hep-ex].

[389] **ATLAS** Collaboration, G. Aad *et al.*, *Search for pair-produced heavy quarks decaying to Wq in the two-lepton channel at $\sqrt{s} = 7$ TeV with the ATLAS detector*. Phys. Rev. **D86** (2012) 012007, arXiv:1202.3389 [hep-ex].

[390] **ATLAS** Collaboration, G. Aad *et al.*, *Search for down-type fourth generation quarks with the ATLAS detector in events with one lepton and hadronically decaying W bosons*. Phys. Rev. Lett. **109** (2012) 032001, arXiv:1202.6540 [hep-ex].

[391] **ATLAS** Collaboration, G. Aad *et al.*, *Search for same-sign top-quark production and fourth-generation down-type quarks in pp collisions at $\sqrt{s} = 7$ TeV with the ATLAS detector*. JHEP **1204** (2012) 069, arXiv:1202.5520 [hep-ex].

[392] **CDF** Collaboration, T. Aaltonen *et al.*, *Search for a Heavy Top-Like Quark in $p\bar{p}$ Collisions at $\sqrt{s} = 1.96$ TeV*. Phys. Rev. Lett. **107** (2011) 261801, arXiv:1107.3875 [hep-ex].

[393] **CDF** Collaboration, T. Aaltonen *et al.*, *Search for heavy bottom-like quarks decaying to an electron or muon and jets in $p\bar{p}$ collisions at $\sqrt{s} = 1.96$ TeV*. Phys. Rev. Lett. **106** (2011) 141803, arXiv:1101.5728 [hep-ex].

[394] M. Aliev, H. Lacker, U. Langenfeld, S. Moch, P. Uwer, *et al.*, *HATHOR: HAdronic Top and Heavy quarks crOss section calculatoR*. Comput. Phys. Commun. **182** (2011) 1034–1046, arXiv:1007.1327 [hep-ph].

[395] **CMS** Collaboration, *Search for T5/3 top partners in same-sign dilepton final state* Tech. Rep. CMS-PAS-B2G-12-012, CERN, Geneva, 2013.

[396] **ATLAS** Collaboration, *Search for heavy top-like quarks decaying to a Higgs boson and a top quark in the lepton plus jets final state in pp collisions at $\sqrt{s} = 8$ TeV with the ATLAS detector* Tech. Rep. ATLAS-CONF-2013-018, CERN, Geneva, Mar, 2013.

[397] A. Azatov and J. Galloway, *Light Custodians and Higgs Physics in Composite Models*. Phys. Rev. **D85** (2012) 055013, arXiv:1110.5646 [hep-ph].

[398] E. Furlan, *Gluon-fusion Higgs production at NNLO for a non-standard Higgs sector*. JHEP **1110** (2011) 115, arXiv:1106.4024 [hep-ph].

[399] A. Azatov and A. Paul, *Probing Higgs couplings with high p_T Higgs production*. JHEP **1401** (2014) 014, arXiv:1309.5273 [hep-ph].

[400] C. Grojean, E. Salvioni, M. Schlaffer, and A. Weiler, *Very boosted Higgs in gluon fusion*. arXiv:1312.3317 [hep-ph].

[401] R. Contino, M. Ghezzi, M. Moretti, G. Panico, F. Piccinini, *et al.*, *Anomalous Couplings in Double Higgs Production*. JHEP **1208** (2012) 154, arXiv:1205.5444 [hep-ph].

[402] F. Hoogeveen, *The Influence of a Heavy Fermion Doublet on Higgs Boson Production via the Gluon Fusion Mechanism*. Nucl. Phys. **B259** (1985) 19.

[403] S. Dawson, E. Furlan, and I. Lewis, *Unravelling an extended quark sector through multiple Higgs production?* Phys. Rev. **D87** (2013) 014007, arXiv:1210.6663 [hep-ph].

[404] C. Delaunay, C. Grojean, and G. Perez, *Modified Higgs Physics from Composite Light Flavors*. JHEP **1309** (2013) 090, arXiv:1303.5701 [hep-ph].

[405] C. Delaunay, T. Flacke, J. Gonzalez-Fraile, S. J. Lee, G. Panico, *et al.*, *Light Non-degenerate Composite Partners at the LHC*. JHEP **1402** (2014) 055, arXiv:1311.2072 [hep-ph].

[406] T. Flacke, J. H. Kim, S. J. Lee, and S. H. Lim, *Constraints on composite quark partners from Higgs searches*. arXiv:1312.5316 [hep-ph].

[407] M. E. Peskin and T. Takeuchi, *Estimation of oblique electroweak corrections*. Phys. Rev. **D46** (1992) 381–409.

[408] G. Altarelli and R. Barbieri, *Vacuum polarization effects of new physics on electroweak processes*. Phys. Lett. **B253** (1991) 161–167.

[409] G. Altarelli, R. Barbieri, and S. Jadach, *Toward a model independent analysis of electroweak data*. Nucl. Phys. **B369** (1992) 3–32.

[410] G. Altarelli, R. Barbieri, and F. Caravaglios, *Nonstandard analysis of electroweak precision data*. Nucl. Phys. **B405** (1993) 3–23.

[411] L. Lavoura and J. P. Silva, *The Oblique corrections from vector - like singlet and doublet quarks*. Phys. Rev. **D47** (1993) 2046–2057.

[412] R. Contino, *The Higgs as a Composite Nambu-Goldstone Boson*. arXiv:1005.4269 [hep-ph].

[413] S. Weinberg, *Precise relations between the spectra of vector and axial vector mesons*. Phys. Rev. Lett. **18** (1967) 507–509.

[414] A. Denner, *Techniques for calculation of electroweak radiative corrections at the one loop level and results for W physics at LEP-200*. Fortsch. Phys. **41** (1993) 307–420, arXiv:0709.1075 [hep-ph].

[415] A. Kapuvari, *Composite Higgs Boson with fermions in the adjoint representation*, 2013. Diploma thesis, KIT.

[416] **ALEPH, DELPHI, L3, OPAL, SLD,LEP Electroweak Working Group, SLD Electroweak Group, SLD Heavy Flavour Group** Collaboration, S. Schael *et al.*, *Precision electroweak measurements on the Z resonance*. Phys. Rept. **427** (2006) 257–454, arXiv:hep-ex/0509008 [hep-ex].

[417] **CMS** Collaboration, S. Chatrchyan *et al.*, *Measurement of the single-top-quark t-channel cross section in pp collisions at* $\sqrt{s} = 7$ *TeV*. JHEP **1212** (2012) 035, arXiv:1209.4533 [hep-ex].

[418] **ATLAS** Collaboration, *Search for anomalous production of events with same-sign dileptons and b jets in 14.3* fb^{-1} *of pp collisions at* $\sqrt{s} = 8$ *TeV with the ATLAS detector* Tech. Rep. ATLAS-CONF-2013-051, CERN, Geneva, May, 2013.

[419] **ATLAS** Collaboration, *Search for pair production of new heavy quarks that decay to a Z boson and a third generation quark in pp collisions at* $\sqrt{s} = 8$ *TeV with the ATLAS detector* Tech. Rep. ATLAS-CONF-2013-056, CERN, Geneva, Jun, 2013.

[420] **ATLAS** Collaboration, *Search for pair production of heavy top-like quarks decaying to a high-*p_{T} *W boson and a b quark in the lepton plus jets final state in pp collisions at* $\sqrt{s} = 8$ *TeV with the ATLAS detector* Tech. Rep. ATLAS-CONF-2013-060, CERN, Geneva, Jun, 2013.

[421] **CMS** Collaboration, S. Chatrchyan *et al.*, *Inclusive search for a vector-like T quark with charge 2/3 in pp collisions at* $\sqrt{s}$*=8 TeV*. Phys. Lett. **B729** (2014) 149–171, arXiv:1311.7667 [hep-ex].

[422] **CMS** Collaboration, *Search for pair-produced vector-like quarks of charge -1/3 in lepton + jets final state in pp collisions at sqrt(s) = 8 TeV* Tech. Rep. CMS-PAS-B2G-12-019, CERN, Geneva, 2013.

[423] C. Csaki, A. Falkowski, and A. Weiler, *The Flavor of the Composite Pseudo-Goldstone Higgs*. JHEP **0809** (2008) 008, arXiv:0804.1954 [hep-ph].

[424] M. Redi and A. Weiler, *Flavor and CP Invariant Composite Higgs Models*. JHEP **1111** (2011) 108, arXiv:1106.6357 [hep-ph].

[425] **ATLAS** Collaboration, G. Aad *et al.*, *ATLAS search for new phenomena in dijet mass and angular distributions using pp collisions at* $\sqrt{s} = 7$ *TeV*. JHEP **1301** (2013) 029, arXiv:1210.1718 [hep-ex].

[426] **CMS** Collaboration, S. Chatrchyan *et al.*, *Search for contact interactions using the inclusive jet* p_T *spectrum in pp collisions at* $\sqrt{s} = 7$ *TeV*. Phys. Rev. **D87** (2013) 052017, arXiv:1301.5023 [hep-ex].

[427] L. Da Rold, C. Delaunay, C. Grojean, and G. Perez, *Up Asymmetries From Exhilarated Composite Flavor Structures*. JHEP **1302** (2013) 149, arXiv:1208.1499 [hep-ph].

[428] M. Redi, *Composite MFV and Beyond*. Eur. Phys. J. **C72** (2012) 2030, arXiv:1203.4220 [hep-ph].

[429] R. Barbieri, D. Buttazzo, F. Sala, D. M. Straub, and A. Tesi, *A 125 GeV composite Higgs boson versus flavour and electroweak precision tests*. JHEP **1305** (2013) 069, arXiv:1211.5085 [hep-ph].

[430] J. Espinosa, C. Grojean, and M. Muhlleitner, *Composite Higgs Search at the LHC*. JHEP **1005** (2010) 065, arXiv:1003.3251 [hep-ph].

[431] R. Contino, M. Ghezzi, C. Grojean, M. Muhlleitner, and M. Spira, *Effective Lagrangian for a light Higgs-like scalar*. JHEP **1307** (2013) 035, arXiv:1303.3876 [hep-ph].

[432] A. Azatov, R. Contino, A. Di Iura, and J. Galloway, *New Prospects for Higgs Compositeness in h -> Z gamma*. Phys. Rev. **D88** (2013) 075019, arXiv:1308.2676 [hep-ph].

[433] **ATLAS** Collaboration, *Combined coupling measurements of the Higgs-like boson with the ATLAS detector using up to 25* fb^{-1} *of proton-proton collision data* Tech. Rep. ATLAS-CONF-2013-034, CERN, Geneva, Mar, 2013.

[434] M. Carena, L. Da Rold, and E. Ponton, *Minimal Composite Higgs Models at the LHC*. arXiv:1402.2987 [hep-ph].

[435] E. Salvioni, *Phenomenology of Compositeness at the LHC*. Dissertation, 2013.

[436] C. Bini, R. Contino, and N. Vignaroli, *Heavy-light decay topologies as a new strategy to discover a heavy gluon*. JHEP **1201** (2012) 157, arXiv:1110.6058 [hep-ph].

[437] R. Gröber, *Higgs pair production in the Composite Higgs Model*, 2011. Diploma thesis, KIT.

[438] T. Figy and R. Zwicky, *The other Higgses, at resonance, in the Lee-Wick extension of the Standard Model*. JHEP **1110** (2011) 145, arXiv:1108.3765 [hep-ph].

Acknowledgements

First of all, I want to thank my advisor Prof. Dr. Margarete Mühlleitner for accepting me as a PhD student on such an interesting subject. I am deeply grateful to her, for teaching me a lot about physics, her constant support and giving me advice whenever needed.

I thank Prof. Dr. Dieter Zeppenfeld very much for agreeing to be the second referee of my dissertation.

I am highly indebted to my collaborators Julien Baglio, Abdelhak Djouadi, Marc Gillioz, Thorben Graf, Christophe Grojean, Andreas Kapuvari, Eva Popenda, Jérémie Quevillon, Heidi Rzehak, Ennio Salvioni, Michael Spira, Juraj Streicher, Kathrin Walz and Alexander Wlotzka, from which I learnt a lot.

I am very thankful to Julien Baglio, Luca Di Luzio, Eva Popenda, Christian Röhr and Kathrin Walz for their useful comments on the manuscript.

Thanks to my office mates Ken Arnold, Francisco Campanario, Hanna Hoffmann, Matthias Kerner, Michael Rauch, Christian Schappacher and Juraj Streicher for various physics discussions and for standing my habit of talking a lot.

A special thanks goes to all the administrators, Johannes Bellm, Bastian Feigl, Christian Röhr and Robin Roth, during my three years of PhD. Without their work, my work would have often not been possible.

My time at the ITP has been very enjoyable. Thanks to all the members for that!

In particular, I want to thank Basti for being wikipedia, Christian for the late night talks, Christian for teaching me the importance of nice colours for the plots, Eva for "composing" the colour reconnection song with me, Franzi for decorating the office door, Johannes for feeding us with "Leberkäs", Nastya for the various shopping tours, Thomas for still standing me after spending two summer schools together and all of them for a lot of fun that we had during the last three years, not only during work times but also on the weekends.

I am very grateful to my parents, Linda and Tini for their support and for always believing that I will succeed.

Finally, I want to thank Luca for all his love, for his patience with me, for staying calm, for doing a lot of stupid things for me and last but not least also for various physics discussions, in particular the ones about the hierarchy problem.